TECHNISCHE UNIVERSITÄT MÜNCHEN

Lehrstuhl für Analytische Lebensmittelchemie

Mass spectrometry based gut meta-metabolomics in obesity and type 2 Diabetes

Alesia Walker

Vollständiger Ausdruck der von der Fakultät für Wissenschaftszentrum Weihenstephan für Ernährung, Landnutzung und Umwelt der Technischen Universität München zur Erlangung des akademischen Grades eines

Doktors der Naturwissenschaften

genehmigter Dissertation.

Vorsitzender: Univ.-Prof. Dr. E. Grill

Prüfer der Dissertation:

1. apl.-Prof. Dr. Ph. Schmitt-Kopplin
2. Univ.-Prof. Dr. M. Rychlik
3. apl.-Prof. Dr. A. Hartmann,
   (Ludwig-Maximilians-Universität München)

Die Dissertation wurde am 14.10.2013 bei der Technischen Universität München eingereicht und durch die Fakultät für Wissenschaftszentrum Weihenstephan für Ernährung, Landnutzung und Umwelt am 25.05.2014 angenommen.

Table of contents

List of Figures

List of Tables

Abbreviations

(-)	negative electrospray ionization mode
(+)	positive electrospray ionization mode
AAM	Arachidonic acid metabolism
ANOVA	Analysis of variance
BA	Bile acid
BW	Body weight
C(x:y)	Fatty acid with x = number of carbon atom and y = number of double bonds
C57J	C57BL/6J
C57N	C57BL/6NTac
CA	Cholic acid
CHNOSP	Carbon, hydrogen, nitrogen, sulfur, phosphor
C_N	Number of carbon atoms
CV	Cross validation
Da	Dalton
DA	Discriminant analysis
db/db	BKS.Cg-dock7^{m} +/+ Lepr^{db}/J
DCA	Deoxycholic acid
DIO	Diet induced obesity
ESI	Electrospray ionization
FT-ICR-MS	Fourier transform ion cyclotron resonance mass spectrometry
GF	Germ free
HFD	high fat diet
KEGG	Kyoto Encyclopedia of Genes and Genomes
LARD	Lard diet
LTB4	Leukotriene B4
MMU	Mus musculus
MS	mass spectrometry
MSA	Multivariate statistical analysis
n	Number of mice
NATs	N-acyl taurines
OPLS	Orthogonal partial least squares
PC	Principal component
PCA	Principal component analysis
p-corr	p-value derived from Pearson correlation
PLS	Partial least squares
ppm	Parts per million
Q2	Goodness of prediction
R2	Goodness of fit
RP	Reverse phase column chemistry
SAFF	Safflower diet
SD	standard diet
T	Tauro
T2DM	Type 2 Diabetes mellitus
TCA	Taurocholic acid
TIC	Total ion chromatogram
TOF	Time of flight
UPLC®/UPLC	Ultra-high pressure liquid chromatography
USA	Univariate statistical analysis
wt	Wildtype

Danksagung

Zu Beginn möchte ich mich bei meinem Doktorvater Prof. Dr. Philippe Schmitt-Kopplin für seine stetige und wertvolle Betreuung und Unterstützung danken. Zudem, möchte ich mich dafür bedanken, dass er mir die Möglichkeit geboten hat, in diesem spannenden Forschungsgebiet eine Doktorarbeit zu absolvieren.

Als nächsten möchte ich bei meinen Kollegen für eine angenehme Atmosphäre, einen wissenschaftlichen Austausch und Hilfsbereitschaft bedanken.

Außerdem möchte ich allen Kooperationspartner danken, die es mir ermöglicht haben verschiedene Facetten und Themengebiete in der Forschung zu ergründen.

Schlussendlich, bedanke ich mich bei meiner Familie, Geschwister und Freunde für all die Unterstützung und insbesondere meinen Eltern, die es mir ermöglicht haben diesen Weg zu beschreiten und zu vollenden.

Die Dissertation wurde in der Abteilung Analytische BioGeoChemie am Helmholtz Zentrum München - Deutsches Forschungszentrum für Gesundheit und Umwelt – erstellt im Rahmen eines Projektes, welches durch Deutsche Zentrum für Diabetesforschung finanziert wurde.

Summary

The gastrointestinal tract is a complex bio-ecological system, consisting of multitude of microbes. Amongst other, the domain of bacteria accounting for the largest proportion of the gut environment, consisting of around 500 species and trillions of bacterial cells. The gut microbiome is an essential part of the mammalian system, exerting multiple biological and chemical functions. The gut microbiome possess an own genome, being 150 times larger than the genome of the mammalian host. The functional output of the exogenous genome is reflected by a dynamic transcription, translation into proteins and metabolism, which reacts to different factors, associated with the host or environment. Recently, the gut microbiome has been discussed to be involved in health or diseases issues. Substantial different microbiome communities were shown to be associated with diseases, influence host energy, and fat metabolism. A research area that is investigating the role of metabolism is called metabolomics. Metabolomics acts in a global and unbiased nature in order to explore the functional output – here in metabolites – and provide new insights and facilitates to generate new strategies. Our strategy was based on the application of metabolomics based methods, especially by means of ultra-high resolution mass spectrometry, that allows us to investigate multiple questions. The focus of the analyses was to reveal the metabolite spectrum – metabolome –of the gut microflora in the context of metabolic disorders. The particularity of thesis was to investigate the metabolome by analyzing the gastrointestinal content of mice to capture the metabolic complexity of the organ. The so-called meta-metabolome in the gut is a mixture of metabolites derived bacterial and host metabolism but also from food ingredients. We could show that the meta-metabolome is changed in type 2 diabetes and diet induced obesity. In a mouse model of type 2 Diabetes, we could unveil the importance of fatty acid metabolism due to altered beta-oxidation. Additionally, we could reveal that taurine and sulfate conjugates of fatty acids, oxylipins, and bile acids were important in discrimination of meta-metabolome between diabetic and healthy mice. In the study of diet-induced obesity, we could also analyze a certain meta-metabolome signature. Here, we reported the importance of several taurine conjugates of C_{24} and C_{27} bile acids, endocannabinoids, but also several other bacterial metabolites including urobilinoids and lignane catabolites. We successfully showed that metabolomics is a powerful tool in systems biology in order to investigate different aspects of health or diseases related issues.

Zusammenfassung

Der Darm ist ein komplexes bio-ökologisches System, bestehend aus einer Vielfalt von Mikroorganismen. Zu diesen gehören unter anderen Bakterien, die im Darm aus rund 500 Spezies und Billionen von bakteriellen Zellen bestehen und damit den größten Anteil der Darmflora ausmachen. Das Darmmikrobiom ist ein essentielles Mitglied des Säugetiers, welches verschiedene biologische und chemische Funktionen ausübt. Das Darmmikrobiom besitzt ein eigenes Genom, das 150-mal grösser ist, verglichen zum Genom des Wirtes, welches eine dynamische Transkription, Proteinbiosynthese und Stoffwechsel betreibt, als eine Reaktion auf verschiedenste Faktoren, die mit dem Wirt oder der Umwelt assoziiert wird. Seit kurzem, werden das Mikrobiom und dessen Funktion in verschiedensten Krankheiten diskutiert. Es wurde gezeigt, dass die mikrobielle Gemeinschaft sich substanziell unterscheidet und bestimmte bakterielle Gemeinschaften mit Erkrankungen assoziiert werden wie Adipositas und ein Einfluss auf den Energie und Fett Metabolismus des Wirtes ausüben. Ein Forschungsgebiet der sich primär mit dem Metabolismus beschäftigt ist Metabolomics. Metabolomics versucht in einer globalen und unvoreingenommenen Art die Funktion der Metabolite zu erforschen und gegebenenfalls neue Ansätze vorzuzeigen. Unsere Hypothese war, dass uns die Anwendung der Metabolomics basierten Methoden, besonders der ultrahoch auflösenden Massenspektrometrie, uns erlaubt verschiedenste Fragestellungen zu analysieren. Der Fokus diese Fragen lag hier speziell in der Analyse des Metaboliten Spektrums – Metabolom –der Darmflora zu ergründen, mit dem Schwerpunkt auf Stoffwechselerkrankungen. Die Besonderheit der Arbeit lag darin, dass zur Erforschung des Metaboloms, der Inhalt des Mausdarms zur Detektion herangezogen wurde um die metabolische Komplexität zu erfassen. Das sogenannte Meta-metabolom im Darm ist eine Mischung aus Metaboliten, die aus dem Stoffwechsel des Wirtes, der bakteriellen Gemeinschaft und Nahrungsbestandteilen stammt. Wir konnten zeigen, dass das Meta-metabolom in Typ 2 Diabetes aber auch in Diät-induzierten Adipositas verändert ist. Dabei sind verschiedenste Arten von Metaboliten-Klassen verändert gewesen, die den Status reflektiert haben. In dem verwendeten Diabetes Mausmodell scheinen vor allem Fettsäuren eine wichtige Rolle zu spielen, als ein Resultat von veränderter ß-Oxidation. Zusätzlich, konnten wir entdecken, dass Taurin- und Sulfatekonjugate von Fettsäuren, oxidierte Fettsäuren und Gallensäuren einen immensen Beitrag zur Unterscheidung zwischen diabetischen und gesunden Mäusen führen. In der Diät-induzierten Adipositas Studie ausgeführt in zwei verschiedenen Mausmodellen konnten wir auch eine bestimmte Meta-metabolom Signatur aufzeigen. Hier scheinen vor allem taurinkonjugierte C_{24} und C_{27} Gallensäuren, Endocannabinoide, bakterielle Metabolite wie zum Beispiel Urobilinoide und Lignane eine wichtige Rolle zu spielen. Wir konnten erfolgreich zeigen, dass Metabolomics, als ein Teil der Systembiologie eine wichtige Rolle in der Erforschung von zahlreichen Fragestellungen des Stoffwechsels darstellt.

Chapter I

GENERAL INTRODUCTION

Metabolomics to decipher the role of gut microbiome

Considering that gut microbiome consists of five hundreds of species and contains 10 times higher number of bacteria cells than our own (Sommer and Backhed 2013), always remember:

You 'll never walk alone

(Oscar Hammerstein II 1945)

Chapter I

1 General Introduction

1.1 Metabolomics

The Term of "Metabolomics" and the related term "Metabonomics" rose up in the late of 90's (Nicholson, Lindon et al. 1999, Fiehn 2002). This field is now rapidly growing and complementing other "-OMICS" techniques such genomics, transcriptomics and proteomics, accounting to the field of systems biology. Thereby metabolomics reflects the functional output of an organism due to different stimuli, related to health or disease topics, including endogenous, xenobiotic, nutritional or bacterial derived compounds (Nicholson and Wilson 2003). But before all upcoming –Metabol - "OMICS" terms metabolome was used firstly to describe and define parallel to the transcriptome and proteome the functional output of metabolites due to genetic modifications in yeasts (Oliver, Winson et al. 1998). Metabolome is defined as – *a full set of metabolites within, or that can be secreted by a given cell type of tissues* (Nicholson and Wilson 2003) -.

Metabolomics aims the – *comprehensive unbiased analysis of all metabolites in a biological system with their identification and quantification* (Fiehn 2002) -.

Metabonomics is defined as – *the quantitative measurement of the multivariate metabolic responses of multicellular systems to pathophysiological stimuli or genetic modifications* (Nicholson, Lindon et al. 1999, Nicholson and Wilson 2003) –.

Another existing discrimination strategy in the field of metabolomics is the way to look on the metabolite responses: **targeted** or **non-targeted** (untargeted) analyses.

The targeted analysis is also often referred as targeted metabolomics or metabolic profiling and belongs to the bottom-up approach in systems biology. Metabolic profiling is defined as – *the quantification of a pre-defined set of metabolites, metabolite classes or metabolic pathways* (Fiehn 2002) -. In fact, the targeted approach should not be a part of metabolomics, because the limitation to a certain *pre-defined set of metabolites* is de facto contradictory to the original aim in metabolomics to identify and quantify *all* metabolites.

Otherwise, any of the existing analytical techniques used for metabolomics studies are able to measure or to claim to identify and quantify *all* metabolites.

The non-targeted analysis often called non-targeted or untargeted metabolomics is a top-down approach in systems biology used for investigation of metabolites without prior limitations and acts in an unbiased way, thereof evaluating global metabolite responses to biological interventions or diseases (Nicholson, Lindon et al. 1999). This approach allows revealing new metabolite classes or pathways. Metabolic fingerprinting is one of the non-targeted metabolomics approaches that aims – *the classification of samples based on metabolite patterns due to biological questions or interventions without quantification* (Fiehn 2002) -. This term should not be interchanged with the metabonomics term – which aims the quantification of metabolic responses.

The term of meta–metabolomics is an extension of non-targeted metabolomics and aims - *the (semi)-quantitative analysis of metabolite patterns in a complex host - microbiome system (including multiple partners) and identify metabolic networks related to health or disease issues* (Turnbaugh and Gordon 2008) -.

Originally, metabolomics studies aimed to investigate drugs toxicity and evaluate their impact on the subjected metabolism (Robertson, Watkins et al. 2011). Nowadays the field of metabolomics is investigating different topics and issues embedding a wide variety of questions related to health or disease (Holmes, Wilson et al. 2008).

1.2 Technologies in metabolomics

One of the popular and widely used techniques for studying metabolite responses and patterns in the metabolomics field is ^{1}H NMR spectroscopy (proton nuclear magnetic resonance) that were initially used in the field of metabolomics. However, the emerging technique of mass spectrometry (MS) and their hyphenation with different separation techniques provides a second powerful tool in the research of metabolomics. The separation techniques coupled to the MS includes gas chromatography (GC), liquid chromatography (LC) or capillary electrophoresis (CE).

1.2.1 Mass Spectrometry

An MS system is mainly composed of ion generating and mass-analyzing components. It gives us information about the elemental composition of molecules and their structures. It does this in three steps namely ionization of the molecules, mass filtration and mass detection. There is either two ways to do this by using an electric or a magnetic field. In a traditional mass spectrometer, a large electromagnet is to deflect a beam of ions. By changing the current in the coils of the magnet, ions with different charge-to-mass ratio can be stilled through the instrument to record the mass spectrum. With powerful magnet, very high resolution can be achieved which allows us to study low and/or high molecular weight molecules in more complex biogeochemical mixtures.

Accordingly, the existing ionization techniques that can be hyphenated to a mass spectrometer are chemical ionization (CI), electron ionization (EI) or atmospheric pressure ionization including the electrospray ionization (ESI), chemical ionization (APCI) and the photo ionization (APPI). However, ESI is the most commonly used ionization technique that serves as an interface between LC and MS for performing metabolomics studies. There is a broad spectrum of mass analyzers ranging from low to high resolution and resolving power – including ion trap, quadrupole, time of flight, orbitrap and Fourier transform ion cyclotron resonance mass analyzer systems (Forcisi, Moritz et al.). In this thesis work, two types of mass analyzers namely Fourier transform ion cyclotron resonance and time of flight MS systems were used to investigate metabolomics studies.

1.2.1.1 Fourier transform ion cyclotron resonance mass spectrometry (FT-ICR-MS)

Fourier transform ion cyclotron resonance mass spectrometry (FT-ICR-MS) is well known by its high resolution and mass accuracy (Marshall, Hendrickson et al. 1998). A mass resolving power from 45.000 to 600.000 can be reached in full scan mode in a mass range of 0.4 Da at m/z 411 with a mass error ≤ 100ppb (Schmitt-Kopplin, Gelencsér et al. 2010). Such advantages allow concrete molecular formula assignment of the detected mass signals and therefore better molecular and elemental classification of studied mixture samples of complex samples but also biological matrices and makes this instrument suitable for metabolomics studies (Brown, Kruppa et al. 2005, Schmitt-Kopplin, Gabelica et al. 2010, Tziotis, Hertkorn et al. 2011, Daniel, Gholami et al. 2013). Ionizable organic compounds can be resolved without prior chromatographic separations. Here, a 12 Tesla solariX™ (Bruker Daltonics, Bremen, Germany) mass spectrometer, equipped with an Apollo II ESI source were used for the acquirement of the FT-ICR mass spectra and subsequent molecular formula assignment. A schematic description of the FT-ICR-MS instrument is shown in Figure 1-1.

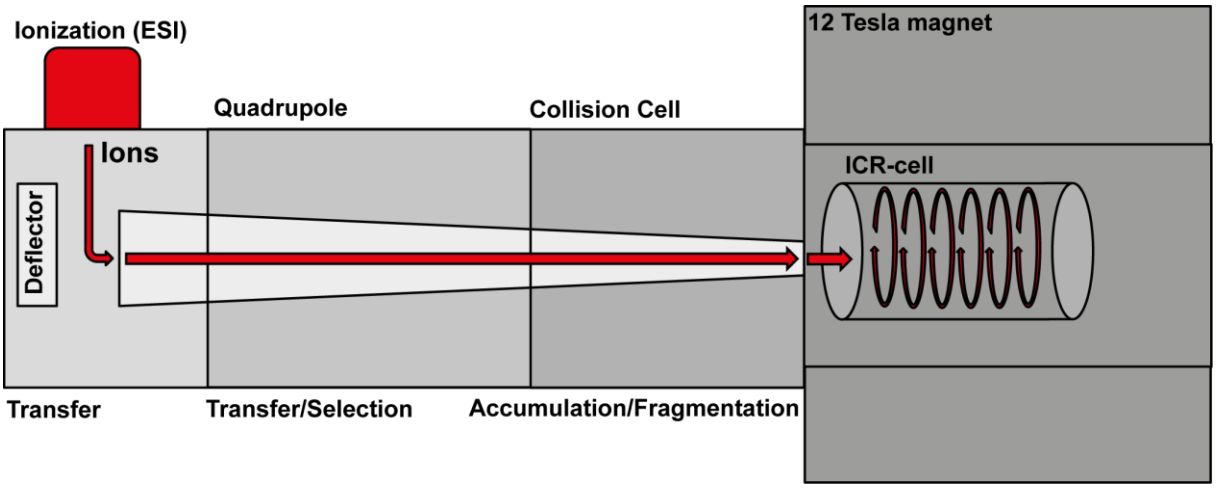

Figure 1-1 Schematic overview of FT-ICR-MS instrument (adapted from solariX™ user manual revision 1, Bruker Daltonics GmbH)

An FT-ICR-MS is assembled of three essential parts, the ionization source, the ion optics and the ICR cell, surrounded by a superconducting cryomagnet (Figure 1-1). The ions are generated by ESI source and forwarded into the FT-ICR-MS instrument under atmospheric pressure (~3 mbar). A deflector guides the ions and forward to ion funnels, passing an octapole unit, where the ions are transferred and focused. The formed ions packages were defined by using a mass selector - here, a quadrupole - (quadrupole in Figure 1-1).

Afterwards, the ions are guided to a multipole that could be coevally used for mass fragmentation experiments or full scan MS acquisitions (collision cell in Figure 1-1). In MS experiments, the ions are accumulated in a pre-selected time in the multipole unit and forwarded to the ICR-cell – the actual mass analyzer-. Before attainment the ICR-cell, several turbo pumps were turned on to adjust the overall pressure of the FT-ICR-MS instrument, which also ascertain the resolving power of the MS instrument (Gross 2011). Accordingly, the key part of all FT-ICR-MS instruments is the ICR-cell, where trapping, excitation and detection of the produced ions are conducted. An ICR-cell is essentially composed of several compartments, consisting of front and back plates liable to the trapping of ions. Moreover, the device of any ICR-cell is consisting of two principal parts namely excitation and detection plates. Thus, the ions trapped in the ICR cell are subjected to a spatial uniform magnetic field - here, 12 Tesla - that forces the ions to move circularly in the ICR-cell following an *ion cyclotron motion* (Marshall, Hendrickson et al. 1998). The radius of ions moving circularly in the ICR-cell is dependent on the mass, its charge and the applied magnetic field. Still, this circular movement is not enough and not applicable to detect the ions (Marshall, Hendrickson et al. 1998, Gross 2011). Additionally, the excitation units of ICR-cell plates apply an electric field and force ions to increase their moving radius with a spiral like movement (Gross 2011). This happens through setting a transverse electric field that excites the ions mass-selectively, resulting that ions reaching their resonance will move to a higher orbit and can be detected. The radius of ions in the higher orbit remains stable during the detection. The frequency is dependent on size of the excited ions. The detector units are measuring induced images currents that evolve through the circulating ions that exceed the detector plates. Then, so called *free induction decay* derived due the cyclotron motion is translated and calculated by a Fourier transformation into a mass signal (Marshall, Hendrickson et al. 1998, Gross 2011). The principle of ion cyclotron resonance ICR is extensively reported by several authors over the past two decades (Marshall and Grosshans 1991, Marshall, Hendrickson et al. 1998, Marshall 2000, Heeren, Kleinnijenhuis et al. 2004).

1.2.1.2 Time of flight mass spectrometry (TOF-MS)

The second mass analyzer performs with time of flight (TOF) principle (Scheme in Figure 1-2), here the maXis™ MS (Bruker Daltonics GmbH). The separation of the generated ions is due to the time of flight ions need, which is given by their size – bigger ions need longer time to travel comparing to smaller ions -. The ions generated by ESI, are passing different stages in the orthogonal TOF-MS system. The first part after ionization performed by ESI is the

stage part where ions are transferred by ion funnels, focusing the generated ions by a multipole and reducing the pressure from ambient environment to $3x10^{-4}$ mbar by turbo pumps. The transfer and focus part is followed by a quadrupole mass analyzer and cooling cell (Figure 1-2; 1 and 2). Whereas the collision cell part is serving as a mass filter prior fragmentation experiments (MS/MS) or further focusing in a full scan rate MS experiments. The collision/cooling cell can be used in MS experiments for further transfer and focusing by decreasing pressure. In MS/MS experiments with collision-induced dissociation (CID) with nitrogen and afterwards the cooling cell rebalance, the increased pressure resulted due to CID experiments. The last part the TOF-MS - the actual mass analyzer - is shown in Figure 1-2, consisting of accelerator, reflector and detector units, with a pressure of $1x10^{-7}$ mbar. The accelerator part is responsible for pushing the incoming ions orthogonally to the reflector, where also the determination of the mass value is taking part due to flying path time from accelerator to detector (drift time, grey arrow). The reflector compensates different kinetic energies from ions with the same mass and correct thereby the time of flight and increases the resolving power (Gross 2011). Finally, the detector converts the ion signals into electrical signals, which is transferred to a digitizer.

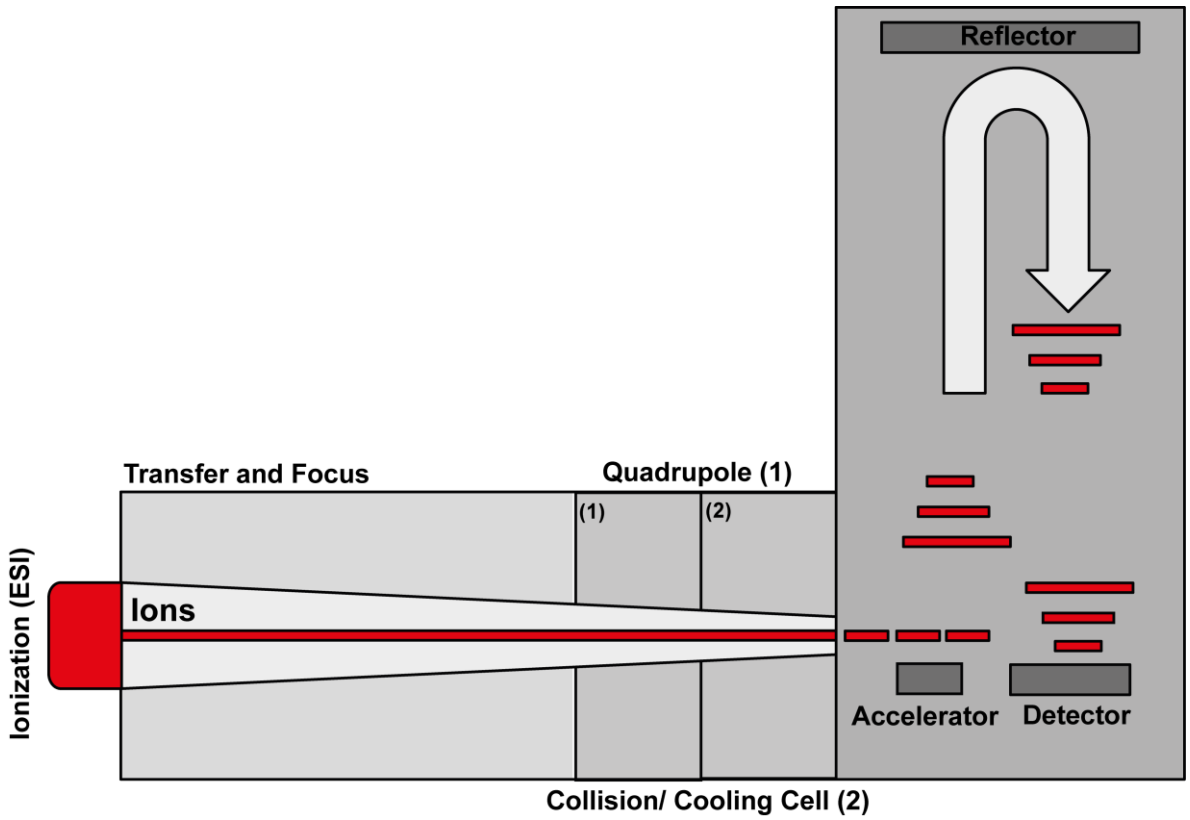

Figure 1-2 Scheme of orthogonal TOF-MS (adapted from maXis™ user manual version 1.1, Bruker Daltonics GmbH)

1.3 Gut microbiome

The intestine of a mammalian system is a complex mixture of trillions of bacteria consisting of around hundreds of different species. The microbiome is the - *sum of the microbial genomes and their environmental interactions* (Turnbaugh and Gordon 2008) – here with the focus on the intestinal ecosystem. The intestinal ecosystem is a term that is defined as a - *complex biological system comprising interrelated factors which counteract in an equal and contrary degree in such a way as to maintain or re-establish equilibrium* (Zoppi 1997) -. The intestinal microbiome such as of humans consists of 100 trillions of bacteria; each individual harbors at least 150 bacterial species and the pan-genome is 150 times larger than the human genome (Medini, Donati et al. 2005, Qin, Li et al. 2010). Gut microbiome exerts strong influences on host functions either in positive or negative manner. The gut microbiome can be regarded as a metabolic active organ within the host, providing compounds serving as an additional energy source (Bergman 1990), maintaining the intestine function (Hooper and Gordon 2001), regulating the host immune system (Kau, Ahern et al. 2011), but is also involved in diseases (Bäckhed, Ding et al. 2004). Recent development of gut microbiome analyses such as culture - independent 16S ribosomal DNA sequencing or 454 pyrosequencing facilitates the research of the gut microbial communities and their functions. Bäckhed *et al.* revealed the importance of *the* gut microbiome and its function in obesity and insulin resistance (Bäckhed, Ding et al. 2004). Colonization of germfree mice resulted in substantial regulation of the host energy metabolism and fat storage. Turnbaugh *et al.* could highlight also the metabolism of gut microbiome, comparing short chain fatty acids (SCFAs) between obese and their lean controls, implying the important role of small metabolites (Ley, Bäckhed et al. 2005, Turnbaugh, Ley et al. 2006). SCFAs are one group of metabolites exhibiting many important biological functions such as an energy source for colonic cells (Bergman 1990). As a consequence of the pioneer studies of Bäckhed *et al.* and Turnbaugh *et al.* the role of gut microbiome has been questioned and implicated in the pathogenesis of nutritional diseases such as obesity (Ley, Bäckhed et al. 2005), endocrine disturbances such as insulin resistance or type 2 diabetes (Larsen, Vogensen et al. 2010, Geurts, Lazarevic et al. 2011). Also, distinct gut microbiome communities were reported in atherosclerosis (Koren, Spor et al. 2011), nonalcoholic fatty liver disease (Henao-Mejia, Elinav et al. 2012), inflammatory bowel diseases (IBD) (Manichanh, Rigottier-Gois et al. 2006, Willing, Dicksved et al. 2010), colorectal cancer (Scanlan, Shanahan et al. 2008, Castellarin, Warren et al. 2012), allergy (Abrahamsson, Jakobsson et al. 2012), irritable bowel syndrome (Rajilić–

Stojanović, Biagi et al. 2011), celiac disease (Di Cagno, De Angelis et al. 2011), liver diseases (Henao-Mejia, Elinav et al. 2012), kidney disorders (Vaziri, Wong et al. 2013) and infections (Lupp, Robertson et al. 2007). The implication of gut microbiome was also discussed for neurodegenerative disorders such as multiple sclerosis (Berer, Mues et al. 2011). In summary, gut microbial community changes were reported in a diversity of diseases we have to be aware and re-think about the cause or the consequence of different microbiome communities (Johnson and Olefsky 2013). Gut microbiome is highly variable between (inter-individual) species, influenced and shaped by diet (Hildebrandt, Hoffmann et al. 2009), antibiotics (Pérez-Cobas, Gosalbes et al. 2012), probiotics (Dinoto, Suksomcheep et al. 2006) and prebiotics (Pan, Chen et al. 2009) but also age (Mariat, Firmesse et al. 2009). The habitants of the intestine are called commensals and the main domain is the bacteria (Hooper and Gordon 2001). Mammals are dominated by two main phyla of bacteria, consisting of *Bacteriodetes* and *Firmicutes*, whereas the *Bacteriodetes* are mainly associated with healthy status and *Firmicutes* are more related to the disease state. This is often referred by observing the ratio between these main phyla but it has to be mentioned that also inconsistent results were reported such as for Duncan *et al.* no changes of this ratio were observed in obesity (Duncan, Lobley et al. 2008). Recently, the so-called enterotypes consisting of three genera: *Bacteroides*, *Prevotella* and *Ruminococcus* were reported in humans and accompanied by different functionalities, evaluated by metagenome analyses (Arumugam, Raes et al. 2011). In rodent studies two distinct enterotypes were reported by Hildebrand *et al.* by observing commonly used laboratory mice strains, they showed different microbial communities at phylum and genera level (Hildebrand, Nguyen et al. 2013, Krych, Hansen et al. 2013). In rodent studies several other factors amongst host genotypes were discussed to contribute and shape the microbial community including strong caging effects, maternal transmission, inter-individual variance, antibiotics and diet (Arthur, Perez-Chanona et al. 2012, Ubeda, Lipuma et al. 2012, Hildebrand, Nguyen et al. 2013).

1.3.1 Application of metabolomics to study the impact of gut microbiome

The complexity given in the intestine of a mammalian and thereof of the circulating metabolome in the intestine is shown in Figure 1-3. In the intestine different systems are able to perform metabolism and produce metabolites (M). In the gut lumen the metabolome is a complex mixture of metabolites derived from bacteria (~500 species) (Sommer and Backhed 2013), food derived compounds, metabolites circulating from gut to the host and vice versa – the so called entero-hepatic system - metabolites coming from the gut epithelium, which consists also of different types of cells (here exemplary enterocytes and M-cells). Thereby, the above mentioned and defined meta-metabolome, which is given in this complex environment can influence the gut microbiome community and vice versa. Interactions of different species may enhance or suppress the abundance of others (Samuel and Gordon 2006).

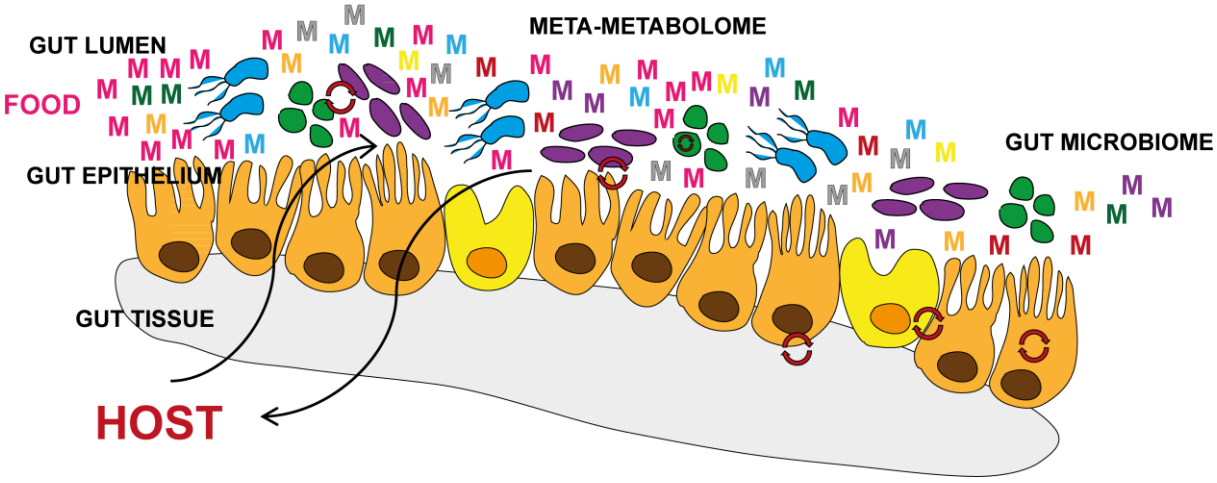

Figure 1-3 A complex environment in the intestine and their meta-metabolome, consisting of circulating metabolites (M) originating from food, host and bacteria

The discrimination of host or gut microbial derived metabolites is truly one of the topics concerned in metabolomics, hence the given complexity in organisms such as mice, rats or humans, consisting of the host itself and their microbiome, here with the focus on the intestinal tract. Therefore, impact of gut microbiome on metabolism was studied primarily by using germfree mice and mice treated with antibiotic drugs. There are several original studies and reviews about host microbial co-metabolism and which metabolites are categorized in this area. Before inventing and calling it metabolomics, several studies were performed to study the impact of gut microbiome in drug metabolism (Bakke, Gustafsson et al. 1980) but also

endogenous metabolites such as bilirubin (Gustafsson and Lanke 1960) or phenolic compounds (Goodwin, Ruthven et al. 1994) or tyrosine (Curtius, Mettler et al. 1976) or isoflavones and lignans (Bowey, Adlercreutz et al. 2003) were investigated. The first global metabolomics approach to study the interaction between host and gut microbiota - after calling it metabolomics - was performed using ^{1}H NMR techniques happened 2002 by Williams *et al.* (Williams, Eyton-Jones et al. 2002) with antibiotic treated rats (1) and followed by Nicholls *et al.* using urine from germfree (GF) rats (2) (Nicholls, Mortishire-Smith et al. 2003). [Both studied the impact of gut microbiota on metabolites by ^{1}H NMR either using antibiotics or germ free animal study design [(1) times cited ISI Web of Science®: 55 or (2) cited ISI Web of Science®: 100 (date 6/12/2013)]. Thus, to study the impact of gut microbiome and their metabolism the application of GF rodents, following their acclimatization or comparing to their conventional controls is truly very helpful to understand the evolving host microbial interactions (Goodwin, Ruthven et al. 1994, Nicholls, Mortishire-Smith et al. 2003, Claus, Tsang et al. 2008). Moreover, going further the colonization of GF mice with one single species provides specifically the functional role of the colonized species and the impact on the host - microbial interactions (Martin, Wang et al. 2007, Marcobal, Kashyap et al. 2013). There are plenty of metabolomics studies given that approached to investigate the impact of gut microbiome either using GF or antibiotic treated mice (Claus, Tsang et al. 2008, Martin, Wang et al. 2009, Wikoff, Anfora et al. 2009, Velagapudi, Hezaveh et al. 2010, Antunes, Han et al. 2011, Chuang, Huang et al. 2012, Lee, An et al. 2012, Matsumoto, Kibe et al. 2012, Marcobal, Kashyap et al. 2013, Sun, Schnackenberg et al. 2013, Zhao, Wu et al. 2013). But using the germfree design needs to be considered carefully because there are a lot of factors differ between GF and "normal" mice, which is not only absence of the gut microbiome (Wostmann 1981).

1.3.2 Gut microbial metabolites

BRIEFLY, changes of gut microbial metabolism are observed and associated with several metabolite classes concerning SCFAs such as butyrate acetate, propionate, methylamines (Al-Waiz, Mikov et al. 1992, Dumas, Barton et al. 2006), phenolic metabolites (Goodwin, Ruthven et al. 1994) such as hippurate following by bile acids (BAs) ("re-promoted" and focused by Nicholson et al. 2003 (Nicholson and Wilson 2003) and other gut microbial metabolites, summarized comprehensively by Nicholson *et al.* (Holmes, Li et al. 2011, Nicholson, Holmes et al. 2012). In detail, gut microbial metabolites are phenylacetylglycine (PAG), trimethylamine-N-oxide (TMAO), 3-hydroxypropionic acid (3-HPP),

4-hydroxypropionic acid (4-HPP), trimethylamine (Goodwin, Ruthven et al. 1994), hippurate, m-hydroxyphenylpropionic acid (m-HPPA) (Williams, Eyton-Jones et al. 2002), which was confirmed by Claus and Tsang *et al.* (Claus, Tsang et al. 2008), showing decreased levels of hippurate, PAG, 4-HPP and 3-hydroxycinnamic acid (3-HCA). Later on, confirmed through GF studies BAs especially deoxycholic acid, lithocholic, hyodeoxycholic and ω-muricholic acid were discussed as co-metabolites derived from gut microbiome (Nicholson and Wilson 2003, Nicholson, Holmes et al. 2005). Not only unconjugated BAs were associated with gut microbiome abundance but also taurine and glycine conjugated BAs appeared to be important comparing GF and conventional rodents (Claus, Tsang et al. 2008, Swann, Want et al. 2011). The deconjugation of BAs through bacteria results in their recirculation in the entero-hepatic system, affects thereof the host metabolism hence bile acids are known to exhibit many biological functions in the host, affecting energy metabolism through receptor dependent actions (Watanabe, Houten et al. 2006). The action of BAs was performed through TGR5 dependent signaling and brown adipose tissue is a key organ where BA signaling occurred (Watanabe, Houten et al. 2006). BAs were not only implicated into regulating host physiology but were also observed to be influenced but also to influence the microbial communities (Islam, Fukiya et al. 2011). Further performed GF studies confirmed but also provide a greater overview and insight in host microbial metabolome impact (Wikoff, Anfora et al. 2009, Velagapudi, Hezaveh et al. 2010). Recently, endocannabinoids (such as 2-arachidonoylglycerol: (2-AG) or arachidonoylethanolamine (AEA) were reported to play an important role as the endocannabinoid system. The endocannabinoid tone was shown to be by the gut microbiome, showing a linkage between the intestinal tract, gut microbiome and the brain axis (Muccioli, Naslain et al. 2010, Velagapudi, Hezaveh et al. 2010).

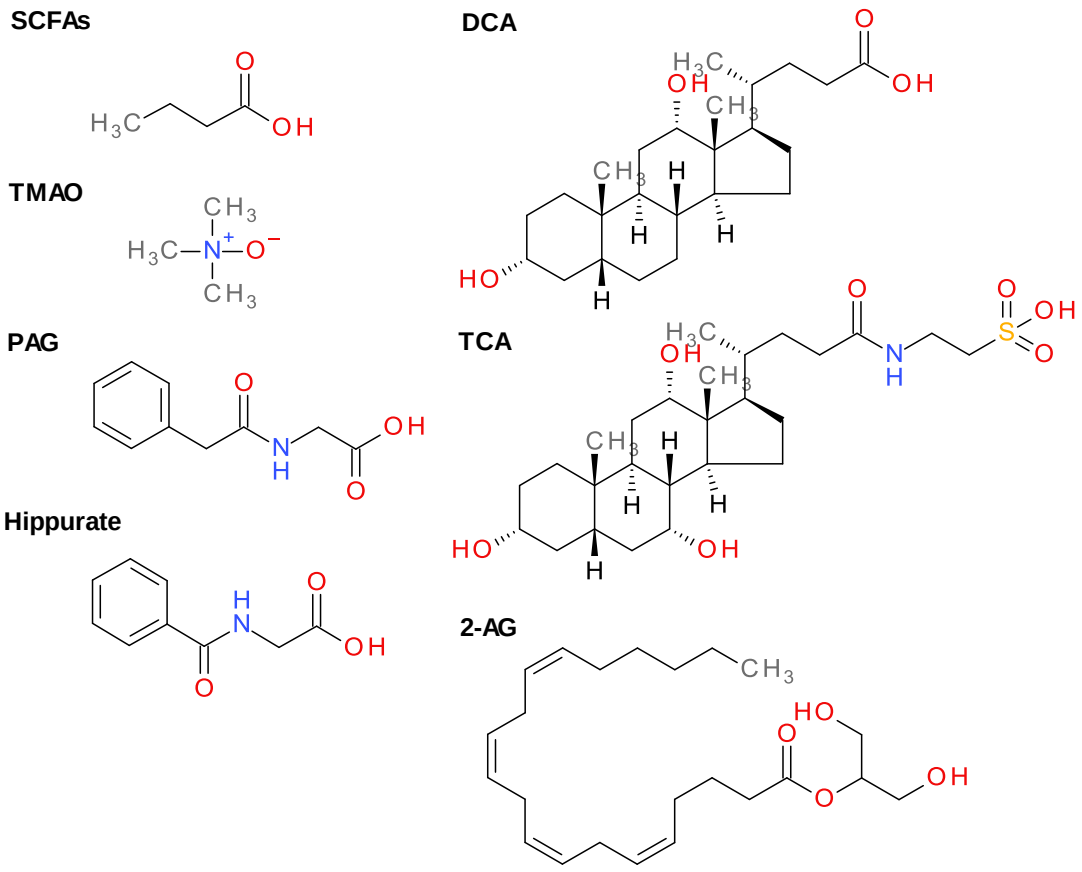

Figure 1-4 Examples of co-microbial metabolites: SCFAs = short chain fatty acids, DCA = deoxycholic acid, TMAO = trimethylamine-N-oxide, PAG = phenylacetylglycine, TCA = taurocholic acid, hippurate and 2-AG = 2-arachidonoylglycerol

1.3.2.1 The prediction of KEGG meta - metabolome

To enlarge the existing knowledge about co-microbial metabolites in the literature we were using a powerful method by accessing information given in databases. In order to illustrate the complexity of the meta-metabolome we used exemplary the Kyoto Encyclopedia of Genes and Genomes (KEGG) database, which possesses complete genomes of 192 eukaryotes, 2451 bacteria and 160 archae (date: 8/28/2013) and contains a large library of metabolites (KEGG compound database) linked with the genome information and thereof with the species. Here, we examine the host – microbial metabolome by including the host – *Mus musculus* (MMU) – as the main study object of this thesis and nine representatives of the bacterial kingdom. Two main divisions are present in mammalian system including *Bacteriodetes* and *Firmicutes: Bacteriodetes vulgatus* (BVU), *Eubacterium rectale* (ERE), *Akkermansia muciniphila* (AMU), *Bacteroides fragilis* YCH46 (BFR), *Bacillus subtilis subsp. subtilis* 6051-HGW

(BSH), *Bacteroides thetaiotaomicron* (BTH), *Clostridium acetobutylicum* (CAC), *Escherichia coli* K-12 MG1655 (ECO) and *Faecalibacterium prausnitzii* L2-6 (FPR). Based on this we could build a pseudo - "phylogenic" dendrogram with the KEGG metabolome, shown in Figure 1-5 consisting of 2236 metabolites. Solely the presence or absence of metabolites of chosen species drives the similarity or dissimilarity between the species.

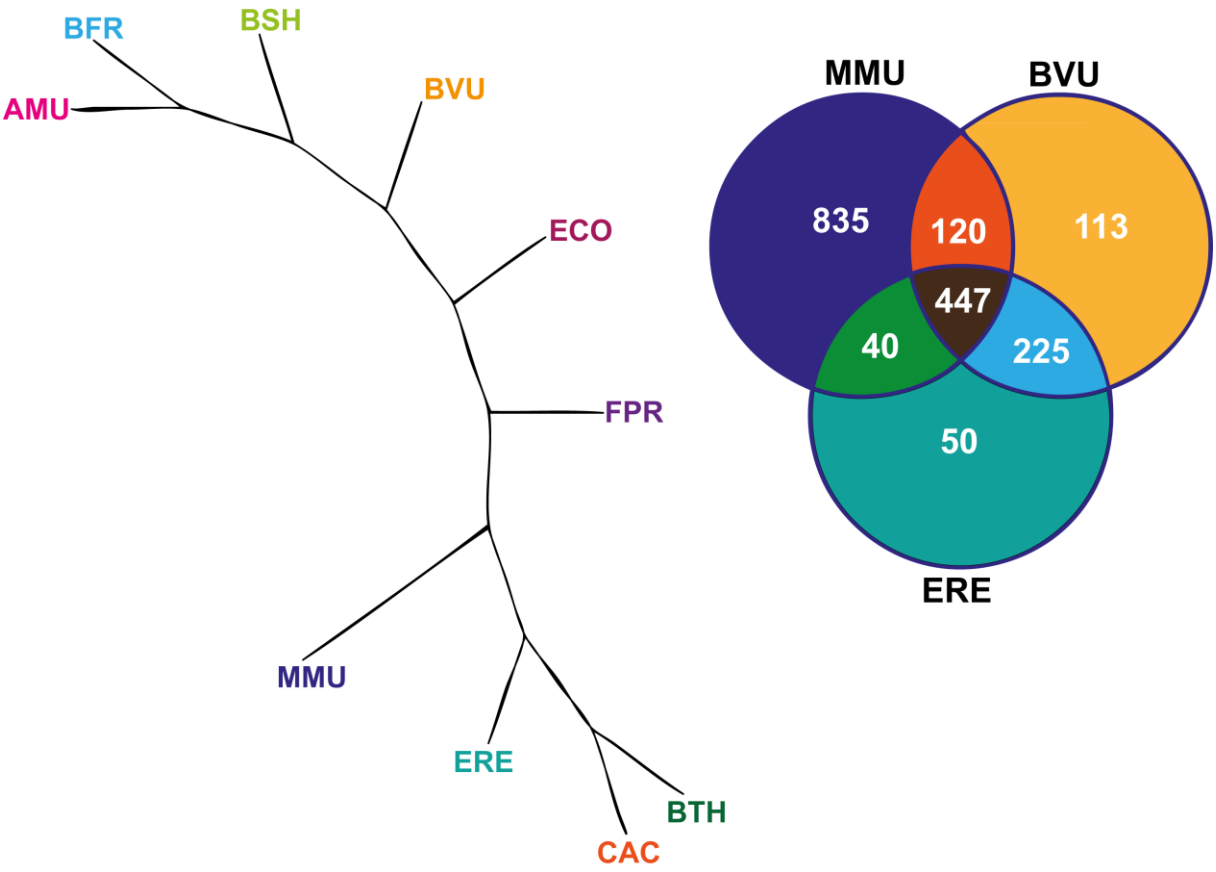

Figure 1-5 "Phylogenic" dendrogram reconstructed from the KEGG meta-metabolome, including one mammalian and nine different bacterial species, clustered due to their metabolome similarities derived from KEGG database; Venn diagram: comparison of three metabolomes of *Mus musculus* (MMU), *Bacteriodetes vulgatus* (BVU) and *Eubacterium rectale* (ERE)

Additionally, we compared their metabolomes of MMU, BVU and ERE and we could observe common but also unique metabolites, shown in a Venn diagram (Figure 1-5). Moreover, we mapped all common metabolites of the ten species into metabolic pathways of KEGG, shown in Figure 1-6, showing the diversity of meta-metabolome involved in different metabolic pathways with different metabolite classes (Figure 1-6).

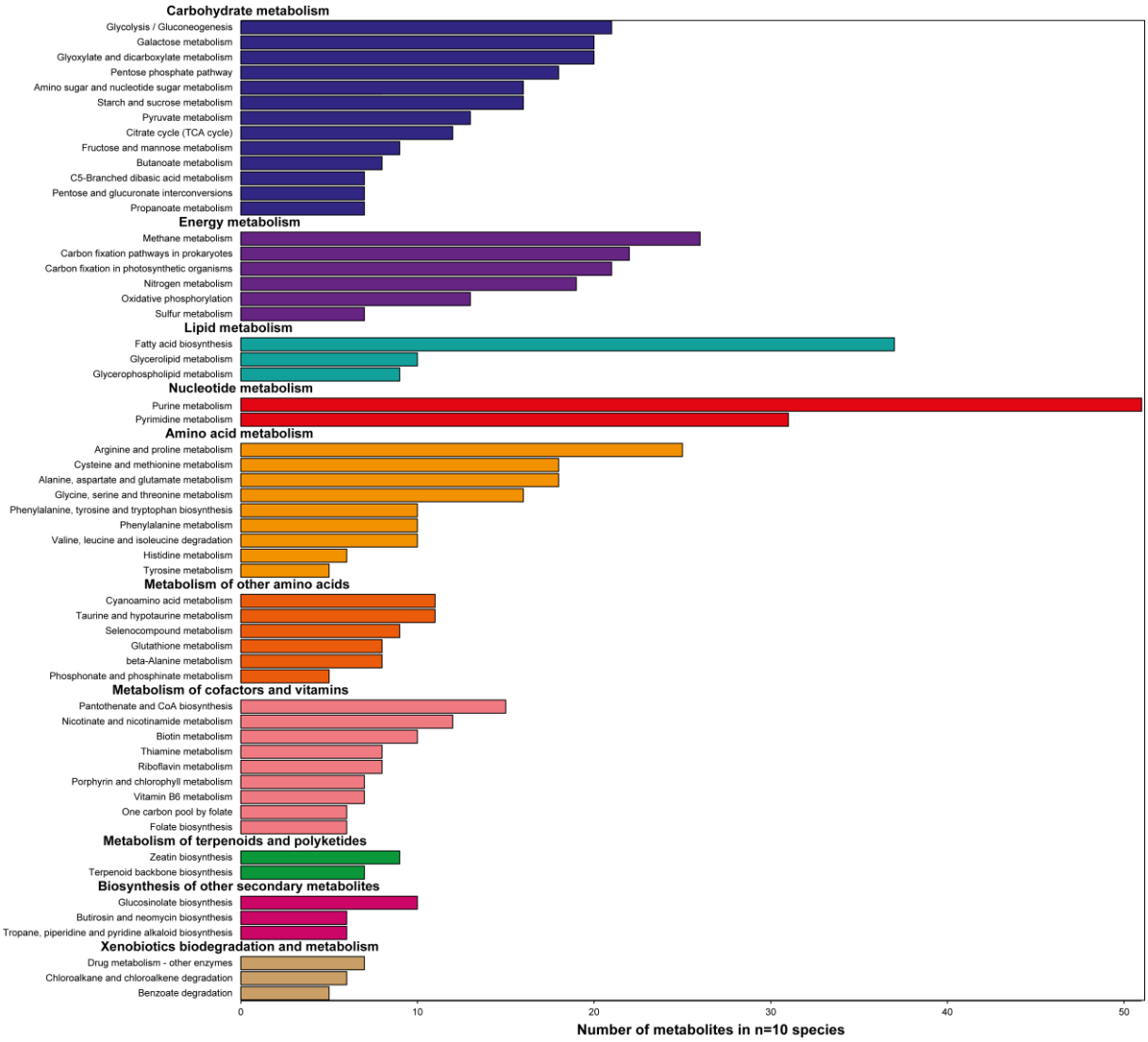

Figure 1-6 KEGG metabolic pathways representing the common meta-metabolome of 10 different species including mammalian organism and bacteria

Thus, the KEGG database provides a powerful tool in order to obtain information about host and microbial metabolome compared to the extensive literature mining. Nevertheless, we need to be aware of the incompleteness of databases. For example the citrate cycle (TCA) is incomplete including KEGG but also other common used databases (Stobbe, Houten et al. 2012). An example of a bacterial metabolite is enterolactone that is derived through bacterial conversion of dietary lignans. Searching the KEGG database this metabolite is not linked to taxonomic, genomic or enzyme information (KEGG compound ID: C18165). Another example is conversion from D-urobilinogen (KEGG compound ID: C05791) to D-urobilin (KEGG compound ID: C05795) which is also discussed to be of bacterial nature especially of *Clostridum* genus (Vítek, Zelenka et al. 2005). The conversion of D-urobilinogen to D-urobilin is not accompanied with any enzyme information and thus no taxonomic information

is given in the KEGG database. A careful usage of literature mining and database knowledge should be applied in order to emphasize host and gut microbial meta-metabolome.

1.3.3 Co - microbial metabolism in diseases

LATER ON, using the information about co - microbial metabolites the patterns of metabolites was investigated particularly related to different diseases; hence the gut microbiome appears to play an important issue in several diseases (Sekirov, Russell et al. 2010). Overall, association of known host-gut microbial derived metabolites in different diseases, observing "the usual suspects" of co-metabolites. First, metabolomics studies of IBDs including Crohn's disease and ulcerative colitis were performed primarily without observing specific co-metabolites but then shifting over to include both host and microbial metabolism (Marchesi, Holmes et al. 2007). The reason for performing gut microbial metabolomics in IBDs is that these diseases are mainly influencing the intestinal tract and their ecosystem. Thereby, the etiology of IBDs is likely driven through a dysbiosis - *an imbalance between commensal and harmful bacteria* (Zoppi 1997) -. Different co-metabolites were observed in IBDs including, small polar metabolites such SCFAs, several methylamines, bile acids, hippurate, 4-cresol sulfate, indoxylsulfate and TMAO (Marchesi, Holmes et al. 2007, Murdoch, Fu et al. 2008, Jansson, Willing et al. 2009, Martin, Rezzi et al. 2009, Williams, Cox et al. 2009, Lin, Helsby et al. 2011). Amongst IBDs, there are several other diseases impacting the health status of the gastrointestinal tract, affecting miscellaneous parts of the intestine (International Statistical Classification of Diseases and Related Health Problems 10^{th} Revision of World Health Organization (WHO 2010)). Taking the ICD-10 classification of digestive system disorders, we could find several metabolomics studies performing the investigation of metabolites in gastrointestinal disorders. Another gastrointestinal disorder named the irritable bowel disease was also associated with distinct microbiome structures and metabolomes, including co-microbial metabolites such as HPPA, hydroxycinnamic acid, tryptamine and putrescine. Among those, putrescine alone is linked to bacterial protein degradation (Li, Ashrafian et al. 2011, Ponnusamy, Choi et al. 2011). A disease of the upper part of digestive system called Barrett's esophagus that can influence the incidence of esophageal cancer were studied in human objects by means of ^{1}H-NMR metabolomics approach resulting in co-microbial metabolites such as acetate, formate, dimethylamine, TMAO, indoxylsulfate (Davis, Schiller et al. 2012). Gastric ulcer in experimental rodent studies were also investigated showing the involvement of co-microbial metabolism including hippurate, dimethylamine and acetate

(Um, Park et al. 2012). Constipation was also linked to metabolome changes but none of them was related to co-microbial metabolites (Rodriguez, Roberts et al. 2013). Celiac disease is an autoimmune disorder, which manifests in hypersensitivity against gluten derived from diet. Moreover, applied metabolomics studies showed co-microbial metabolites such as m-HPPA, indoxylsulfate and PAG (Bertini, Calabrò et al. 2008). A further disorder of the gastrointestinal tract, classified by ICD-10 into neoplasm is cancer that can affect all parts of the tract. Here, metabolomics studies were performed studying esophageal, gastric and colorectal studies (Ikeda, Nishiumi et al. 2012). Concerning the esophageal cancer none of the given metabolomics studies could show co-microbial metabolites (Wu, Xue et al. 2009, Ikeda, Nishiumi et al. 2012, Zhang, Xu et al. 2013). However, one study applying 1H-NMR metabolomics could show several co-microbial metabolites involved in the esophageal cancer discrimination including 4-HPPA, SCFAs, hippurate, acetate, formate, trimethylamine and dimethylamine (Wu, Xue et al. 2009). In a xenograft mouse model of human gastric cancer a research group could report the involvement of TMAO, hippurate, 3-indoxylsulfate and trimethylamine (Kim, Yang et al. 2012). Colorectal cancer was also associated with co-microbial metabolites including p-cresol, hydroxyhippurate, phenylacetate, phenylacetylglutamine, p-hydroxyphenylacetate, tryptamine, putrescine, hippurate and m-HPPA amongst several other metabolites (Qiu, Cai et al. 2010).

The question of the link between bacterial metabolism and non-intestinal diseases associations such as of obesity or type 2 diabetes (Williams, Lenz et al. 2005) or fatty liver diseases (Dumas, Barton et al. 2006) was investigated since different microbial communities were shown for colonized GF mice or *ob/ob* mice (Bäckhed, Ding et al. 2004). Co-microbial metabolites such as methyl, dimethyl-, trimethylamine, p-cresol, m-HPPA, m-HPPA sulfate, phenylsulfate and hippurate were found in rodent models of T2DM including *db/db* mice or *fa/fa* rats (Williams, Lenz et al. 2005, Waldram, Holmes et al. 2009, Connor, Hansen et al. 2010). Atherosclerosis was shown to be promoted by TMAO (Wang, Klipfell et al. 2011). Nonalcoholic fatty liver disease was associated with different co-microbial signatures including several methylamines, TMAO but also bile acids such as glycocholate, taurocholate and glycochenodeoxycholate (Dumas, Barton et al. 2006, Kalhan, Guo et al. 2011). Co-microbial metabolites were also reported in parasitic infections (Wang, Holmes et al. 2004). Microbial metabolism was also observed in drug-toxicity studies applying ^{1}H-NMR techniques (Connor, Wu et al. 2004, Ohta, Masutomi et al. 2009). As mentioned above, distinct gut microbiome community was shown for a plenty of disorders, which is likely concordantly followed by different microbial metabolites. Systemic responses to altered gut

microbiome are reflected in host metabolome and as mentioned above different metabolites can be associated with an altered gut microbiome community and measured in plasma but also urine samples. Biological matrices used as readouts of metabolite patterns of gut microbial impact were dominated through plasma and urine analyses. A small number of metabolomics studies were performed by using the intestinal matrices. Maybe the reason of this is that plasma/serum or urine samples are established matrices and well known for usage in clinical practice and they are fluids and easy to handle, compared to fecal samples. Applying an ISI Web of Science® search containing metabolomics (metabolom*; date of search 9/12/2013) and 19 different terms used in gastrointestinal and gut microbial research, shown in Figure 1-7. The number of found original publications was not greater than 200 whereas about 177 articles were found for gut and metabolom*, followed intestine or intestinal and colon or colonic term in conjunction with metabolom*. There are around 98 articles combining the research of gut microbiota and metabolomics (Figure 1-7).

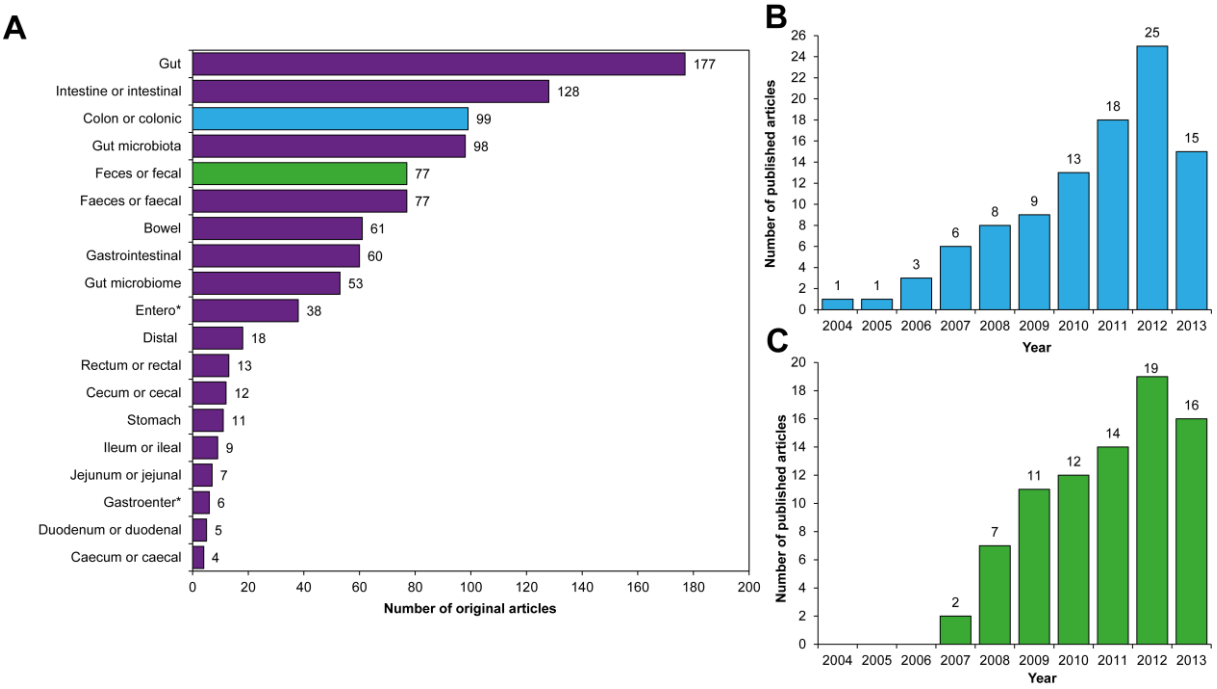

Figure 1-7 A Number of original articles found within the ISI Web of Science® search containing metabolom* and several terms of gastrointestinal research area; B: Number of published articles in year (2004-2013/9/12/2013) for metabolom* and colon or colonic search term; C: B: Number of published articles in year (2004-2013/9/12/2013) for metabolom* and feces or fecal search term

Looking in the detail, the rise of interest studying metabolomics with colon or colonic terms started at 2004 (Figure 1-7, B) with the major interest in colon cancer as reflected in most

cited paper in this publication of Hirayama *et al.* investigating metabolites in stomach and colon cancer (Hirayama, Kami et al. 2009). Fecal metabolomics has his beginnings in the year of 2007 (Figure 1-7, C). Here, the most cited publication did investigate the role of metabolome in Crohn's disease by applying a MS based metabolomics approach in fecal water extracts (Jansson, Willing et al. 2009).

1.4 Main Objectives

The thesis is arranged into three main chapters including two chapters related to health or diseases issues and we questioned the role of gut meta-metabolome in Type 2 Diabetes and obesity. Type 2 Diabetes was studied in a genetic driven mouse model, which bears a mutation in the leptin receptor. Gut meta-metabolome was also examined in obesity whereas two different C57BL/6 mouse strains were taken. Strain susceptibility and the development of obesity were studied by feeding three different diets. In both studies, we were curious whether the gut meta-metabolome is associated with the phenotype and which metabolites are reflected and changed especially in the gut microbiome environment. Hence, different sequence based gut microbiome and metagenome studies already showed the important role of bacteria we want to elaborate the functional output, here in metabolites and metabolism of host and bacteria. Particularly, to investigate the gut meta-metabolome the content of gastrointestinal organs of mice was collected and analyzed. Intestinal samples provide a complex matrices consisting of a mixture of host cells, bacteria, food and their metabolites as shown in Figure 1-3, assembling a host-microbiome environment. To unveil the impact of meta-metabolome different analytical and statistical tools commonly applied in metabolomics were taken to evaluate and elaborate the gut microbial metabolome. Moreover, in this thesis all metabolomics studies were performed with MS based techniques.

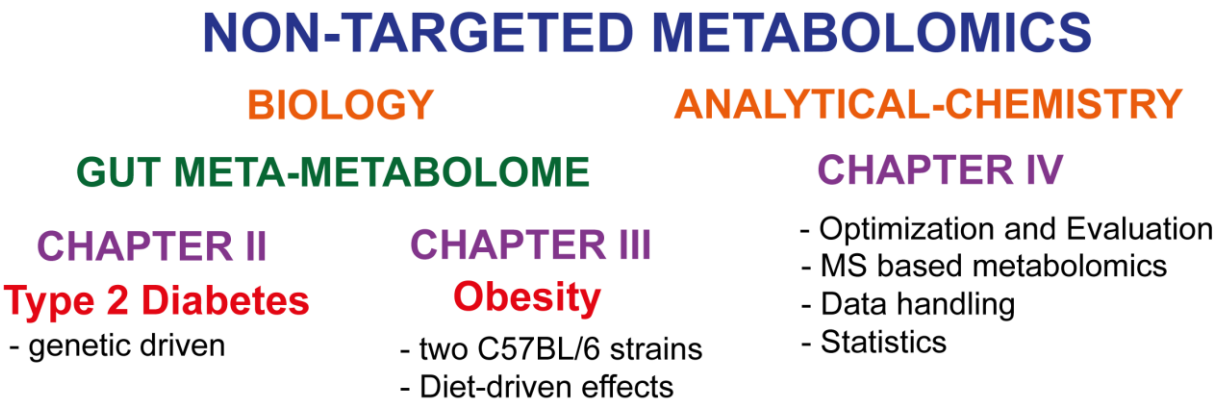

Figure 1-8 Overview of the thesis: this work is divided into a biological and analytical chemistry related topics. Chapter II and III outlined the role of gut meta-metabolome in a type 2 Diabetes and obesity. The research of Diabetes was performed in a genetic – driven mouse model. Additionally, anti-diabetic treatments applying metformin or sglt-2 inhibitor were conducted. The linkage between obesity and its association with gut meta-metabolome was questioned by using two different C57BL/6 strains and their susceptibility to three different diets. More important, before handling metabolomics studies the analytical and chemical tools need to be optimized and evaluated. In chapter IV sample collection, metabolite extraction, the analysis of metabolites by means of MS was conducted. MS based metabolomics resulted in multivariate data which was undertaken through an appropriate data handling and statistical analysis in order to interpret the data and link the elaborated metabolites into a biological context of health or disease.

Chapter II

META-METABOLOMICS IN TYPE 2 DIABETES

OVERVIEW

ABSTRACT

Investigation of type 2 Diabetes (T2DM) by applying a metabolomics approach can be performed by using animal experiments or clinical trials. Here, a genetic mouse model, commonly used for research of T2DM, was used to study the pathophysiology with the focus on gut meta-metabolome. We applied a MS based metabolomics approach to study gut meta-metabolome differences between T2DM and healthy mice. The extensive data elaboration using different tools including multivariate statistical analyses or mass difference network based approach derived a deeper insight into several metabolite classes. In summary, we could find several metabolite classes affected in T2DM mice including taurine and sulfate conjugate of fatty acids, bile acids and arachidonic acid metabolism pathway.

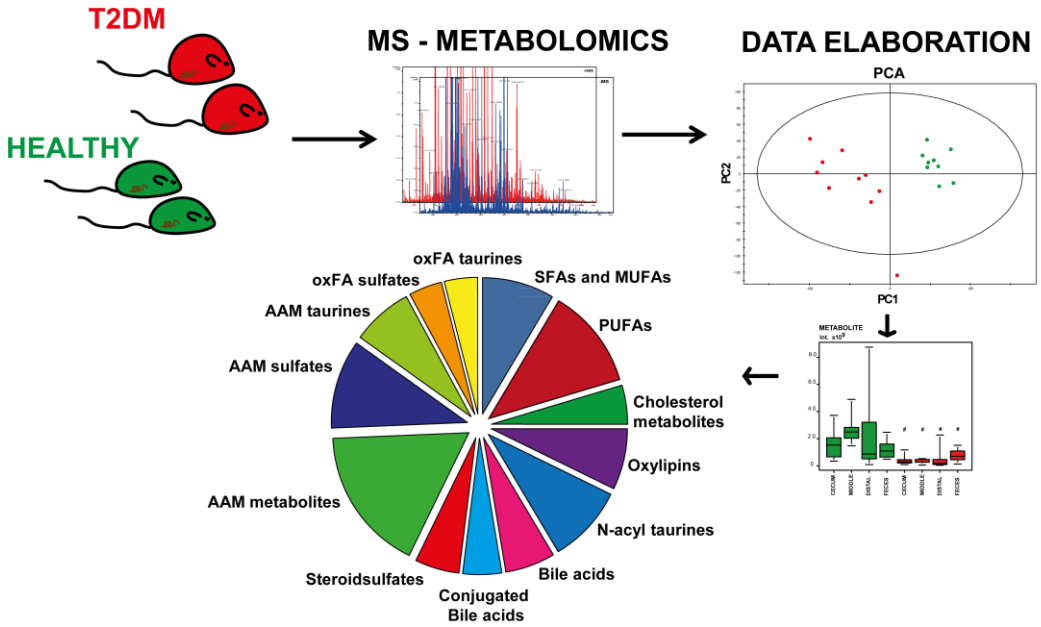

Chapter II

2 Metabolomics in Type 2 Diabetes

2.1 Introduction

Type 2 Diabetes (T2DM) is defined as an endocrine disease (WHO 2010), where several factors has been discussed and investigated to be involved in the pathogenesis of T2DM. The risk factors for developing T2DM might be driven by genetic susceptibility, but also environmental exposure. T2DM is a chronic disease characterized by high blood glucose levels or hyperglycemia. The deregulation of blood glucose levels in T2DM is a consequence of insulin resistance in the peripheral system and later on the failure of pancreatic ß-cells to produce insulin (Alberti and Zimmet 1998). The origin of insulin resistance is likely derived through factors that are secreted by adipose tissue especially the visceral fat such as pro-inflammatory cytokines and hormones, influencing the insulin receptor actions and sensitivity to insulin itself (Kahn, Hull et al. 2006). Different risk factors are discussed in T2DM that are mainly lifestyle including diet, especial western style, physical inactivity and obesity (Lieberman 2003). In recent years, several groups performed metabolomics studies as a research tool to investigate the role of metabolites in T2DM, summarized in Table 1 (Friedrich 2012, Dunn 2013, Lu, Xie et al. 2013).

The role of metabolites in T2DM can be investigated by using animal or human studies (Friedrich 2012). In animal studies T2DM pathophysiology can be investigated by either using genetic or diet driven T2DM rodent studies but also induced experimentally by drugs (indicated as “Others” in Table 1). In genetic rodent studies of T2DM, two prominent models are used for metabolomics studies, predominantly the leptin receptor deficient *db/db* mice or the Zucker *fa/fa* rats (Major, Williams et al. 2006, Salek, Maguire et al. 2007). In *db/db* mice, which is the genetic mouse model used in this thesis, metabolism are already examined applying different analytical techniques such as ^{1}H NMR and LC-MS of urine samples (Salek, Maguire et al. 2007, Altmaier, Ramsay et al. 2008, Gipson, Tatsuoka et al. 2008, Connor, Hansen et al. 2010, Patterson, Bonzo et al. 2011, Li, Wang et al. 2013). Exploring the metabolites involved especially in the discrimination of *db/db* mice several metabolite classes and pathways have been already reported before. Salek *et al.* observed several compound

classes including amino acids such as methionine and glutamate, but also creatine or trimethylamine. Moreover, gut microbial metabolites including hippurate, meta-hydroxyphenylpropionic acid and indoxylsulfate are changed in *db/db* mice, indicating gut microbial metabolism in T2DM (Salek, Maguire et al. 2007). In contrast, the investigation of Altmaier *et al*. could highlight metabolite classes consisting of carnitines and also several lipid classes such as phosphatidylcholines (PCs) or sphingosylphosphocholines (Altmaier, Ramsay et al. 2008). Xu *et al.* could show that triglycerides, PCs, glycerophosphocholines, glucose, glycogen and choline are related to the classification between wiltdtype and *db/db* mice and thus the possible involvement of methylamine metabolism. Additionally, co-microbial metabolites such as TMAO and bile acids are changed in *db/db* mice (Xu, Zhang et al. 2009). Connor *et al.* could find further co-microbial metabolites differentiating in *db/db* mice such as methyl, dimethyl-, trimethylamine, p-cresol, m-HPPA, m-HPPA sulfate, phenylsulfate and hippurate and confirmed thereby the involvement of gut microbiome (Connor, Hansen et al. 2010). Moreover, several gut microbiome studies could already report and reveal different microbial patterns in *db/db* mice (Geurts, Lazarevic et al. 2011). Another study by Patterson *et al.* that applied a more targeted metabolomics approach could observe different glycine betaine, pipecolic acid, proline and glucose levels following them over a time period of 12 weeks (Patterson, Bonzo et al. 2011).

Table 1 Summary of metabolomics studies performed either in animal or human subjects

	Author	Year	Type of biological matrix	Species	Analytical technique	Animal model
Animal studies						
Genetic- driven	(Williams, Lenz et al. 2005)	2005	Urine	Rats	NMR, HPLC-MS	*fa/fa*
	(Granger, Plumb et al. 2005)	2005	Urine	Rats	LC-MS	*fa/fa*
	(Welthagen, Shellie et al. 2005)	2005	Spleen tissue	Mice	GC-MS	NZO
	(Major, Williams et al. 2006)	2006	Plasma	Rats	GC-MS	*fa/fa*
	(Plumb, Johnson et al. 2006)	2006	Plasma	Rats	UPLC-MS	*fa/fa*
	(Serkova, Jackman et al. 2006)	2006	Liver and blood	Rats	NMR	*fa/fa*
	(Salek, Maguire et al. 2007)	2007	Urine	Human, mice, rats	NMR	***db/db***
	(Gika, Theodoridis et al. 2008)	2008	Urine	Rats	UPLC-MS	*fa/fa*
	(Altmaier, Ramsay et al. 2008)	2008	Plasma	Mice	LC-MS	***db/db***
	(Xu, Zhang et al. 2009)	2009	Liver and kidney	Mice	NMR	***db/db***
	(Waldram, Holmes et al. 2009)	2009	Plasma and urine	Rats	NMR	*fa/fa*
	(Connor, Hansen et al. 2010)	2010	Urine	Mice	NMR	***db/db***
	(Zhao, Zhang et al. 2010)	2010	Urine	Rats	NMR	*fa/fa*
	(Patterson, Bonzo et al. 2011)	2011	Urine	Monkeys, mice	UPLC-MS	***db/db***
	(Tsutsui, Maeda et al. 2011)	2011	Plasma, hair, liver and kidney	Mice	UPLC-MS	ddY-H
	(Saadat, Iglay Reger et al. 2012)	2012	Urine	Mice	NMR	***db/db***
	(Li, Wang et al. 2013)	2013	Serum, urine	Mice	GC-MS	***db/db***
Others						
	(Huang, Yin et al. 2011)	2011	Liver	Rats	UPLC-MS	Streptozotocin
	(Ugarte, Brown et al. 2012)	2012	Serum	Rats	UPLC-MS	Streptozotocin
Diet - driven						
	(Shearer, Duggan et al. 2008)	2008	Serum	Mice	NMR	
	(Fearnside, Dumas et al. 2008)	2008	Plasma	Mice	NMR	Different strains
	(Kim, Yang et al. 2009)	2009	Urine	Rats	NMR	
	(Kim, Kim et al. 2010)	2010	Liver and serum	Mice	UPLC-MS, GC-MS	
	(Li, Hu et al. 2010)	2010	Plasma and liver	Mice	HPLC-MS, GC-MS	Two different strains
	(Lin, Yang et al. 2011)	2011	Plasma and liver	Rats	HPLC-MS	
Human studies						
	(Messana, Forni et al. 1998)	1998	Plasma	Human	NMR	
	(Van Doorn, Vogels et al. 2007)	2007	Plasma	Human	NMR	
	(Zhang, Wang et al. 2009)	2009	Serum	Human	NMR	
	(Bao, Zhao et al. 2009)	2009	Serum	Human	GC-MS	
	(Li, Xu et al. 2009)	2009	Plasma	Human	GC-MS	
	(Zhao, Fritsche et al. 2010)	2010	Plasma, Urine	Human	UPLC-MS	
	(Lucio, Fekete et al. 2010)	2010	Plasma	Human	FT-ICR-MS	
	(Zhao, Peter et al. 2009)	2010	Plasma	Human	UPLC-MS	
	(Suhre, Meisinger et al. 2010)	2010	Plasma	Human	LC-MS, GC-MS	
	(Fiehn, Garvey et al. 2010)	2010	Plasma	Human	GC-MS	
	(Mihalik, Goodpaster et al. 2010)	2010	Plasma	Human	HPLC-MS	
	(Wang, Larson et al. 2011)	2011	Plasma	Human	LC-MS	

(Mihalik, Michaliszyn et al. 2012)	2012	Plasma	Human	HPLC-MS
(Würtz, Mäkinen et al. 2012)	2012	Serum	Human	NMR
(Wang-Sattler, Yu et al. 2012)	2012	Serum	Human	FIA MS
(Floegel, Stefan et al. 2013)	2013	Serum	Human	FIA MS

FIA = Flow injection analysis

However, also metabolomics in clinical studies with T2DM or pre-diabetic applied to human has gained a lot of interest (Table 1). This rise of interest is related to the urge of discovering and evaluating new biomarkers and their application in early diagnostic research (Friedrich 2012, Dunn 2013, Lu, Xie et al. 2013). Recently, our group highlighted the role of metabolomics in investigating T2DM pathophysiology in human subjects with insulin resistance (Lucio, Fekete et al. 2010). Major interest in T2DM metabolomics research is to find biomarkers that are associated with the pre-diabetic status of patients in order to interfere and prevent further progress from insulin resistance to T2DM (Lu, Xie et al. 2013).

2.2 Overview – Goals

Investigation of T2DM by applying a metabolomics approach can be performed by using animal experiments or clinical trials, summarized in Table 1. Here, a genetic mouse model, commonly used for research of T2DM was used to study the pathophysiology with the focus of gut meta-metabolome. For this approach we used ten weeks old homozygous BKS.Cg-*dock7*^{m} *+/+ Lepr*^{db}*/J* (*db/db*) mice. The goal herein was to discover the metabolite patterns of intestinal samples in *db/db* mice and their non-diabetic controls (*wt*) by using MS based metabolomics approach with the focus on FT-ICR-MS experiments. As mentioned above, the *db/db* mice have a mutation in the leptin receptor and develop obesity after one month, fasting hyperglycemia after 10 days of age and hyperinsulinaemia after eight weeks and provide therefore a good model for T2DM research (Sharma, McCue et al. 2003, Breyer, Böttinger et al. 2005).

2.2.1 Study design: Drug challenge in *db/db* mice

The main purpose of the study is to investigate the role of two different drugs, the combinatory treatment and their action on the blood glucose levels and the effect on the gut meta-metabolism in *db/db* mice. The drugs are metformin (MET) and SLGT-2 inhibitor (SGLT) and a combined treatment (COMBI). These drugs are applied for a period of two weeks by oral gavage, shown in the scheme (Figure 2-1). Detailed information about study design is described in chapter 5.1.1.

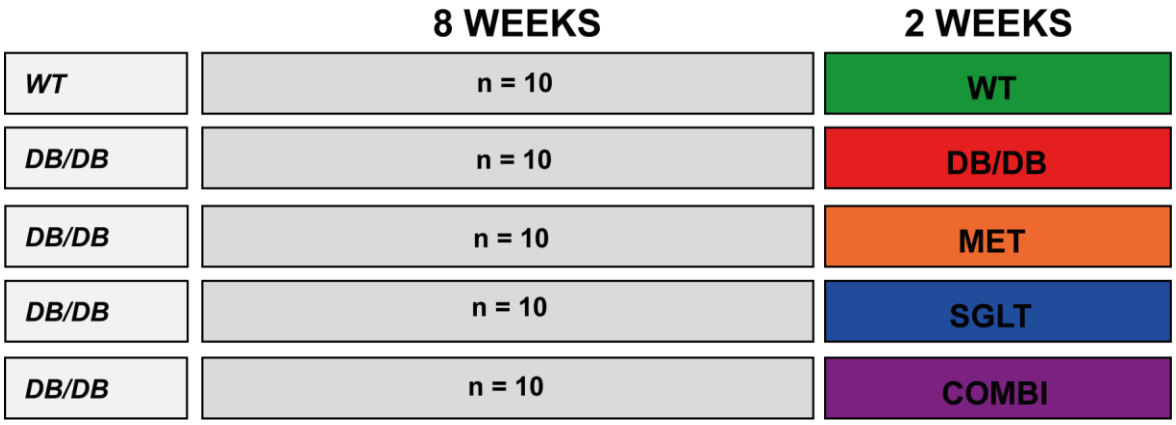

Figure 2-1 Study design of drug challenge of *db/db* mice for two weeks

Metformin is used as a hypoglycemic drug for type 2 diabetes patients and has several influences on different organs of humans, e.g. increase of the glucose uptake in the muscles, decrease of the gluconeogenesis in the liver and effect on the lipid metabolism. The approach of our investigation is to reveal, whether the drug application has an effect on gut meta-metabolome and which meta-metabolites of the intestinal tract are associated with the diabetic status of the *db/db* mice. Especially, our focus is to investigate the meta-metabolome of the gastrointestinal tract because none of the given metabolomics studies of T2DM are related to the metabolite compounds of intestinal or fecal samples (Table 1). This is accompanied by a non-targeted metabolomics approach based on MS analyses. Therefore, the luminal content of cecum, colon (proximal, middle and distal) and feces were collected, whereas proximal samples were excluded from further analyses due to low number of samples per each group. Plasma samples were also provided for the non-targeted metabolomics measurements. First, analyses in a non-targeted metabolomic manner were performed by FT-ICR-MS. Metabolite identification was performed by MS/MS experiments according to the description in chapter 4.4.2.

2.3 Results and Discussion

2.3.1 General: Body weight and blood glucose

We monitored the body weight changes after two weeks of the drug challenge, observing significantly higher body weight differences between *wt* and *db/db* mice with a p-value<0.001 (p-value = 1.78×10^{-9}, Students t-test) (Figure 2-2, A). Different body weight were also observed at the beginning of the experiments (starting conditions of body weight: $\bar{x}$ (*wt*) =

22.21 g; $\bar{x}$ (*db/db*) = 47.5 g; $\bar{x}$ (*db/db* MET) = 47.31 g; $\bar{x}$ (*db/db* SGLT) = 47.41 g and $\bar{x}$ (*db/db* COMBI) = 47.31 g for all groups n=10).

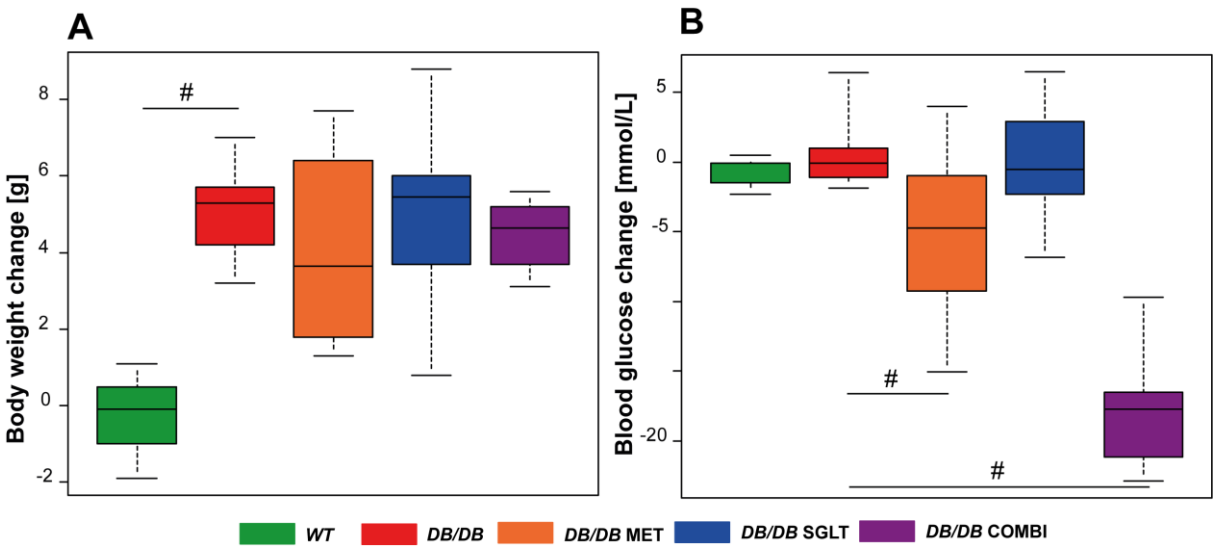

Figure 2-2 Body weight and blood glucose changes in *wt, db/db* mice and *db/db* mice after MET, SGLT and COMBI

The drug application for a period of two weeks did not alter body weight in the *db/db* mice concerning the MET, SGLT or the COMBI treatment (Figure 2-2, A). Blood glucose was reduced significantly after MET (p-value = 0.01, Students t-test) and COMBI (p-value = 1.86×10^{-10}, Students t-test) treatment compared to the untreated *db/db* mice (starting conditions for blood glucose in mmol/l: $\bar{x}$ (*wt*) = 6.66; $\bar{x}$ (*db/db*) = 27.00; $\bar{x}$ (*db/db* MET) = 27.01; $\bar{x}$ (*db/db* SGLT) = 27.01 and $\bar{x}$ (*db/db* COMBI) = 27.25 for all groups n = 10).

2.3.2 The role of meta-metabolome in *db/db* mice during drug challenge

The collected samples of cecum, colon and feces were extracted by methanolic protein precipitation (see chapter 4.3.3). Several processing and filtration steps followed then, shown in chapter 4.5. Afterwards the filtered mass signals lists were subjected to multivariate statistical analyses (MSA). First, a principal component analysis (PCA) was applied for all filtered mass lists to gain on overview about the possible separation between the five groups. To get an overview we observed the first two generated PCs of the models for the analyses of all gastrointestinal matrices and plasma measured in negative mode of FT-ICR-MS, shown in Figure 2-3, A and for positive mode for feces and plasma samples Figure 2-3, B.

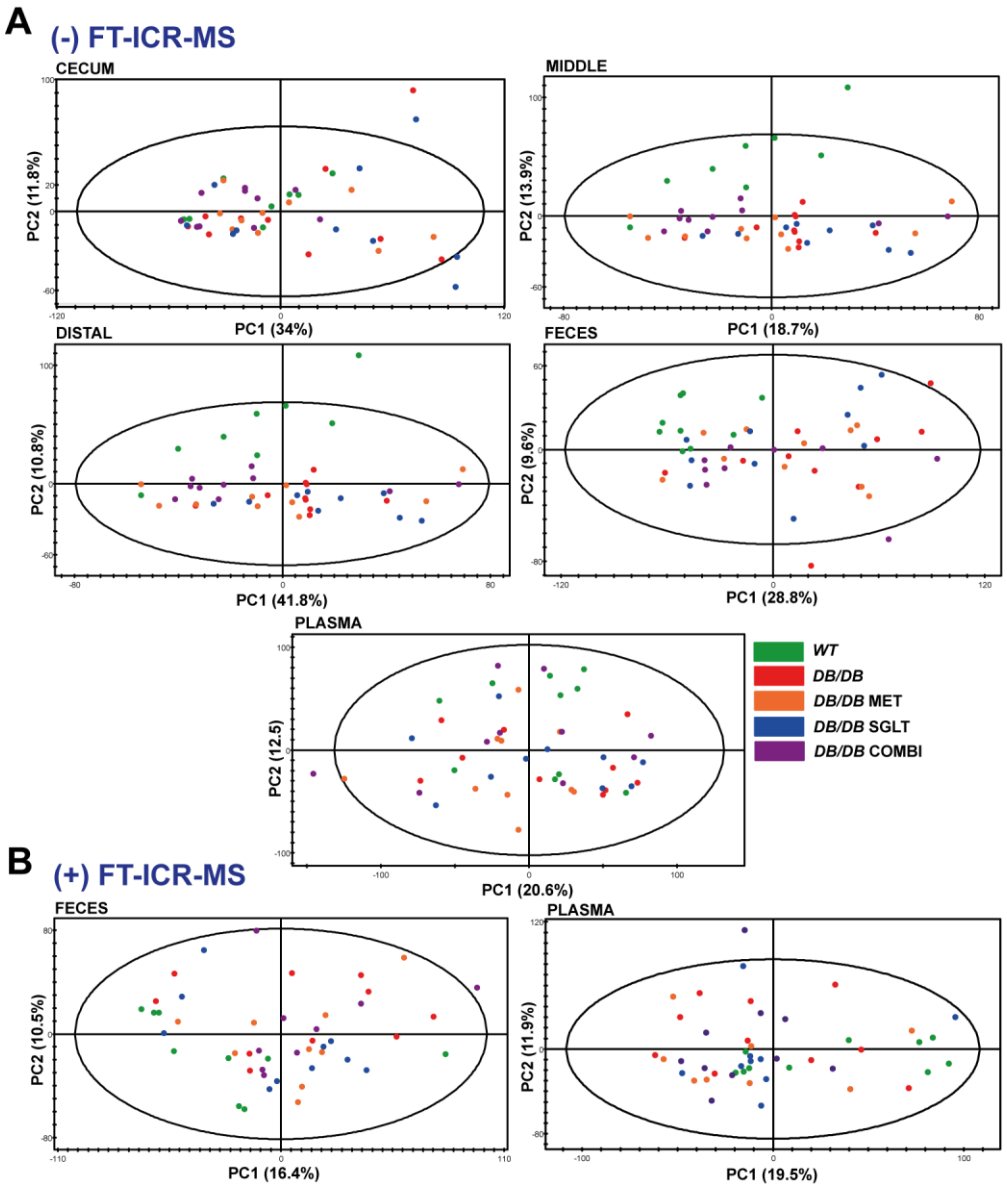

Figure 2-3 Unsupervised PCA scores plots of gut meta-metabolome samples including cecum, middle, distal, feces and plasma samples, analyzed in (-) FT-ICR-MS mode (A) displaying *wt* (green dots), *db/db* (red dots) mice being treated with MET (orange dots), SGLT (blue dots) and COMBI (purple dots) for 2 weeks; (B) feces and plasma samples analysis in (+) FT-ICR-MS mode

The separation based on PCA scores scatter plot was sufficient but in order to classify and discriminate the mass signals responsible for the separation we performed for every matrix an OPLS/O2PLS-DA. First, a model was generated for the group of *wt* and *db/db* mice to extrapolate the mass signals responsible for the separation. These mass signals were given in "variable importance projection" – VIP list and were taken for further analyses. To test whether the different drug challenges impact the VIP mass signals contributing for the *db/db*

and *wt* separation, we took these mass signals and generated new models by including solely the mass signals VIP list. Every generated model was also 7-fold cross-validated (CV-ANOVA). We could find valid models for *db/db* vs. *wt* for middle, distal content, feces samples and plasma for (-) FT-ICR-MS mode (Table 1). In positive mode, only plasma samples could show a valid model for comparison between *db/db* and *wt* mice (Table 1). All generated models we examined by OPLS/O2PLS-DA in order to evaluate the drug challenge impact on intestinal metabolome could not pass the CV-ANOVA step resulting in non-significant p-values (see Table 1).

Table 2 OPLS/O2PLS-DA models of different group comparison

(-) FT-ICR-MS			
	R^2Y(cum)	**Q^2(cum)**	**p-value (CV-ANOVA)**
Group comparison		**CECUM**	
wt vs. *db/db*	0.97	0.67	0.08490
db/db vs. *db/db* MET	0.85	1	0.40693
db/db vs. *db/db* SGLT	-	-	-
db/db vs. *db/db* COMBI	0.68	0.44	0.05452
		MIDDLE	
wt vs. *db/db*	0.94	0.77	0.00044
db/db vs. *db/db* MET	1	0.34	0.96800
db/db vs. *db/db* SGLT	-	-	-
db/db vs. *db/db* COMBI	0.98	0.48	0.23502
		DISTAL	
wt vs. *db/db*	0.9	0.68	0.01624
db/db vs. *db/db* MET	0.96	0.51	0.26756
db/db vs. *db/db* SGLT	0.96	0.23	0.90708
db/db vs. *db/db* COMBI	0.82	0.47	0.15032
		FECES	
wt vs. *db/db*	0.97	0.76	0.00332
db/db vs. *db/db* MET	-	-	-
db/db vs. *db/db* SGLT	0.24	0.03	0.77135
db/db vs. *db/db* COMBI	-	-	-
		PLASMA	
wt vs. *db/db*	0.99	0.82	0.00120
db/db vs. *db/db* MET	1	0.48	0.73189
db/db vs. *db/db* SGLT	0.77	0.09	0.80902
db/db vs. *db/db* COMBI	0.85	0.47	0.03938
(+) FT-ICR-MS			
		FECES	
wt vs. *db/db*	0.99	0.51	0.33287
db/db vs. *db/db* MET	0.99	0.56	0.36081
db/db vs. *db/db* SGLT	0.35	0.15	0.26210
db/db vs. *db/db* COMBI	-	-	-
		PLASMA	
wt vs. *db/db*	0.99	0.75	0.00246
db/db vs. *db/db* MET	0.99	0.36	0.73620
db/db vs. *db/db* SGLT	-	-	-
db/db vs. *db/db* COMBI	0.94	0.06	0.98708

Afterwards, additionally an univariate statistical analysis (USA) was performed in order to confirm the results derived from OPLS/O2PLS-DA. First, the significance between *wt* and *db/db* mice was calculated by using a non-parametric univariate statistical test (Mann-Whitney test). These significant mass signals were used to perform again a pair wise comparison between *db/db* and the drug treated *db/db* mice (*db/db* vs. *db/db* MET, *db/db* vs. *db/db* SGLT, *db/db* vs. *db/db* COMBI) to see if the treatment had an effect on the changed

mass signals. Most differences aroused between the *wt* and the *db/db* mice concerning the mass signals detected in cecum, middle, distal, fecal and plasma samples. Most significant mass signals were calculated for fecal samples (3412) followed by plasma (2815) in neg. mode, middle content (1222), cecal content (977) and 557 in distal content (Figure 1-2). Therefore, only feces and plasma samples were measured in positive mode achieving 1797 significantly different mass signals for feces and 1733 for plasma samples (Figure 2-4).

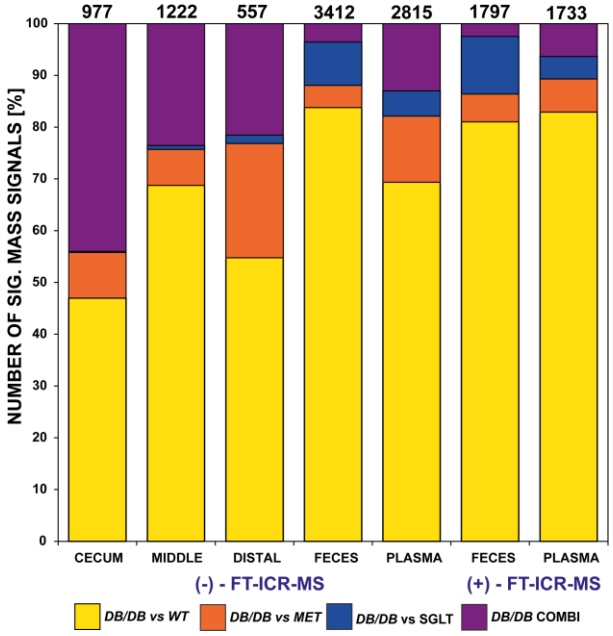

Figure 2-4 Univariate statistical analysis and comparison of drug challenge in *db/db* mice; 100 % are always representing all significant mass signals between *db/db* and *wt* mice, the number of significant mass signals between *db/db* and *wt* mice are displayed on the top of the bar plots

Furthermore, the results nicely show that there were differences in the number of the significant mass signals between *db/db* and *wt* between the samples in negative mode with FT-ICR-MS. In the bar plot 100% are representing the number of significant mass signals between *db/db* and *wt* in each sample type of the gastrointestinal tract and plasma. Then, the proportion of significantly changed mass signals due to drug treatment was calculated, resulting in different percentages of mass signals changed after treatment. The lowest changes could be shown for SGLT treatment mice, resulted in significantly changes of 2 (0.2%) mass signals for cecal content, 9 mass signals (0.7%) for middle content, 9 mass signals (1.6%) for distal content, 285 mass signals (8.3%) for feces and 137 mass signals (4.9%) for plasma samples in neg. mode (Table). Moreover, slight differences could be elaborated for MET treatment, accounting 146 (4.3%) different mass signals in feces, 123 (22.1%) in distal and

around 85 (7%) in middle and 86 (8.8%) cecal content. The COMBI treatment had a larger effect the metabolism in the gastrointestinal tract accounting for 430 (44%) for cecal content, 288 (24%) for middle content, 120 (22%) for distal content, 122 (4%) for feces and 366 (16%) for plasma samples. For positive mode, the MET group resulted in 97 (5.4%) significantly changed mass signals and 111 (6.4%) for plasma. In SGLT comparison, we found 199 different mass signals (11%) for feces and 75 mass signals (4%) for plasma samples that were changed. In the COMBI group, we found 45 mass signals (2.5%) in feces samples and 110 mass signals (6.3%) for plasma samples, affected after drug treatment.

Table 3 Univariate statistical analysis of mass signals derived from FT-ICR-MS experiments of four matrices from *wt* and *db/db* mice and the respective comparison of drug challenge, performed with Mann-Whitney test

	(-) FT-ICR-MS					(+) FT-ICR-MS	
Group comparison	**CECUM**	**MIDDLE**	**DISTAL**	**FECES**	**PLASMA**	**FECES**	**PLASMA**
wt vs. *db/db*	977	1222	557	3412	2815	1797	1733
db/db vs. *db/db* MET	86	85	123	146	359	97	111
db/db vs. *db/db* SGLT	2	9	9	285	137	199	75
db/db vs. *db/db* COMBI	430	288	120	122	366	45	110

The results from univariate statistical analyses again confirm and underline the results derived from OPLS/O2PLS-DA, that the drug challenge had only slight impact on gastrointestinal metabolome. However, we could show valid multivariate OPLS/O2PLS-DA models for cecal and plasma metabolome after COMBI treatment. Moreover, the drug challenge with MET, SGLT or COMBI did not affect body weight during the 2 weeks (Figure 2-2, A). Solely, in the *db/db* MET and *db/db* COMBI group we could find decreased blood glucose levels (Figure 2-2, B). Hence, the COMBI treatment could decrease blood glucose level to a higher extent compared to MET treatment and additionally we could find valid OPLS/O2PLS-DA models for cecal and plasma metabolome, we did elaborate the metabolome changes in chapter 2.3.10. Still, our major interest was to focus on the differences between *db/db* and *wt* mice to describe the metabolome changes due to diabetes status of the *db/db* mice. By evaluating the different metabolomic composition between *db/db* and *wt* mice, we can probably find some metabolites that were also altered due to drug stimulation. Concerning the gastrointestinal matrices and thereof the changes between *db/db* and *wt* mice, the best results derived from OPLS/O2PLS-DA were shown for middle content and feces samples. Looking in detail for significant differences by univariate statistical test the feces samples had the highest number of significant mass signals (Figure 2-4). Therefore, we were focusing on the variations between *db/db* and *wt* mice by using the results of the measurements of fecal metabolome. Moreover, feces samples are easily to collect and provide non-invasive matrices

to perform metabolomic analyses (see detailed results about fecal metabolome between *db/db* and *wt* mice in Chapter 2.3.3).

2.3.2.1 Cholesterol and primary bile acid metabolism in *db/db* mice – metabolite patterns in the intestine

One of the metabolite classes known to be changed between *db/db* and *wt* mice are primary bile acids, hence the enzyme cholesterol 7 alpha-hydroxylase (CYP7A1) was shown to be up-regulated in the liver of *db/db* mice and an increased bile acid content for feces samples (Watanabe and Ayugase 2010). This enzyme is involved in the biosynthesis of primary bile acid pathway from cholesterol. In *db/db* mice the level of cholic acid was significantly decreased in *db/db* mice compared to *wt* mice in all four gastrointestinal matrices (Figure 2-5, A). The up-regulation of the enzyme resulted in lower levels of CA in the gastrointestinal tract in diabetic mice. We had expected a higher level of CAs in the gastrointestinal tract in diabetic mice as shown before (Watanabe and Ayugase 2010). Unfortunately, CA differences could not be obtained in plasma samples due to low abundance. The next step was to determine the changes related to the secondary bile acid synthesis and therefore we examined the levels of deoxycholic acid (DCA). There were no obvious or significant differences concerning cecum, middle and distal DCA levels comparing *wt* and *db/db* mice (Figure 2-5, B). Interestingly, DCA levels in feces and plasma samples were significantly altered comparing *wt* and *db/db* mice (Figure 2-5, B and C). Accordingly, we observed all possible and detected C_{24} BAs and their patterns between *db/db* and *wt* mice and their behavior in all four gastrointestinal matrices. We could find 23 different C_{24} BAs and the sum of all found BAs showed in total higher levels in *wt* mice compared to diabetic mice (Figure 2-5, D).

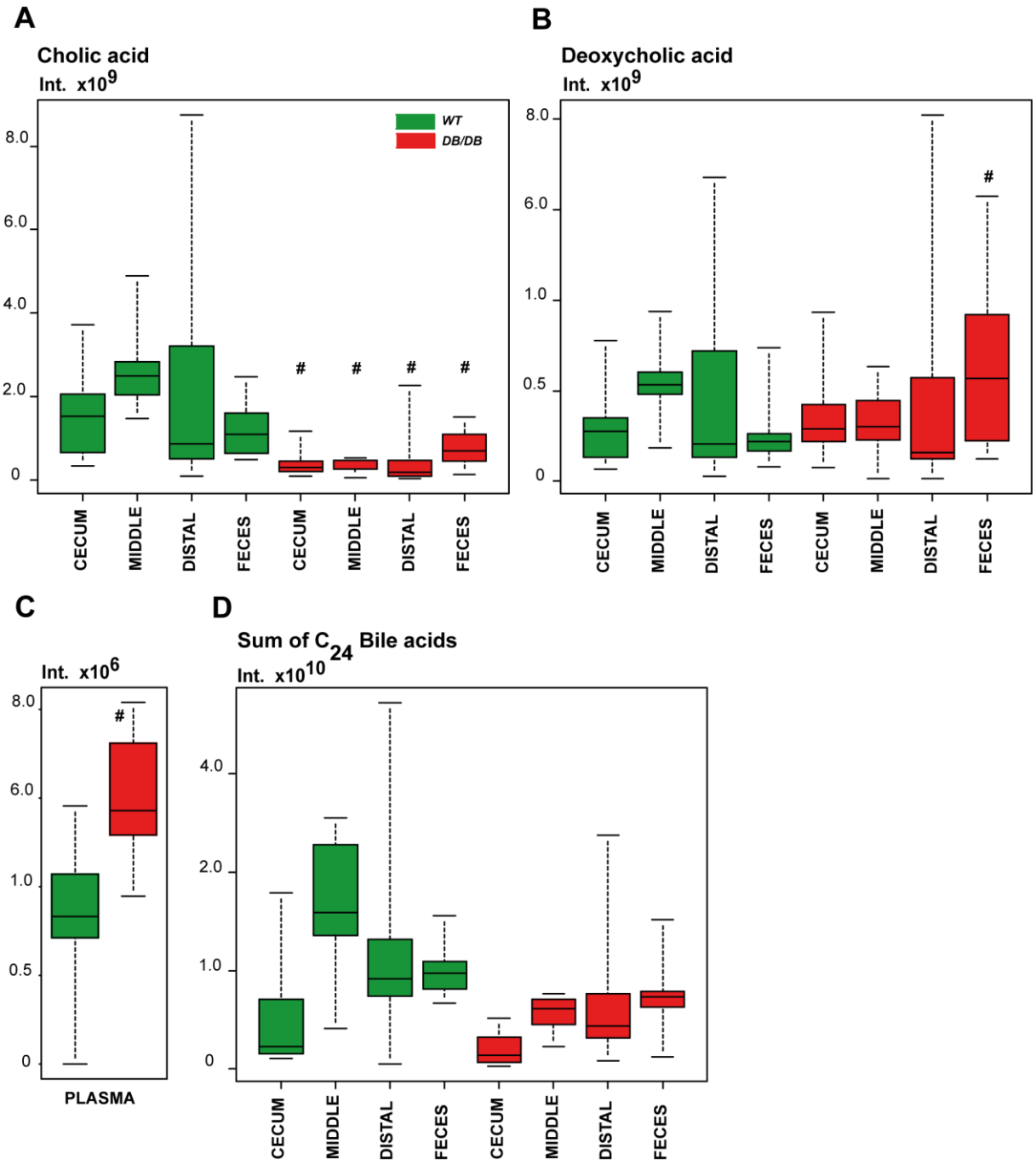

Figure 2-5 Bile acids comparison between *db/db* and *wt* mice; A: Cholic acid; B: Deoxycholic acid; C: Deoxycholic acid in plasma; D: Overall behavior of sum of all C_{24} bile acids; # p-value <0.05 (Mann-Whitney test), detailed information are given Table 15 of appendix (Chapter 6)

Still we need to consider the individual behavior of the BAs, as for example shown for CA and DCA, whereas DCA did not show the same behavior like CA and the sum of all C_{24} BAs (Figure 2-5, A, B and D). Moreover, the enzyme deregulation is not only affecting the bile acid metabolism but also the cholesterol derivatives that are involved in the BA biosynthesis. The first step of the enzyme is the conversion of cholesterol into hydroxycholesterol; thereof

we examined the levels of cholesterol and hydroxycholesterol in the gut and their possible difference between *wt* and *db/db* mice. Cholesterol was not detected in all matrices but hydroxylcholesterol showed increased patterns in diabetic mice in middle and feces samples but not in cecal or distal samples and likely confirmed thereby the up-regulated behavior of the enzyme (Figure 2-6, A).

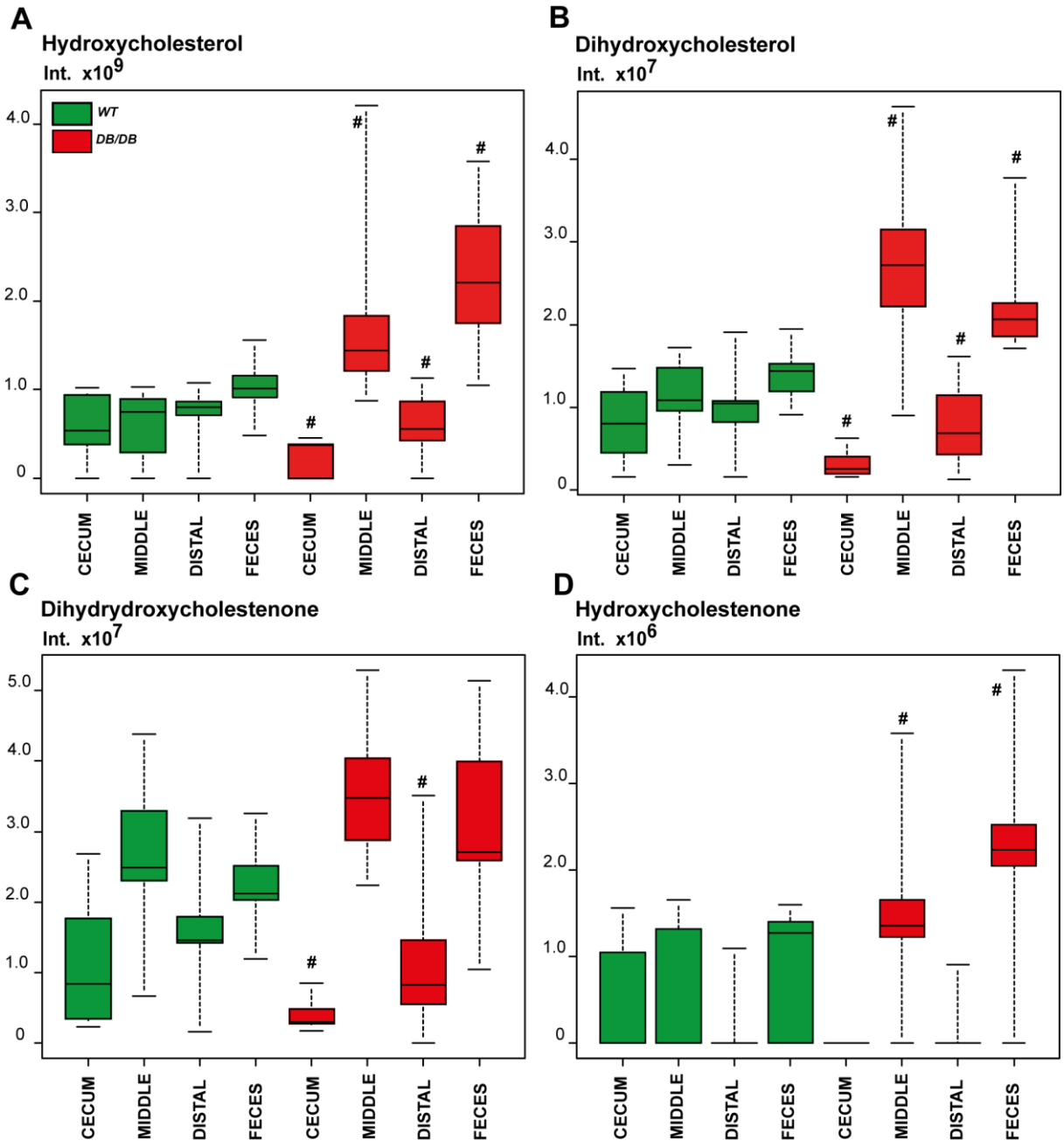

Figure 2-6 Cholesterol metabolites part I; # p-value <0.05 (Mann-Whitney test), detailed information are given Table 15 of appendix (Chapter 6)

Going deeper, we could show increased patterns for dihydroxycholesterol (Figure 2-6, B), dihydroxycholestone (Figure 2-6, C) and hydroxycholestenone (Figure 2-6, D) in diabetic mice but we saw that the behavior of the last two metabolites are getting similar to the *wt* mice levels, shown in Figure 2-6.

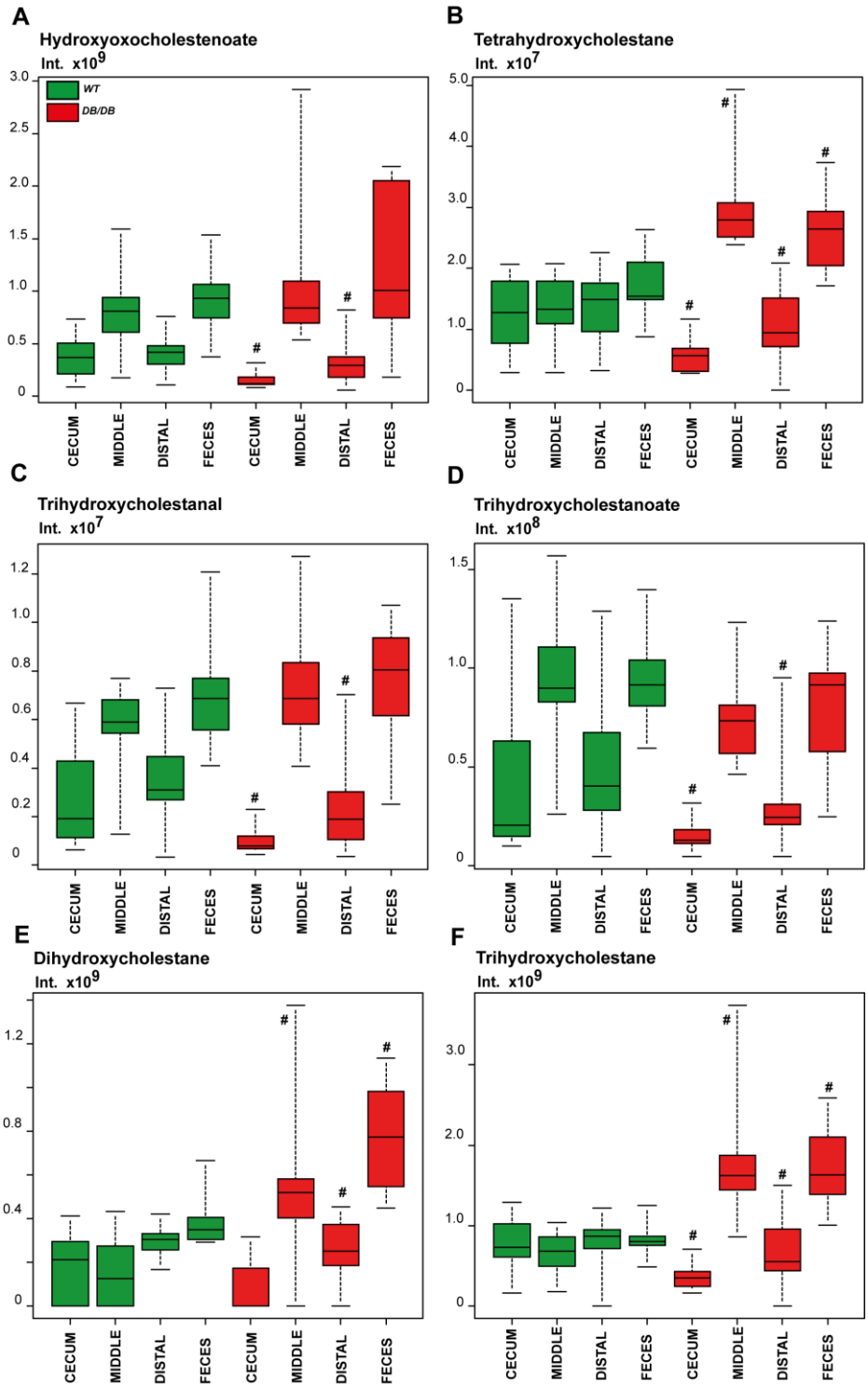

Figure 2-7 Cholesterol metabolites part II; # p-value <0.05 (Mann-Whitney test), detailed information are given Table 15 of appendix (Chapter 6)

For hydroxyoxocholestenoate (Figure 2-7, A), tetrahydroxycholestane (Figure 2-7, B), trihydroxycholestenal (Figure 2-7, C), trihydroxycholestanoate (Figure 2-7, D), dihydroxycholestane (Figure 2-7, E) and trihydroxycholestane (Figure 2-7, F) we observed lower levels in *db/db* mice in cecal and distal samples and higher levels in middle and fecal samples. Trihydroxycholestanoate (Figure 2-7, D) showed overall decreased patterns whereas only cecal and distal levels were significantly different. The behavior of the cholesterol derivatives was different, including the gastrointestinal matrices and we need to consider this behavior while interpreting the data (Figure 2-6 and Figure 2-7). The enzyme CYP7A1 was shown to be expressed uniquely in liver (Jones, Repa et al. 2012). Other enzymes involved in the bile acid biosynthesis are also predominantly expressed in liver (Jones, Repa et al. 2012). Interestingly, overexpression of CYP7A1 in mice resulted in a protection against high fat induced obesity, fatty liver and insulin resistance and showed higher levels of bile acids in the gastrointestinal tract of the transgenic mice (Li, Owsley et al. 2010). The expression of CYP7A1 was also stimulated by re-feeding after a fasting period, concluding food intake affects bile acid metabolism, reporting higher bile acid content in the intestine due to restricted feeding (Li, Owsley et al. 2010). Moreover, the *db/db* mouse strain is known to have increased food intake (hyperphagia) (Bivona, Park et al. 2011) and hyperphagia was shown to change the bile acid pool (Young, McNamara et al. 1983). In contrast, fasted *ob/ob* mice and streptomycin treated mice (type 1 diabetes mouse model) had still higher CYP7A1 mRNA levels compared to their wildtype controls, which found to be due to epigenetic control mechanism (Li, Owsley et al. 2010).

2.3.3 Differences of the fecal metabolome between *db/db* and *wt* mice

Hence, both MSA and USA showed the best results for fecal samples; therefore, we were focusing in this chapter on the fecal metabolome differences between *db/db* and *wt* mice. Firstly, a PCA was applied for both modes without the drug treated groups. As a result, the score scatter plot that revealed already the presence of two distinct groups *of db/db* and *wt mice* (Figure 2-8), which will be further investigated through supervised approaches with the focus on the results of negative mode.

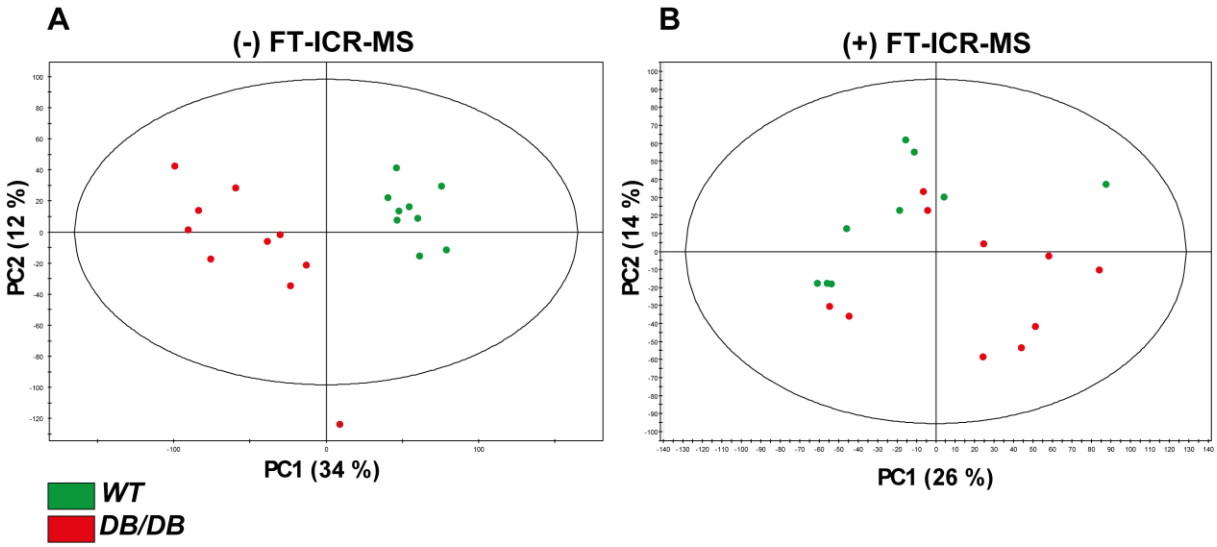

Figure 2-8 PCA scores scatter plot of fecal metabolome of *db/db* and *wt* mice analyzed in (-) FT-ICR-MS (A) and (+) FT-ICR-MS mode (B)

Moreover there were no strong outliers detected, hence almost all scores are distributed within the confidence region or ellipse (95% of Hotelling's T^2 Range). The group's separation and consequently the putative mass signals responsible for the group forming were investigated with different techniques. One is the analysis with an Orthogonal Partial Least Squares regression OPLS/O2PLS-DA with an OSC (orthogonal signal correction) (Wiklund, Johansson et al. 2007). The model resulted in good fit results obtaining good values for $R^2Y(cum) = 0.97$ and $Q^2(cum) = 0.76$ (with an overall significance of p-value = 0.00332197 and with 7-fold CV, Table 2, 2.3.2). The scores plot derived from OPLS/O2PLS-DA model is presented in Figure 2-9, A displayed a clear discrimination between *db/db* and *wt* mice. The mass signals that were responsible for this discrimination are selected from the S-PLOT (Figure 2-9, B).

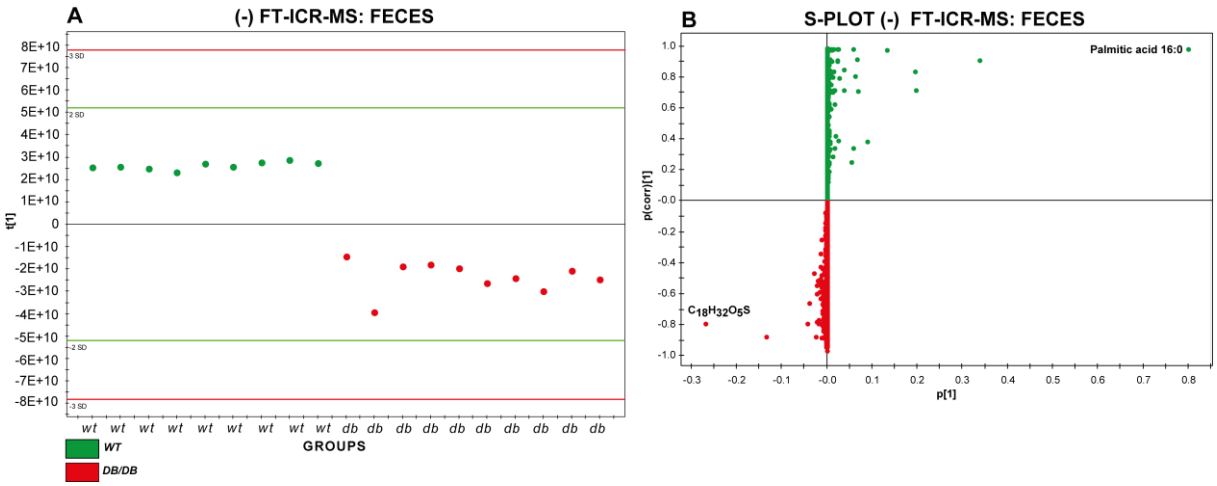

Figure 2-9 A: OPLS/O2PLS-DA scores scatter plot of fecal metabolome of *db/db* and *wt* mice analyzed in (-) FT-ICR-MS; B: S-Plot of the contributing mass signals to the separation between *db/db* and *wt* mice

2.3.3.1 KEGG metabolic pathway analysis of fecal meta-metabolome

As shown above, due to dys-regulated enzyme (CYP7A1) the primary bile acid biosynthesis and all metabolite classes were affected between *wt* and *db/db* mice in different intestinal samples (Chapter 2.3.2.1). Therefore, we took the mass signals that were significantly changed and afterwards we performed an annotation with MassTRIX. Subsequently, a KEGG pathway assignment was performed in order to see which pathways are involved in the separation between diabetic and *wt* mice. Therefore, we took all KEGG metabolites and assigned them into metabolic pathways of KEGG. Different pathways were involved in the separation between *wt* and *db/db* mice including biosynthesis of steroid hormones, unsaturated fatty acids and primary bile acids as well as arachidonic acid, alpha-linolenic acid and linoleic acid metabolism, shown in Figure 2-10.

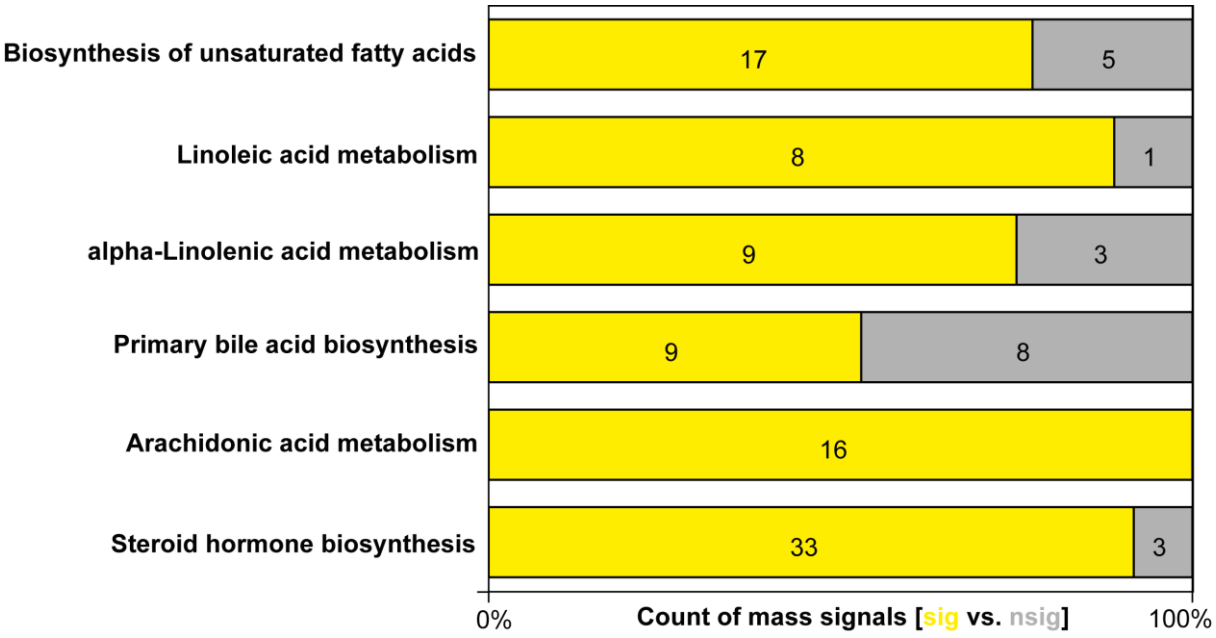

Figure 2-10 KEGG metabolic pathway analysis and comparison of significant (sig) versus not significant (nsig) mass signals

For example, in arachidonic acid metabolism pathway all assigned mass signals were also significantly changed between *db/db* and *wt* mice (Figure 2-10). Steroid hormone biosynthesis has the highest number of significant mass signals, shown in Figure 2-10. These results indicate already the immense changes in the metabolism of diabetic mice and confirm the results of the deregulated primary bile acid biosynthesis, showed in chapter 2.3.2.1 for the different intestinal matrices.

2.3.4 Comparative analyses of metabolite classes between *db/db* and *wt* mice

2.3.4.1 Fatty acids comparison in *db/db* mice vs. *wt* mice

The KEGG pathway analyses showed that different metabolic pathways and thereof different metabolite classes were involved in discriminating *db/db* and *wt* mice. Moreover, two mass signals highly discriminating *wt* mice, concerning palmitic acid C16:0 and an unknown mass signal given through molecular formula of $C_{18}H_{32}O_5S$ representing *db/db* mice are highlighted in the S-PLOT (Figure 2-9, B). We used this information to extrapolate different metabolite classes. In the S-Plot palmitic acid (C16:0) was one of top metabolites discriminating *wt* and *db/db* mice, highly increased in *wt* mice, displayed in the fold change plot. But, also other FAs were observed to be significantly increased in *wt* mice including lauric acid (C12:0),

myristic acid (C14:0), palmitoleic acid (C16:1), oleic acid (C18:1), stearic acid (C18:0), nonadecanoic acid C(19:0), icosenoic acid (C20:1), icosanoic acid (C20:0), docosadienoic acid (C22:2) docosenoic acid (C22:1), docosanoic acid (C22:0), tetracosenoic acid (C24:1) and tetracosanoic acid (C24:0). Interestingly, all FAs discriminated for *wt* mice were grouped to the saturated or mono-unsaturated class, except linoleic acid (C18:2) and linolenic acid (C18:3). Contrarily, in *db/db* mice unsaturated FAs were significantly increased, including arachidonic acid (C20:3), icosapentanoic acid (C20:5) and docosahexanoic acid (C22:6), trisotrienoic acid (C23:3), pentacosatrienoic acid (C25:3), pentacosadienoic acid C25:2), hexacosatrienoic acid (C26:3), heptacosadienoic acid (C27:2), octacosadienoic acid (C28:2), nonacosadienoic acid (C29:3), nonacosadienoic acid (C29:2), dotriacontatetraenoic acid (C32:4), hexatriancontahexaenoic acid (C36:4), octatriacontahexaenoic acid (C38:6) Octatriacontapentaenoic acid C(38:5), shown in fold change plot in Figure 2-11. We could also confirm four different fatty by applying MS/MS experiments, including palmitic acid C(16:0), icosenoic acid (C20:1), arachidonic acid (C20:3) and linoleic acid (C18:2), mentioned in chapter 5.2.1 in Figure 5.2.1.1 A –D.

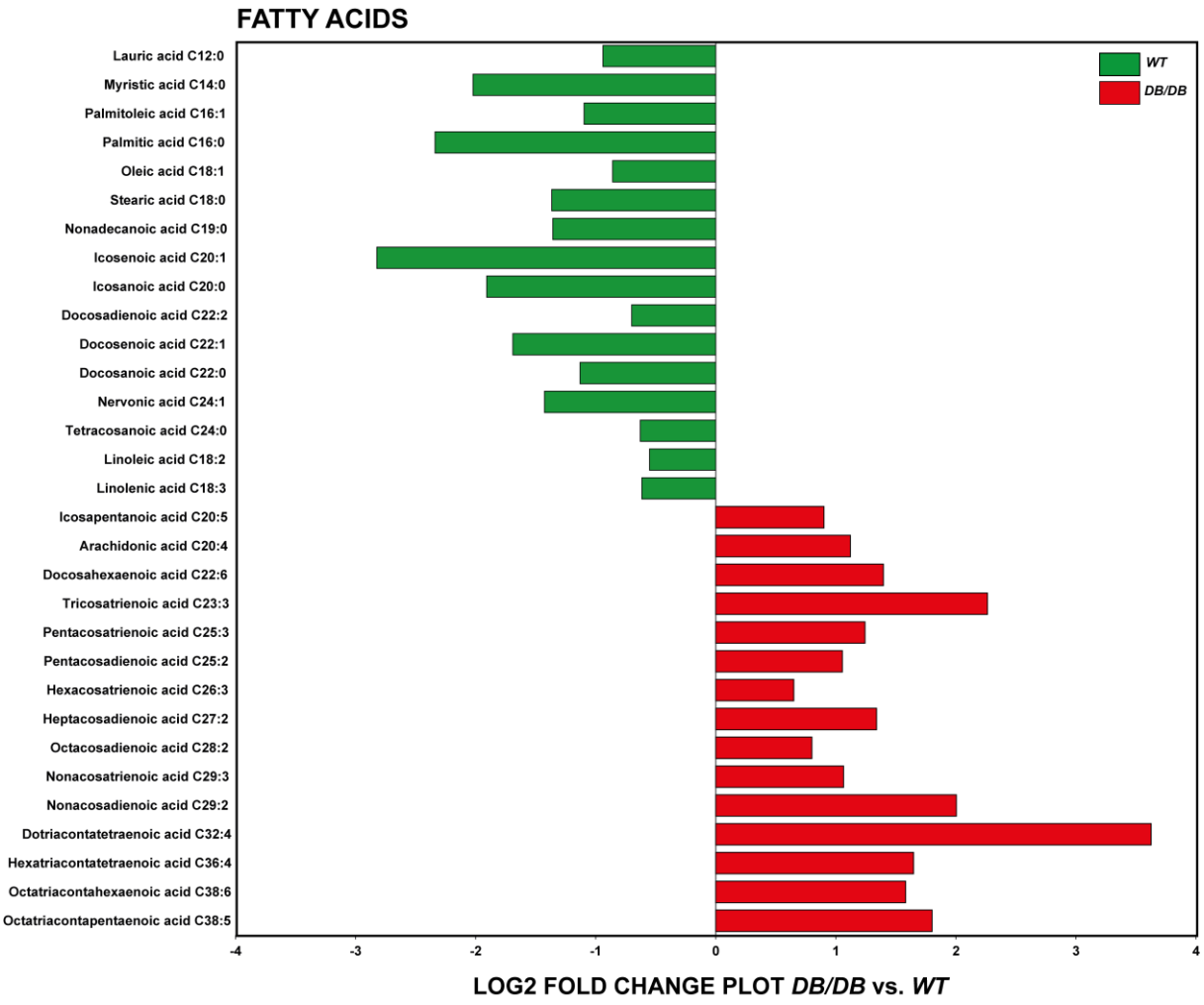

Figure 2-11 Fold change plot of fatty acids changed between *db/db* and *wt* mice in fecal samples; all displayed metabolites were significant with a p-value <0.05 (Mann-Whitney test), detailed information are given Table 16 of appendix (Chapter 6)

In the non-diabetic *wt* mice, the metabolite group of un- and monounsaturated FAs were significantly increased. The lower levels of these FAs in *db/db* mice indicate lower excretion of FAs due to higher ß-oxidation in liver and their systemic distribution. In fact, in blood samples higher levels of free FAs were already shown before and also higher ß-oxidation was measured in the liver of *db/db* mice (Seo, Choi et al. 2008). In addition, in our study the fecal samples exhibit the reverse behavior of free FAs comparing to blood samples of diabetic mice. In another study using Zucker rats for investigating diabetes, several FAs including octanoic acid, nonanoic acid, oleic acid, arachidonic acid were increased in plasma samples (Major, Williams et al. 2006). In our study we could not confirm results concerning oleic or arachidonic acid. No significant changes were shown for these FAs in plasma samples by

comparing *db/db* and *wt* mice, shown in Figure 2-12. Octanoic and nonanoic acid was not be detected in plasma samples.

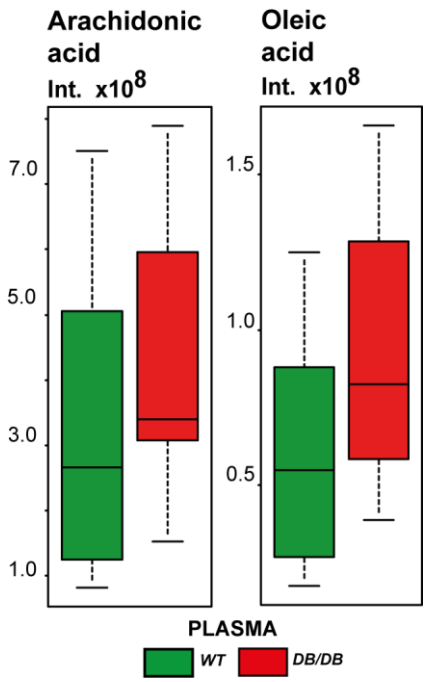

Figure 2-12 Arachidonic and oleic acid in plasma samples of *wt* and *db/db* mice; no significant changes could be calculated by Mann-Whitney test

The compound class of FAs seemed also to be very indicative of changed metabolism in T2DM showed throughout in human species, whereas we could confirm this for fecal sample but plasma samples (Major, Williams et al. 2006, Zhao, Peter et al. 2009, Suhre, Meisinger et al. 2010, Zhao, Fritsche et al. 2010).

2.3.4.2 Oxylipins changes in *db/db* mice

A further class of fatty acids, so called oxylipins (here especially C18 oxylipins of oleic, linoleic, linolenic and stearic acid) appeared to be an important factor discriminating diabetic and *wt* mice (Figure 2-13). Oxylipins are classes of bioactive FA metabolites with many structural members, bearing for example hydroxyl groups.

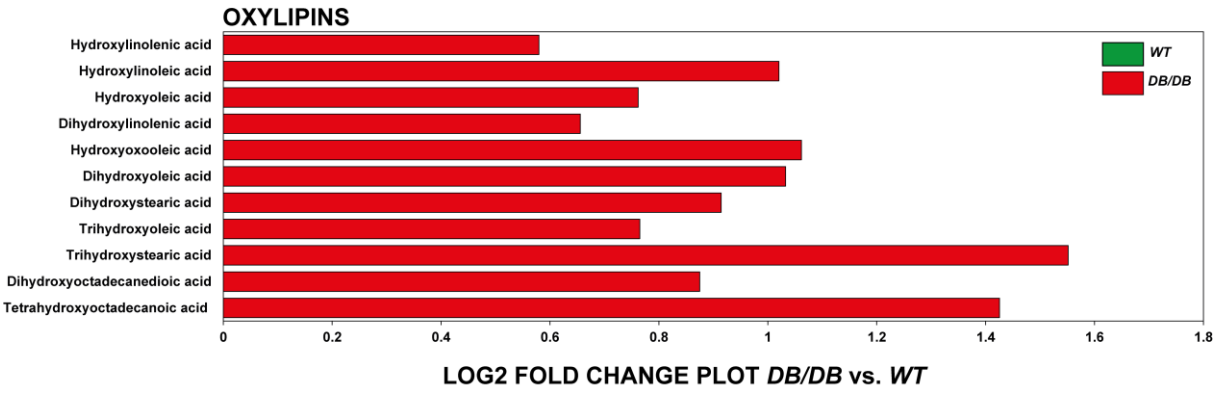

Figure 2-13 Fold change plot of oxylipins changed between *db/db* and *wt* mice in fecal samples; all displayed metabolites were significant with a p-value <0.05 (Mann-Whitney test), detailed information are given Table 16 of appendix (Chapter 6)

Here, we observed increased patterns of hydroxylinoleic acid (MS/MS spectrum in Figure 5-2, A), hydroxyoleic acid (MS/MS spectrum in Figure 5-2, B), hydroxyoxooleic acid (MS/MS spectrum in Figure 5-2, C), dihydroxyoleic acid (MS/MS spectrum in Figure 5-2, D), trihydroxyoleic acid, hydroxylinolenic acid, dihydroxylinolenic acid, dihydroxystearic acid, dihydroxyoctadecanedionic acid, trihydroxystearic acid and tetrahydroxystearic acid in *db/db* mice, shown in Figure 2-13. Hatley *et al.* reported about the presence for oxylipins of linoleic and arachidonic acid in urine samples of *db/db* mice (Hatley, Srinivasan et al. 2003). Lipoxygenases are the enzymes that are responsible for the synthesis of oxylipins of linoleic acid and arachidonic acid as the first step of the arachidonic acid metabolism and are likely involved in pathophysiology of diabetes (Hatley, Srinivasan et al. 2003, Grapov, Adams et al. 2012).

2.3.4.3 N-acyltaurines in *db/db* mice

A further fatty class so called N-acyltaurines (NATs) that are in general taurine conjugates of fatty acids were discovered in fatty acid amide hydrolase (FAAH) deficient mice (Saghatelian, Trauger et al. 2004). They could observe four different NATs with alkyl chains of C22:0, C23:0; C24:1 and C24:0, following by reports of NATs of polyunsaturated FAs (Saghatelian, McKinney et al. 2006). We could assign four different fatty acids conjugated with taurine including arachidonic acid (NAAT, C20:4) (MS/MS spectrum in Figure 5-3, A), linoleic acid (NLAT, C18:2) (MS/MS spectrum in Figure 5-3, B), oleic acid (NOAT, C18:1) were throughout significantly increased in *db/db* mice (Figure 2-14). Only a taurine conjugate of palmitic acid (NPAT, C16:0) was increased in *wt* mice. Moreover we could find ten other

FAs taurine conjugates, displayed in the fold change plot, consisting of C16:1, C16:2, C16:3, C16:4, C18:3, C18:4, C18:5, C19:1, C20:5 and C24:0 containing FAs (Figure 2-14). All new taurine conjugates were exclusively increased in diabetic mice (Figure 2-14).

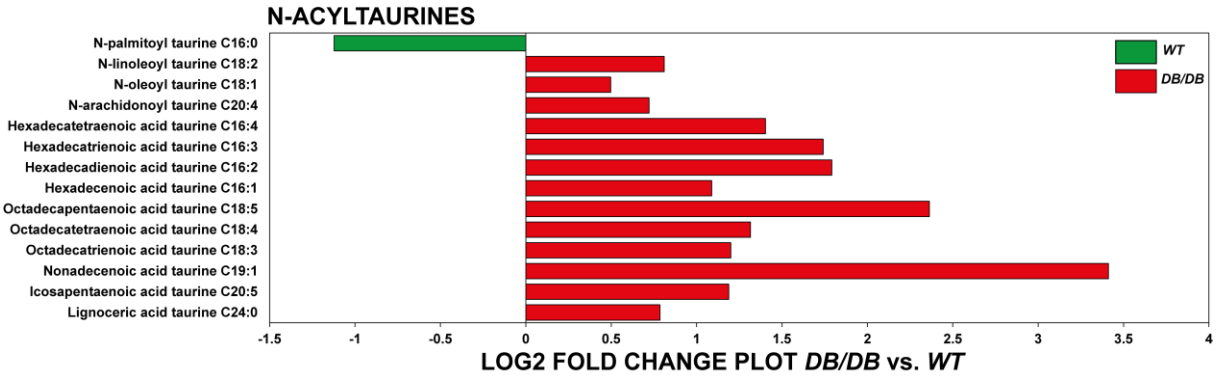

Figure 2-14 Fold change plot of N-acyltaurines changed between *db/db* and *wt* mice in fecal samples; all displayed metabolites were significant with a p-value <0.05 (Mann-Whitney test), detailed information are given Table 16 of appendix (Chapter 6)

NATs were recently discovered as a new class of lipids detected firstly in brain and spinal cord tissues and were highly accumulated in FAAH deficient mice (Saghatelian, Trauger et al. 2004). Subsequently, NATs were also found in liver and kidney tissues, activating transient receptor potential family of cation channels and degraded in a FAAH dependent manner (Saghatelian, McKinney et al. 2006). Geurts *et al*. reported also a decreased FAAH expression in subcutaneous fat tissue of diabetic mice, which is concordantly with higher levels of NATs in our *db/db* mouse study (Geurts, Lazarevic et al. 2011). Long *et al.* studied the impact of FAAH inhibition compared to FAAH deficient mice and showed different distribution of NATs long chain FAs highly accumulated in brain such as C22:0 or NATs of polyunsaturated FAs in liver and kidney such as C20:4 and C22:6. They found similar levels of NATs in liver and plasma (absolute concentrations in liver about 5 nmol/g and plasma about 0.2 nmol/g), concluding NATs could probably act as endocrine signaling molecules. Recently, a group confirmed this assumption by revealing that two NATs of arachidonic (NAAT) and oleic acid (NOAT) were involved in insulin signaling (Waluk, Vielfort et al. 2013). NATs also activate transient receptor potential family of calcium channels (TRPV1 and TRPV4) and especially NATs of NAAT and NOAT exhibited anti-proliferative effects (Saghatelian, McKinney et al. 2006). Furthermore insulin signaling is performed via activation of TRPV1 in pancreatic ß-cells by increasing intracellular calcium levels (Waluk, Vielfort et al. 2013). The expression of TRPV1 containing nerve fibers were reported in the mucosa, in the submucosal layer and myenteric plexus of rectum and distal colon of mice (Matsumoto, Kurosawa et al. 2009). The

distribution of FAAH was throughout similar in intestine and inhibition of FAAH resulted in decreased intestinal motility (Capasso, Matias et al. 2005). Concerning NAAT and NOAT, we were also curios about the distribution of these two metabolites in intestinal samples of *wt* and *db/db* mice to see whether we might observe changes in the gastrointestinal tract. Increasing levels were analyzed from cecum to fecal samples in *wt* mice, shown in Figure 2-15, A and B.

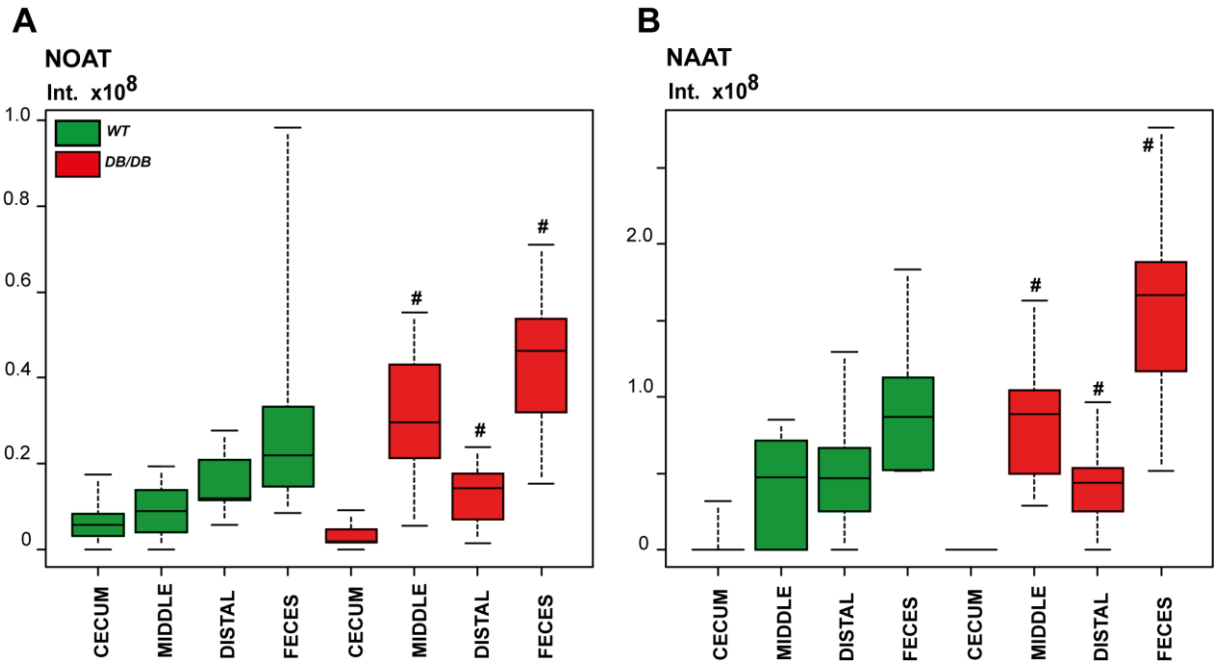

Figure 2-15 Comparison of two NATS and their distribution along the intestine of *wt* and *db/db* mice; A: N-oleoyltaurine (NOAT); B: N-arachidonoyltaurine (NAAT), # p-value <0.05 (Mann-Whitney test), detailed information are given Table 17 of appendix (Chapter 6)

Comparing the behavior of these NATs with *db/db* mice we found significantly increased NOAT and NAAT levels in middle, distal and fecal samples by completely different patterns in *db/db* mice compared to *wt* mice (Figure 2-15). The NATs somehow oscillate by starting with low levels in cecum, increasing in middle, decreasing in distal content and increasing again in fecal samples (Figure 2-15). Moreover, an enzyme was identified by Reilly *et al.* performing the conjugation of FAs with taurine and was called acyl-coenzyme A:amino acid N-acytransferase (ACNAT) which is localized in peroxisomes and expressed in liver and kidney (Reilly, O'Shea et al. 2007). They showed successfully taurine conjugation of different chain varying acyl-CoAs, including C10:0, C12:0, C14:0, C16:0, C18:0, C20:0 and C24:0 Acyl-CoAs, with preferences for the C18:0 acyl chain. Moreover, ACNAT could use BAs CoAs as substrates with lower conjugation rates compared to FAs CoAs.

2.3.4.4 Bile acids patterns in *db/db* mice

As discussed above in chapter 2.3.2.1, the deregulation of the enzyme cholesterol 7 α-hydroxylase could show different patterns of cholesterol metabolites in the intestinal samples between *db/db* and *wt* mice (Figure 2-5, Figure 2-6 and Figure 2-7). In addition, the KEGG pathway analyses of fecal samples revealed that the primary bile acid biosynthesis pathway showed a high number of significantly assigned mass signals, shown in chapter 2.3.3.1 and in Figure 2-10. We could find eight different C_{24} BAs that were increased in *db/db* mice and two BAs cholic acid and ketodeoxycholic acid (ketoDCA) were decreased in *db/db* mice compared to *wt* mice (Figure 2-16).

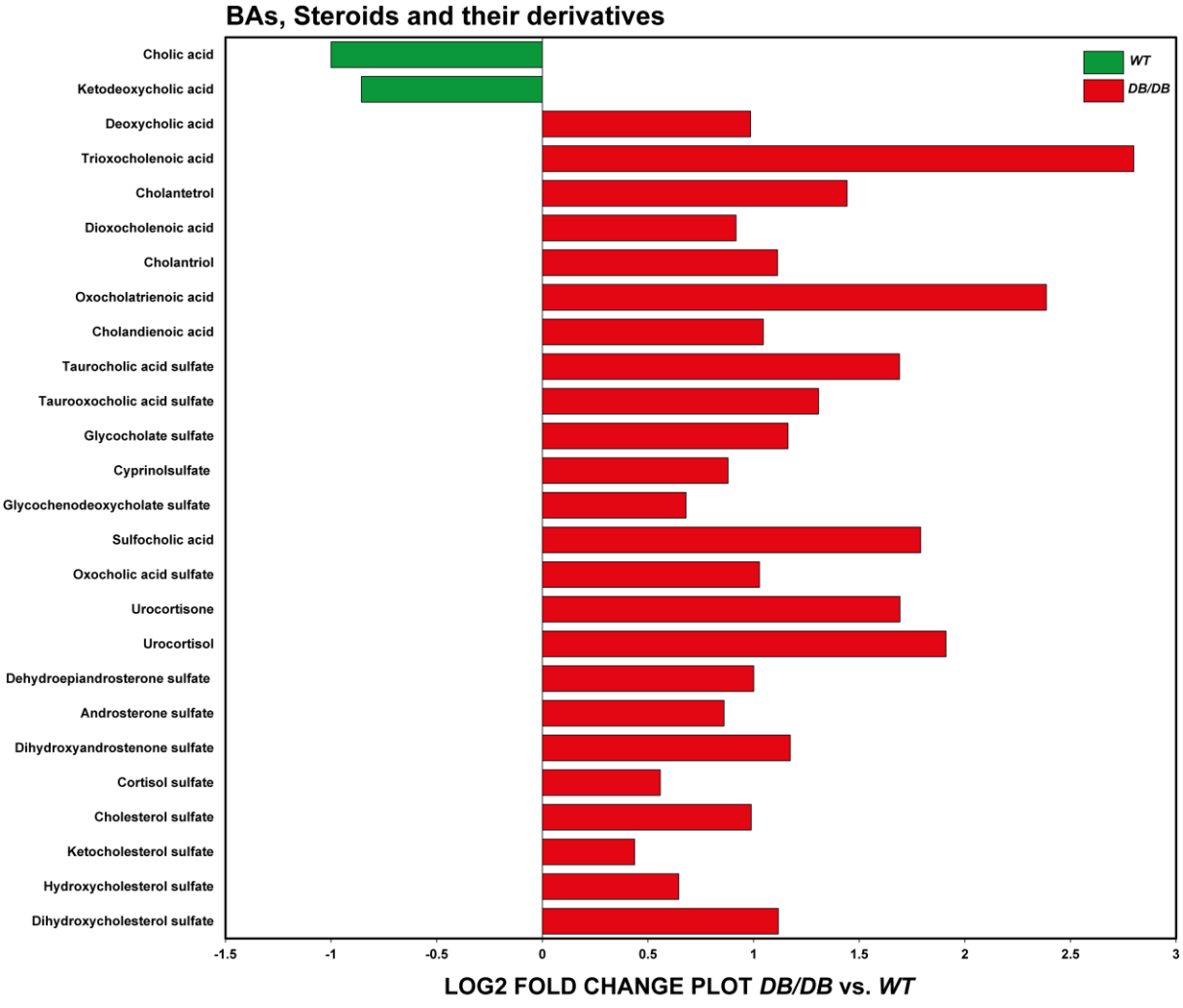

Figure 2-16 Fold change plot of bile acids, conjugated bile acids (sulfates) and sulfate conjugated steroids changed between *db/db* and *wt* mice in fecal samples: all displayed metabolites were significant with a p-value <0.05 (Mann-Whitney test), detailed information are given Table 16 of appendix (Chapter 6)

The BAs were DCA (MS/MS spectrum in Figure 5-4, A), ketoDCA (MS/MS spectrum in Figure 5-4, B), trioxocholenoic acid, cholantetrol, cholantetrol, dioxocholenoic acid, oxocholatrienoic acid and cholandienoic acid. Moreover, sulfate conjugates of taurocholic acid (MS/MS spectrum in Figure 5-5, A), taurooxocholic acid (MS/MS spectrum in Figure 5-5, B), cholic acid (MS/MS spectrum in Figure 5-5, C), oxocholic acid (MS/MS spectrum in Figure 5-5, D), cyprinol (MS/MS spectrum in Figure 5-5, F), glycochehodeoxycholic acid and glycocholic acid were throughout significantly increased in *db/db* mice (Figure 2-16). As mentioned above in chapter 2.3.2.1, several cholesterol metabolites but also their sulfate conjugates were increased in the intestine of *db/db* mice (Figure 2-16). We could detect raised levels of urocortisol and urocortisone as cholesterol sulfate (MS/MS spectrum in Figure 5-5, E), ketocholesterol sulfate, hydroxy- and dihydroxycholesterol sulfate and further sulfate steroid-metabolites including dehydroepiandrosterone, androsterone, dihydroxyandrosterone and cortisol (Figure 2-16). A difference of cholic acid (CA) was already shown for *db/db mice*, *ob/ob* mice and streptomycin treated mice, which were caused by alteredCYP7A1 levels. These were regulated by food intake (Li, Owsley et al. 2010). Studies with human subjects with T2DM revealed that BAs metabolism is in fact an important pathway and metabolites including DCA and CA were changed due to T2DM (Brufau, Stellaard et al. 2010, Zhao, Fritsche et al. 2010). The treatment of diabetic mice with cholic acid decreased significantly the blood glucose levels in *db/db* mice (Jiang, Wang et al. 2007). Different steroids and BAs are found to be conjugated with sulfate and revealed different patterns in diabetic mice. The formation of sulfate metabolites is performed by different sulfotransferases (SULTs) exhibiting substrate specificities and affinities (Klaassen and Boles 1997, Alnouti 2009). Interestingly, in our study dehydroepiandrosterone sulfate (DHEAS) was increased in *db/db* mice, but feeding experiments of DHEA and DHEAS could prevent the diabetic status in the mouse strain assuming negative feedback through oral administration of DHEA on systemic synthesis and regulation of DHEA (Coleman, Leiter et al. 1984). Steroid sulfotransferases are responsible for controlling the activity of steroids such as androgens and estrogens. In male *db/db* mice DHEA sulfotransferase (SULT2A1) activity was shown to be suppressed but estron sulfotransferasase (SULT1E1) was increased (Leiter, Chapman et al. 1991). In our study, sulfate conjugates of steroids were overall significantly increased in the diabetic mouse strain in fecal samples. For example BAs sulfate conjugation is also performed by SULT2A1 which possesses a broad substrate specificity (Alnouti 2009). The dysregulation of the mentioned SULTs reflects thereof the significant differences of the sulfated steroids and bile acids, measured in the diabetic mice. BA sulfates were found to be

elevated in urine and serum samples of patients with hepatobiliary diseases and in inflammatory bowel diseases in conjunction with altered microbial community (Makino, Shinozaki et al. 1974, Duboc, Rajca et al. 2012). We are assuming that this major dysregulation of sulfur containing metabolites also impacts the microbial community in diabetic mice, which needed to be validate The ability of sulfate de-conjugation of BAs was already indicated for example in *Clostridium spp.* (Van Eldere, Robben et al. 1988).

2.3.4.5 Arachidonic acid metabolism in *db/db* mice

As already mentioned above in Figure 2-10, arachidonic acid metabolism revealed the highest proportion of significant mass signals between *db/db* and *wt* mice in feces samples. Many metabolites of AAM are isomers and the comparison resulted in 16 different molecular species, shown in Figure 2-10, including different prostaglandins classes such as prostaglandins, prostacyclines and leukotrienes. These compounds are exhibiting many important biological functions and play an essential role in mediating inflammation (Ricciotti and FitzGerald 2011). Thus, rapid degradation of active compounds is important in order to avoid the prolonged biological response, thus detecting prostaglandins, which are very unstable and rapidly converted *in vivo*, in fecal samples are very unlikely. The AAM pathway consists of 75 different compounds, whereas 19 compounds do differ by their different molecular composition. Some of the mass signals and isomers were excluded from further analyses because the enzymes were not given in the mouse species (KEGG database information). Rapid conversion or degradation was shown for Leukotriene A4, Leukotriene B4 (LTB4), different HPETEs, Prostaglandin H2, E2, D2, I2, Thromboxane A2, 15-Keto-prostaglandin F2alpha, Prostaglandin G2, Thromboxane B2 and Leukotriene B4 (Hamberg, Svensson et al. 1974, Kindahl, Edqvist et al. 1976, Fitzpatrick, Gorman et al. 1977, Fitzpatrick and Wynalda 1981, Pifer, Cagen et al. 1981, Jubiz, Rådmark et al. 1982, Davies, Bailey et al. 1984, Naccache, Molski et al. 1984, Peter, Bosu et al. 1987, Baumert, Huber et al. 1989, MacMillan and Murphycor 1995, Fiedler, Simon et al. 2001). This finally resulted in 8 metabolites with different elemental composition regarding arachidonic acid, hydroxyarachidonic acid (HETE), 2,3-dinor-8-iso prostaglandin F2α, 2,3-Dinor-8-iso prostaglandin F1α, hydroxyleukotriene B4 (OH-LTB4) and carboxyleukotriene B4 (COOH-LTB4) and such as 6-keto-prostaglandin E1 (6-Keto-PGE1) and 6-keto-prostaglandin F1α (6-keto PGF1α). These could be possible metabolites of AAM. In terms of the metabolite LTB4, two metabolites OH-LTB_4 and COOH-LTB_4 were compounds that resulted as intermediates in the degradation/deactivation pathway of LTB4 (Fiedler, Simon et al. 2001). LTB_4 is a

potent chemotactic agent produced from arachidonic acid via the 5-lipoxygenase pathway and converts granulocytes to an inflammatory state (Fiedler, Simon et al. 2001). The ω-oxidation of LTB_4 happens in the liver mediated by the cytochrome P450 system. OH-LTB_4 is oxidized to COOH-LTB_4 that is biologically inactive (Fiedler, Simon et al. 2001). Harper *et al*. could find further metabolites involved in the degradation of LTB_4 as a result of further ω-oxidation of the metabolite COOH-LTB_4 to COOH-dinor LTB_4 (Harper, Garrity et al. 1986). Shirley *et al*. found also that the metabolite COOH-dinor-LTB4 reacts with taurine for subsequent removal and excretion (Shirley and Murphy 1990). Prostacyclin is potent vasodilator and inhibits platelet aggregation, but this factor is very unstable and is rapidly converted to 6-keto PGF1α and oxidized to 6-keto-PGE1.This deactivation pathway has been determined for few organisms (Pace-Asciak, Carrara et al. 1977, Sun and Taylor 1978, Rosenkranz, Fischer et al. 1980). Infusion experiments of 6-keto-PGF1α (1) revealed further oxidation steps including ß- and ω-oxidation of this metabolite (Figure 2-17) that resulted in identification of two new metabolites called 2,3-dinor, 6-keto-PGF1α (2) and dinor ω-1-hydroxy-6-keto-PGF1α (3). The reaction can be followed by further oxidation of the hydroxylgroup of dinor ω-1-hydroxy-6-keto-PGF1α to dinor ω-1-oxo-6-keto-PGF1α (3) as an intermediate to a further oxidation resulting in a carboxylgroup at the ω-end of the side chain, resulting in COOH-2,3-dinor 6-keto-PGF1α (4).

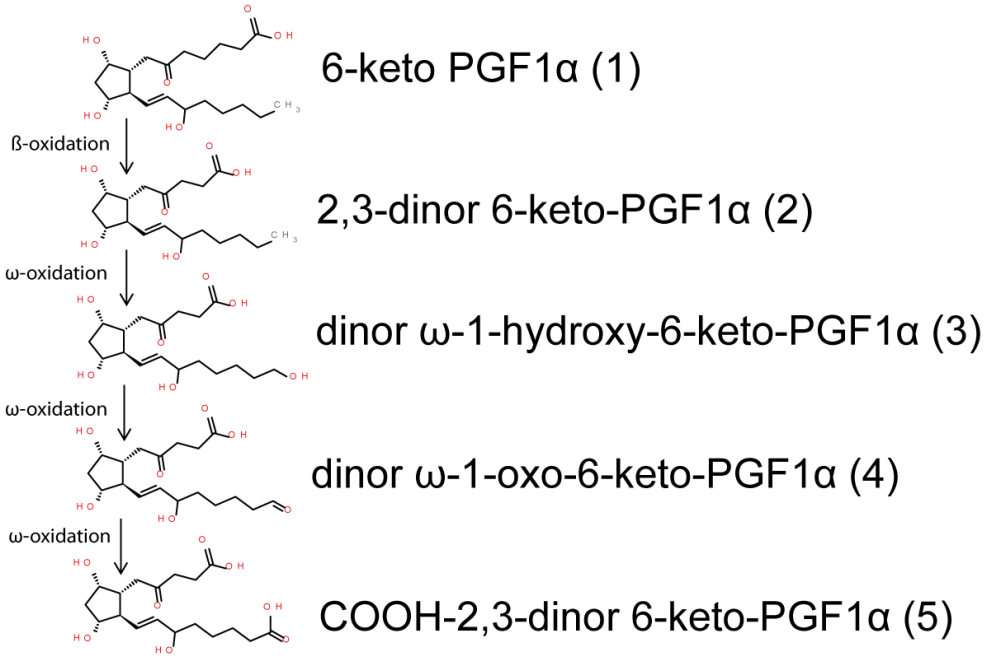

Figure 2-17 An example of four step reaction by ß- and ω-oxidation of the AAM metabolite 6-keto PGF1α (1) to COOH-2,3-dinor 6-keto-PGF1α (5)

Moreover, the metabolite can undergo further ß-oxidation step to tetranor-PGF1α by further hydroxylation to hydroxy-tetranor-PGF1alpha and dehydrogenation to tetrahydroxyprostanoic acid. All possible metabolites derived from different oxidation steps and that we found are summarized in heatmap, showing also the behavior of the metabolites between *db/db* and *wt* mice that were in total significantly increased in *db/db* mice (Figure 2-18).

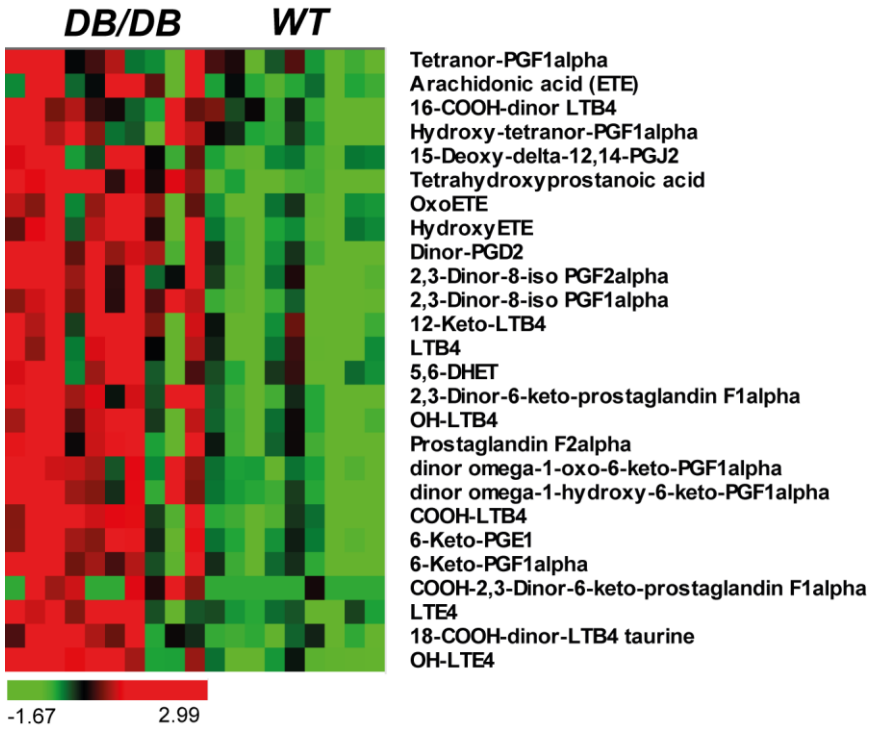

Figure 2-18 Summary of arachidonic acid pathway and their metabolites found in fecal samples of *db/db* and *wt* mice: all metabolites were significantly changed between *db/db* and *wt* mice with a p-value <0.05 (Mann-Whitney test), detailed information are given Table 16 of appendix (Chapter 6)

As mentioned for the metabolite 6-keto-PGF1α that ß- and ω-oxidation are possible reaction steps in the prostaglandine metabolism, we investigated other metabolites of AAM, possibly metabolized by ß- or ω-oxidation pathway. Furthermore, we were observing whether taurine conjugates of AAM metabolites were found in the samples since taurine conjugates of COOH-dinor $LTB_{4,}$ HETE and DiHETEs were already reported before (Shirley and Murphy 1990, Turman, Kingsley et al. 2008). The latter two metabolites are derived through oxidation of N-arachidonoyltaurine in a lipoxygenase (LOX) dependent manner (Turman, Kingsley et al. 2008). Also, we were searching for sulfate conjugates hence sulfate conjugation is one of major pathway of phase 2 reaction of CYP450 systems (Klaassen and Boles 1997, Alnouti 2009). In general, a ß-oxidation is an enzymatic catalysis of fatty acids, resulting in a

shortening of a C_2H_4 unit. The ω-oxidation is an oxidation of methyl group to a carboxyl group at the end of a side chain of a FA. Taurine and sulfate conjugation are enzyme catalyzed reactions performed for metabolites such as bile acids, drugs but also fatty acids such arachidonic acid (Klaassen and Boles 1997, Saghatelian, Trauger et al. 2004, Alnouti 2009). Moreover, in chapter 2.3.4.3 we could show that several NATs of FAs changed between *db/db* and *wt* mice. Thus, maybe taurine conjugation is also occurring for AAM metabolites.

2.3.5 Mass difference analyses to reveal arachidonic acid co - metabolites applying NetCalc

To extrapolate new metabolites of AAM pathway we applied a new approach the so-called mass difference analysis. Therefore we generated a mass difference list with exact mass differences for ß-oxidation ($-C_2H_4$; 28.0313), ω-oxidation (introduction of O_2 and reduction of H_2: +29.974174), taurine ($+C_2H_5NOS$: +107.0041) and sulfate ($+SO_3$: 79.956816) conjugation. By using this approach, we can found direct links that were connected through these mass differences and reveal thereof new metabolites. The calculation of mass difference was defined within a narrow error range of 0.2 ppm, which is a unique possibility of FT-ICR-MS measurements. The use of four mass differences resulted in highly disconnected network. Therefore, we enlarged the network calculation by using 22 different mass differences (as described in chapter 4.5.3). We filtered all metabolites from AAM metabolism (29 metabolites) and their respective mass signals, described in 4.5.3 and a mass difference network was generated, shown in Figure 2-19. All red nodes are metabolites from AAM pathways surrounding by different nodes (representing other mass signals). The size of nodes indicates the number of found connections (big node: high number of connections). The network was done by Yifan Hu algorithm (see details in chapter 2.3.8).

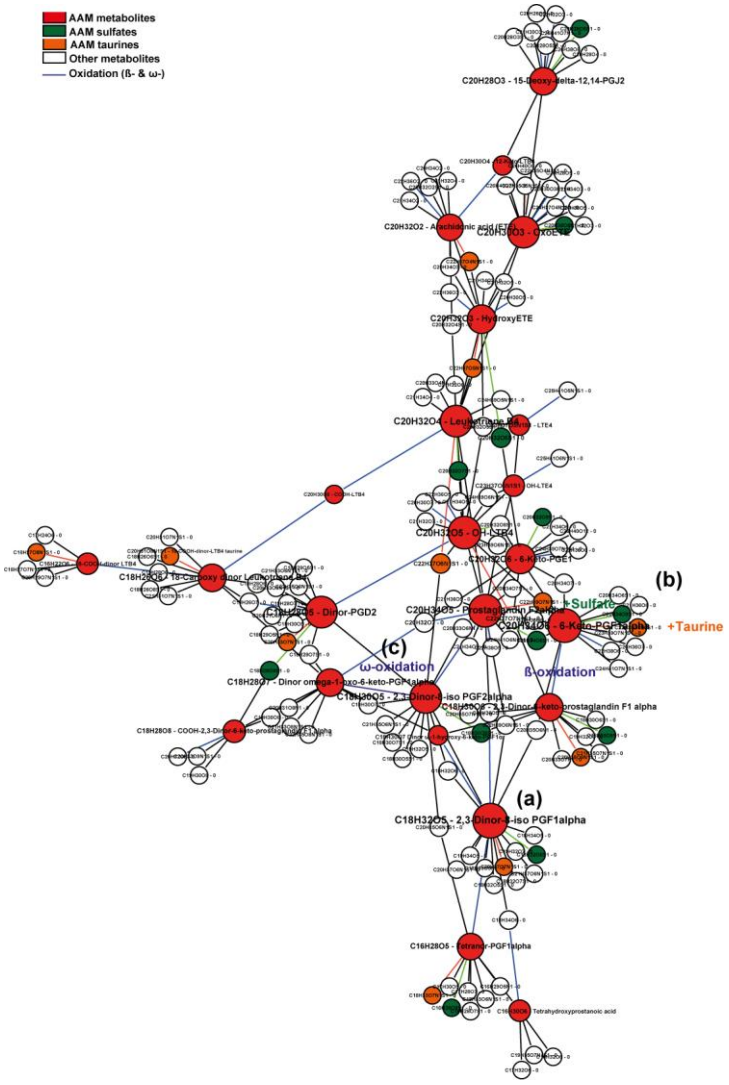

Figure 2-19 Mass difference analysis and network visualization for discovery of novel AAM metabolites; nodes are representing the metabolites, edges the mass differences; red nodes are metabolites from AAM, green nodes are sulfate conjugates of AAM metabolites, orange nodes are taurine conjugates of AAM metabolites, the mass difference of ß- and ω-oxidation is highlighted through blue edge color, sulfate conjugation through green colored edges and taurine through orange colored edges

The node 2, 3-dinor, 6-keto-PGF1α (a) is an example of a node with highest amount of connections: 18 connections from 22 possible connections. We could also find the searched mass differences for ß- and ω-oxidation (blue line), sulfate (green nodes) and taurine (orange nodes) conjugation. An example of such connections is shown for 6-Keto PGFα (b) which contains three connections of ß-oxidation, sulfate and taurine conjugation shown in Figure 2-19. A ω-oxidation step is demonstrated for 2, 3-Dinor-8-iso-PFGα to Dinor ω-keto-PGFα (c) (Figure 2-19). By using this approach, we could show that several sulfate and taurine

metabolites of AAM pathway were found in fecal matrices. Moreover, these new conjugates revealed a significantly differential behavior between *db/db* and *wt* mice, summarized in the heatmap of Figure 2-20.

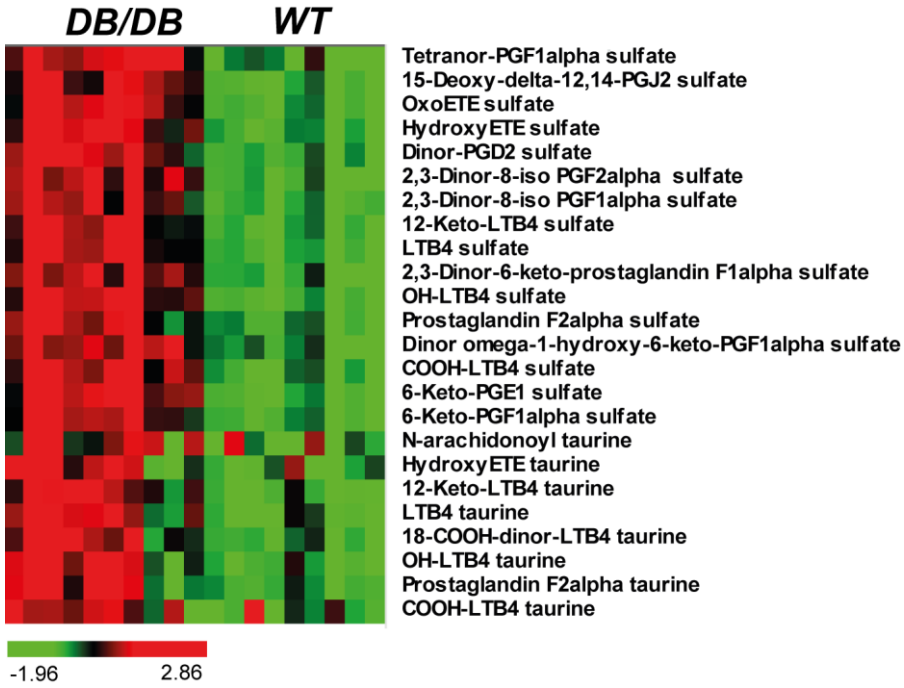

Figure 2-20 Heatmap of sulfate and taurine conjugates of AAM metabolites that differ significantly between *db/db* and *wt* mice in fecal samples; all displayed metabolites were significant with a p-value <0.05 (Mann-Whitney test), detailed information are given Table 16 of appendix (Chapter 6)

We could describe 16 different sulfate conjugates and 8 different taurine conjugates of AAM metabolism (Figure 2-20). Additionally, we could confirm two conjugated metabolites such as 2, 3-Dinor-8-iso prostaglandin F1alpha sulfate and 15-Deoxy-delta-12,14-PGJ2 sulfate by MS/MS experiments (MS/MS spectra in Figure 5-6 A and B). As discussed above taurine conjugates were already d for COOH-dinor $LTB_{4,}$ HETE and DiHETEs (Shirley and Murphy 1990, Turman, Kingsley et al. 2008). We could confirm and find that sulfate conjugates play an important role in metabolism of AAM pathway and were increased in diabetic mice. Another possibility is to map the new metabolites into KEGG metabolic pathways. As an example, we selected therefore the sulfate conjugation.

2.3.5.1 KEGG metabolic pathway enrichment analysis – sulfate conjugation

Another approach to determine new metabolites is to use the mass signals and subtracted each mass signal from the theoretical mass of SO_3 (- 79.956816). All subtracted mass signals were then uploaded for a new annotation in MassTRIX. We derived new annotated mass signals and their annotated putative metabolite name. The pseudo-annotated metabolites can now be mapped into metabolic pathways of KEGG to illustrate which metabolites are sulfate conjugated. Furthermore, we took two different species *Mus musculus* (MMU) as the host and *Bacteriodetes vulgatus* (BVU) as one of the representative of the gut microbiome, which is in fact very restrictive (gut microbiome ~ 500 species). For the mapping, we excluded all isomeric compounds and counted the number of the mass signals. For comparison, we used also the results from "normal" annotation step and compared these metabolites against the pseudo-annotated metabolites (+/- SO_3: shown in Figure 2-21

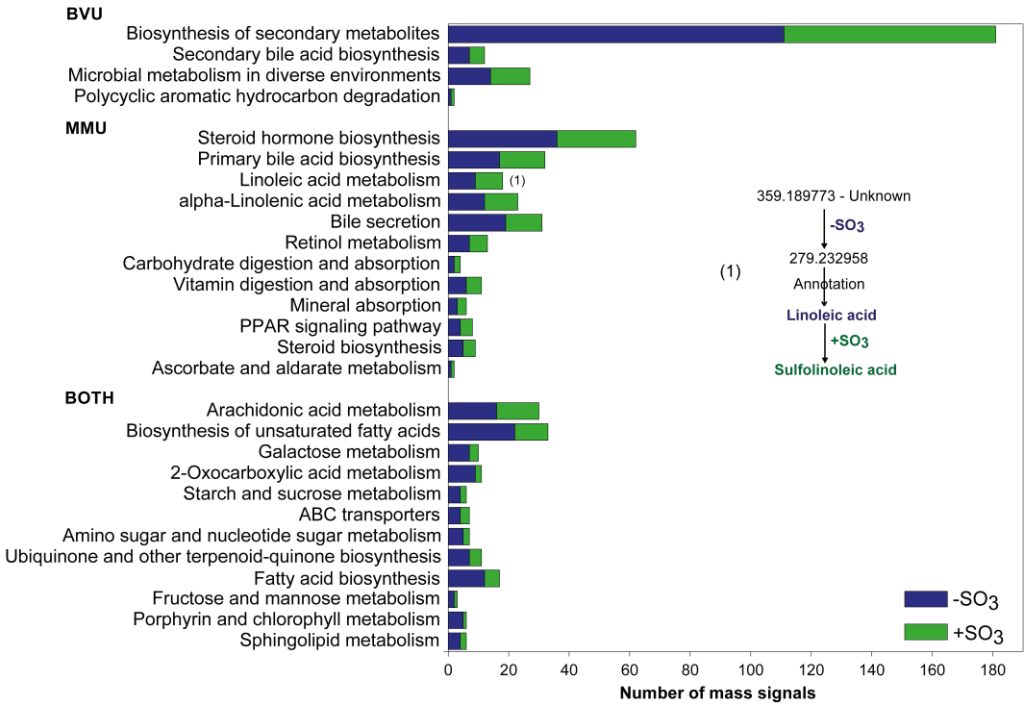

Figure 2-21 KEGG metabolic pathway enrichment with sulfate conjugates: blue bars are annotated metabolites, green bars metabolites that were found by an in-silico subtraction of SO_3; green bars are annotated metabolites that were found after subtraction: one example is shown for the linoleic acid metabolism – (1): the mass signal in neg. mode with the experimental mass of 359.189773 was an unknown with molecular formula of $C_{18}H_{32}O_5S$, the subtraction of SO_3 (-79.956816) resulted in mass of 279.232958 which was annotated as linoleic acid, resulted in sulfolinoleic acid after respective SO_3 addition

The mapping resulted into 28 different metabolic pathways (MP), whereas 12 pathways were matched for both organisms, 12 other MPs were exclusively found in MMU and 4 MPs in BVU (Figure 2-21). Sulfate conjugated metabolites could be mapped into different pathways predominantly in AAM, steroid hormone biosynthesis, biosynthesis of unsaturated fatty acids and biosynthesis of secondary metabolites, whereas biosynthesis of secondary metabolites represents different pathways. For example, the sulfated metabolites of AAM we already described in Chapter 2.3.5. A large of number of sulfated metabolites of primary BA biosynthesis we also already described in Chapter 2.3.4.4. Interestingly, we could find that amongst AAM pathway other fatty acids metabolic pathways were also playing an important role due to sulfate conjugation such as the linoleic acid metabolism (9 different metabolites with different mass signals). Taken linoleic acid metabolism, we illustrated the procedure for the in-silico deconjugation, shown in Figure 2-21 (1). The mass signal with experimental mass of 359.189773 in (-) FT-ICR-MS mode could not be annotated before and was determined as an unknown (see chapter 4.5.4). The subtraction with $-SO_3$ (79.956816) resulted in 279.232958, which could be successfully annotated in MassTRIX as the metabolite linoleic acid and was mapped into the respective pathway. Additionally, we could confirm that the unknown metabolite is sulfolinoleic acid, described in chapter 2.3.6.1. This approach can be very helpful to get further information about this mass signal, highly discriminative for the diabetic mice (S-Plot, Figure 2-9). Additionally, this assists to reveal and to describe new metabolites such as sulfate conjugates. For this is important to elaborate and to know which kind of conjugation steps could occur in the specific matrices.

2.3.6 Novel sulfur containing metabolites in *db/db* mice

2.3.6.1 Sulfate conjugated metabolites: oxylipins sulfates

As described above with KEGG metabolic pathway analysis one of most discriminant mass signals shown in the S-Plot (Figure 2-9), separating *db/db* and *wt* mice was a sulfated metabolite $[M-H]^-$. 359.189773. The molecular formula is $C_{18}H_{31}O_5S^-$ (neutral molecular formula, $C_{18}H_{32}O_5S$). Identification experiments applying MS/MS approach (MS/MS spectrum in Figure 5-7, A) could show a loss of HSO_3, indicating that this mass signal is identified as a fatty acid containing a sulfate (as assumed in Chapter 2.3.5.1), named sulfolinoleic acid (found by molecular formula search in PubChem) (Figure 2-23, C). This metabolite is highly discriminant between *db/db* and *wt* mice and increased in fecal samples of diabetic mice. The behavior of sulfolinoleic acid in the intestinal samples of *wt* and *db/db*

mice is shown in Figure 2-23. The metabolite is very highly abundant due to high intensity values ($x10^{10}$) and is significantly changed in distal and feces samples but the changes were more pronounced in fecal samples (Figure 2-23).

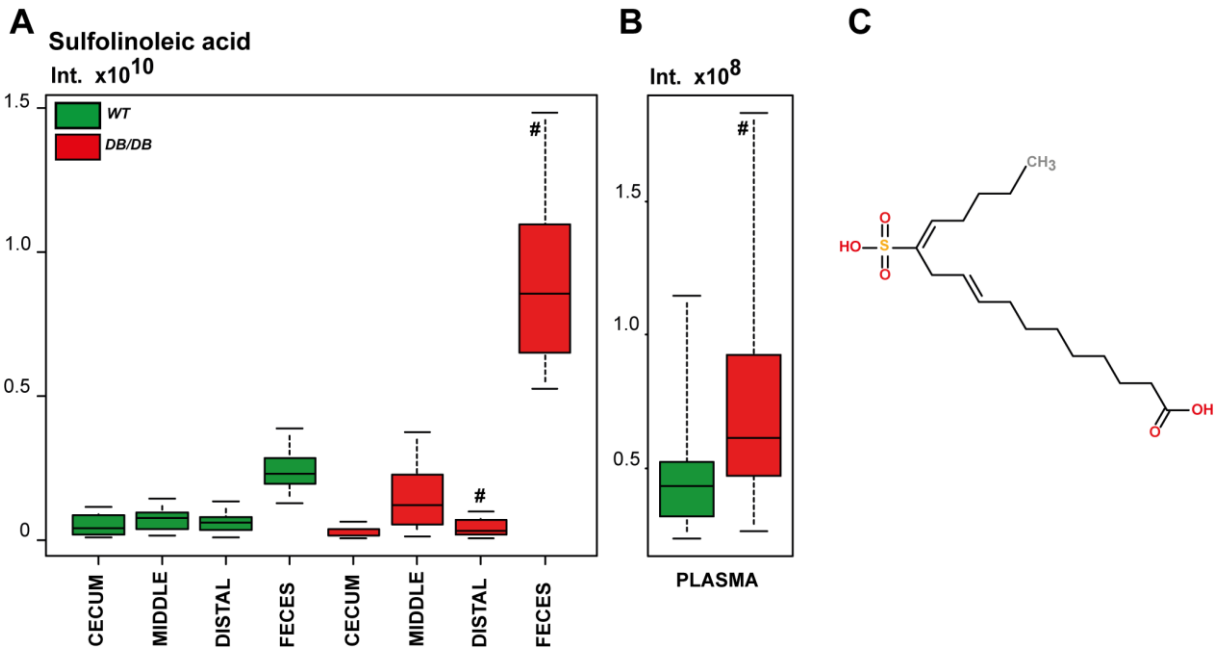

Figure 2-22 A: Sulfolinoleic acid pattern in all four intestinal samples from *wt* and *db/db* mice; B: Sulfolinoleic acid pattern in plasma samples in *wt* and *db/db* mice C: Most plausible structure of sulfolinoleic acid found in PubChem; detailed information are given Table 16 of appendix (Chapter 6)

Moreover, we could also find the same mass signal in plasma samples, significantly increased in *db/db* mice (Figure 2-23, B). With the information of possible sulfated metabolites (especially sulfated FAs), we performed further MS/MS experiments with a predefined precursor list of all possible sulfate conjugates derived through subtraction of SO_3. Then we searched the MS/MS spectra for the typical fragments of HSO_3 and neutral losses of SO_3 in our performed MS/MS experiments. We could find five other sulfate conjugates of oxylipins such as hydroxylinoleic acid sulfate (MS/MS spectrum in Figure 5-7, C), hydroxylinolenic acid sulfate (MS/MS spectrum in Figure 5-7, D), dihydroxylinoleic acid sulfate (MS/MS spectrum in Figure 5-7, D), dihydroxyoleic acid sulfate (MS/MS spectrum in Figure 5-7, E) and also a unique nonadecadienoic acid sulfate (MS/MS spectrum in Figure 5-7, B), that were all increased in *db/db* mice (Figure 2-23).

2.3.6.2 Taurine conjugated metabolites: oxylipins taurines

The same MS/MS screening approach used above, we performed also for the specific loss of taurine of $C_2H_6NO_3S^-$ [124.0070] and we found six different oxylipins. They were hydroxylinolenic acid taurine (MS/MS spectrum in Figure 5-8, A), hydroxylinoleic acid taurine (MS/MS spectrum in Figure 5-8, B), hydroxyoleic acid taurine (MS/MS spectrum in Figure 5-8, C), dihydroxystearic acid taurine (MS/MS spectrum in Figure 5-8, D), dihydroxyeicosadienic acid taurine (MS/MS spectrum in Figure 5-8, E) and dihydroxyeicosanoic acid taurine (MS/MS spectrum in Figure 5-8, F). All taurine conjugates of oxylipins, except hydroxylinolenic acid taurine and hydroxylinoleic acid taurine, were increased in *db/db* mice (Figure 2-23).

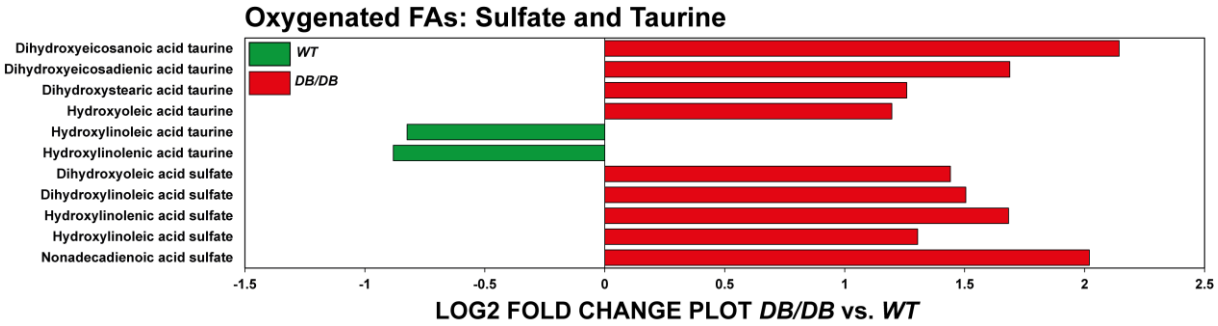

Figure 2-23 Fold change plot of sulfate and taurine conjugates of oxylipins, especially oxylipins; all displayed metabolites were significant with a p-value <0.05 (Mann-Whitney test), detailed information are given Table 16 of appendix (Chapter 6)

2.3.6.3 Other N-acyl Fatty acids with amino acids

We could identify different types of fatty acids conjugate with taurine and sulfate playing an important role in discriminating *db/db* and *wt* mice. Several other n-acyl amino acids were significantly changed. We filtered all mass signals of possibly annotated N-acyl fatty acids and subjected them to MS/MS experiments ((MS/MS spectrum in Figure 5-9, A-B)). We could successfully identify three different fatty acid conjugated with amino acids (Figure 2-24), including N-palmitoyl valine (Figure 2-24, A) significantly increased in fecal and decreased in distal samples of *db/db* mice. Additionally, we could find N-oleoyl (iso)leucine (Figure 2-24, B) and N-palmitoyl (iso)leucine (Figure 2-24, C) that were significantly decreased in distal samples of *db/db* mice and showed an increased tendency in fecal samples of *db/db* mice for N-oleoyl (iso)leucine and decreased tendency for N-palmitoyl (iso)leucine.

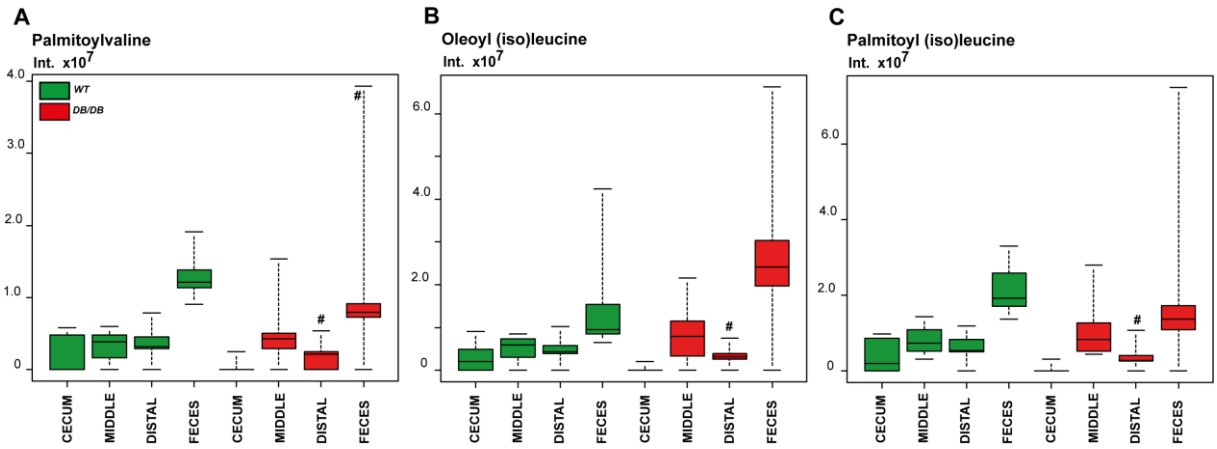

Figure 2-24 N-acyl conjugated amino acids and their patterns in four intestinal matrices comparing *wt* and *db/db* mice, # p-value <0.05 (Mann-Whitney test), detailed information are given Table 17 of appendix (Chapter 6)

2.3.7 Plasma changes between *db/db* and *wt* mice based on KEGG metabolic pathway analyses

This work is focused on metabolome differences in terms of intestinal samples; still we want to describe the plasma metabolite differences between *db/db* and *wt* mice. For this approach, we selected all metabolites, which were significantly changed between *db/db* and *wt* mice. Subsequently we mapped them into KEGG metabolic pathways. Most of mapped metabolites were increased in *db/db* mice and different pathways were involved in the differentiation. The pathways are displayed in the fold change plot, shown in Figure 2-25, A.

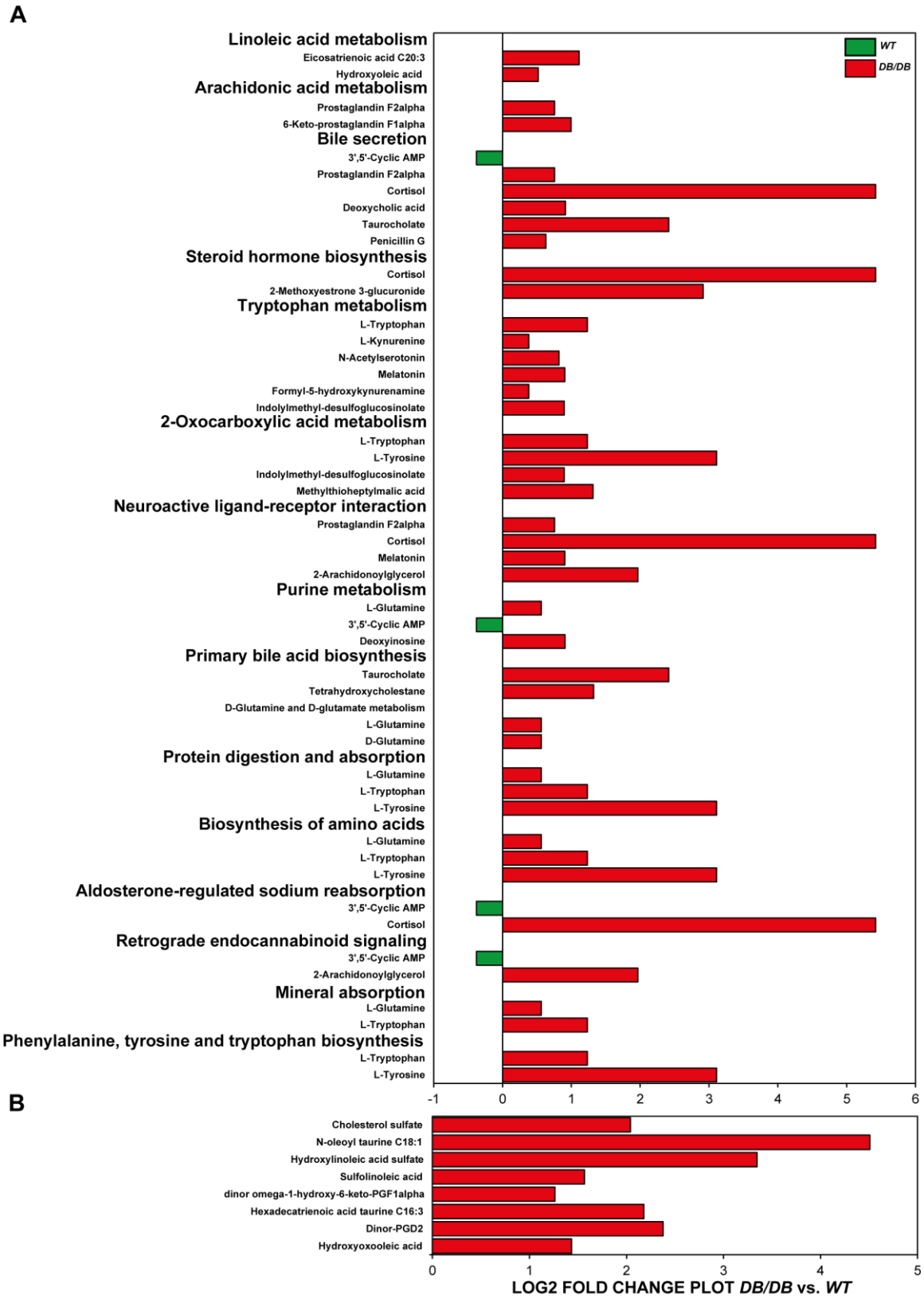

Figure 2-25: A Plasma metabolome changes between *db/db* and *wt* mice based on KEGG metabolic pathway comparison; B: Other metabolites significantly changed between *db/db* and *wt* mice; all displayed metabolites were significant with a p-value <0.05 (Mann-Whitney test), detailed information are given Table 18 of appendix (Chapter 6)

Several metabolites including AAM metabolites, BAs and FAs were increased in *db/db* mice, shown in Figure 2-25. Only 3',5'-cyclic AMP was increased in *wt* mice, involved in four different metabolic pathways of KEGG. Observing the metabolites that were additionally described in fecal metabolome we could elaborate eight different metabolites that were increased in *db/db* mice including sulfolinoleic acid as described in chapter 2.3.6.1, also cholesterol sulfate or the NAT of oleic acid, shown in Figure 2-25, B.

2.3.8 Correlation studies and mass difference analyses between fecal and plasma samples of *db/db* mice

2.3.8.1 Correlation studies between feces and plasma samples

For this approach, we used all mass signals that were significant between *db/db* and *wt* mice concerning feces (brown) but also plasma (pink) samples, measured in negative mode. We performed a NetCalc molecular formula calculation resulting in 1619 molecular formulas with elemental composition (CHNOSP). We performed a Pearson correlation between fecal and plasma mass signals to extrapolate the mass signals that correlate highly between the different matrices. We plotted that correlations that represents the top ten that correlate positive with each other (green) or negatively (orange), shown in Figure 2-26. For positive correlation, all mass signals significantly increased in *db/db* mice in both matrices. For negative correlation, mass signals from fecal samples were significantly increased in *wt* mice and in plasma samples, whereas all involved mass signals were significantly increased in *db/db* mice (Figure 2-26). Most signals we could only annotate by their molecular formula, except fatty acids significantly increased in *wt* mice of fecal samples. As an example we plotted the most negative and positive correlated metabolites from fecal and plasma samples in order to illustrate the behavior the metabolite in the matrices. In Figure 2-26 (1) the fecal metabolite nonadecanoic acid and the plasma metabolite with molecular formula of $C_{20}H_{30}O_9$ is shown and their behavior between *db/db* and *wt* mice. In Figure 2-26 (2) a positive correlation between the fecal metabolite with molecular formula $C_{27}H_{43}O_8N_1S_1$ and the plasma metabolite with molecular formula of $C_{32}H_{60}O_6$, showing similar behavior of both metabolites in *wt* and *db/db* mice in both matrices.

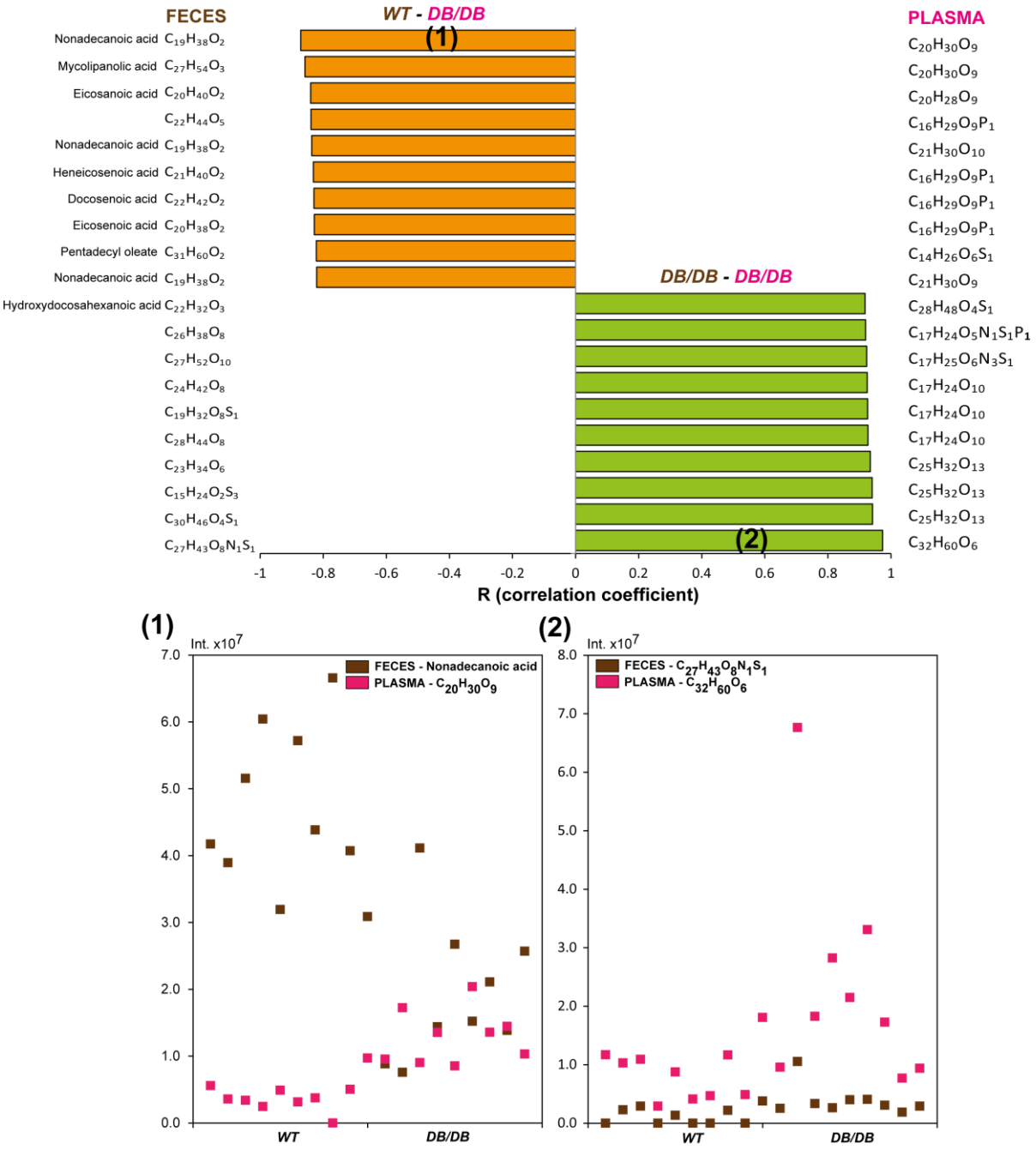

Figure 2-26 Pearson correlation studies between feces (brown) and plasma (pink) metabolites of *db/db* and *wt* mice; mass signals that were not annotated are given by their molecular formula; all displayed metabolites were significant with a p-value <0.05 (Mann-Whitney test) between db/db and *wt* mice; On the left side metabolites from feces and right side metabolites from plasma are displayed; Orange plots are negative correlating metabolites between feces and plasma and their respective correlation coefficient (R), Green plots show positive correlation between feces and plasma metabolites; (1) Detailed plot about the strongest negative correlation between fecal and plasma metabolites of nonadecanoic acid and $C_{20}H_{30}O$; (2) Detailed plot about the strongest positive correlation between fecal and plasma metabolite of $C_{27}H_{43}O_8N_1S_1$ and $C_{32}H_{60}O_6$

2.3.8.2 Mass difference analyses between fecal and plasma samples

For this approach, we took all mass signals that were significant between *db/db* and *wt* mice concerning feces but also plasma samples, measured in negative mode. We performed a mass difference analyses using NetCalc software that resulted in 1619 molecular formulas with elemental composition (CHNOSP). For the mass difference analyses, we selected 22 different mass differences, including mass differences such as taurine and sulfate conjugation shown in Table 11. We could find 4851 different edges between the 1619 mass signals. The overall abundance of the counted mass differences is shown in Figure 2-27.

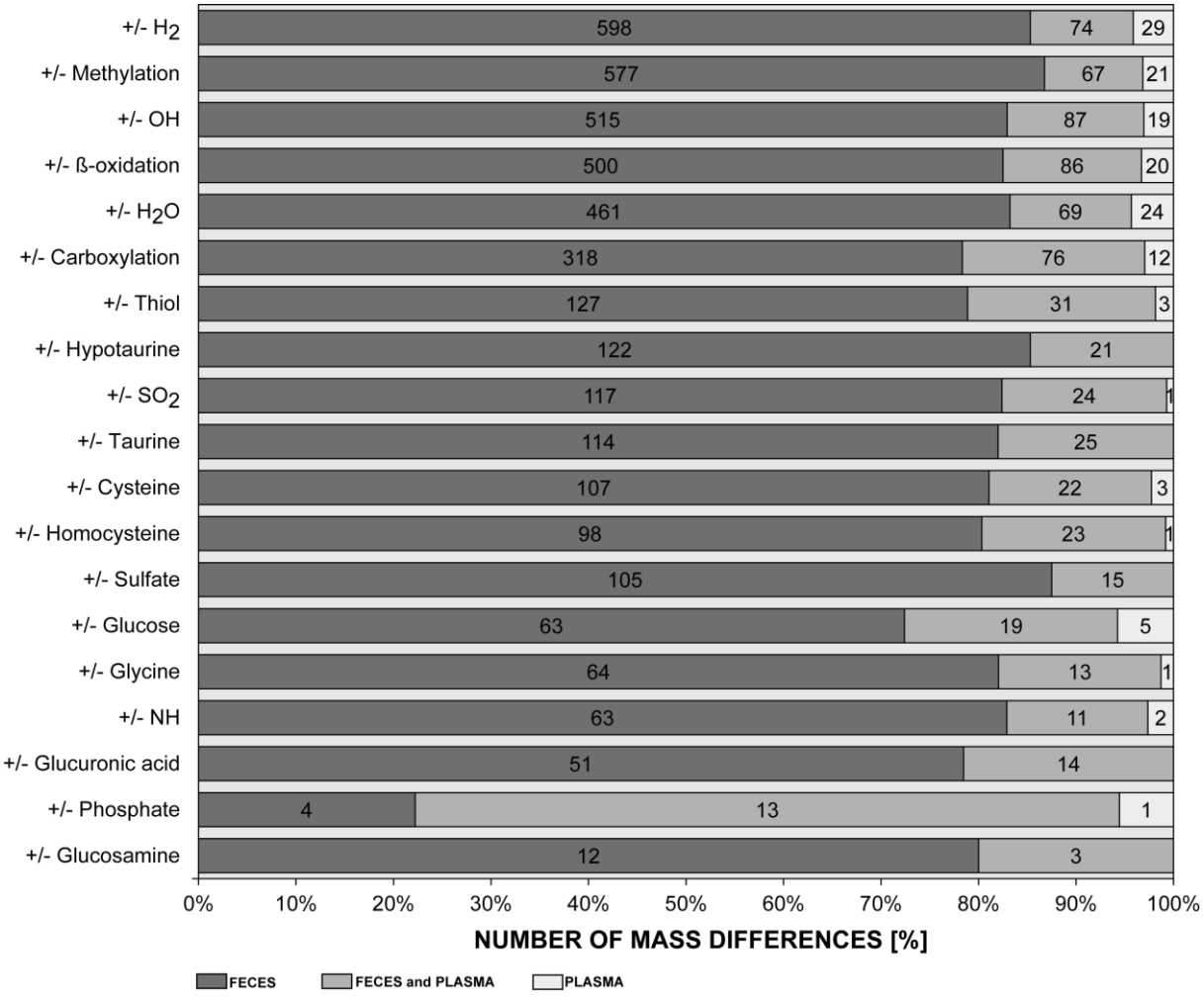

Figure 2-27 Count of mass differences found by mass difference analyses of mass signals significant between *db/db* and *wt* mice solely between fecal mass signals in dark grey, between fecal and plasma mass signals in grey and uniquely between plasma mass signals in light grey

The highest count of mass differences was found between mass signals of fecal samples (4016), between fecal and plasma mass signals we found 693 connections and 142 connections were found plasma-plasma mass signals. This is due to that 1375 mass signals

were originated from fecal data matrix and 244 mass signals from plasma samples. Furthermore, the mass differences reference list is generated based on the knowledge derived from handling with mass signals and data matrices from intestinal samples and not plasma samples. This should be adapted appropriately, which was not a part of this work. Next, we took the data matrix containing mass signals and their connections, appeared between fecal and plasma samples to visualize the connections by using a mass difference based network approach. A mass difference network is a network consisting of nodes (mass signals) and edges (mass differences such as +/- sulfate), that were generated by NetCalc calculations. Afterwards you obtain a simple list consisting of mass signals, including source and target nodes (mass signals, Table 11) connected by edges which are weighted through the different mass differences. We were using Gephi 0.8.1 beta version (Bastian, Heymann et al. 2009), an open source network visualization software package, allowing visualizing complex and highly connected networks such as a generated mass difference networks. Herein, we used the Yifan Hu algorithm, which simply attract highly connected nodes (also represented by the size of the nodes, big nodes) and repulse less connected nodes (small nodes). The generated graph is shown in Figure 2-28, consisting of two large sub graphs emerged by the Yifan Hu algorithm. The graph is colored by matrices type: feces (green nodes) and plasma (red nodes) and common mass signals are highlighted through blue colored nodes.

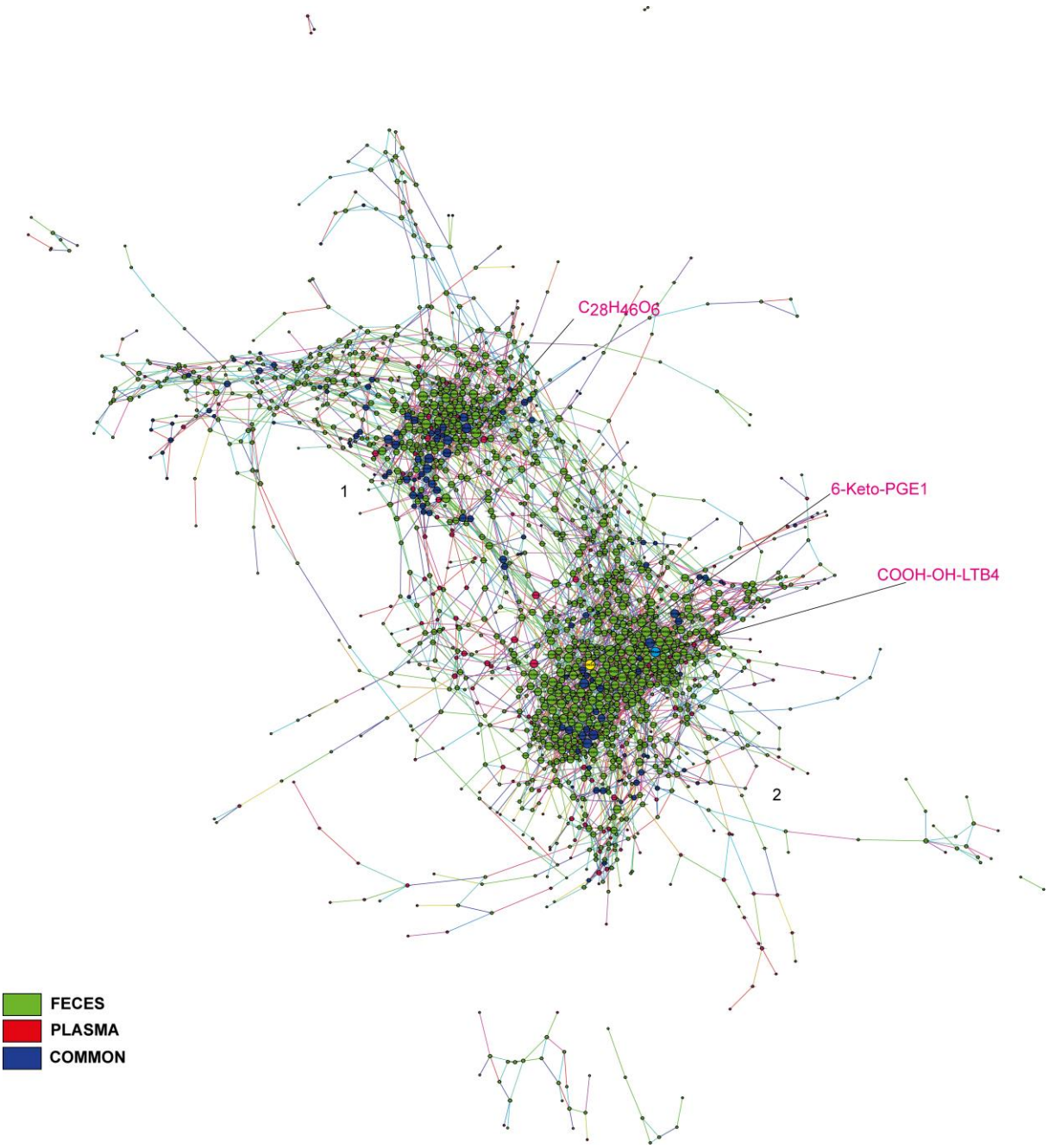

Figure 2-28: Mass difference network between mass signals of feces samples and plasma samples, green nodes representing mass signals from feces samples and red nodes representing mass signals from plasma samples, blue nodes are common shared mass signals

The generated network is mainly dominated by green nodes originating from mass signals of fecal samples. The node with the highest amount of edges (20 found mass differences) was found in feces samples and was 6-Keto-PGE1 (yellow node: $[M-H]^-$: 367.212623; $C_{20}H_{32}O_6$) a metabolite from AAM pathway. The highest connected node in plasma samples was COOH-OH-LTB4 (lightblue node: $[M-H]^-$: 381.191852; $C_{20}H_{30}O_7$), which is also metabolite from AAM pathway derived possibly through hydroxylation and ω-oxidation of LTB4. Both

mass signals are significantly increased in *db/db* mice, in either fecal or plasma samples. We could show that both biological matrices were represented by metabolites derived from AAM pathway, which is one of the significant pathways, described in chapter 2.3.4.5. The network is divided into two big sub graphs because highly connected nodes from one network are not connected directly to the highly nodes from the other network. Such an example is the highly connected node 6-Keto-PGE1 of network 2 and the highly connected node with the molecular formula of $C_{28}H_{46}O_6$ of network 1 and no direct or indirect connections were found between these both. This means the mass difference list that we took for generating the network could not provide a connection between these both (Table 11).

2.3.9 Comparative analyses of fecal metabolome patterns between *db/db* and *wt* mice using UPLC-TOF-MS

This study was also investigated using the UPLC-TOF-MS system. Fecal samples of *db/db* and *wt* mice were separated using a RP column (C8, Waters© Acquity™ UPLC® BEH™ C8 column (1.7 µm, 2.1 × 150 mm)). Here we focused on data derived from (-) UPLC-TOF-MS mode. The processed data using MZmine 2 contained 2271 features was then also subjected to MSA (Pluskal, Castillo et al. 2010). The data reduction using PCA showed a sufficient separation of *db/db* and *wt* mice, whereas the first component declares 24.3 % and the second component 9.6 % of total variance. A non-parametric univariate test Mann-Whitney test was used for the calculation of significant features between *db/db* and *wt* mice, resulting in 621 significant features. Afterwards we compared the metabolites derived through the FT-ICR-MS elaboration and extrapolated the overlaying significantly changed metabolites between FT-ICR-MS and UPLC-TOF-MS experiments. We found 45 different metabolites that were also significant between *db/db* and *wt* mice in UPLC-TOF-MS experiments. These metabolites that were also found in UPLC-TOF-MS were shown in the heatmap (Figure 2-29, B) and were metabolites of AAM pathway, FAs, sulfate conjugates of FAs, taurine conjugates of FAs but also BAs such DCA, ketoDCA and TCA sulfate (RTs are also displayed in min). The analyses with UPLC-TOF-MS confirmed additionally that certain metabolites were important discriminating *db/db* and *wt* mice.

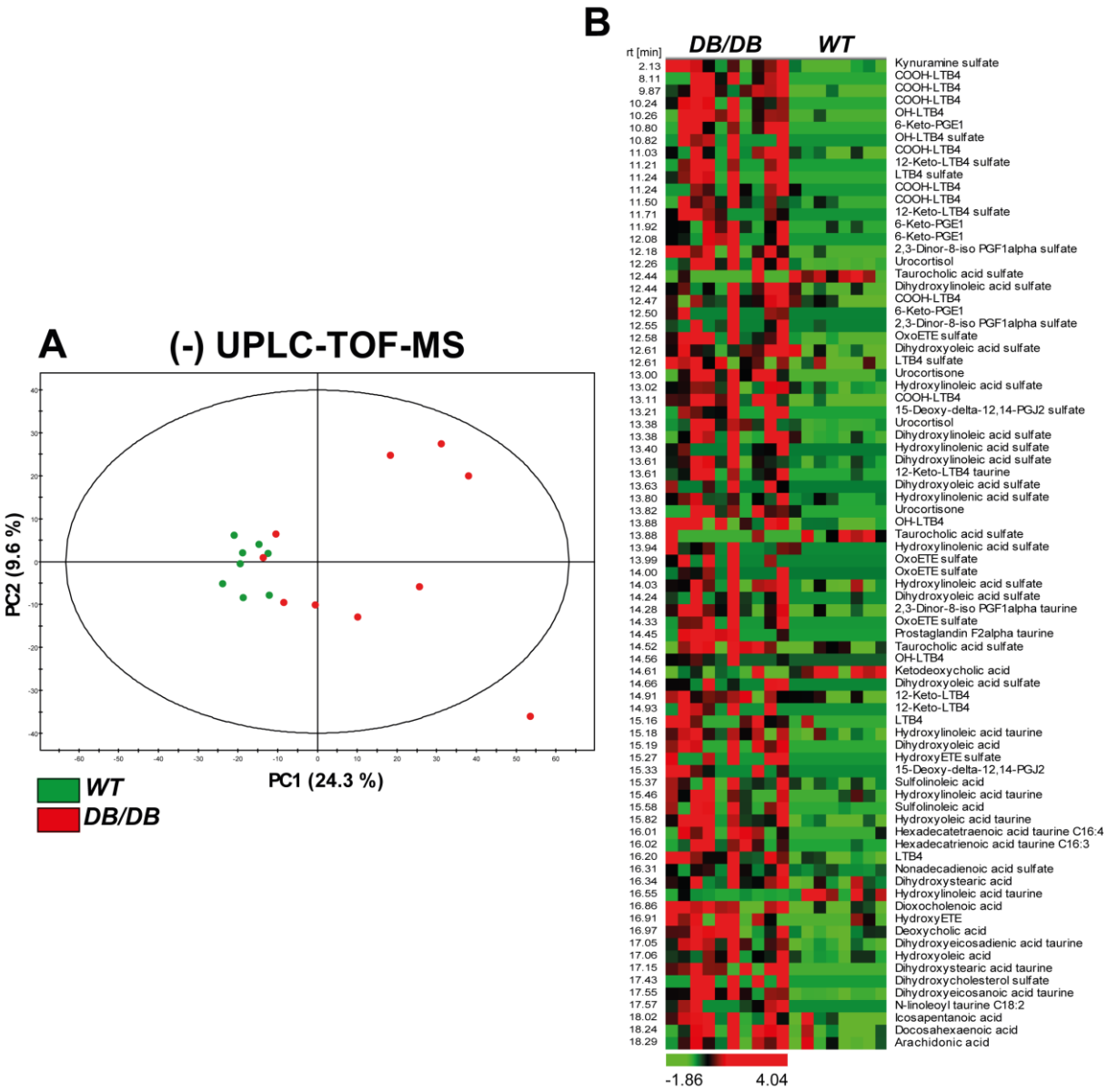

Figure 2-29 A: PCA scores scatter plot derived from analyses of fecal samples of *db/db* and *wt* mice using (-) UPLC-TOF-MS; B: Heatmap visualization of significantly changed metabolites with their respective retention time (rt) in min between *db/db* and *wt* mice; all displayed metabolites were significant with a p-value <0.05 (Mann-Whitney test), detailed information are given Table 19 of appendix (Chapter 6)

2.3.10 Metabolome analyses of COMBI treatment in *db/db* mice

As described in chapter 2.3.2, we could demonstrate by means MSA that the COMBI treatment changed significantly the metabolome of cecum and plasma compared *wt* and *db/db* mice, derived through significant models of OPLS/O2PLS-DA (Table 2). Moreover, concerning the cecum samples we could show that 430 mass signals out from 977 that were significant in *db/db* and *wt* mice, were changed again after COMBI treatment. Concerning the

plasma samples, 366 mass signals from 2815 (significantly changed between *db/db* and *wt* mice) were altered due to COMBI treatment. To evaluate which metabolites were affected by COMBI treatment we took all metabolites, which were elaborated from the comparison of fecal metabolome between *db/db* and *wt* mice. Then, we compared the metabolites whether they were changed after COMBI treatment based on our previous collected knowledge about changed metabolite classes and pathways.

Concerning the cecal metabolome, we could identify several metabolite classes that were affected after COMBI treatment of *db/db* mice for two weeks. As shown in Figure 2-30 several metabolite classes we elaborated from fecal metabolome comparison were changed after COMBI treatment. These classes were AAM metabolites, some FAs, two cholesterol metabolites including hydroxyoxocholestenoate and tetrahydroxycholestane and five NATs of fatty acids and taurine conjugates of oxygenated FAs (Figure 2-30, A).

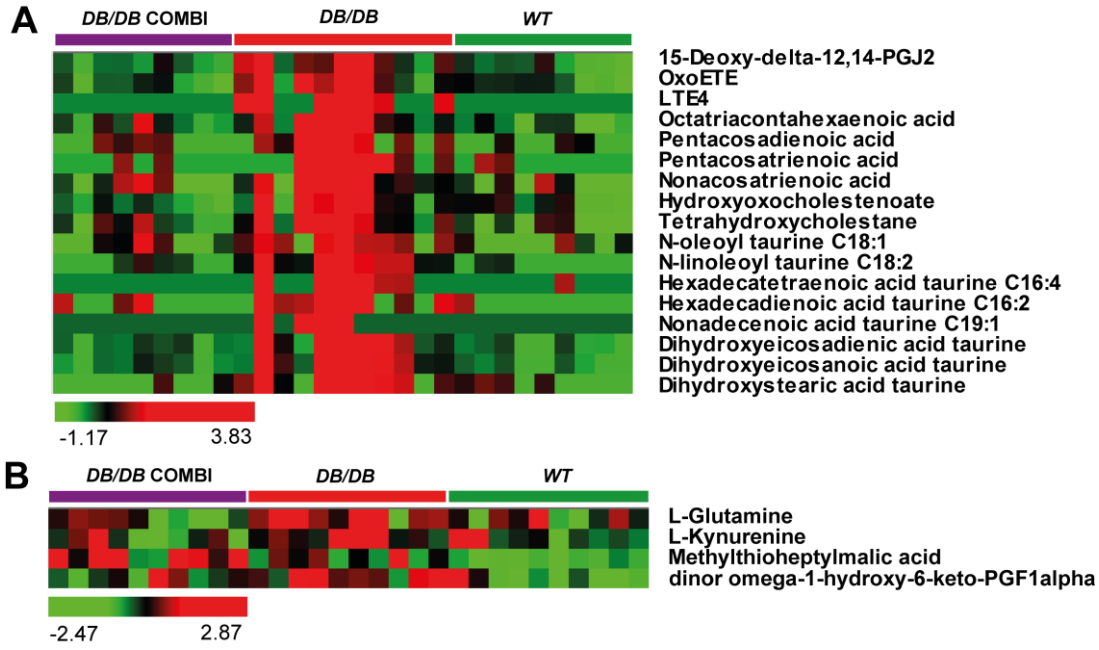

Figure 2-30 A Cecal metabolome changes after COMBI treatment of *db/db* mice; B: Plasma metabolome changes after COMBI treatment of *db/db* mice; all displayed metabolites were significant with a p-value <0.05 (Mann-Whitney test), detailed information are given Table 20 of appendix (Chapter 6)

Concerning the plasma metabolome, we could find only a few metabolites, that were already elaborated before, shown in Figure 2-30 B. The metabolites were L-Glutamine, L-Kyrenine, methylthioheptymalic acid and the dinor ω-1-hydroxy-6-keto-PGF1α from AAM pathway.

2.3.11 Topographical Variation in *wt* mice

This study allows us to follow the metabolite signature along the gastrointestinal tract (topographical variation or distribution of metabolites). For this purpose, we used the measurements done with (-) FT-ICR-MS of the luminal contents from cecum, colon (middle, distal) and feces samples of *wt* mice because their metabolism in the intestine somehow represents the "healthy" status of a mouse. First, we aligned all different data matrices. We performed several filtration steps including the 10 % abundance filter and NetCalc molecular formula calculation. Annotation of the mass signals was done with MassTRIX. First, the data were subjected to PCA analyses to get an overview of the behavior of the different intestine matrices. We showed the results of thirst three PCs: PC1 vs. PC2 (Figure 2-31, A) and PC2 vs. PC3 (Figure 2-31, B). The first two components demonstrated that samples of middle and feces were clustering closely and cecum and distal samples were closer to each other (Figure 2-31, A). In the next two components only feces samples clearly separates from all other samples (Figure 2-31, B).

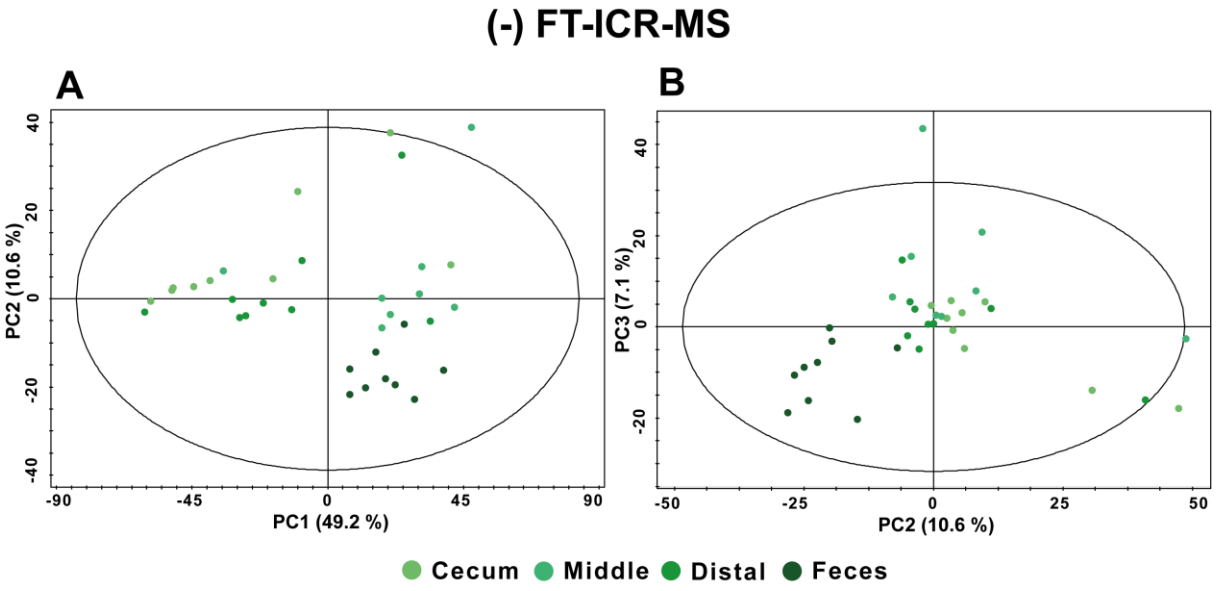

Figure 2-31 PCA scores scatter plot of four different intestinal matrices from *wt* mice including cecum, middle, distal content and feces, measured in (-) FT-ICR-MS; A: PCA of PC1 and PC2; B: PCA of PC2 and PC3

In order to extrapolate which mass signals are responsible for the separation we performed additionally a univariate non-parametric test (Kruskal Wallis test; p-value<0.05). In sum, 1423 mass signals were significantly changed between all four intestinal matrices. In order to reveal the mass signal patterns decreasing or increasing from cecum to feces we performed

subsequently a Pearson correlation (p-corr<0.05; resulted in 728 mass signals) and extrapolate the top 25 mass signals, following the desired pattern (Figure 2-32). In Figure 2-32, (A), a heatmap shows the pattern of the decreasing mass signals. In Figure 2-32, (B), a further heatmap summarized the increased patterns of the mass signals. Decreasing patterns were found for retinol, pantheteine or fatty acids such as oxodecenoic acid (Figure 2-32; A). Increasing patterns were observed for oxylipins such as hydroxyoleic acid and dihydroxystearic acid or several NATs of FAs or oxygenated FAs for example palmitic acid or hydroxyoleic acid (Figure 2-32, B). These metabolites classes were also responsible for the separation of *db/db* and *wt* mice in fecal samples see chapter 2.3.3. The metabolite N-palmitoyl valine revealed the highest positive correlation coefficient with 0.75 and p-corr=1.84650x10-^{7} (Figure 2-32, B). The metabolite dodecylphenol was responsible for highest negative correlation resulted in a correlation coefficient of -0.67 and p-corr=3.0515x10^{-5} (Figure 2-32, A). We also observed the distribution of the main bile acids and their sulfate and taurine conjugates including LCA, DCA, CA, DCA sulfate, CA sulfate, TLCA, TDCA and TCA. There were no prominent changes in term of increasing or decreasing patterns (Figure 2-32, C). There are few studies given, exploring and comparing metabolite patterns of intestine for example small intestinal samples from rats (Wang, Tang et al. 2005) or human gut biopsy samples (Wang, Holmes et al. 2007) or comparison of conventional and ex-germ free mice but also specific colonized mice (Martin, Wang et al. 2009) or a comprehensive comparison of age and intestinal topography of rats (Tian, Zhang et al. 2011). Most of them were performed by using ^{1}H NMR metabolic profiling approach. Thus the comparison was with our study was very difficult due to different techniques used for metabolomics, hence the mentioned studies measured small metabolites consisting of for example amino acids and SCFAs (Martin, Wang et al. 2009).

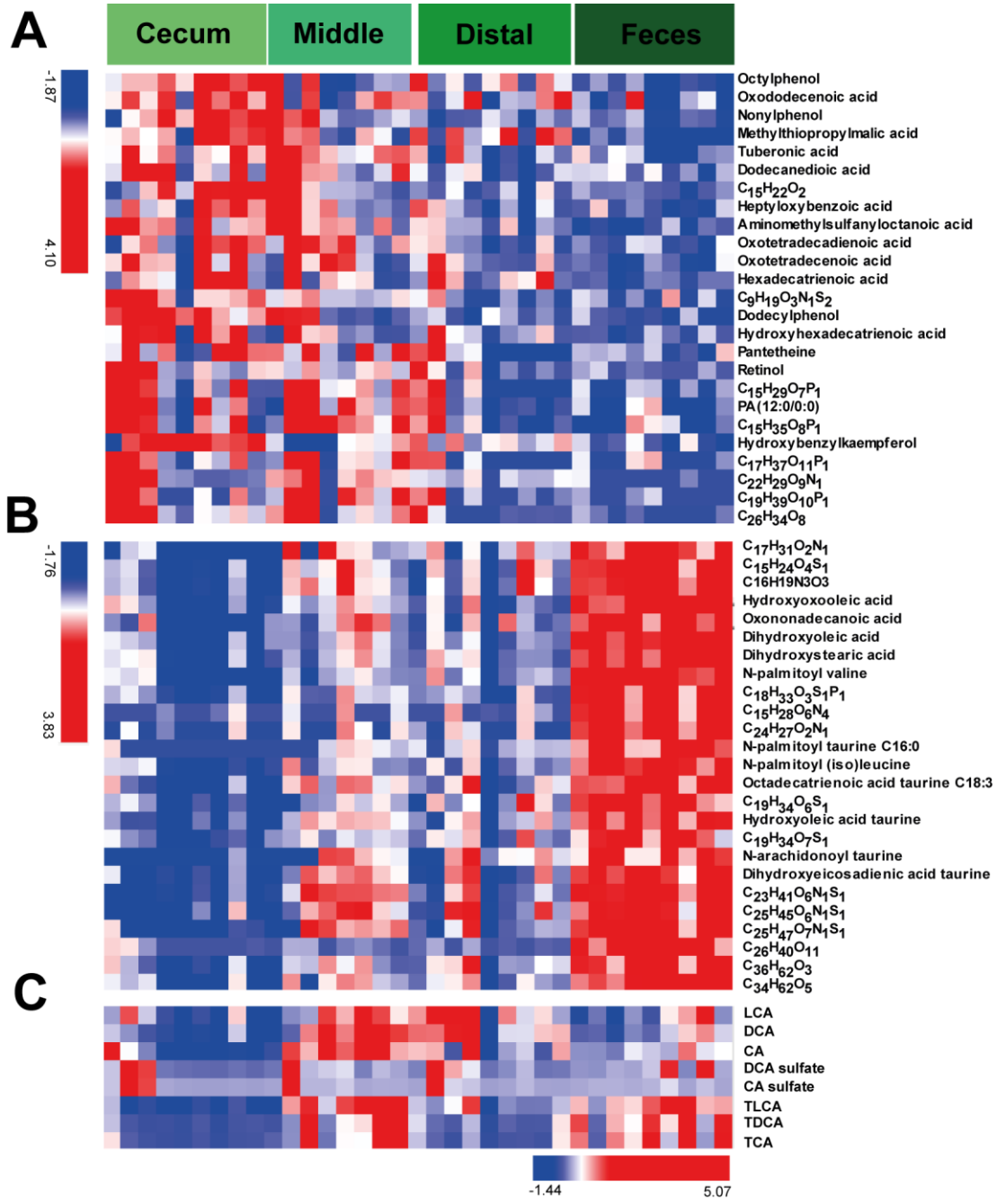

Figure 2-32 A: Top 25 metabolites decreasing from cecum to feces; B: Top 25 metabolites increasing from cecum to feces; C: the patterns of BAs and their sulfate and taurine conjugates; correlation was calculated by Pearson correlation algorithm with p-corr < 0.05; detailed information are given Table 21 of appendix (Chapter 6)

2.4 Summary and Conclusion

Here, we presented a non-targeted metabolomics approach in revealing metabolites in T2DM applying predominantly a FT-ICR-MS approach of intestinal samples and plasma samples from a commonly used mouse model for T2DM. Furthermore, we validated the role of two drugs metformin and a SGLT-2 inhibitor and their impact of intestinal metabolome. The drug application could not show any significant changes on the intestinal metabolome, except the combination of both drugs. Due to this fact, we were focusing on the gut metabolome changes between *db/db* and *wt* mice, especially the feces samples due to the best discrimination results. The data elaboration could highlight different metabolite classes involved in the differentiation between *db/db* and *wt* mice. Major metabolite classes that were affected were fatty acids and their derivatives including oxylipins, bile acids and we could find that taurine and sulfate conjugates of several classes play an immense role in discriminating *db/db* and *wt* mice. Distinct appearance of free fatty acids in diabetic mice is underlying previous reports about changes in ß-oxidation in diabetic subjects. A further class of oxylipins indicates a change in the lipoxygenation. Additionally, the so-called N-acyltaurines were majorly elevated in *db/db* mice likely due to a deregulation of ACNAT or FAAH enzymes responsible for con- or deconjugation of N-acyltaurines. Recently, N-acyltaurines were also discussed to be involved in insulin signaling. Gut bacterial metabolism in db/db mice is reflected through different bile acids and their sulfate conjugates signatures of feces and other gastrointestinal matrices. Taurine and sulfate conjugates as well as degradation metabolites of arachidonic acid metabolism were found to be increased in *db/db* mice. Finally, oxylipins conjugated with sulfate and taurine were revealed to play in the fecal metabolome of *db/db* mice comparing to *wt* mice. Here, we have to mention that especially the conjugates were not given in any metabolite database such HMDB, KEGG or Lipid Maps. Concerning, the N-acyltaurines fatty we could find ten metabolites were not present in these databases. We could find three different sulfate conjugates of bile acids and steroids. In arachidonic acid metabolism we could elaborated five metabolites, sixteen new sulfate conjugates and eleven new taurine conjugates. Moreover, eight different sulfate conjugates and six taurine conjugates of oxylipins were unveiled with the non-targeted metabolomics approach to play an important role in discriminating diabetic and healthy mice. We brought a new insight of possible sulfate and taurine conjugation especially of fatty acids and oxylipins, which need to be investigated

Chapter III

META-METABOLOMICS IN OBESITY

OVERVIEW

ABSTRACT

Here, we studied two different factors in developing obesity in mice. We investigated the role of three diets and genotype susceptibility due to high fat feeding in two C57BL6 mouse strains. By applying a comprehensive and unbiased metabolomics based on MS technique, we could observe the meta-metabolome association related to diet or genotype and body weight changes. High fat feeding resulted in different phenotype of the C57BL6 strains, which was also reflected in distinct cecal-metabolome. We could elaborate different metabolite classes ranging from bile acids, their taurine and sulfated conjugates but also several bacterial derived metabolites including lignans and urobilinoids.

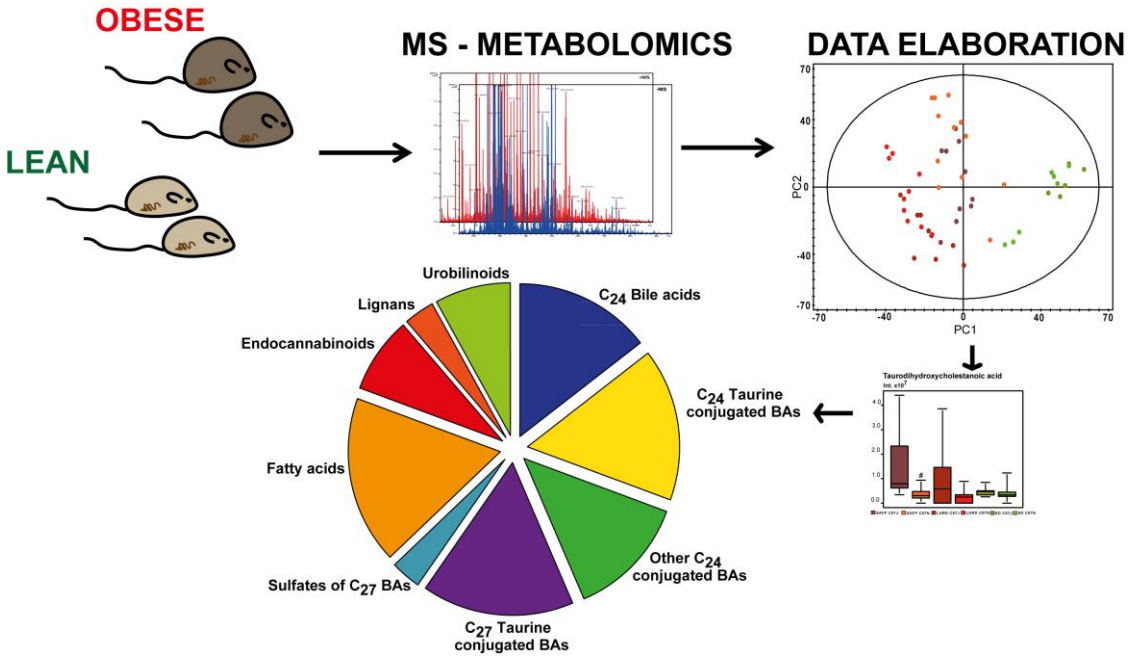

Chapter III

3 Metabolomics in Obesity

3.1 Introduction

According the world health organization (WHO) obesity is defined by excess of body mass index equal or greater than 30 kg/m^2 and classified into nutritional disorders (WHO 2010). The development of overweight or obesity is majorly associated with lifestyle habits including nutrition and the lack of physical activity (Popkin, Kim et al. 2006). Obesity was discussed to be one of the risk factors for developing insulin resistance and T2DM (Kahn and Flier 2000) and could be linked to changes in the gut community composition in different independent studies (Kahn and Flier 2000, Turnbaugh, Ley et al. 2006, Bäckhed, Manchester et al. 2007). Also, obesity plays a key role in developing coronary artery diseases including stroke and myocardial infarction, metabolic syndrome and cancer (Eckel, Grundy et al. , Haslam and James).

As mentioned above T2DM was investigated by applying a metabolomics approach using rodent (genetic or diet-induced) or human studies, summarized in Table 1. We performed an ISI Web of Science® search (date: 9/19/2013) with the terms of obesity and metabolomics and excluding diabetes to avoid cross citations of Table 1.

Table 4 Metabolomics studies of obesity

	Author	Year	Type of biological matrix	Species	Analytical technique	Animal model
Animal studies						
Genetic- driven	(Yetukuri, Katajamaa et al. 2007)	2007	Liver	Mice	UPLC-MS	*Ob/ob*
	(Serkova, Jackman et al. 2006)	2006	Liver and blood	Rats	NMR	*fa/fa*
	(Atherton, Gulston et al. 2009)	2009	Liver, heart and white adipose tissues	Mice	NMR	PPAR-α-nul
	(Lindeque, Hidalgo et al. 2013)	2013	Plasma, Gastrocenmius, Liver and Brain	Mice	LC-MS and GC-MS	*Metallothionein KO mice*
	(Kim, Jung et al. 2010)	2010	Urine		NMR	AHNAK$^{-/-}$
Others	(Velagapudi, Hezaveh et al. 2010)	2010	Serum	Mice	GG-MS	*GF vs. CONV-R*
	(Oresic, Seppanen-Laakso et al. 2009)	2009	Eyes (retina and lenses)	Mice	UPLC-MS	*GF vs. CONV-R*
	(Ma, Zhang et al. 2011)	2011	Serum	Rats	GC-MS	*ovariectomized*
Diet - driven	(Mutch, Grigorov et al. 2005)	2005	Liver	Mice	GC	
	(Xie, Su et al. 2007)	2007	Urine	Rats	CE and capillary LC-UV	
	(Cox, Williams et al. 2009)	2009	Serum	Monkeys	GC-MS	
	(Bertram, Larsen et al. 2012)	2012	Liver	Rats	NMR	
	(Spagou, Theodoridis et al. 2011)	2011	Plasma	Mice	GC-MS	
	(Shi, Wahlang et al. 2012)	2012	Liver	Mice	FT-ICR-MS	
	(Song, Wang et al. 2013)	2013	Plasma	Rats	NMR	
	(Kim, Kim et al. 2010)	2010	Liver and serum	Mice	UPLC-MS, GC-MS	
	(Kim, Yang et al. 2009)	2009	Urine	Rats	NMR	
	(Christensen, Hedemann et al. 2012)	2012	Plasma	Pigs	LC-MS	
	(Ji, Ernest et al. 2012)	2012	Abdominal adipose tissue	Chicken	LC-MS	
Human studies	(Raman, Ahmed et al. 2013)	2013	Feces	Human	GC-MS	
	(Calvani, Miccheli et al. 2010)	2010	Urine	Human	NMR	
	(Oberbach, Bluher et al. 2011)	2011	Serum	Human	FIA-MS	
	(Szymanska, Bouwman et al. 2012)	2012	Serum	Human	NMR and UPLC-MS	

We could find several original publications studying obesity related metabolites, which used biological matrices including urine, plasma but tissue samples. Also one group studied obesity associated metabolites in fecal samples but in a more targeted metabolomics approach (Raman, Ahmed et al. 2013). In addition, the question of gut microbiota in obesity has been approached by two studies applying a metabolomics approach by using an GF mouse model (Oresic, Seppanen-Laakso et al. 2009, Velagapudi, Hezaveh et al. 2010).

3.2 Overview – Goals

To examine diet-induced obesity (DIO), we took two different sub strains the C57BL6/J (C57J) and C57BL6/N (C57N) and fed them with three different diets (safflower oil (SAFF), lard diet (LARD) and standard chow diet (SD)). These two sub strains differ, apart from several SNPs, in the nicotinamide nucleotide transhydrogenase (nnt) gene, which bears a missense mutation in strain C57BL/6J (Toye, Lippiat et al. 2005, Mekada, Abe et al. 2009). The NNT is a proton pump of the inner membrane of the mitochondrial membrane, affecting NADH/NAD^+ ratio and consequently NADH accumulates in the mitochondrium (Olgun 2009, Wong, Blair et al. 2010). The sub strain C57N presents thereby the wild type with a normal expression of NNT gene. Previous studies showed different phenotypes of the substrains, depending on the diet, being applied (Nicholson, Reifsnyder et al. 2010). Our goal was to examine the effects of the SAFF and LARD diet on body weight and genotype susceptibility due to the high fat diets (HFD) of SAFF and LARD. Moreover, we investigated the role of cecal meta-metabolome and the influence of genotype or diet related changes.

3.3 Study design of diet induced obesity (DIO)

For a short overview, the study set up is shown in Figure 3-1. Two different sub strains the C57BL6/J (C57J) and C57BL6/N (C57N) were subjected two three different diets (SAFF, LARD and SD) for a period of three weeks at an age of 14 weeks. For detailed information on animal experiments, please see chapter 5.1.2.

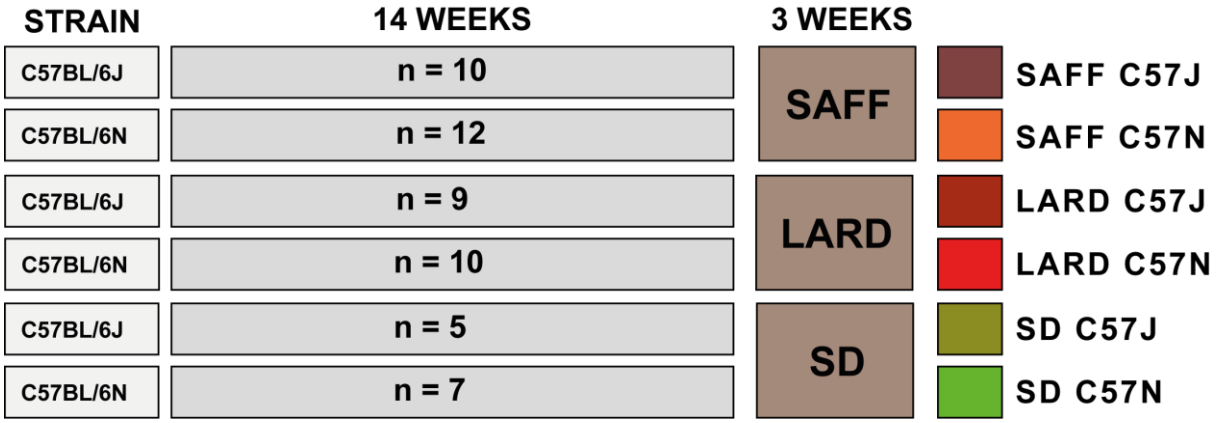

Figure 3-1 Study design of diet induced obesity in C57J and C57N mice

3.4 Results and Discussion

3.4.1 General – Body weight changes

The application of different diets (SAFF, LARD and SD) resulted in substantial body weight changes in C57N on SAFF and LARD diets compared to C57J strain (Figure 3-2). In addition, a significant body weight change was detected between SAFF C57N and LARD C57N. The significance was calculated with a univariate statistical test called Welch test (SAFF C57J vs. C57N: # p - value = 0.02129; SAFF C57J vs. C57N: ‡ p - value = 0.00001 and SAFF C57N vs. LARD C57N: a p - value = 0.03068).

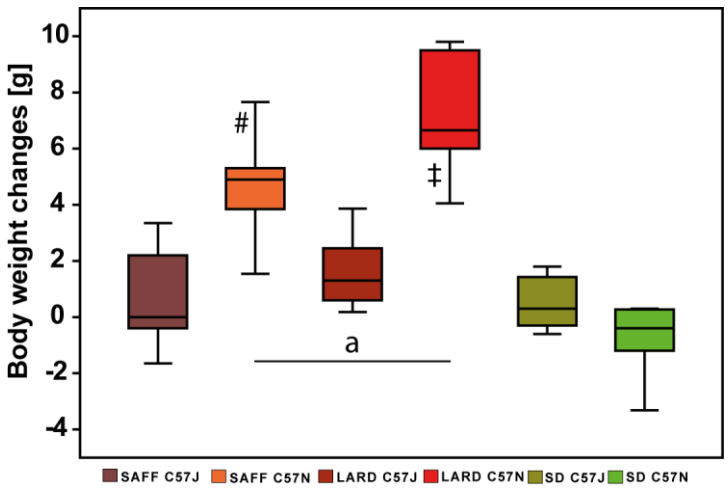

Figure 3-2 Body weight changes after 3 weeks of dietary challenge of C57J and C57N mice

3.4.2 Global analysis of cecal meta-metabolome due to DIO

To extrapolate whether these body weight changes are also associated with changes of cecal metabolome a non-targeted metabolomics approach was performed using FT-ICR-MS. The luminal content of cecum was extracted as described in chapter 4.3.2. The mass peak lists were aligned using Matrix Generator within an error ppm of one. Several filtration steps followed then, applying a 10 % abundance filter and filtration with means of Netcalc molecular formula calculation. The resulted matrix was subjected to further multivariate statistical analyses (MSA). First a PCA was performed, that showed a good separation in the first two components, whereas 19.8 % are representing the first component and 17.7 % the second component of the (-) FT-ICR-MS mode (Figure 3-3). Visually, the scores plot in Figure 3-3 showed a group consisting of LARD and SAFF containing both sub strains and another group consisting of two sub strains on the SD diet either for (-) or (+) FT-ICR-MS mode. The major separation of the cecal metabolome was also due to fed diet.

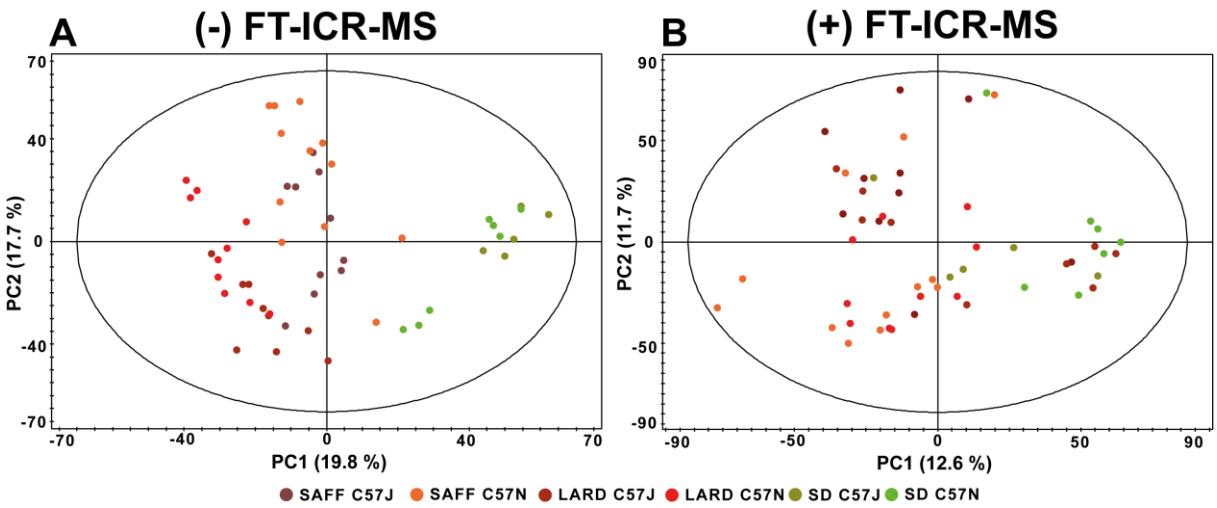

Figure 3-3 PCA scores scatter plots displaying the cecal metabolome of C57J and C57N mice after the application of three different diets (SAFF, LARD and SD) measured in (-/+) FT-ICR-MS mode

In order to discriminate between the sub strains on the different diets, we performed a pair wise comparison (genotype and diet) by using two different OPLS/O2PLS-DA with or without orthogonal signal correction to generate and validate different models (SAFF C57J vs. C57N; SAFF C57J vs. LARD C57J; SAFF C57N vs. LARD C57N; LARD C57J vs. C57N; SD C57J vs. C57N). For the orthogonal signal correction, we were using the values of the body weight changes to generate different OPLS/O2PLS-DA models. For every generated model of interest, the robustness of the model has been tested with cross-validation analysis of variance (CV-ANOVA). Significant OPLS/O2PLS-DA models (without OSC) were generated for SAFF C57N vs. LARD C57N, SAFF C57J vs. LARD C57J and SAFF C57J vs. C57N, shown in Table 5. Applying OSC the comparison of LARD C57J vs. C57N and SAFF C57J vs. C57N showed significant p-values after CV-ANOVA (Table 6).

Table 5 OPLS/O2PLS-DA results from different model comparison

Models – (-) FT-ICR-MS)	R^2Y(cum)	Q^2(cum)	p- value (CV-ANOVA)
SAFF C57J vs. SAFF C57N	0.98	0.61	0.014
SAFF C57J vs. LARD C57J	0.99	0.85	0.001
SAFF C57N vs. LARD C57N	0.99	0.90	0.00002
LARD C57J vs. LARD C57N	0.99	0.73	0.062
SD C57J vs. SD C57N	0.99	0.70	0.24

Table 6 Orthogonal signal corrected OPLS/O2PLS-DA results from different model comparison

Models	R^2Y(cum)	Q^2(cum)	p- value (CV-ANOVA)
SAFF C57J vs. C57N	0.78	0.57	0.004
SAFF C57J vs. LARD C57J	0.36	0.16	0.256
SAFF C57N vs. LARD C57N	0.77	0.51	0.058
LARD C57J vs. C57N	0.74	0.55	0.0019
SD C57J vs. C57N	0.82	0.36	0.6511

Indeed, the discrimination of SAFF C57J vs. C57N showed in both OPLS/O2PLS-DA models the best results. The model generated after OSC is shown in scores scatter plot generated from OPLS/OPLS-DA (Figure 3-4).

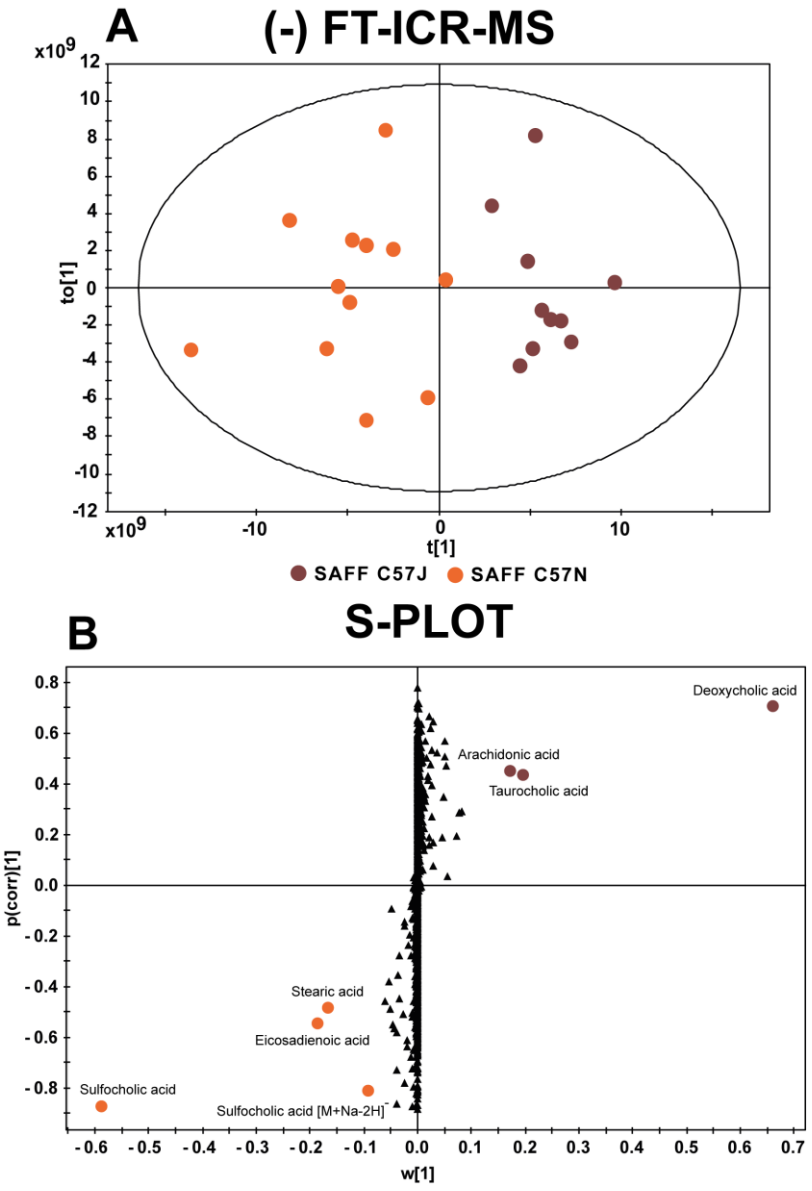

Figure 3-4 A: OPLS/O2PLS-DA scores scatter plot of cecal metabolome of C57J and C57N mice on SAFF diet measured in (-) FT-ICR-MS mode; B: S-Plot displaying mass signals highly discriminative between C57J and C57N mice on SAFF diet

The mass signals responsible for the separation are shown the S-Plot derived from the model from the comparison of SAFF C57J vs. C57N (Figure 3-4, B). The annotation of the mass signals was performed with MassTRIX and not annotated mass signals (unknowns) are represented by their molecular formula. Moreover, the significance was also confirmed by calculating the p-value of pair wise comparison of both genotypes on SAFF, LARD and SD diet. A non-parametric univariate test Mann-Whitney test was used for the calculation. A Venn diagram was constructed with all significant mass signals (in total 1185 mass signals), shown in Figure 3-5. We could find 862 significant mass signals differed between C57J and C57N mice on SAFF diet. Nine hundred forty four (944) mass signals were significantly changed between C57J and C57N on LARD diet. On SD diet, we could find 412 significantly changed mass signals. Moreover, 449 mass signals were uniquely changed between C57J and C57N mice on SAFF diet, 563 mass signals on LARD diet and 292 mass signals in SD diet. Overall, 26 mass signals were common in all three comparisons and significantly changed between C56J and C56N in all three diets. In the heatmap, the most abundant (calculated by the arithmetic mean of all intensity values for each mass signal) mass signals (Top 50) are shown Figure 3-6, that different between C57J and C57N on SAFF, LARD and SD diet.

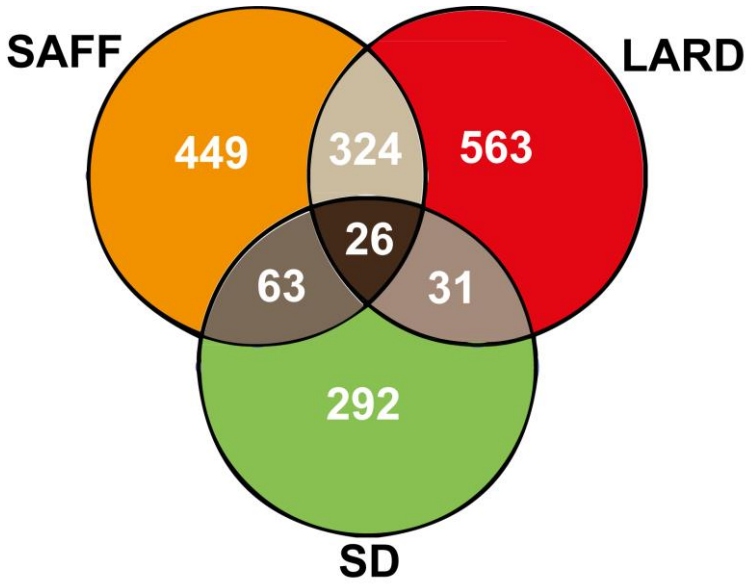

Figure 3-5 Venn diagram of all significantly changed mass signals between C57J and C57N mice on SAFF, LARD and SD diet

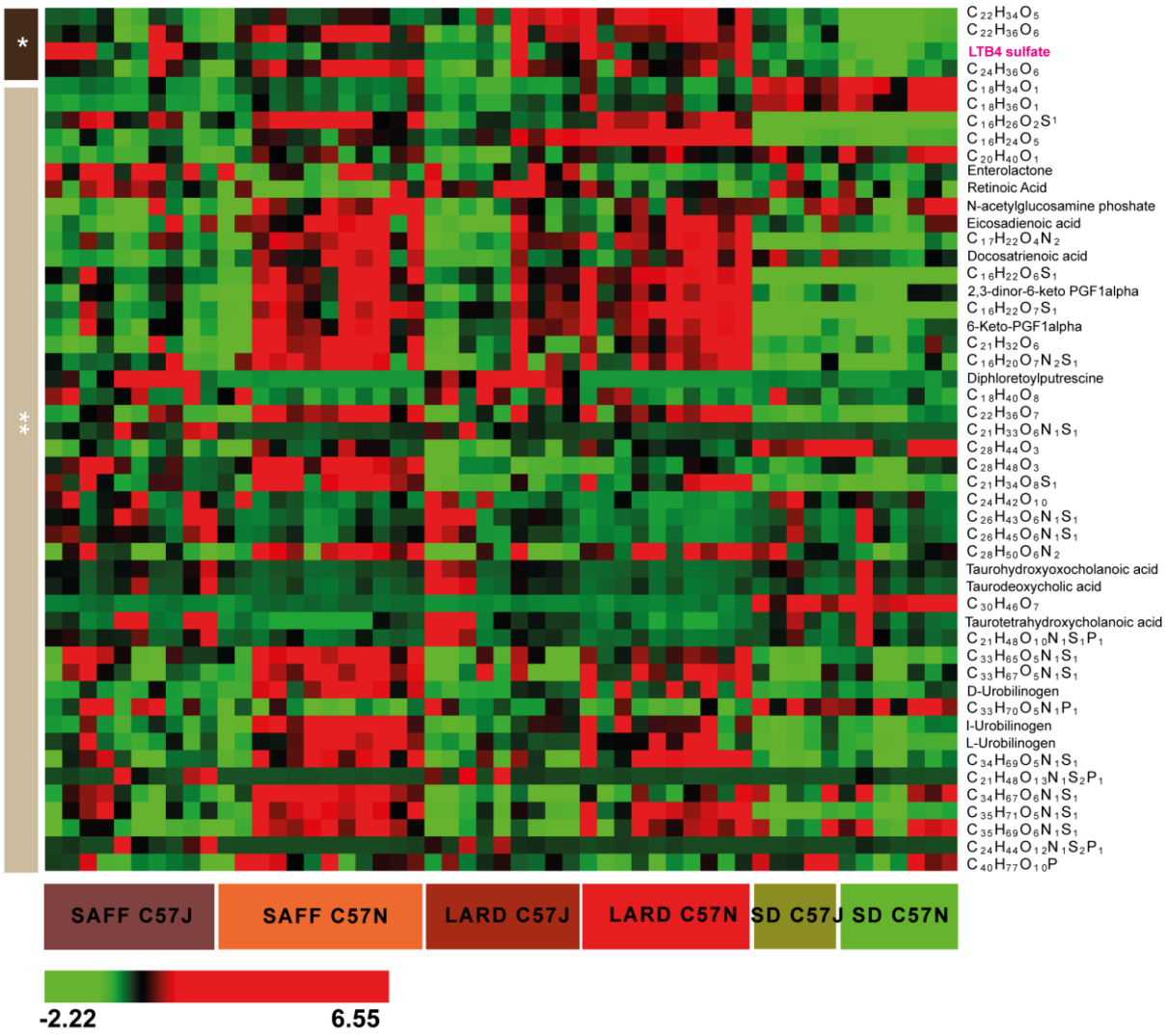

Figure 3-6 Top 50 most abundant and significant mass signals between C57J and C57N on SAFF, LARD and SD diet; all displayed metabolites were significant with a p-value <0.05 (Mann-Whitney test); Not annotated mass signals are indicated by their molecular formulas, detailed information are given Table 22 of appendix (Chapter 6)

Four of these mass signals also differed C57J and C57N on SD diet (*, brown color, Figure 3-6). All others mass signals did differ significantly between C57J and C57N on SD diet (**, beige color, Figure 3-6). One of these mass signals with molecular formula of $C_{20}H_{32}O_7S_1$ (pink) we could already observe in Chapter 2.3.5 which was one of the sulfated metabolites from AAM pathway so called LTB4 sulfate. LTB4 sulfate was significantly decreased in C57N on SAFF diet, increased in C57N on LARD diet and decreased in C57N on SD diet (Figure 3-7). The presence of LTB4 sulfate could be confirmed by (-) TOF MS/MS fragmentation experiments given in Figure 5-10. A typical fragment of HSO_4 and a neutral loss of SO_3 were shown for LTB4 sulfate (Figure 5-10).

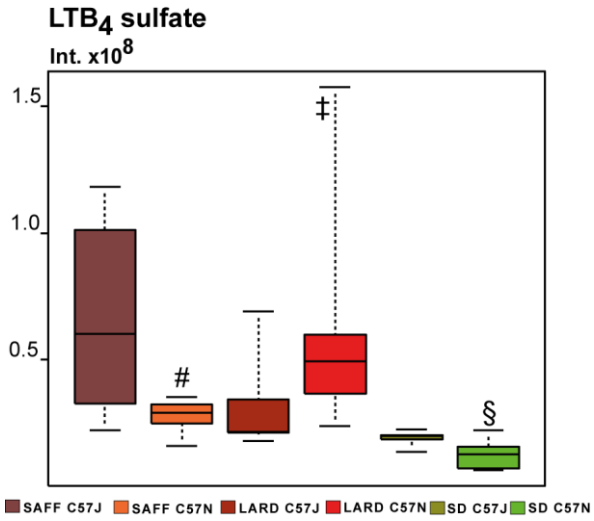

Figure 3-7: LTB4 sulfate was significantly between C57J and C57N in all three diets: # p-value = 0.02955; ‡ p-value = 0.01430; $ p-value = 0.042357 (Mann Whitney test)

3.4.3 Correlation studies: metabolites and body weight changes

Next, we examined an association between the values of body weight changes of all groups and the metabolome data in order to investigate possible mass signals correlating positively with body weight changes in all six groups. We evaluated these correlations by calculating p-values for every mass signal and took the top 50 significant mass signals, shown in Figure 3-8. Mass signals that were correlating positively with body weight changes with correlation value (R) above 0.6, are shown in Figure 3-8.

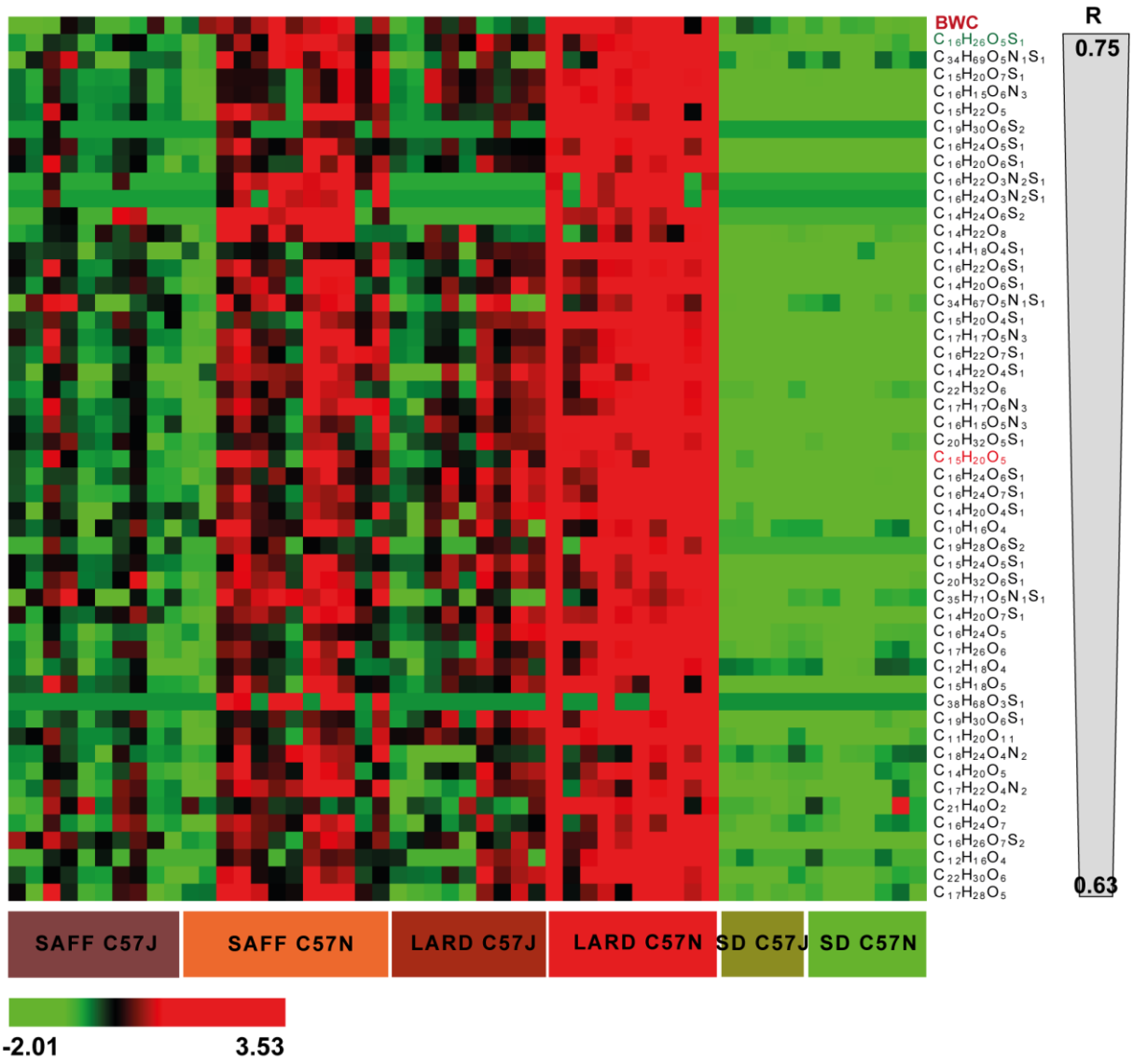

Figure 3-8 Top 50 mass signals correlated positively with body weight changes; Correlation was performed by Pearson algorithm with p-corr<0.05; Not annotated mass signals are indicated by their molecular formulas; detailed information are given Table 23 of appendix (Chapter 6)

The mass signal with the highest correlation coefficient was annotated by the molecular formula of $C_{16}H_{26}O_5S_1$ (green label). This mass signal was significantly increased in C57N mice on SAFF and LARD diet. Subsequently, performed identification by MS/MS experiments were not possible due to low abundance Then we decided to extrapolate mass signals out of top 50 with highest intensity values of arithmetic mean of all samples. This mass signal derived a correlation value over 0.7 and p-corr = $1.4x10^{-9}$ and was annotated as the molecular formula of $C_{15}H_{20}O_5$ (red label). This mass signal was also annotated in MassTRIX as a plant metabolite, which was a false positive annotation. We performed (-) TOF MS/MS experiments and MS/MS spectrum is shown in Figure 5-11. Unfortunately, it

was not possible to find plausible structures in order to identify the unknown metabolite. The metabolite was highly increased in C57N mice on SAFF and LARD diet, compared to SD diet and was significantly changed between C57J and C57N mice on SD diet and LARD diet.

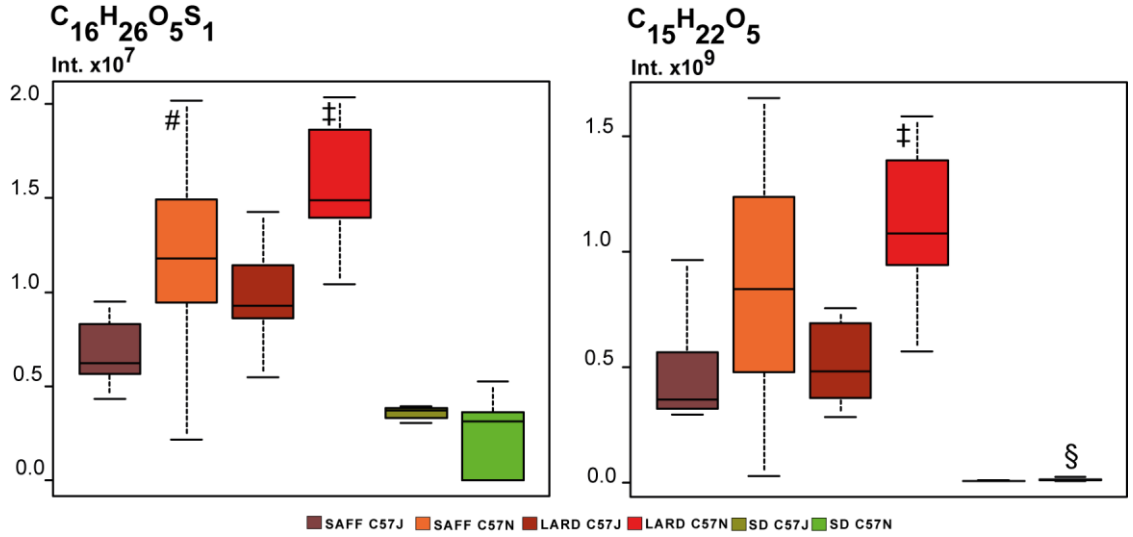

Figure 3-9 Two metabolites highly positively correlating with body weight changes in C57J and C57N mice after 3 weeks of dietary intervention p-corr (A)= 5.91744 x10-11; p-corr (B)= 1.41677x10-9; Group comparison: A: # p-value = 0.00835; ‡ p-value = 0.00145; (Mann Whitney test); B: # p-value = 0.00060; § p-value = 0.02835 (Mann Whitney test)

3.4.4 Cecal meta-metabolome changes between C57J and C57N after SAFF diet for three weeks

Due to the best results derived from OPLS/O2PLS-DA model comparison, showed for C57J and C57N mice on SAFF diet we were focusing on describing and interpreting the results based on this comparison. The group of C57SAFF diet could be discriminated through four different mass signals annotated as sulfocholic acid, eicosadienoic acid and stearic acid (Figure 3-4, B). The fourth mass signal appeared to be an adduct of sulfocholic acid $[M+Na-H]^-$, whereas a performed Pearson correlation between both mass signals obtained a value over 0.96. The group of SAFF B6J could be represented by three mass signals annotated as deoxycholic acid (DCA), taurocholic acid (TCA) and arachidonic acid (AA). Afterwards we were plotting sulfocholic acid as one representative of the C57N and DCA as the second representative of C57J to see the differences for all six groups, shown in Figure 3-10. DCA was increased in C57J on SAFF diet.

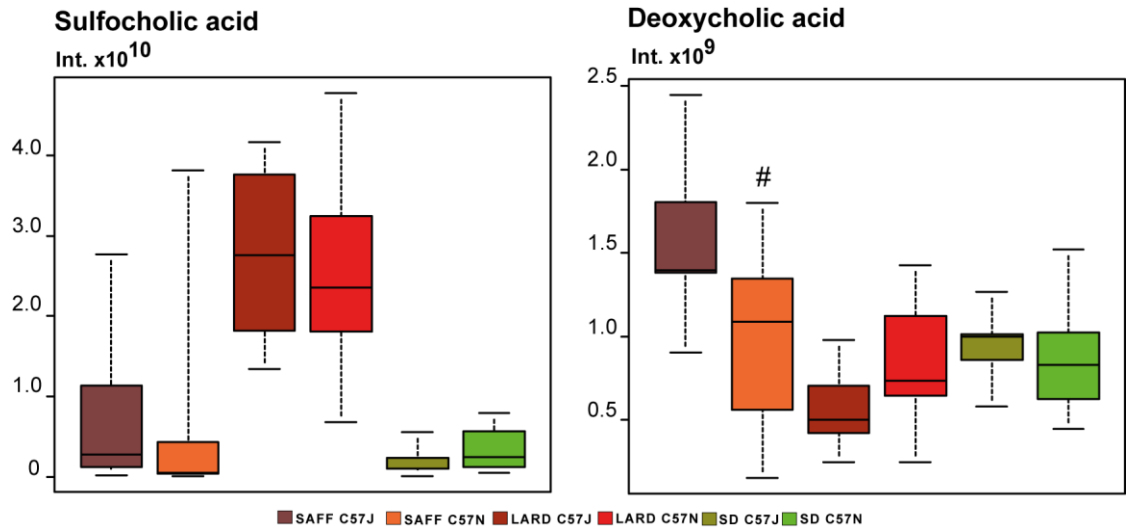

Figure 3-10 Two B derived from S-Plot that were highly discriminative for C57J and C57N mice; A: Sulfocholic acid; B: Deoxycholic acid; B: # p-value = 0.02496 (Mann Whitney test)

Other diets did not show any significant results. Sulfocholic acid did not show any significant results due to univariate statistical analysis but we observed higher levels in C57J and C57N mice on LARD diet. DCA and TCA are bile acids (BAs) and play an important role in discriminating the two groups of C57J and C57N on SAFF diet. Using this knowledge, we were looking specifically for further BAs especially C_{24} BAs and their conjugates (taurine, glycine and sulfate).

3.4.4.1 Different Patterns of C_{24} Bile acids

The OPLS/O2PLS-DA model could highlight already the important role of two BAs DCA (MS/MS spectrum in Figure 5-12) and TCA (MS/MS spectrum in Figure 5-13, B). Accordingly, we could find increased and significant different levels of oxocholanoic acid, oxocholenoic acid and cholandienoic acid in C57J mice (Figure 3-11). Increased but not significant patterns were observed for cholic acid (CA) and lithocholic acid (LCA) (Figure 3-11).

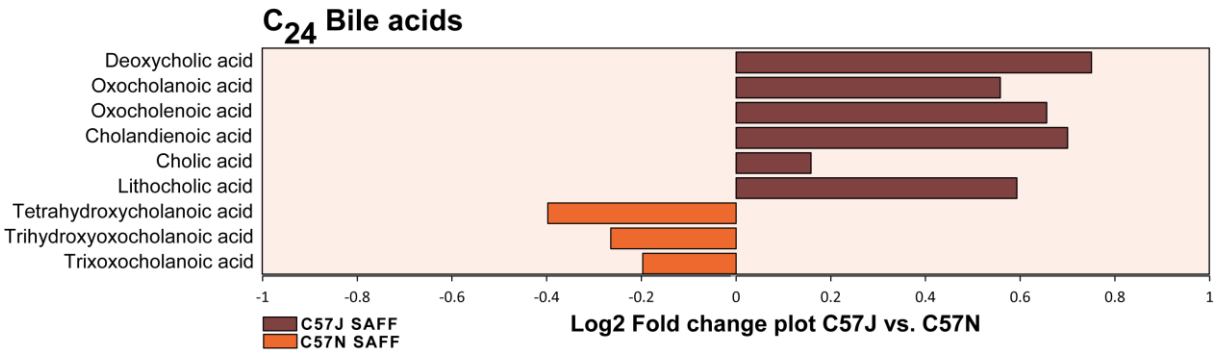

Figure 3-11 All C_{24} BAs significantly changed between C57J and C57N; all displayed metabolites except cholic and lithocholic acid were significantly altered with a p-value <0.05 (Mann-Whitney test), detailed information are given Table 24 of appendix (Chapter 6)

Contrary, other BAs such as hydroxycholic acid, trihydroxyoxocholanoic acid and trioxocholanoic acid were increased in the luminal content of cecum in C57JN mice, shown in Figure 3-11 and thus likely reflected different bacterial activity of the gut microbiome. DCA is one of the major secondary BA derived through dehydroxylation of bacteria in the gut. Narushima *et al.* indicates that *Bacteroides* is the main bacterial genus that is responsible for the dehydroxylation of CA to DCA (Narushima, Itoha et al. 2006). Interestingly, an increase of BAs was also observed in feces of diabetic mice (*ob/ob* mice) with elevated levels of CA and DCA (Li, Francl et al. 2012). Thus, could be explained through different regulation of bile acid pool, which is related to the disease state. Transgenic mice overexpressing cholesterol 7α-hydroxylase, which is involved in the biosynthesis of BAs from cholesterol, were resistant against diet-induced weight gain and development of fatty liver with elevated BAs concentration in the intestine (Li, Owsley et al. 2010). BAs are known to exert several biological effects *in vivo*, such as playing a role on lipid and cholesterol metabolism but also acting as signaling molecules and activating nuclear hormone receptors (Watanabe, Houten et al. 2006, Lefebvre, Cariou et al. 2009). Administration of CA to obese HFD-fed C57J mice led to a decrease in their body weight and improvement of insulin sensitivity. This effect was also observed in KK-A^y mice, which showed increased levels of CA, DCA, TCA and TDCA in liver and intestine, what were also observed in our study in cecal samples of C57J mice fed with a HFD. The difference of CA levels in the mentioned study of the Watanabe group is due to the supplemented CA in the diet (Watanabe, Houten et al. 2006). But also overexpression of enzymes involved in the biosynthesis of BAs were shown to play a key role in the regulation of body weight (Li, Owsley et al. 2010). Both studies indicated that energy expenditure was changed and they reported a higher CO_2 production and O_2 consumption.

Microarray studies revealed altered gene expression of cholesterol and BA synthesis in liver and genes in energy expenditure in brown adipose tissue including an increased conversion of thyroxine to triiodothyronine by type 2 deiodinase. The action of BAs is most likely transmitted by TGR5 dependent signaling in brown adipose tissue rather than in liver (Watanabe, Houten et al. 2006). Taken together, our results indicate that there are differences of BAs biosynthesis in C57J and C57N mice. Thus, elevated patterns of certain BAs in the intestine can be associated with higher energy expenditure in the lean phenotype of C57J mice.

3.4.4.2 C_{24} Taurine conjugated BAs differed between C57J and C57N mice

As a further BAs involved in the discrimination of C57J and C57N mice was the taurine conjugate of CA (TCA). Furthermore, we could find nine other taurine conjugated C_{24}-BAs derivatives. Significantly increased tauro (T)BAs were observed in C57J mice (Figure 3-12), including taurooxocholenoic acid (A), taurooxocholanoic acid (B), taurolithocholic acid (C), taurodioxocholanoic acid (D), taurohydrocyoxocholanoic acid (E), taurodeoxycholic acid (TDCA) (F), taurohydroxyoxocholanoic acid (G), TCA (H), taurohydroxycholanoic acid (I) and the sulfate conjugate of TCA: taurocholic acid sulfate (J). Confirmation was done by means of (-) TOF-MS/MS with a confirmation of taurodeoxycholic acid and TCA (MS/MS spectrum in Figure 5-13, A-B). The possible structures of the TBAs are displayed in Figure 3-13.

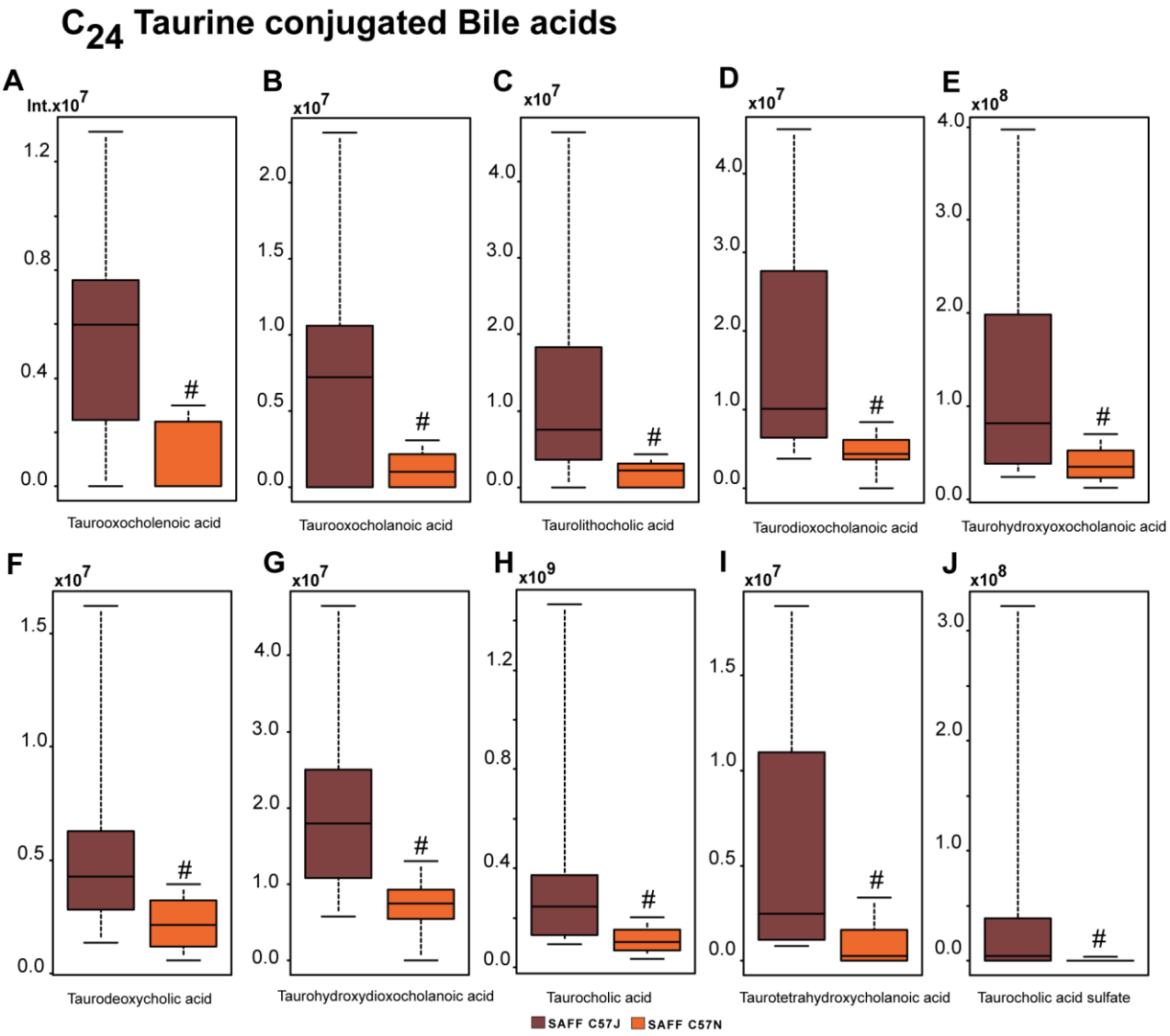

Figure 3-12 C_{24} Taurine conjugated BAs between C57J and C57N mice on SAFF diet; A: # p-value = 0.00630; B: # p-value = 0.02421; C: # p-value = 0.01316; D: # p-value = 0.00457; E: # p-value = 0.01469; F: # p-value = 0.00561; G: # p-value = 0.00123; H: # p-value = 0.00457; I: # p-value = 0.00632; J: # p-value = 0.00670 (Mann-Whitney test)

The prominent changes of TBAs in C57J and C57N on SAFF diet rose up a question how the behavior is due to other two diets in C57J or C57N mice. Therefore, we plotted TCA as an example of the TBAs (Figure 3-14). We could observe that C57N mice had lower levels of TCA either on SAFF or on LARD diet. SD diet did not change the TCA levels between the two diets (Figure 3-14).

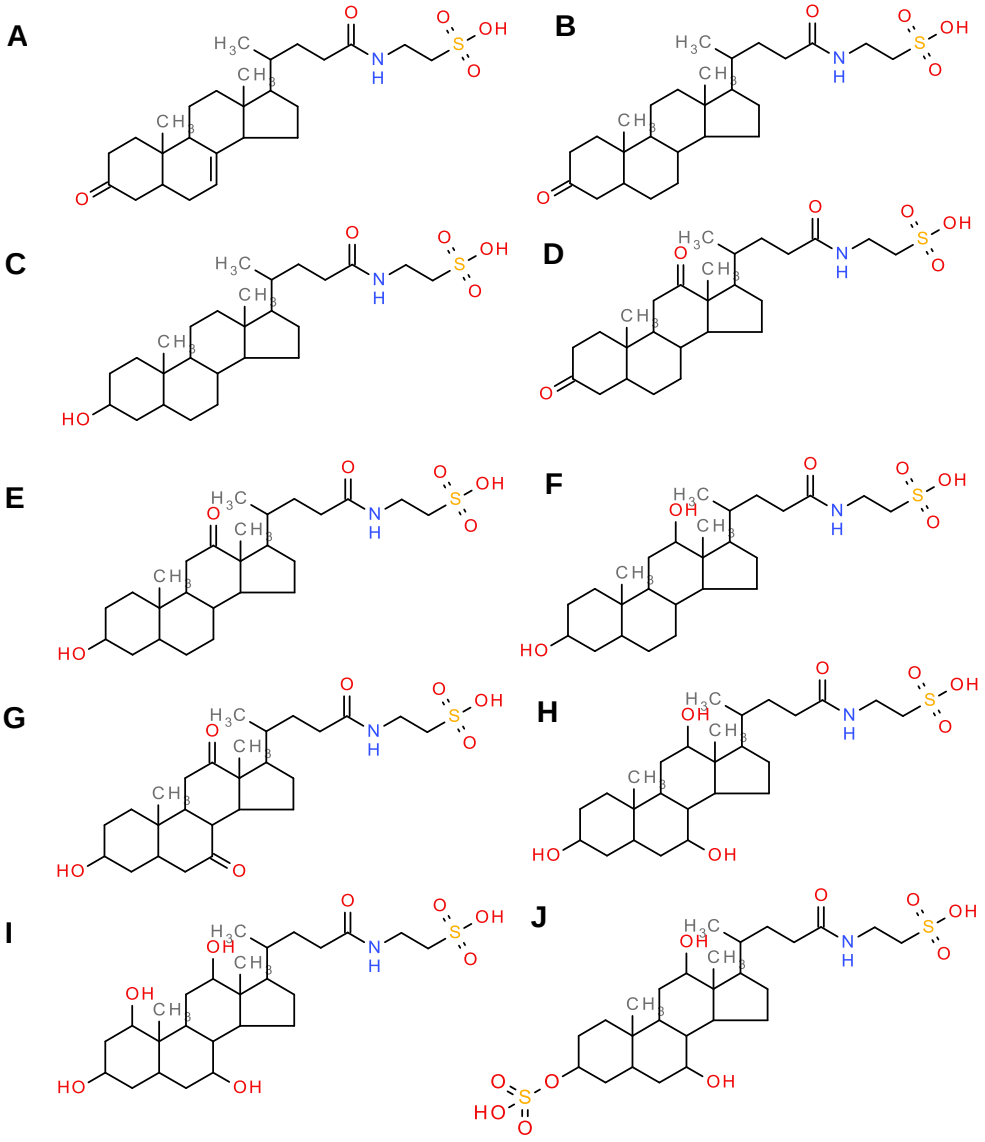

Figure 3-13 C_{24} Taurine conjugated BAs changed significantly between C57J and C57N mice on SAFF diet in cecal samples; A: taurooxocholenoic acid, B: taurooxocholanoic acid, C: taurolithocholic acid, D: taurodioxocholanoic acid, E: taurohydrocyoxocholanoic acid, F: taurodeoxycholic acid , G: taurohydroxyoxocholanoic acid, H: TCA, I: taurohydroxycholanoic acid, J:taurocholic acid sulfate

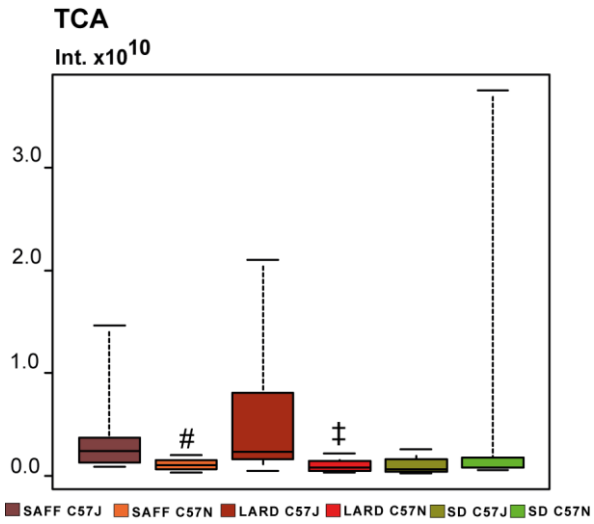

Figure 3-14 Taurocholic acid (TCA) pattern between C57J and C57N mice on SAFF, LARD or SD diet: # p-value = 0.00457; ‡ p-value = 0.01789 (Mann Whitney test)

All others TBAs showed the similar behavior in SAFF and LARD diet comparing the C57J and C57N mice. These results underlined that diet could possibly influence the behavior of TBAs in mice. Watanabe *et al.* could observe, that the patterns of TBAs can be modulated by several factors especially diet, the supplementation with specific bile acids or farnesoid X receptors agonists (Watanabe, Horai et al. 2011). TBAs are higher in germfree mice compared to their conventional controls and are changed after antibiotic treatment resulted in higher levels of TCA and tauro-ß-muricholic acid (Claus, Tsang et al. 2008, Swann, Want et al. 2011). Recently, El Aidy *et al.* described that TBAs are decreasing during conventionalization of germfree mice (El Aidy, Merrifield et al. 2012). As discussed above BAs play a crucial role in energy expenditure, also TCA and TDCA could increase thyroid hormone deiodinase type 2 mRNA and activity. This enzyme is involved in the conversion of inactive thyroxine to its active hormone triiodothyronine through a cAMP dependent manner, taking place in brown adipose tissue (Watanabe, Houten et al. 2006). Moreover, TBAs did not affect cAMP levels in the liver but the action of TBAs was specifically taken part in brown adipose tissue (Wimmer, Hohenester et al. 2008). Lower abundance of TBAs in cecal content of C57JN mice could also be explained through an increase in their deconjugation by specific bacteria that are using sulfur containing taurine as an energy source (Ridlon, Kang et al. 2006, Devkota, Wang et al. 2012). Devkota *et al.* showed that saturated fat (milk-derived) increased the percentage of TCA in bile that was responsible for a significant increase of a member of Deltaproteobacteria, *B. wadsworthia* (Devkota, Wang et al. 2012). The combination of a diet rich in saturated fat, mono-association with *B.wadsworthia* and simultaneous supplementation

with TCA induced and progressed colitis in IL10$^{-/-}$ mice. Martin et al. observed higher levels of TBAs in ileal flushes of human baby flora colonized germfree mice in comparison to conventional mice, which might be explained by changes in the abundance of *Enterobacteria* and *Bacteroides* in human baby flora colonized germfree mice (Martin, Dumas et al. 2007). In this study, elevated TBAS were more associated with the lower body weight changes of C57J mice and are more comparable with germfree mice, which also show leaner phenotype, compared to their conventional raised mice. This implicates that specific gut bacteria in C57N mice utilize the excreted TBAs as an energy source what might be responsible for the observed decrease of TBAs in obese mice (Van Eldere, Robben et al. 1988).

3.4.4.3 Other conjugated C_{24} Bile acids altered between C57J and C57N mice on SAFF diet

The glycine (G) conjugates of CA and DCA found to be significantly different between C57J and C57N mice on SAFF diet. Interestingly all three main G conjugated and sulfated (S) BAs of CA, DCA and LCA were detected and were significantly increased in C57J mice. Especially GCAS were increased 3-fold compared to C57N mice. Discovery of increased BA conjugates revealed that the sulfated form of LCA (SLCA) is increased in C57J mice, but also other sulfated BAs (CA and DCA) were detected but did not allow for discrimination between lean and obese mice in our study (Figure 3-15). The behavior of sulfocholic acid in the other diets is shown in Figure 3-10. Swann *et al.* showed that glycine conjugated BAs were decreased in germfree mice in different tissues (Swann, Want et al. 2011). Conjugation of LCA with sulfate provides a protection against the hepatotoxic effect of LCA through involving the cytochrome P450 enzyme Phase II reactions. In term, the sulfate conjugation of LCA was shown to be independently of microbial abundance/composition and catalyzed by SULTA2 (Deo and Bandiera 2008, Meinl, Sczesny et al. 2009).

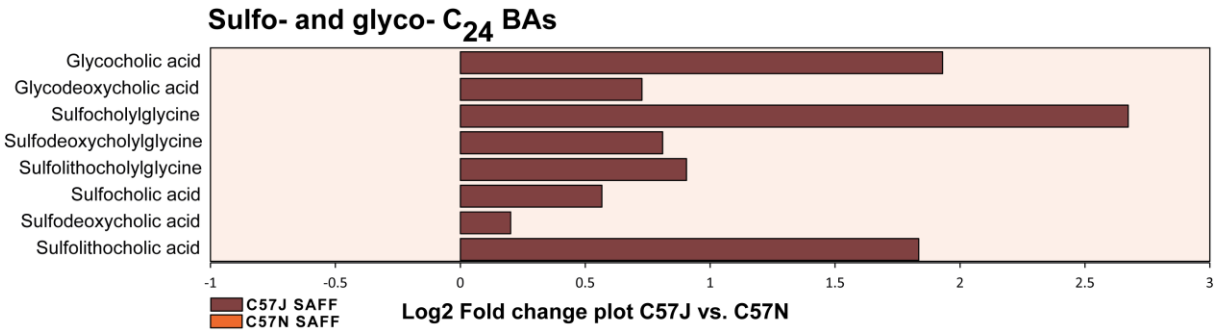

Figure 3-15 Fold change plot of other conjugated BAs, including sulfates and glycine conjugates and their patterns between C57J and c57N mice; all displayed metabolites except sulfocholic and sulfodeoxycholic acid were significant with a p-value <0.05 (Mann-Whitney test), detailed information are given Table 24 of appendix (Chapter 6)

3.4.4.4 C_{27} Taurine conjugated BAs differed between C57J and C57N mice

Amongst C_{24} TBAs, we could find several C_{27} TBAS that were significantly decreased in C57N mice (Figure 3-16) such as taurotrihydroxycholestanoic (H) acid and taurodihydroxycholestanoic acid (E) that were annotated and already described in MassTRIX database. Moreover, we could find eight additional C_{27} TBAs including taurodihydrocholestenoic acid (A), taurocholestenoic acid (B), taurodioxocholestanoic acid (C), taurodihydroxycholestenoic acid (D), taurodihydroxyoxocholestenoic acid (F), taurodihydroxycholestenoic acid (G), taurotetrahydroxycholestenoic acid (I) and taurotetrahydroxycholestanoic acid (J), with increased ratio in C57J mice. The occurrence of taurodihydroxycholestenoic acid was also confirmed by (-) TOF MS/MS experiments (MS/MS spectrum in Figure 5-14, A).

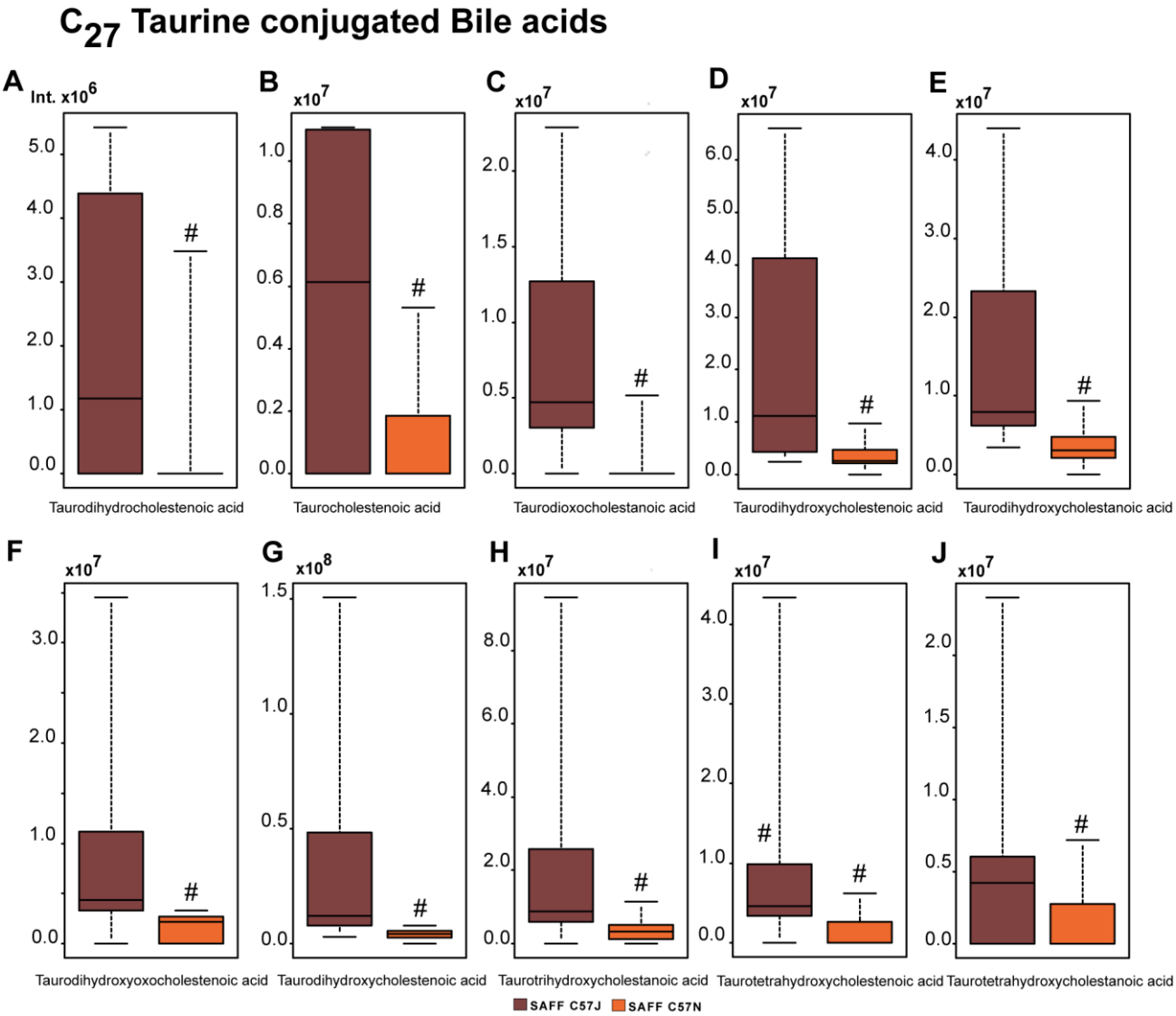

Figure 3-16 C_{27} Taurine conjugated BAs between C57J and C57N mice on SAFF diet, found in cecal content; A: # p-value = 0.02599; B: # p-value = 0.01057; C: # p-value = 0.00397; D: # p-value = 0.00456; E: # p-value = 0.00456; F: # p-value = 0.00735; G: # p-value = 0.00371; H: # p-value = 0.02252; I: # p-value = 0.00773; J: # p-value = 0.04102 (Mann Whitney test)

We observed the same pattern of taurine conjugated C_{27} BAs compared to C_{24} BAs with similar increased levels in C57J mice. Additionally, we compared the pattern of taurodihydroxycholestanoic acid in whole study and observed significantly increased patterns in C57J mice on SAFF and LARD diet (Figure 3-16).

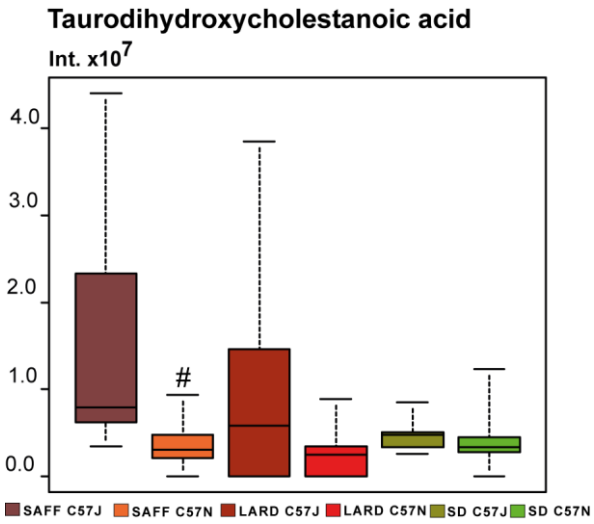

Figure 3-17 Taurodihydroxycholestanoic acid pattern between C57J and C57N mice on SAFF, LARD and SD diet: # p-value = 0.00456 (Mann-Whitney test)

Some C_{27} TBAs such as tauropenta-, taurotetra- and taurotrihydroxycholestanoic acid were already described and observed in urine of patients with Zellweger syndrome or Refsum's disease or with peroxisomes dysfunction in the liver (Lawson, Madigan et al. 1986, Libert, Hermans et al. 1991).

3.4.4.5 Sulfates of C_{27} Bile acids in C57J and C57N mice

Moreover, we also could find that two sulfate conjugates of C27 BAs were also increased in C57J mice of SAFF diet (Figure 3-18). Here we found dihydroxyoxocholestanoic acid sulfate (Figure 3-18, A) and dihydroxycholestenoic acid sulfate (Figure 3-18, B) decreased in C57N mice. Moreover, this increase was specific in C57J on SAFF diet and was not observed in C57J on LARD diet. In mice on SD diet no differences were shown but levels of for example were decreased compared to the other two diets (Figure 3-18). Dihydroxyoxocholestanoic acid sulfate was identified successfully, shown in MS/MS spectrum of Figure 5-14, B.

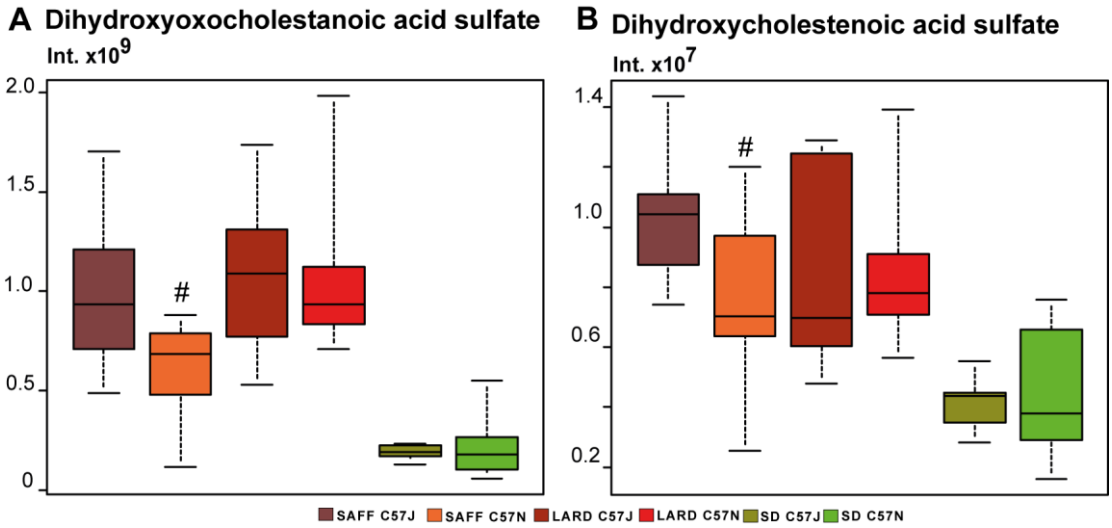

Figure 3-18 Sulfate conjugates of C_{27} BAs between C57J and C57N on SAFF, LARD or SD diet, found in cecal content; A: # p-value = 0.02955; B: # p-value = 0.01760 (Mann Whitney test)

3.4.4.6 Fatty acids and Eicosanoids in C57J and C57N mice

In the S-Plot several fatty acids including arachidonic acid, stearic acid and eicosadienoic acid observed to be discriminative between C57J and C57N mice, whereas arachidonic acid (MS/MS spectrum in Figure 5-15, A) was significantly increased in C57J mice and eicosadienoic acid (MS/MS spectrum in Figure 5-15, B) was significantly increased in C57N mice (Figure 3-4). Moreover, we could find increased levels of docosahexaenoic acid, eicosapentaenoic acid, retinoic acid, LTB4 and hydroxyarachidonic acid in C57J mice (Figure 3-19) that have been shown to modulate PPAR activity (Krey, Braissant et al. 1997).

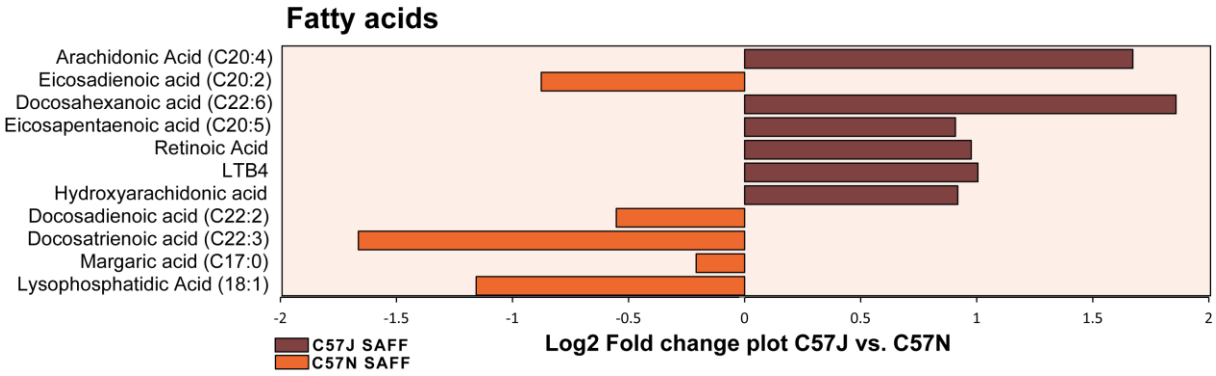

Figure 3-19 Fold change plot of fatty acids differed significantly between C57J and C57N mice on SAFF diet; all displayed metabolites were significant with a p-value <0.05 (Mann-Whitney test), detailed information are given Table 24 of appendix (Chapter 6)

In our study significant increased levels of docosadienoic acid, docosatrienoic acid as well as margaric acid (C17:0) were found in C57N mice (Figure 3-19). Fatty acids are known to act as endogenous ligands of Peroxisome Proliferator-Activated Receptors (PPAR) (Krey, Braissant et al. 1997). Several studies revealed that these receptors are involved in fatty acid and lipid homeostasis finding out that PPARα is responsible for catabolic metabolism of lipids and PPARγ is a regulator of adipogenesis (Chawla, Repa et al. 2001). Lysophosphatidic acid (LPA (C18:1)) is another bioactive lipid that is known to mediate adipocyte proliferation and differentiation, associated with a downregulation of PPARγ expression (Nobusue, Kondo et al. 2010). The presence of LPA in cecum is associated with obesity in C57JN mice.

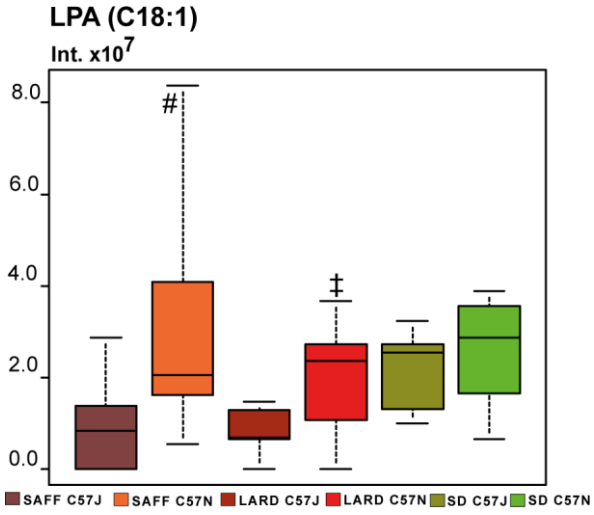

Figure 3-20 The behavior of LPA (C18:1) in cecal samples of C57J and C57N mice on SAFF, LARD and SD diet; # p-value = 0.00453; ‡ p-value = 0.03041; (Mann-Whitney test)

These results were consistent with the results of the study of Federico *et al.*, who pointed the promoting role of LPA in DIO study in mice (Federico, Ren et al. 2012).

3.4.4.7 Endocannabinoid like metabolites in C57J and C57N mice

Muccioli *et al.* showed the involvement of the endocannabinoid system in obesity (Muccioli, Naslain et al. 2010). They measured increased CB1mRNA levels in colon of *ob/ob* mice and their modulation by several factors such as antibiotics, absence of bacteria, HFD and prebiotics. In terms of anandamides, arachidonoylethanolamide (AEA) and 2-Arachidonoylglycerol (2-AG) are endogenous ligands for CB1 whereas AEA levels were reduced in obese mice fed with prebiotics and 2-AG was not affected (Muccioli, Naslain et al. 2010). In our study no changes were observed for 2-AG in cecum samples between C57J and

C57N mice on SAFF diet and AEA of arachidonic acid was not detected (Figure 3-21, A). But, solely comparing the impact of different diets we could see that the applied diets influence the levels of 2-AG independently of the genotype (Figure 3-21, A) (ANOVA p-value: $5.88x10^{-6}$).

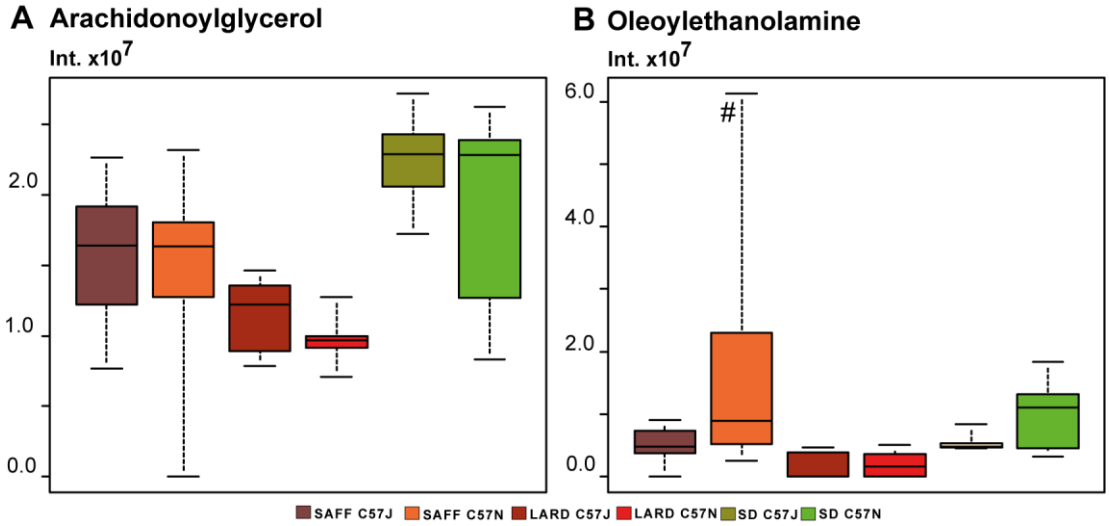

Figure 3-21 Two endocannabinoids alterations between C57J and C57N mice on SAFF, LARD or SD diet in cecal samples: B: # p-value = 0.02955 (Mann-Whitney test)

In SAFF and LARD diet we observed lower levels of 2-AG (Figure 3-21, A) which underlined the HFD influence shown by Muccioli *et al.* (Muccioli, Naslain et al. 2010). Interestingly, other endocannabinoid like molecules were increased in obese C57JN mice, primarily consisting of saturated/mono-unsaturated FAs (stearic acid, oleic acid, erucic acid, 20:1 and 20:2 fatty acids), shown in Figure 3-22. Previous studies demonstrated that oleoylethanolamine (OEA) is not involved in the activation of the endocannabinoid system like AEA but modulates satiety and decreases body weight (Capasso and Izzo 2008). It was suggested that OEA is mediating these functions through activation of PPARα, whereas stearoylethanolamine and AEA had no effect on PPARα. Contrary, in this study stearoylethanolamine is likely associated with the obese status of C57N strain. Elevated levels of OEA in cecal samples might lead to a lower OEA abundance and likely decreased activity in the organism that could result in a decrease on the activation of PPARα pathway and a decreased lipid catabolism (Fu, Gaetani et al. 2003). Interestingly, LARD and SD diet could not influence the levels of OEA between C57J and C57N mice, shown in Figure 3-21, B. In total, these results and the decreased levels of certain fatty acids and eicosanoids in C57N confirm moreover the differently regulated PPAR pathways in C57 mice (Chapter 3.4.4.6).

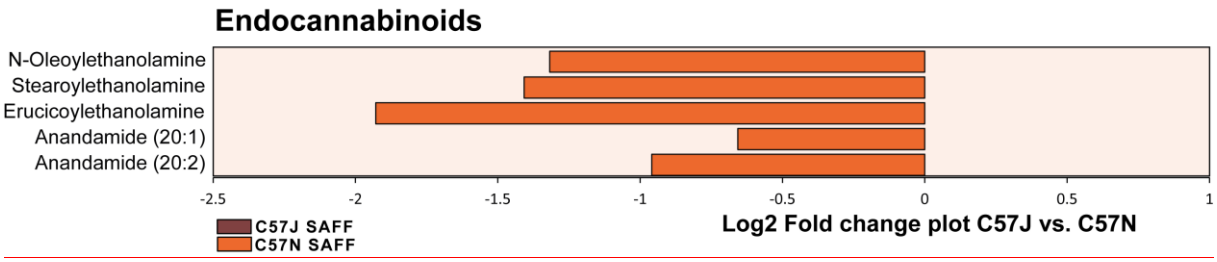

Figure 3-22 Fold change plot of endocannabinoids differed significantly between C57J and C57N mice on SAFF diet in cecal samples; all displayed metabolites were significant with a p-value <0.05 (Mann-Whitney test), detailed information are given Table 24 of appendix (Chapter 6)

3.4.4.8 Lipid changes between C57J and C57N mice

We could also determine significantly increased ratios of ceramides, lysophosphatides (LysoPAs), phosphatides (PAs), lysophosphocholines (LysoPCs), phosphoethanolamines (PEs), and phosphoglycerols (PGs) in C57N mice. Previously, a study in *ob/ob* mice depicted predominantly changes of tri- and diacylglycerols, phosphoglycerols and ceramide species (Yetukuri, Katajamaa et al. 2007). Increased ratios were shown for example for the ceramide species Cer(18:1/18:0) and Cer(18:1/16:0) in liver of *ob/ob* mice. In our study, elevated levels of different ceramide species predominantly with saturated fatty acid moieties were observed: Cer(34:0), Cer(36:0) or Cer(40:0). Also, our study is indicating that lipid profiles in intestinal samples may also linked with the HFD-induced obesity in C57N sub strain (Samad, Hester et al. 2006).

Table 7 Lipid changes between C57J and C57N fed with SAFF diet

[M-H]$^-$	Compound Name	Monoisotopic mass	C57J	C57N	log2 fold change	Increased	p-value	Molecular Formula
Ceramides								
538.52044	Cer(34:0)	539.527714	2.9E+07	4.7E+07	-0.71	C57N	0.00155	$C_{34}H_{69}NO_3$
552.53605	Cer(35:0)	553.543321	7.8E+06	1.2E+07	-0.57	C57N	0.04095	$C_{35}H_{71}NO_3$
566.55144	Cer(36:0)	567.558711	1.8E+07	3.9E+07	-1.14	C57N	0.00372	$C_{36}H_{73}NO_3$
622.61441	Cer(40:0)	623.621683	4.6E+06	7.8E+06	-0.77	C57N	0.00562	$C_{40}H_{81}NO_3$
636.63002	Cer(41:0)	637.637295	1.0E+06	1.6E+06	-0.65	C57N	0.00526	$C_{41}H_{83}NO_3$
648.62990	Cer(42:1)	649.637172	6.5E+06	9.9E+06	-0.60	C57N	0.00835	$C_{42}H_{83}NO_3$
678.67681	Cer(44:0)	679.684083	3.3E+05	1.9E+06	-2.54	C57N	0.02926	$C_{44}H_{89}NO_3$
LysoPA; PA								
379.18945	PA(14:1)	380.196730	2.7E+06	4.9E+05	2.43	C57J	0.02175	$C_{17}H_{33}O_7P$
421.27251	PA(18:0)	422.279784	3.0E+06	8.7E+06	-1.55	C57N	0.00535	$C_{21}H_{43}O_6P$
435.25176	PA(18:1)	436.259036	9.4E+06	2.9E+07	-1.62	C57N	0.00453	$C_{21}H_{41}O_7P$
479.31399	PA(21:0)	480.321263	6.6E+06	2.7E+06	1.26	C57N	0.02886	$C_{24}H_{49}O_7P$
671.46527	PA(34:2)	672.472549	8.4E+05	3.1E+06	-1.90	C57N	0.01268	$C_{37}H_{69}O_8P$
673.48151	PA(34:1)	674.488784	1.7E+06	6.1E+06	-1.82	C57N	0.00762	$C_{37}H_{71}O_8P$
LysoPC; PE								
411.23883	LysoPC(10:0)	412.246105	2.9E+07	4.7E+07	-0.70	C57N	0.02497	$C_{18}H_{39}NO_7P$
514.29393	LysoPC(18:4)	515.301204	3.0E+07	4.2E+06	2.84	C57J	0.02647	$C_{26}H_{46}NO_7P$
676.49243	PE(31:0)	677.499702	1.1E+07	1.7E+07	-0.60	C57N	0.01761	$C_{36}H_{72}NO_8P$
688.49191	PE(32:1)	689.499185	3.7E+06	7.2E+06	-0.98	C57N	0.00685	$C_{37}H_{72}NO_8P$
690.50803	PE(32:0)	691.515309	1.6E+06	1.1E+07	-2.74	C57N	0.00068	$C_{37}H_{74}NO_8P$
702.50784	PE(33:1)	703.515114	1.0E+07	1.8E+07	-0.87	C57N	0.00242	$C_{38}H_{74}NO_8P$
704.52337	PE(33:0)	705.530643	3.1E+05	3.2E+06	-3.35	C57N	0.00152	$C_{38}H_{76}NO_8P$
716.52375	PE(34:1)	717.531023	1.0E+07	1.9E+07	-0.94	C57N	0.00242	$C_{39}H_{76}NO_8P$
718.53882	PE(34:0)	719.546097	1.0E+06	2.2E+06	-1.16	C57N	0.00222	$C_{39}H_{78}NO_8P$
728.52349	PE(35:2)	729.530764	1.0E+06	1.7E+06	-0.79	C57N	0.01173	$C_{40}H_{76}NO_8P$
730.53905	PE(35:1)	731.546323	6.5E+05	4.8E+06	-2.88	C57N	0.00105	$C_{40}H_{78}NO_8P$
740.52299	PE(36:3)	741.530262	1.1E+06	3.6E+06	-1.70	C57N	0.02006	$C_{41}H_{76}NO_8P$
PG								
483.27278	PG(16:0)	484.280053	8.8E+06	1.5E+07	-0.80	C57N	0.00562	$C_{22}H_{45}O_9P$
495.30946	PG(P-18:0)	496.316736	4.9E+05	3.0E+06	-2.63	C57N	0.02404	$C_{24}H_{49}O_8P$

505.25706	PG(18:3)	506.264335	2.1E+07	6.0E+07	-1.49	C57N	0.00686	$C_{24}H_{43}O_9P$
509.28837	PG(18:1)	510.295646	3.3E+06	8.9E+06	-1.42	C57N	0.01414	$C_{24}H_{47}O_9P$
511.30397	PG(18:0)	512.311249	4.6E+06	9.1E+06	-0.98		0.01213	$C_{24}H_{49}O_9P$
677.47594	PG(30:1)	678.483215	6.8E+06	1.5E+07	-1.10		0.00562	$C_{36}H_{71}O_9P$
689.47592	PG(31:1)	690.483194	2.7E+05	1.7E+06	-2.68		0.04621	$C_{37}H_{71}O_9P$
691.49209	PG(31:1)	692.499364	1.9E+07	4.4E+07	-1.18		0.00835	$C_{37}H_{73}O_9P$
703.49222	PG(32:1)	704.499496	1.6E+06	6.7E+06	-2.06		0.00320	$C_{38}H_{73}O_9P$
707.48703	PG(31:0)	708.494310	7.0E+06	1.4E+07	-1.01		0.00458	$C_{37}H_{73}O_{10}P$
721.50270	PG(32:0)	722.509972	8.0E+06	2.2E+07	-1.43		0.00155	$C_{38}H_{75}O_{10}P$
721.53936	PG(33:0)	722.546631	1.0E+06	3.2E+06	-1.70		0.02036	$C_{39}H_{79}O_9P$
731.52340	PG(34:2)	732.530678	3.5E+07	7.3E+07	-1.06		0.01761	$C_{40}H_{77}O_9P$
733.53860	PG(34:1)	734.545871	4.6E+06	1.1E+07	-1.21		0.00835	$C_{40}H_{79}O_9P$
749.53353	PG(34:0)	750.540804	3.5E+06	8.4E+06	-1.27		0.00799	$C_{40}H_{79}O_{10}P$
757.53857	PG(36:3)	758.545850	2.0E+06	6.2E+06	-1.60		0.00699	$C_{42}H_{79}O_9P$
761.53408	PG(35:1)	762.541352	7.3E+06	1.5E+07	-1.05		0.00835	$C_{41}H_{79}O_{10}P$
761.57043	PG(36:0)	762.577706	3.2E+05	2.2E+06	-2.83		0.02404	$C_{42}H_{83}O_9P$
763.54988	PG(35:0)	764.557152	5.8E+05	3.4E+06	-2.55		0.01435	$C_{41}H_{81}O_{10}P$
771.51785	PG(36:3)	772.525128	4.6E+05	2.4E+06	-2.39		0.01792	$C_{42}H_{77}O_{10}P$
775.54962	PG(36:1)	776.556895	1.3E+07	3.1E+07	-1.25		0.00562	$C_{42}H_{81}O_{10}P$
801.56563	PG(38:2)	802.572908	2.8E+06	1.2E+07	-2.13		0.00139	$C_{44}H_{83}O_{10}P$

3.4.4.9 Bacterial derived metabolite patterns between C57J and C57N mice: Lignans and urobilinoids

Enterolactone and enterodiol are metabolites that are produced by intestinal bacteria and have been reported to exert beneficial effects in a mammalian system(Woting, Clavel et al. 2010). In our study, the precursor plant lignans matairesinol, secoisolariciresinol and lariciresinol did not differ between the two mice strains, but the bacterial converted metabolites enterolactone and enterodiol were increased in cecal content of C57J mice on SAFF and LARD diet. SD diet did not influence levels of both metabolites between C57J and C57N mice (Figure 3-23). The presence of enterolactone in cecal samples was confirmed by (-) TOF-MS/MS experiments (MS/MS spectrum in Figure 5-16, A). Studies showed that low concentrations of enterolactone in human plasma were positively correlated with obesity (Sonestedt, Borgquist et al. 2008). Recently, a study revealed that administration of secoisolariciresinol in obese mice reduces in HFD-induced body weight. Subcutaneous injection of enterolactone and enteridiol tended to decrease body weight of obese mice (Tominaga, Nishi et al. 2012).

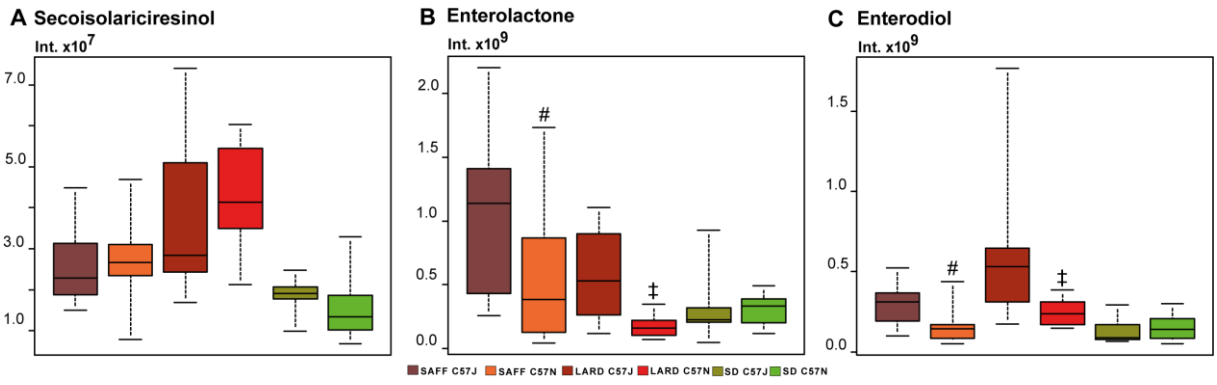

Figure 3-23 Lignans and their metabolites enterolactone and enterodiol patterns in C57J and C57N mice after SAFF, LARD or SD diet in cecal samples; B: # p-value = 0.03485; ‡ p-value = 0.00550; C: # p-value = 0.00835; ‡ p-value = 0.00705 (Mann-Whitney test)

Several bilirubin degradation compounds were increased in C57N including urobilinogens and urobilins. In detail, we observed higher levels of D-, L- and I-Urobilinogen and increased levels of D- and L-Urobilin in C57N mice (Figure 3-24). The presence of L-Urobilin was confirmed by (-) TOF-MS/MS experiments (MS/MS spectrum in Figure 5-16, B).

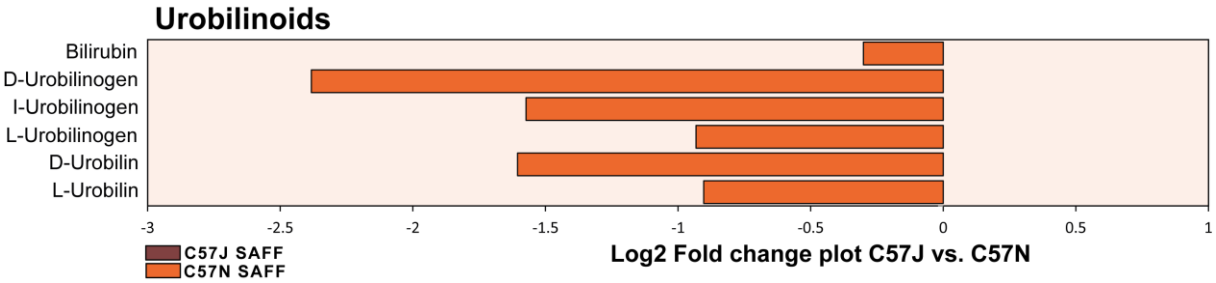

Figure 3-24 Fold change plot of urobilinoids between C57J and C57N mice on SAFF diet in cecal samples; all displayed metabolites except bilirubin were significant with a p-value <0.05 (Mann-Whitney test), detailed information are given Table 24 of appendix (Chapter 6)

The degradation of bilirubin occurs through intestinal bacteria but interestingly the levels of bilirubin were not changed between C57J and C57N (Tiribelli and Ostrow 2005). The increased presence of so-called urobilinoids resulted likely due to different microbial communities in C57J and C57N mice. In germfree mice no urobilinoid formation was observed but the amount of bilirubin was comparable with the sum of bilirubin and all urobilinoids, detected in conventional mice (Gustafsson and Lanke 1960). Until now, several bacterial strains were found to contribute to bilirubin catabolism: such as unclassified *Clostridium* species, *E.coli* (Gustafsson and Lanke 1960) *Clostridium perfringens*, *Clostridium ramosum* and *Clostridium difficile* (Vítek, Zelenka et al. 2005) and *Bacteriodes fragilis* (Fahmy, Gray et al. 1972, Jedlitschkys, Volkls et al. 1991). Besides this, the absence of bacteria like in germfree mice, but also antibiotic treatment decreased markedly the fecal excretion of urobilinoids but also the fecal bilirubin concentration (Vítek, Zelenka et al. 2005). Lower urobilinoids in feces were also dependent on the applied antibiotic drug (Vítek, Zelenka et al. 2005). Next, we showed the behavior of urobilinoids L-urobilin and L-urobilinogen as well as bilirubin in all groups and the impact of the diets. The patterns of L-Urobilinogen were significantly increased in C57N mice on SAFF and LARD diet, whereas L-Urobilin was significantly increased in C57N on SAFF diet but not in LARD diet fed mice. We could also see the different behavior of urobilinoids is dependent on the applied diets. The levels of urobilinoids were increased in mice on SAFF and LARD diet (Figure 3-25).

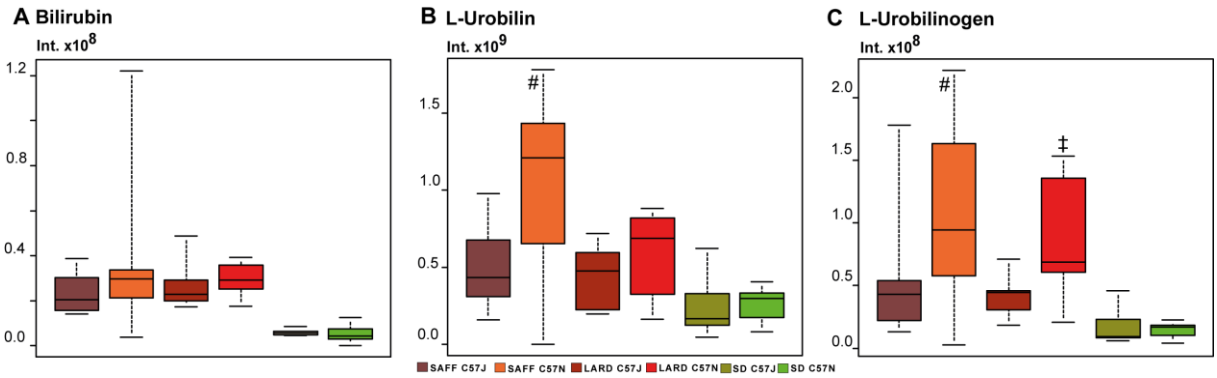

Figure 3-25 Bilirubin and two urobilinoids L-Urobilin and L-Urobilinogen patterns comparing cecal samples of C57J and C57N mice on SAFF, LARD and SD diet: A: # p-value = 0.02496; B: # p-value = 0.02100; ‡ p-value = 0.00898 (Mann-Whitney test)

The levels of bilirubin were increased in SAFF and LARD diet mice compared to the SD diet mice (Figure 3-25, A). Thus, we assume that diet could be also one of the factors that affect the levels of urobilinoids in mice.

3.4.4.10 Novel metabolites identified between C57J and C57N mice

According the comparison of C57J and C57N on SAFF diet we revealed that one mass signal obtained the highest p-value of 0.00011 (Mann-Whitney test). The mass signal was also significantly increased in C57J mice on LARD diet, but not SD diet (Figure 3-26, A). This mass signal with experimental mass value of $[M-H]^-$: 383.197532 and the neutral molecular formula composition of $C_{22}H_{28}N_2O_4$ were then subjected to MS/MS identification experiments (Figure 4-10).

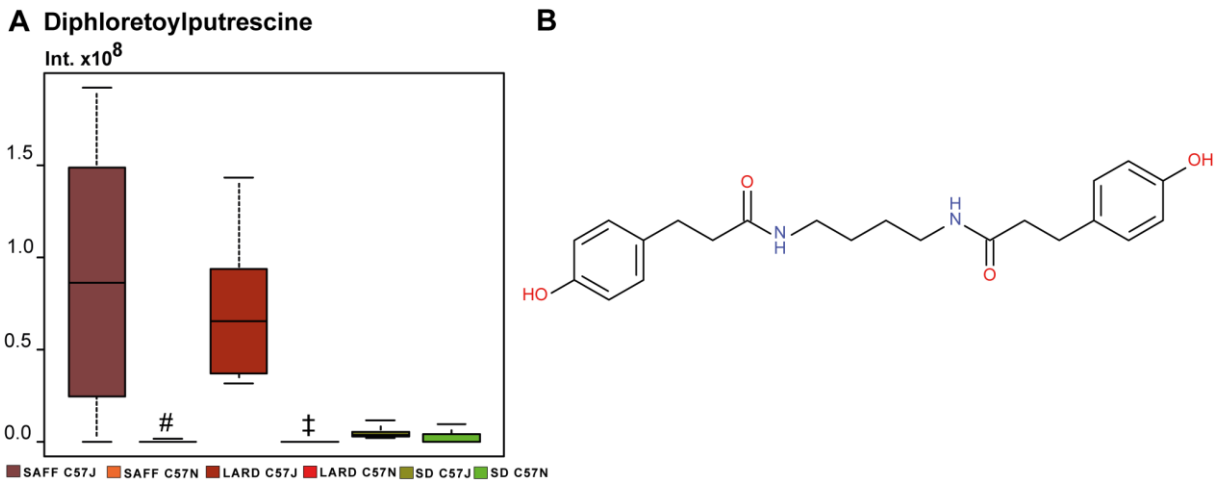

Figure 3-26 A novel metabolite called diphloretoylputrescine identified in cecal content of C57J mice and its pattern between C57J and C57N mice on SAFF, LARD or SD diet; B: # p-value = 0.00011; ‡ p-value = 0.00007 (Mann-Whitney test)

The most plausible metabolite that we considered due to the given MS/MS fragments is shown in Figure 3-26, B. The MS/MS spectrum of this metabolite and detailed fragmentations are shown in Figure 5-17. This metabolite is likely consisting of two molecules of hydroxyphenylpropionic acid (also known as phloretic acid or dihydrocoumaric acid) and a putrescine molecule as the linkage (Figure 3-26). This metabolite is likely produced through an enzymatic condensation of the carboxyl group of phloretic acid and the amino group of putrescine. The metabolite is so-called diphloretoylputrescine and belongs to the class of polyamine conjugates. Phloretic acid is a degradation product of the tyrosine metabolism and putrescine is originated through microbial degradation of proteins (Booth, Masri et al. 1960, Welters, Dejong et al. 1999). Previously, related polyamine conjugates with different phenol containing molecules such as coumaric, ferulic and caffeic acid were discovered, predominantly in plants (Moreau, Nuñez et al. 2001, Choi, Lee et al. 2007). Especially, the conjugates dicoumaroylputrescine and diferuoylputrescine were shown to be anti-inflammatory and inhibit nitric oxide production in macrophages (Kim, Min et al. 2012).

3.4.5 Comparative analysis of cecal meta-metabolome pattern between C57J and C57N mice on SAFF diet using UPLC-TOF-MS

Here, again the focus was to examine the differences of cecal metabolome between the two strains after SAFF diet. Cecal samples of C57J and C57N mice were separated using a RP column (C8, Waters© Acquity™ UPLC® BEH™ C8 column (1.7 µm, 2.1 × 150 mm)). Here we focused also on the data derived from (-) UPLC-TOF-MS mode. The LC-MS data was then processed with an MzMine, resulted in 1580 features in subsequent subjection with MSA. The data reduction using PCA showed a sufficient separation of C57J and C57N mice, whereas the PC1 declares 27.2 % and the PC2 explains 10.5 % of the total variance (Figure 3-27, A). Furthermore, a non-parametric univariate test Mann-Whitney test was used for the calculation of significant features between C57J and C57N on SAFF diet, resulting in 240 significant features. Afterwards we compared the metabolites derived through the FT-ICR-MS elaboration and extrapolated the overlaying significantly changed metabolites between FT-ICR-MS and UPLC-TOF-MS experiments. We found 17 different metabolites, which matched in both analyses. The metabolites that were also found in UPLC-TOF-MS analysis are shown in the heatmap (Figure 3-27, B). We could find conjugated BAs, especially the taurine conjugates, the lignane catabolites enterolactone and enterodiol and urobilinoids that discriminateC57J and C57N mice, shown in Figure 3-27, B.

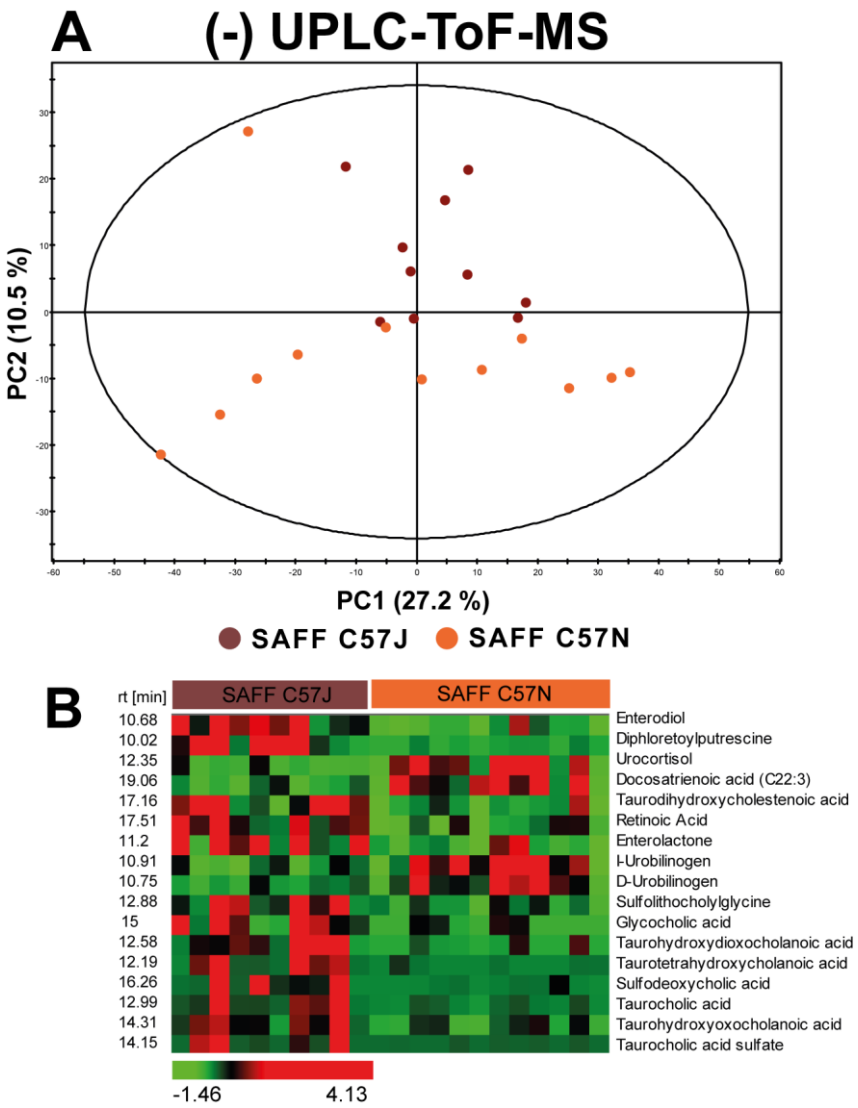

Figure 3-27 A: PCA scores scatter plot of cecal metabolome including C57J and C57N mice on SAFF diet by using (-) UPLC-TOF-MS analysis B: A heatmap visualizing the significantly changed metabolites found by comparison of (-) UPCL-TOF-MS with (-) FT-ICR-MS measurements; all displayed metabolites are significant with a p-value <0.05 (Mann-Whitney test), detailed information are given Table 26 of appendix (Chapter 6)

3.4.6 Cecal meta-metabolome changes between C57J and C57N, dependent on the fed diet

As next, we determined all mass signals that were only significant in one diet between C57J and C57N but remained unchanged in the other two (Figure 3-5, Venn diagram, orange, red and green). We filtered only on the top 10 of highly abundant mass signals that were significantly different between C57J and C57N on a specific diet but not in the other two diets.

3.4.6.1 Altered metabolites between C57J and C57N fed with SAFF diet

The analyses of the unique metabolites significantly changed between C57J and C57N after three weeks of SAFF diet are summarized in Table 8. In detail, these metabolites were unsaturated FAs, BAs, sulfated C_{27} BAs and L-Urobilin but also sulfated phytosterines (Table 8).

Table 8 Uniquely differed metabolites between C57J and C57N after SAFF diet

[M-H]$^-$	Compound Name	Monoisotopic mass	C57J	C57N	log2 fold change	Increased	p-value	Molecular Formula
303.232832	Arachidonic Acid (C20:4)	304.2402172	2.96E+09	1.09E+09	1.44	C57J	0.01760	$C_{20}H_{32}O_2$
327.233001	Docosahexanoic acid (C22:6)	328.2402172	5.76E+08	1.80E+08	1.68	C57J	0.01222	$C_{22}H_{32}O_2$
365.233356	Urocortisol	366.2406114	2.79E+08	8.21E+08	-1.55	C57N	0.04791	$C_{21}H_{34}O_5$
391.285157	Deoxycholic acid	392.292644	1.57E+10	9.86E+09	0.67	C57J	0.02496	$C_{24}H_{40}O_4$
423.275108	Tetrahydroxycholanoic acid	424.282474	5.43E+08	8.17E+08	-0.59	C57N	0.01760	$C_{24}H_{40}O_6$
427.26193	Deoxycholic acid [M+Cl]-	427.261497	5.54E+08	2.52E+08	1.14	C57J	0.00155	$C_{24}H_{40}O_4Cl$
479.319867	Campesterylsulfate (Phytosterine)	480.3273128	4.55E+08	3.05E+08	0.57	C57J	0.00097	$C_{28}H_{48}O_4S_1$
493.335481	Stigmastenylsulfate (Phytosterine)	494.342962	5.39E+08	2.88E+08	0.90	C57J	0.00242	$C_{29}H_{50}O_4S_1$
527.268213	Dihydroxyoxocholestanoic acid sulfate	528.2756744	9.67E+08	6.10E+08	0.66	C57J	0.02955	$C_{27}H_{44}O_8S_1$
593.334357	L-Urobilin	594.3417176	5.20E+08	1.04E+09	-1.00	C57N	0.02496	$C_{33}H_{46}N_4O_6$

3.4.6.2 Altered metabolites between C57J and C57N fed with LARD diet

The unique metabolites that discriminated C57J and C57N on LARD diet were predominantly fatty acids such as oleic acid or icosatrienoic acid, lithocholic acid, hydroxyalphatocopherol and sarcostin, shown in Table 9. All shown metabolites were exclusively increased in C57N mice.

Table 9 Uniquely differed metabolites between C57J and C57N fed with LARD diet

[M-H]⁻	Compound Name	Monoisotopic mass	C57J	C57N	log2 fold change	Increased	p-value	Molecular Formula
241.217339	Pentadecanoic acid	242.224568	2.5E+08	4.1E+08	-0.70	C57N	0.00710	$C_{15}H_{30}O_2$
281.248393	Oleic acid	282.2558664	9.1E+09	1.5E+10	-0.71	C57N	0.03376	$C_{18}H_{34}O_2$
299.259197	Hydroxystearic acid	300.2664306	9.4E+08	2E+09	-1.09	C57N	0.02748	$C_{18}H_{36}O_3$
305.248438	Icosatrienoic acid	306.2558664	2.4E+09	4.4E+09	-0.89	C57N	0.00044	$C_{20}H_{34}O_2$
329.248637	Docosapentanoic acid	330.2558664	6.1E+08	1.1E+09	-0.84	C57N	0.00705	$C_{22}H_{34}O_2$
331.264194	Docosatetraenoic acid	332.2715156	7.1E+08	1.2E+09	-0.78	C57N	0.02748	$C_{22}H_{36}O_2$
375.29046	Lithocholic acid	376.297729	3.4E+08	6.3E+08	-0.89	C57N	0.02224	$C_{24}H_{40}O_3$
381.228178	Sarcostin	382.2355264	4.7E+08	8.3E+08	-0.82	C57N	0.04126	$C_{21}H_{34}O_6$
445.368713	Hydroxyalphatocopherol	446.375975	2.1E+08	4.6E+08	-1.10	C57N	0.00081	$C_{29}H_{50}O_3$
483.205666	Unknown	484.2130776	5.5E+07	5.7E+08	-3.38	C57N	0.01430	$C_{24}H_{36}O_8S_1$

3.4.6.3 Altered metabolites between C57J and C57N fed with SD diet

In SD diet, we also found different metabolites that were changed significantly between C57J and C57N. However, it was difficult to classify these metabolites based on the annotation, shown in Table 10. However, we could observe six different C_{29} containing metabolites that were overall increased in C57J mice (Table 10). Moreover, performed MS/MS experiments could not provide sufficient information about the metabolites to identify clearly the annotated metabolites.

Table 10 Uniquely differed metabolites between C57J and C57N fed with SD diet

[M-H]⁻	Compound Name	Monoisotopic mass	C57J	C57N	log2 fold change	Increased	p-value	Molecular Formula
301.165733	Glycerol tributyrate	302.1729296	4.8E+07	1.8E+08	-1.90	C57N	0.01182	$C_{15}H_{26}O_6$
343.321753	1-O-Octadecylglycerol	344.3290274	2.9E+08	1.8E+08	0.70	C57J	0.02835	$C_{21}H_{44}O_3$
457.295837	Unknown	458.3032082	5.1E+08	1.8E+08	1.49	C57J	0.00448	$C_{28}H_{42}O_5$
459.311441	Stoloniferone G	460.3188574	1.2E+08	7.5E+07	0.63	C57J	0.01182	$C_{28}H_{44}O_5$
469.296007	Minabeolide	470.3032082	4.4E+08	2.6E+08	0.76	C57J	0.00737	$C_{29}H_{42}O_5$
471.311515	Unknown	472.3188574	7.3E+09	3E+09	1.25	C57J	0.00448	$C_{29}H_{44}O_5$
473.32706	Acetoxydihydroxycalciferol	474.3345066	1.5E+09	4.8E+08	1.61	C57J	0.00448	$C_{29}H_{46}O_5$
485.290813	Hydrocortisone cypionate	486.2981232	1.4E+09	6.3E+08	1.16	C57J	0.00737	$C_{29}H_{42}O_6$
519.27839	Unknown	520.2858444	1.6E+08	7.2E+07	1.13	C57J	0.00737	$C_{29}H_{44}O_6S_1$
535.273697	Unknown	536.2807594	1.8E+08	5.9E+07	1.62	C57J	0.00448	$C_{29}H_{44}O_7S_1$

3.4.7 Diet induced alterations in cecal meta-metabolome of C57 mice

Our next approach was to observe the differences in the metabolome that were significantly changed due to the diets. Therefore, we performed a univariate ANOVA analysis. We could find 2839 mass signals from 3903 mass signals that were significantly altered between all three diets. Different diets had a large impact on cecal metabolome independently from the mouse genotype and obesity related changes.

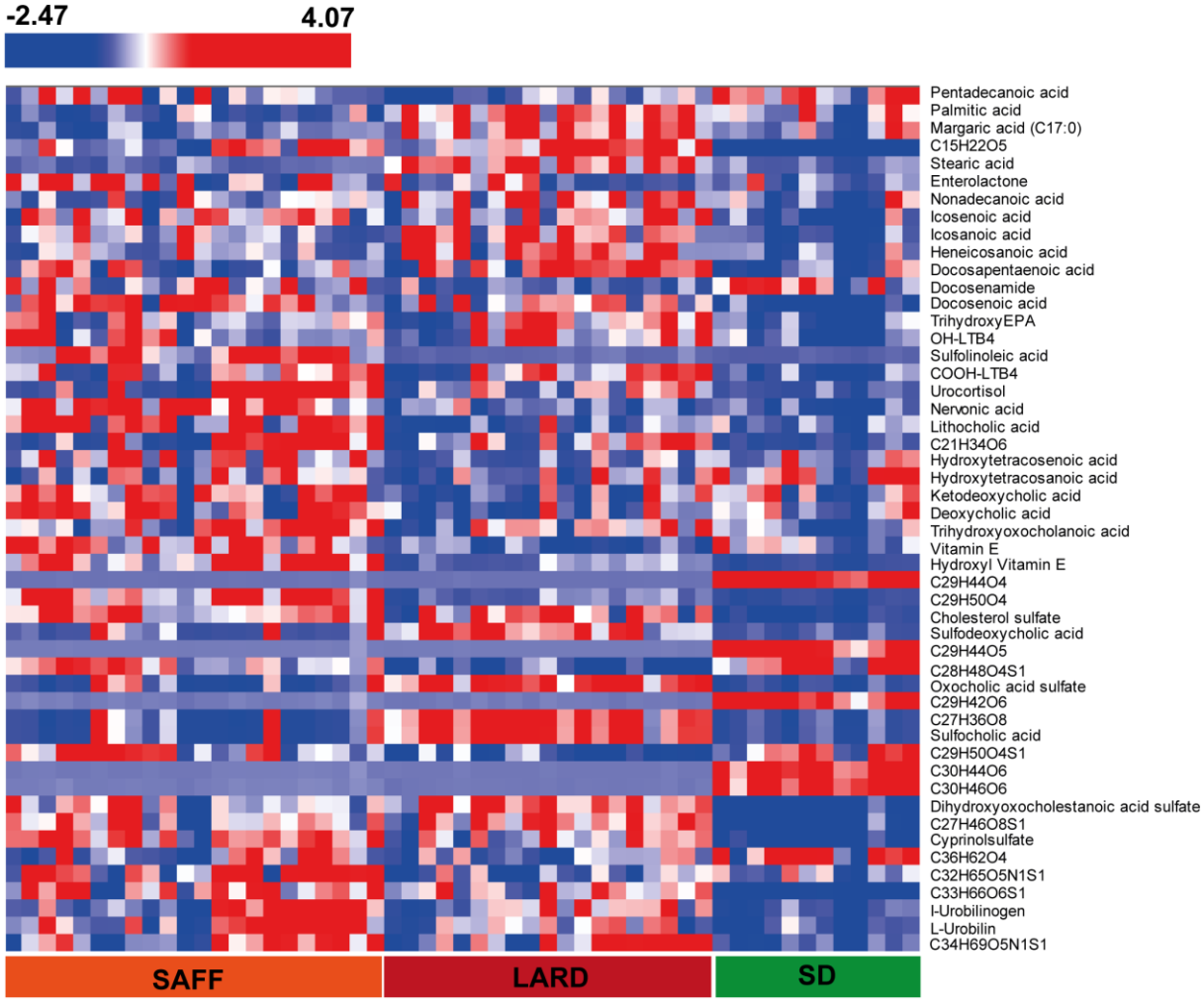

Figure 3-28 Top 50 highly abundant mass signals differed significantly between SAFF, LARD and SD diet; all displayed metabolites were significant with a p-value <0.05 (ANOVA); Not annotated mass signals are indicated by their molecular formulas

We extrapolated then all significant and highly abundant mass signals that were responsible for the discrimination between SAFF, LARD and SD diet. The mass signals responsible for the separation due to different diet were displayed in the heatmap (Figure 3-28). Different

metabolites were affected and differed due to diets such as fatty acids, bile acids but also lignans and urobilinoids (Figure 3-28 and Figure 3-29). For example, palmitic acid was increased in cecal metabolome in SAFF fed mice (Figure 3-29, A) compared to other diets. The AAM metabolite COOH-LTB4 was increased in SAFF and LARD diet (Figure 3-29, B). The bile acid DCA (Figure 3-29, C) and the lignane catabolite enterolactone (Figure 3-29, D) were increased in SAFF diet mice. Vitamin E was increased in SAFF and decreased in LARD diet compared to SD diet (Figure 3-29, E). Sulfolinoleic acid was highly increased in SAFF diet compared to other diets (Figure 3-29, F).

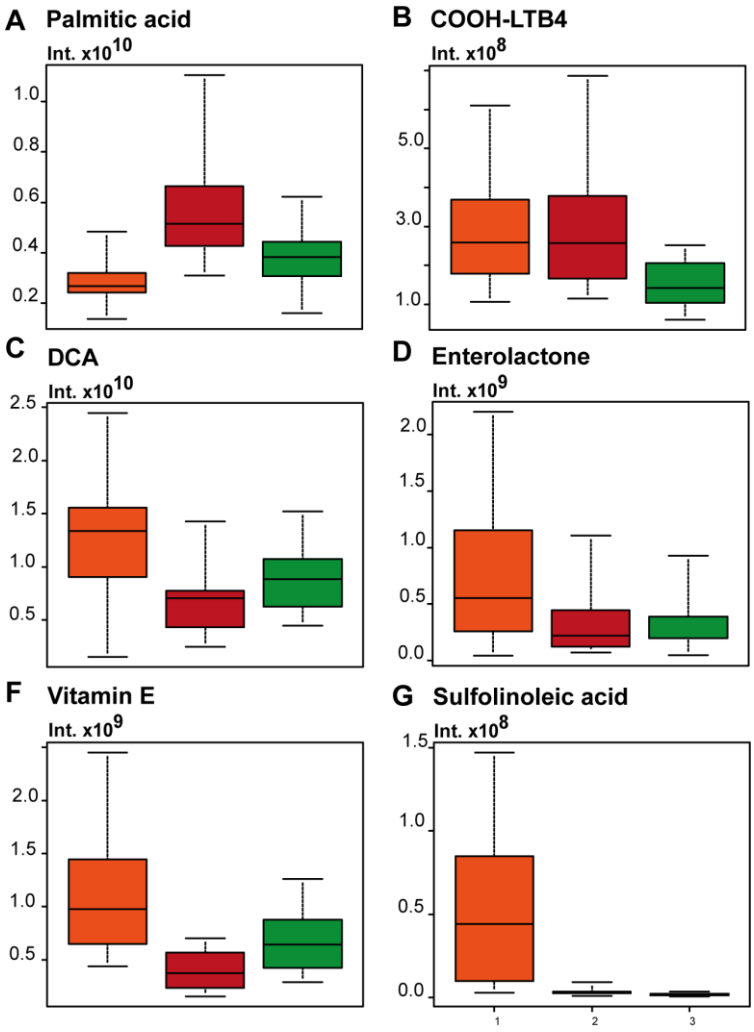

Figure 3-29 Six metabolites differed significantly between the diets A: Palmitic acid p-value (ANOVA) = 1.47061E-06; B: COOH-LTB4 p-value (ANOVA) = 7.31956E-03; C: DCA p-value (ANOVA) = 9.20414E-04; D: Enterolactone p-value (ANOVA) = 6.08204E-03; E: Vitamin E p-value (ANOVA) = 6.81139E-06; D: Sulfolinoleic acid p-value (ANOVA) = 4.26401E-07; detailed information are given of appendix (Chapter 6)

Several metabolomics studies were conducted in order to study the effect of high fat diets on obesity and/or insulin resistance. In our study, the C57N mouse strain developed obesity on SAFF and LARD diet compared to the SD diet. The advantage of our study was that the C57N mouse strain developed obesity on SAFF or LARD diet compared to the lean C57J mouse strain. Thus, we can differentiate between diet-related effects and obesity-related effects as we considered only the differences of C57J and C57N on the SAFF diet. Shearer *et al.* compared high-fat fed C57BL/6J mice to chow fed mice by applying a ^{1}H-NMR metabolic profiling study of sera plasma for 12 weeks (Shearer, Duggan et al. 2008). They reported about metabolites involved in the energy metabolism like citrate and amino acids such as leucine. Another study performed a GC-MS based metabolomics approach with insulin – resistant mouse strain compared to the control wildtype strain and the effect of diet containing safflower diet (Li, Hu et al. 2010). For example, TCA was significantly decreased in liver and plasma samples due to diet in wild type mice but not the insulin resistant mice. In our study, TCA was changed between C57J and C57N mice on SAFF diet and LARD diet but the different diets did not affect the TCA levels. In our study, decreased TCA levels were strongly associated with body weight increase in C57N on SAFF and LARD study. They showed that palmitic acid was increased in wildtype mice associated with both diets. Here, palmitic acid was significantly increased in LARD diet in both strains. This is probably due to the LARD diet composition with high content of palmitic acid in diet. In another study of high-fructose diet, metabolite profiles were investigated in rats by LC-MS/MS metabolomics approach (Lin, Yang et al. 2011). High-fructose diet revealed increased blood glucose levels at the beginning and after an oral glucose tolerance test but the rats had lower body weights compared to the control rats (Lin, Yang et al. 2011). They could find different lipids such as phosphatidylcholines, lysoPCs and lysoPEs that were changed after high fructose diet measured in plasma, liver and skeletal muscles samples from rats (Lin, Yang et al. 2011). We could already observe different lipid patterns between C57J and C57N on SAFF diet that were related to the body weight changes in C57N mice. We could observe different ceramides, PA, lysoPCs, PEs and PGs.

3.5 Summary and Conclusion

Here, in this study we investigated the role of different diets and genotype susceptibility of two sub strains of C57BL/6 mice. We could show that both diet and genotype influences the phenotype resulting in increased body weight in C57N mice. By applying an unbiased metabolomics approach, we highlighted the meta-metabolome differences, especially by focusing on the analysis of one diet in two substrains. For example, bile acids were key metabolites that were changed in C57J and C57N mice. Bile acids are known to exert many biological functions such as regulating energy expenditure in receptor dependent manner. The different signature of bile acids can be also regarded as a functional output of different bacterial community and their metabolism. Especially, the systematic behavior of taurine conjugates of C_{24} and C_{27} BAs between C57J and C57N mice indicated the appearance of distinct gut microbial communities in cecal samples. Taurine deconjugation of bile acids is a specific feature belonging to bacterial metabolism. Bile acids and their conjugates either taurine or sulfates are known to be co-microbial metabolites, studied before in germ free and antibiotic treated mice. We have to mention that six taurine conjugated C_{24} bile acids, eight taurine conjugated C_{27} bile acids and the sulfates of C_{27} bile acids were not given in any metabolomics database including HMDB, KEGG or Lipid Maps. Fatty acids but also lipids were altered providing an insight into lipid metabolism of obesity related changes in gastrointestinal samples, here in cecum, a biological matrix that were never considered before to be an matrix for a global lipidomics approach. In the context of bacterial metabolism, we could highlight the role of lignane metabolites and urobilinoids but also novel metabolites. Moreover, the novel metabolite diphloretolyputrescine was never reported before in a mammalian system and its function is probably unknown. Additionally, is the signature of several metabolites is affected by the applied diet, the probable genotype susceptibility and majorly to the resulted body weight changes after the specific diet experiment. Host and bacterial meta-metabolome were altered and in future, several targets could be approached in order to reveal the mechanism due to DIO and genotype susceptibility of the C57BL/6 sub strains.

Chapter IV

METABOLOMICS – ANALYTICAL CHEMICAL DEVELOPMENT

OVERVIEW

Prior to performing a metabolomics study several steps are needed in order of appropriate metabolite extraction, application of the analytical tools, the data processing, statistical analyses, handling the multivariate containing data and extrapolation of important biological meaning.

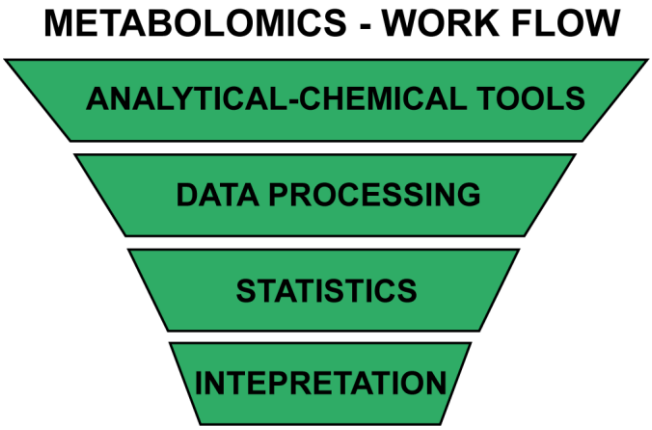

Chapter IV

4 Non targeted meta - metabolomics – Workflow

4.1 Overview

In order to perform an appropriate non-targeted meta-metabolomics study several processing steps are needed to be evaluated, concerning sample collection, preparation, the analytical biochemical analyses, data alignment, filtration, the multivariate statistical analysis and data elaboration in terms of annotation, identification and interpretation of important metabolites and connect them into biological context (Figure 4-1).

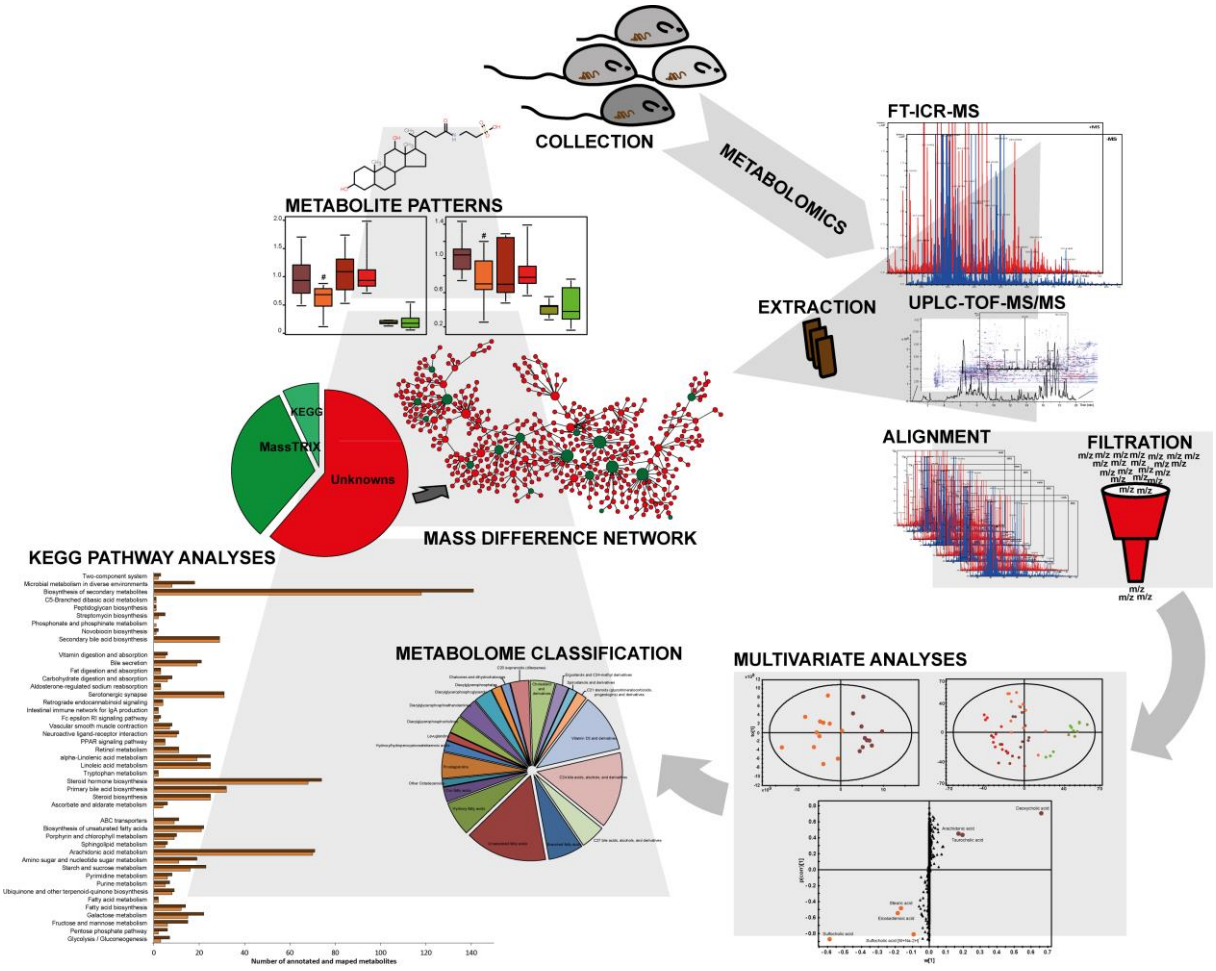

Figure 4-1: Scheme of the gut meta-metabolomics workflow for intestinal samples

4.2 Sample collection

In every performed study, the mice were euthanized with isoflurane and the complete gastrointestinal tract was immediately removed from each animal. All instruments for handling with microbial samples were treated with ethanol and were scarfed for sterile condition. The gastrointestinal tract was divided into five parts: stomach, duodenum, jejunum, ileum and cecum. The colon was divided into proximal, middle and distal part. The luminal content of the cecum and the proximal, middle and the distal part of the colon of each group was collected in Eppendorf tubes and immediately snap-frozen, quenched in liquid nitrogen and preserved at -80°C prior to further experiments. Additionally, feces droppings were collected in the cages after sacrification of the mice and stored at -80°C conditions. For the main experiments of non-targeted metabolomics of each study, the luminal content or feces was taken. Details about the matrices that were taken for metabolomics studies are then given in the respective chapters.

4.3 Evaluation of sample preparation for intestinal samples

The first step after sampling the luminal content was to investigate the best extraction procedure that was suitable for a high-throughput procedure for a non-targeted metabolomics approach.

4.3.1 Comparison of different solvents for metabolite extraction

For this approach, five different solvent systems were used: Acetone (AT), Acetonitrile (ACN), Methanol (MEOH), Water (H_2O) and a mixture of 50:50 MEOH/H_2O. The solvents except H2O were pre-chilled in -20°C and the sample pooling was done on dry ice to avoid any enzymatic degradation. Also two different homogenization steps were compared by using a vortex shaker (VS) and ultrasonic bath system (US). For this experiment a mixture of different parts of the intestinal content were taken and pooled together (cecum and colon samples). About 1 mL of cooled solvent was taken for the extraction. The homogenization was either performed for 30 seconds (VS) on 30 min on ice (US) was done in the sonication step. Afterwards, the homogenized samples were centrifuged at 14000 rpm for 10 min and the supernatant was taken for further analyses. The analyses was performed in (-) FT-ICR-MS and (-) UPLC-MS mode. For (-) FT-ICR-MS measurements about 100 µl were diluted in 400

µl of pure methanol. For the UPLC-MS analyses, about 500 µL were evaporated and dried samples were reconstituted in 100 µL of 10% MEOH, ACN or AT.

4.3.1.1 Results of solvent comparison of (-) FT-ICR-MS and (-) UPLC-TOF-MS experiments

The comparison of the solvent extractions system resulted in highest number of mass signals in MEOH for VS homogenization type and MEOH/H_2O for US homogenization type for (-) FT-ICR-MS (Figure 4-2, A). As an example, we displayed a mass range of a nominal mass of 343 Da (Figure 4-3, A and B). We could observe that MEOH, MEOH/H_2O and H_2O had a higher number of mass signals in a nominal mass range in both homogenization types, VS and US, and higher intensities values compared to AT and ACN. Through the comparison of number of detected features in (-) UPLC-TOF-MS experiments, we could observe that MEOH derived the highest number of features either for VS- or US- homogenization types (Figure 4-2, B).

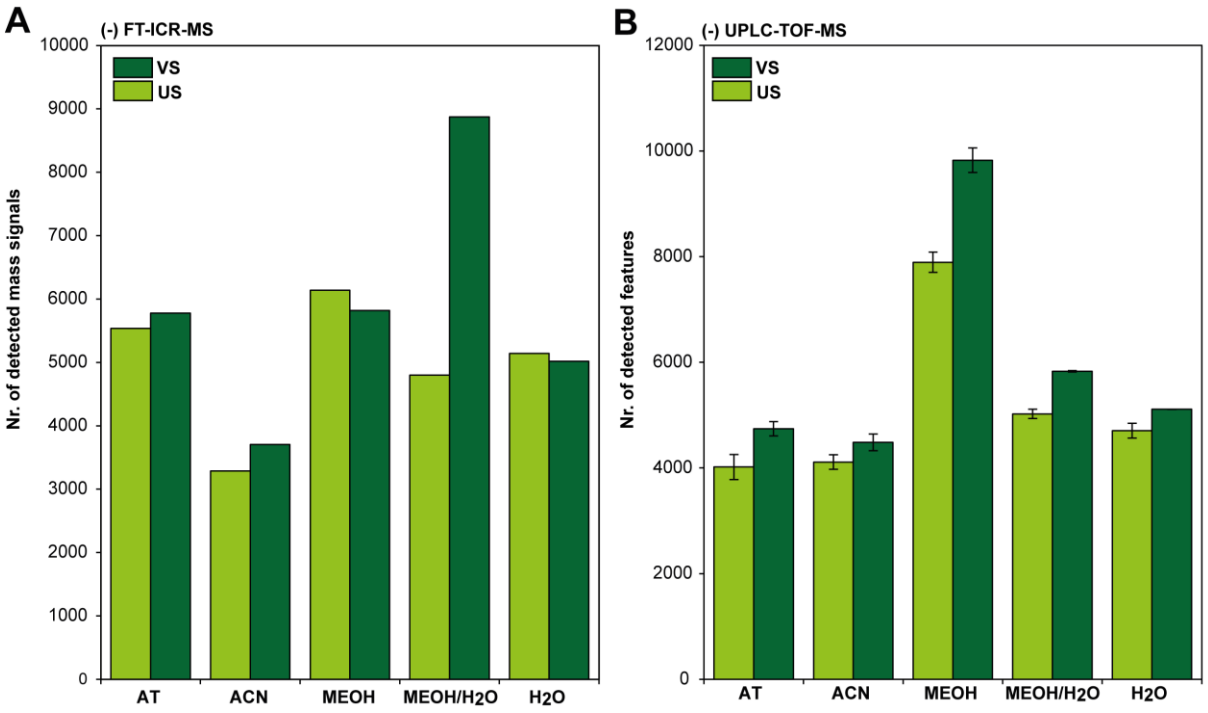

Figure 4-2 Sample preparation evaluation of different solvents and homogenization types in terms of number of detected mass signals

Next, we viewed the total ion chromatograms (TICs) of the extraction procedures (Figure 4-4). We could see that TICs of VS and US did not show big differences concerning the individual solvents except higher intensity values (Figure 4-4, A and B). Already through

visual comparing, we could see that the AT showed the worst TIC with low intensities in total, compared to other solvents.

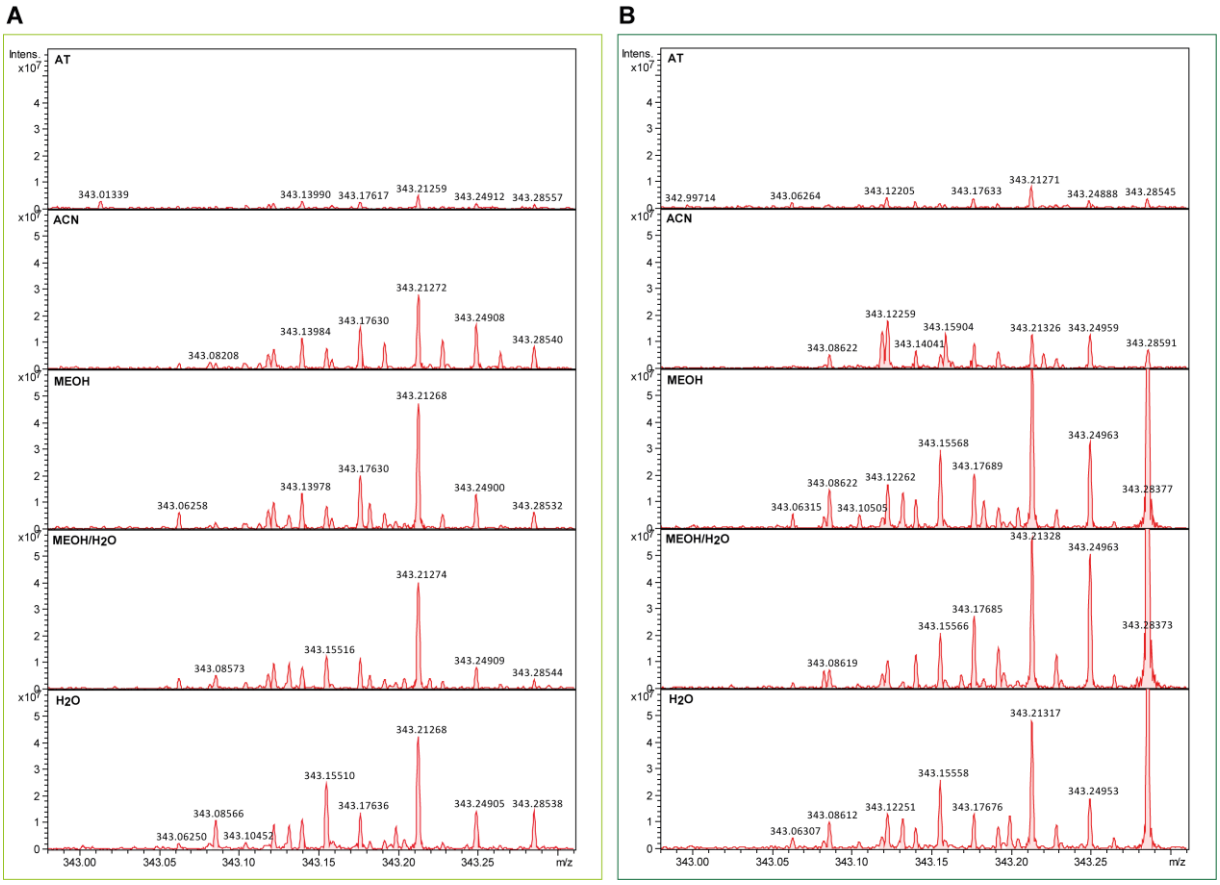

Figure 4-3 A mass range of nominal mass 343 Da showing the abundance of mass signals per nominal mass and their intensity values according to different solvent systems and homogenization types (A and B)

We divided the chromatograms into four different sections (Figure 4-4; 1-4). We could observe that MEOH/H_2O and H_2O had higher LC peaks in area 1, containing polar compounds which did not retain on a RP chemistry. Additionally, LC peaks in section 2 and 3 were higher in MEOH, MEOH/H_2O and H_2O compared to AT and ACN and even better for the US homogenization type. Especially, the LC peaks in section 3 in MEOH&US showed higher intensities compared to all others. The LC peaks in section 4 showed the best results for ACN and MEOH, whereas MEOH in combination with US reached the highest intensity values, compared to all others. By combining both results from (-) FT-ICR-MS and (-) UPLC-TOF-MS we decided that MEOH was the better solvent extraction type for these samples followed by US homogenization. The disadvantage of this method is obviously due to the extraction time of 30 minutes and was not suitable for high-throughput performance of about

200 samples. However, the VS method did not result in homogeneous suspension, shown in Figure 4-5, A.

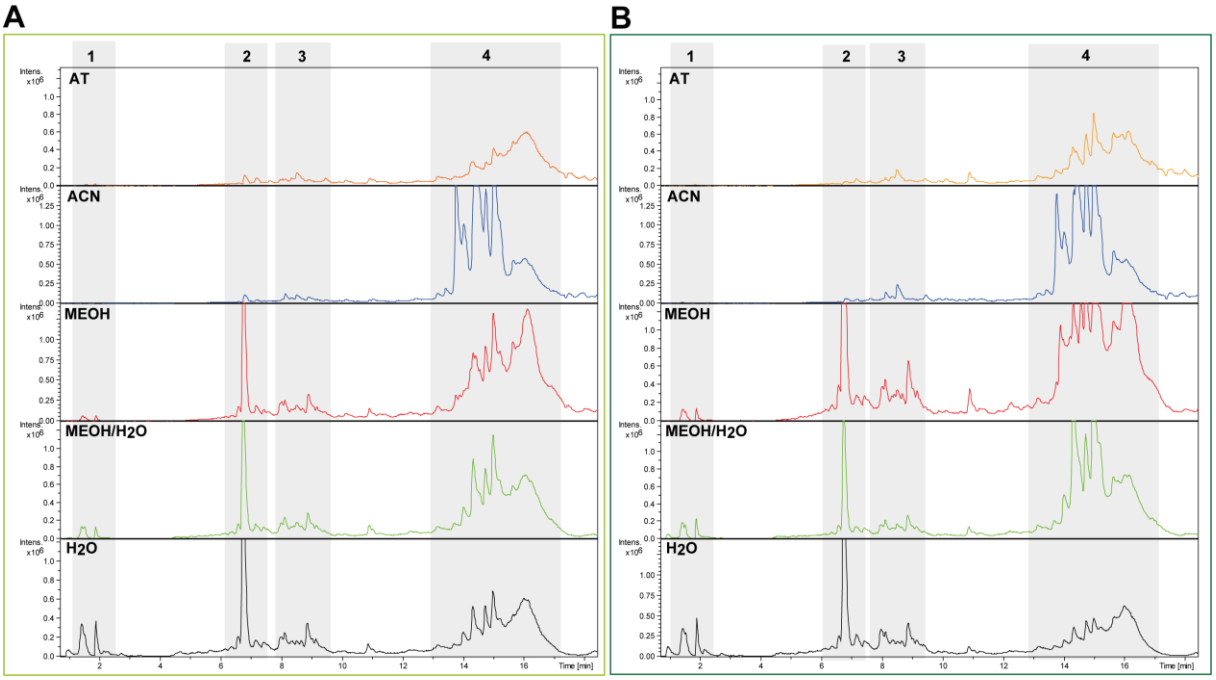

Figure 4-4 Total ion chromatograms of the solvent extraction procedure and the homogenization types derived from (-) UPCL-TOF-MS measurements

4.3.2 Optimization of the homogenization procedure

Based on the results shown above, further experiments were performed to evaluate the best and fastest homogenization for a large sample set for metabolite profiling. Therefore, 4 different homogenization steps were compared containing the previously mentioned vortex shaker (VS), ultrasonic bath system (US) and TissueLyser II system by using different beads: glass beads (GB) and ceramic beads (CB) (Figure 4-5). The extraction times were 30 sec for VS, 30 min on ice for US and 5 min with 30 Hz for TissueLyser II system, respectively. For the extraction, 1 mL of pre chilled MEOH (-20°C) was used due to the best extraction efficiency, as already shown above. Afterwards all samples were centrifuged to remove crude particulates and the supernatants were taken, 500 µL were evaporated and the dried samples were re-diluted in 100 µL of 10% methanol for subsequent (-) UPLC-TOF-MS. The homogenization methods US, GB and CB resulted in homogenous suspension compared to the VS system, shown in Figure 4-5, A, B, C and D.

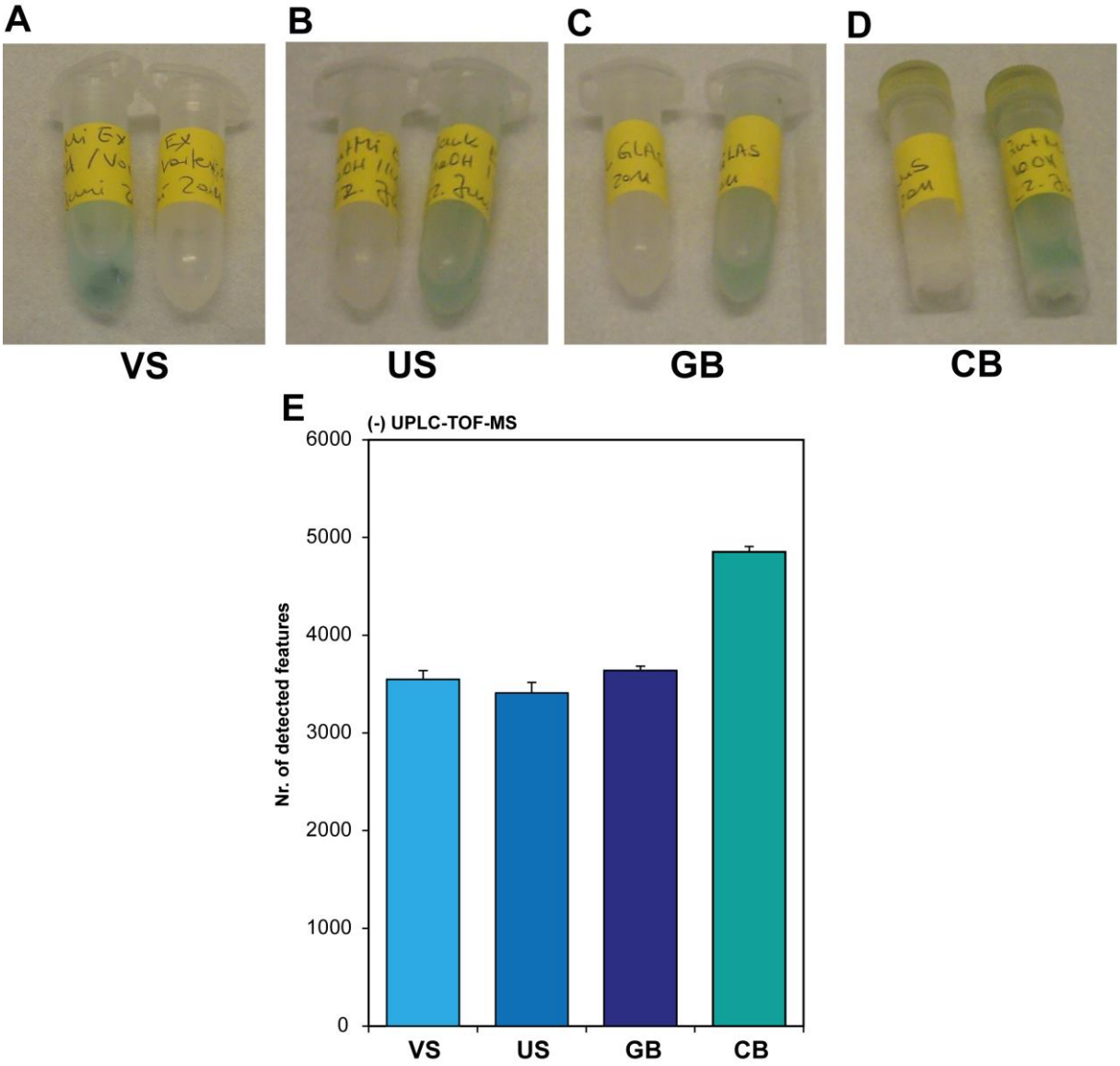

Figure 4-5 A-D: Four different homogenization procedures including vortex shaker (VS), ultrasonic bath system (US) and TissueLyser II system by using different beads: glass beads (GB) and ceramic beads (CB); E: Comparison of number of detected features applying four different homogenization procedures, measured by (-) UPLC-TOF-MS

The analyses of the measurements resulted in the highest detected number of features in CB, followed by GB (Figure 4-5, E). In addition, we could observe these differences in the TIC comparison, shown in Figure 4-5, E, with highest TIC for CB but very similar LC peaks for all extraction types (Figure 4-6). Taken all together, we decided to apply a methanolic extraction with the CB extraction homogenization type.

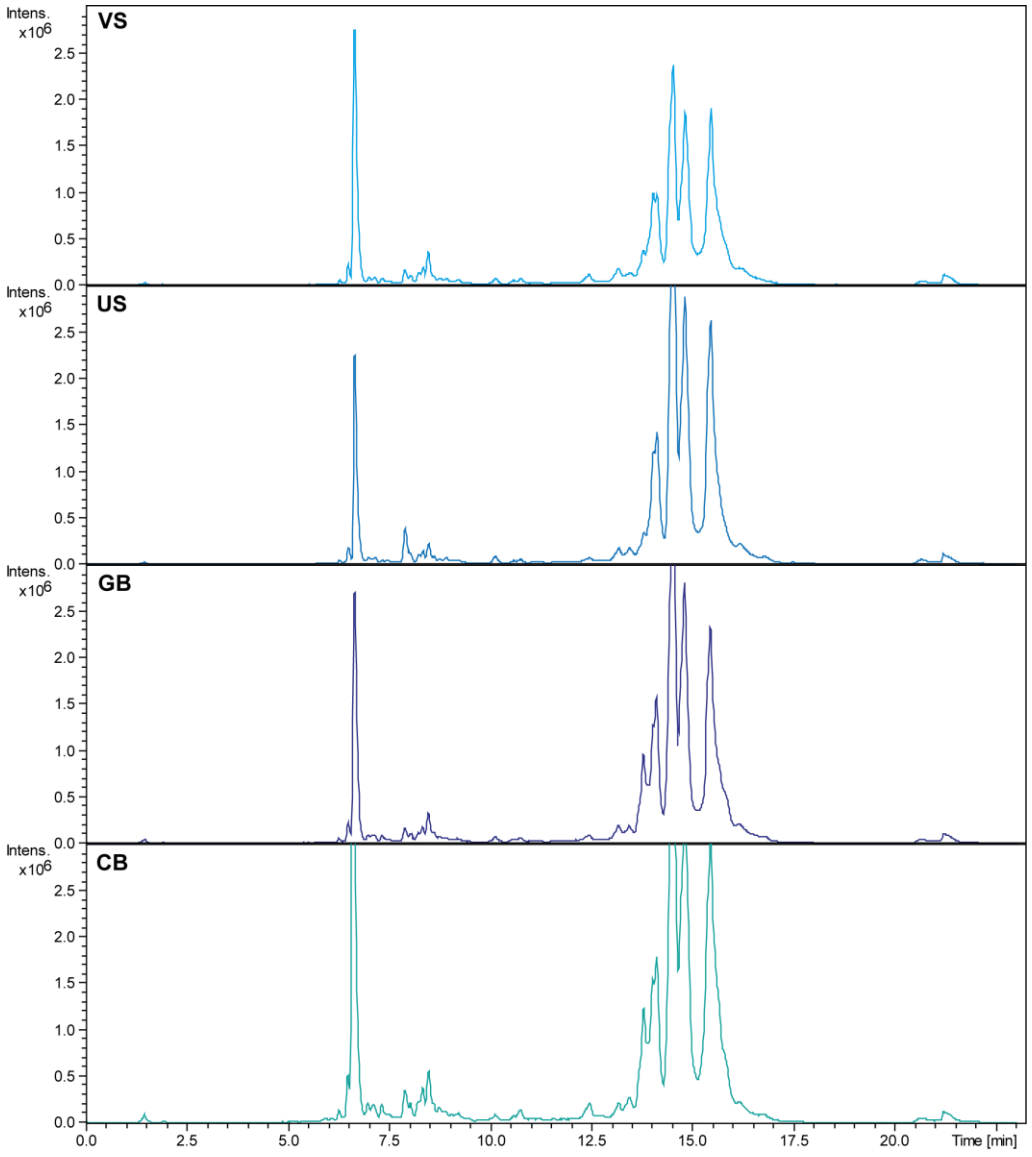

Figure 4-6 Total ion chromatograms of four different homogenization types: vortex shaker (VS), ultrasonic bath system (US) and TissueLyser II system by using different beads: glass beads (GB) and ceramic beads (CB)

4.3.3 Final sample extraction procedure: methanolic extraction for non-targeted meta-metabolomics studies

The sample preparation was always done under sterile conditions. All instruments were scarfed with methanol and after each sample; the instruments were cleaned with pure water, following by pure methanol. Original samples were always cooled on dry ice and cut aliquots were stored on dry ice before extraction. After extraction, the samples were stored on normal ice (+4°C). Samples from the intestine of mice (~10 mg) were placed in ceramic bead tubes (NucleoSpin® Bead Tubes, MACHEREY-NAGEL GmbH & Co. KG) combined with a metal

bead (QIAGEN®) on dry ice. After the addition of 1 mL of cold (-20°C) methanol (Fluka, Sigma Aldrich, HPLC-grade) the homogenization was performed in TissueLyser II (QIAGEN®) for 5 minutes at a rate of 30 Hz to homogenize and disrupt the bacterial cells and extract the metabolites of the gut microbiome. Then, the samples were centrifuged two times at 14.000 rpm for 10 min at 4° C and the supernatant was collected for the non-targeted metabolomics MS analyses.

4.4 Analytical chemical tools – MS based approach

4.4.1 UPLC-TOF-MS/MS

4.4.1.1 Comparison of different RP chemistries for separation with UPLC coupled to TOF MS

In order to perform chromatographic separation of intestinal samples we evaluated different column, packed with different reverse phase chemistries for metabolomics studies using LC-MS. The chromatography was performed by means of ultra performance liquid chromatography (UPLC®) (ACQUITY™ UPLC system Waters®, Milford, MA) coupled to a time of flight mass spectrometer (TOF) (maXis™, Bruker Daltonics GmbH).

The following columns were taken for the comparison:

- Waters© Acquity™ UPLC® BEH™ C8 column (1.7 µm, 2.1 × 150 mm): BEH™ C8
- Waters© Acquity™ UPLC® BEH™ C18 column (1.7 µm, 2.1 × 150 mm): BEH™ C18
- Phenomenex©, Kinetex®, C18 column (1.7 µm, 2.1 × 150 mm): Kinetex® C18

We performed the analyses in both modes of UPLC-TOF-MS using

(+) UPLC-TOF-MS

A: 10 % methanol with 0.1 % formic acid (FA)

B: 0.1 % FA in pure methanol

(-) UPLC-TOF-MS

A: 10% methanol with 5 millimolar (mM) ammonium acetate (NH_4Ac)

B: 100% pure methanol with 5 mM NH_4Ac

Different gradient times of 30, 20, 10 and 7.5 minutes (min) were applied. The gradients are displayed in Figure 4-7. The flow was set to 0.2 mL/min with the column temperature at 40° C.

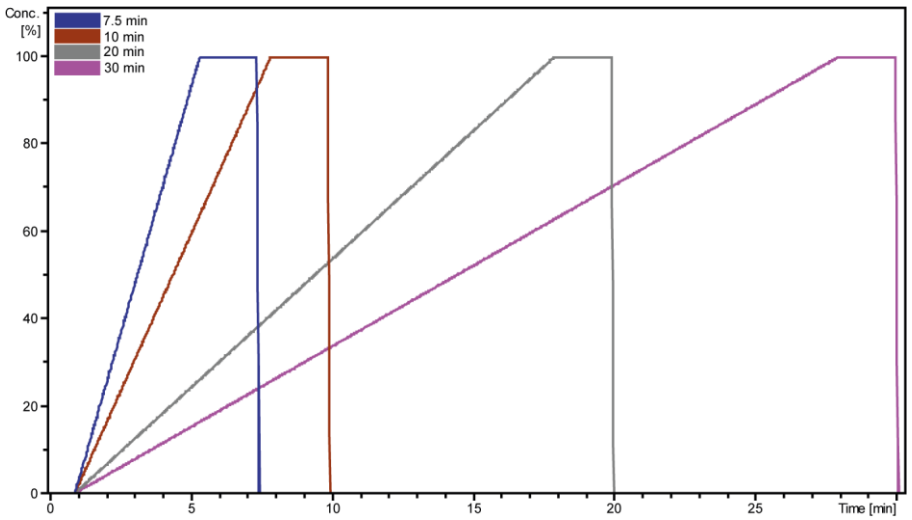

Figure 4-7 Gradients used for comparison of the RP columns

4.4.1.2 Results of column comparison in (+/-) UPLC-TOF-MS

The raw data was exported to .mzxml format and processed with MZmine 2.0. For the evaluation, the amounts of detected features were taken as criteria for the comparative analyses. In terms of feature detection the best results were shown for the Kinetex® C18 column including both (+/-) UPLC-TOF-MS modes, shown in Figure 4-8, A and B, followed by BEH™ C8 for 20, 10 and 7.5 minutes. BEH™ C8 showed the highest number of detected features in the run of 30 min of (+) UPLC-TOF-MS mode. Exemplarily, we checked also the TICs of the analyses, here for the 7.5 min separation (Figure 4-8, C-D). In (+) UPLC-TOF-MS the separation was quite good and no obvious differences were observed (Figure 4-8, C). In contrast, the Kinetex® C18 did not show any good separation ability, especially between 5 and 7 min, compared to the other two columns in the (-) UPLC-TOF-MS mode (Figure 4-8, D). Considering these results, we excluded the use of Kinetex® C18 and based on higher feature detection for BEH™ C8 we decided to use this column for experiments performed with UPLC-TOF-MS-technique.

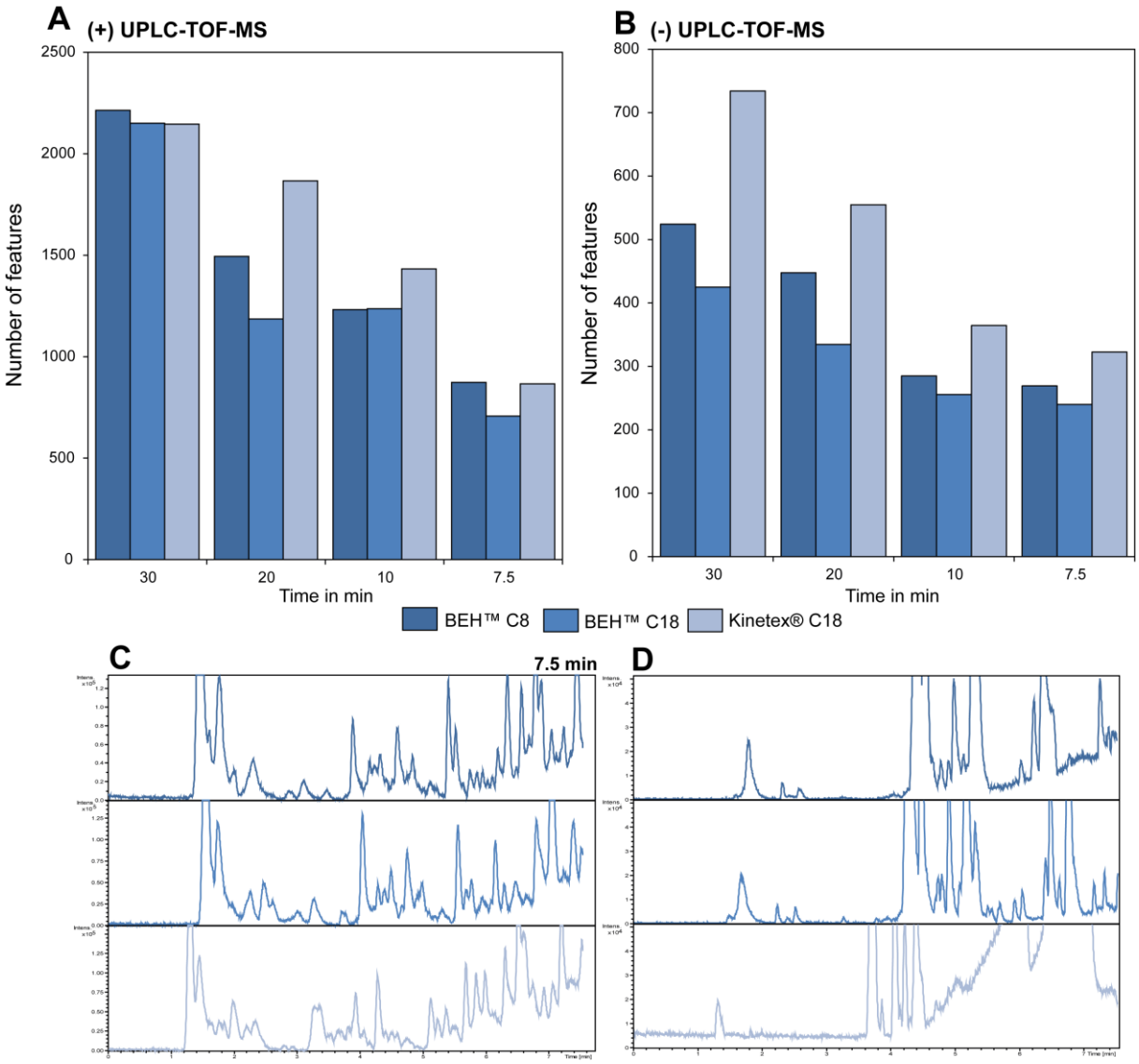

Figure 4-8 A-B: RP column comparative analyses in (+/-) UPLC-TOF-MS by elaborating the number of detecting features and applying different gradients and times; C-D: Exemplarily TICs of 7.5 min run of the three RP chemistries that were measured in (+/-) UPLC-TOF-MS

4.4.1.3 Additives system evaluation for UPLC-TOF-MS

We checked two different additive systems for (+) UPLC-TOF-MS mode, displayed below, to enhance the ionization power in positive mode:

1. Methanol with 0.1 % FA

A: 10 % methanol with 0.1% FA

B: 100 % pure methanol with 0.1% FA

2. Acetonitrile with 0.1 % FA

A: 10 % acetonitrile with 0.1 % FA

B: 100 % acetonitrile with 0.1 % FA

Other conditions for this analysis were a runtime of 10 min, flow rate of 0.2 mL/min column temperature of 40°C and we took the BEH™ C18 column for the separation. For (+) UPLC-TOF-MS mode the buffer system 2 provided a higher number of features as shown in Figure 4-9 A. Moreover, chromatographic separation was better with system 2 compared to system 1, revealing more LC peaks in one analyses (Figure 4-9, B).

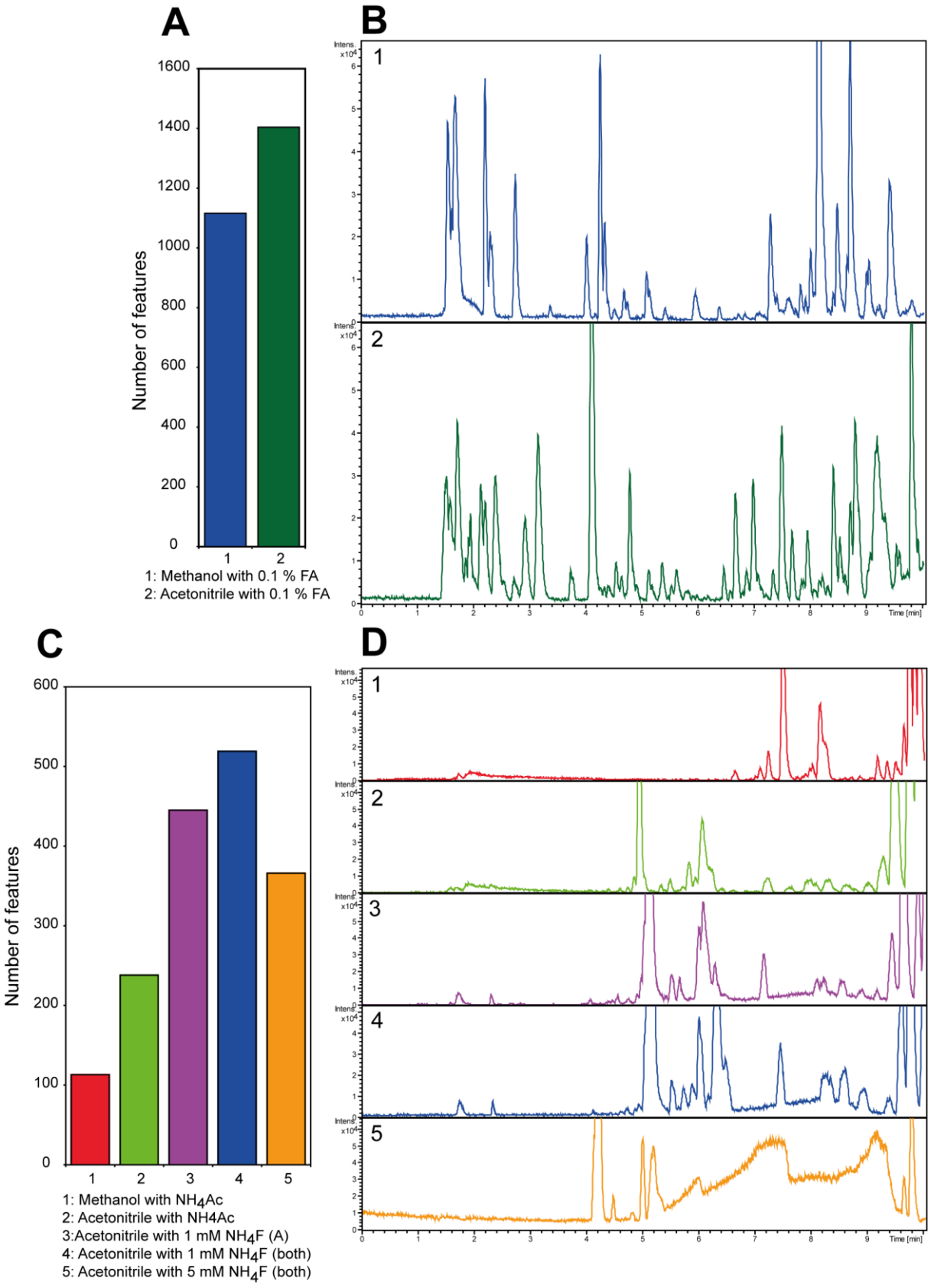

Figure 4-9 A-B: Additives evaluation in (+) UPLC-TOF-MS mode and their respective TICs; C-D: Additive evaluation in (-) UPLC-TOF-MS mode and their respective TICs

We checked five different additive systems for (-) UPLC-TOF-MS mode, displayed below to enhance the ionization power in negative mode:

1. Methanol with NH_4Ac

A: 10% methanol with 5 millimolar (mM) ammonium acetate (NH_4Ac)

B: 100% pure methanol with 5 mM NH_4Ac

2. Acetonitrile with NH_4Ac

A: 10% acetonitrile (ACN) with 5 mM NH_4Ac

B: 100% pure methanol with 5 mM NH_4Ac

3. Acetonitrile with 1 mM NH_4F (only A)

A: 10% ACN with 1 mM ammonium fluoride (NH_4F)

B: 100% ACN

4. Acetonitrile with 1mM NH_4F (both)

A: 10% ACN with 1 mM NH_4F

B: 100% ACN with 1 mM NH_4F

5. Acetonitrile with 5mM NH_4F (both)

A: 10% ACN with 5 mM NH_4F

B: 100% ACN with 5 mM NH_4F.

Other conditions for this analysis were a runtime of 10 min, a flow rate of 0.2 mL/min as well as a column temperature of 40°C with the BEH™ C8 column for the separation. As shown in Figure 4-9, the best solvent buffer system was the Nr. 4 followed by Nr. 3. The addition of NH_4F resulted in higher ionization capability in (-) UPLC-TOF-MS mode compared to the NH_4Ac addition. Observing the LC peaks, shown in Figure 4-9 D, the buffer system of Nr.2 showed better behavior followed by Nr.4 and Nr.3. Similar results were already shown before by Yanes *et al.* (Yanes, Tautenhahn et al. 2011).

4.4.2 Identification experiments using MS/MS concept

4.4.2.1 FT-ICR-MS/MS

First, we performed MS/MS experiments using a FT-ICR-MS approach to unveil an unknown mass signal that was especially important in chapter 2.3.4, derived from statistical analysis it was the most discriminative mass signal for *db/db* mice, which was not annotated in mentioned metabolite databases used for annotation, see chapter 4.5.4. The MS and MS/MS (20 eV) spectra for the mass signal of $[M-H]^-$ (359.18982) are shown in Figure 4-10 A. To obtain sufficient fragment counts (mass signal values highlighted in red) we acquired 200 scans, which took about 10 minutes. Increasing the collision energy above 20 eV resulted in the loss of the parent mass signal. The disadvantage of this method was obvious due to the lack of automatization and long acquisition-time for every mass signal subjected to fragmentation experiments. Therefore, we decided to use the UPLC-TOF-MS/MS function to perform fragmentation experiments.

4.4.2.2 UPLC-TOF-MS/MS

All MS/MS spectra, shown in this thesis were done by using predominantly the (-) UPLC-TOF-MS/MS. Before MS/MS analyses separation was performed using the BEH™ C8 column with a total runtime of 20 min, a flow rate of 0.2 mL/min and a column temperature of 40°C. The separation was performed by using the (3) acetonitrile with 1 mM NH_4F (only A) from chapter 4.4.1.3. The (-) TIC of representative intestinal matrices is shown in Figure 4-10 B. The fragmentation experiments were performed in automated MS/MS mode of TOF (Figure 4-10 C). The parameters for automated MS/MS fragmentation were set to a number of 5 precursor ions, shown in Figure 4-10 C. This automated MS/MS function chooses always the 5 highest detected mass signals and intensity values over 1000 (red, Figure 4-10 C) and subjected them into fragmentation experiments. The advantage is the fast scan rate of TOF-MS/MS because it acquired 5 MS/MS spectra at a scan rate of 5 Hz. The disadvantage was that less abundant peaks were skipped and no MS/MS spectrum was given. To overcome this problem, we generated a precursor mass list of the desired mass signals and their retention time and subjected them into the automated MS/MS experiments (shown in Figure 4-10 D). Thereby we searched for specific mass signals with high importance in chapter 2.3.3, that were possible sulfate and taurine conjugates of fatty acids.

Another advantage of the UPLC-TOF-MS/MS experiments was the chromatographic separation, to overcome the ion suppression effects present in FT-ICR-MS/MS experiments. As one example, we took the mass signal of 410. 237112 ($[M-H]^-$), shown in Figure 4-10 E. The mass spectrum is analyzed in (-) FT-ICR-MS and the mass signal showed a low intensity value, almost disappearing in the background-noise. Additionally, in FT-ICR-MS the minimum isolation width is 0.1 Da, which means there are still a plenty of other mass signals (shown, for example the nominal mass of 410 in Figure 4-10 E), which could not be excluded in fragmentation experiments. The analysis with (-) UPLC-TOF MS resulted in an extracted ion chromatogram (EIC of 410.2360, Figure 4-10 E) with high intensities of the mass signal (Figure 4-10 F), which allows to perform further MS/MS experiments. Thus, we performed preferentially UPLC-TOF-MS/MS experiments to confirm the annotated metabolites, but also to reveal new metabolites.

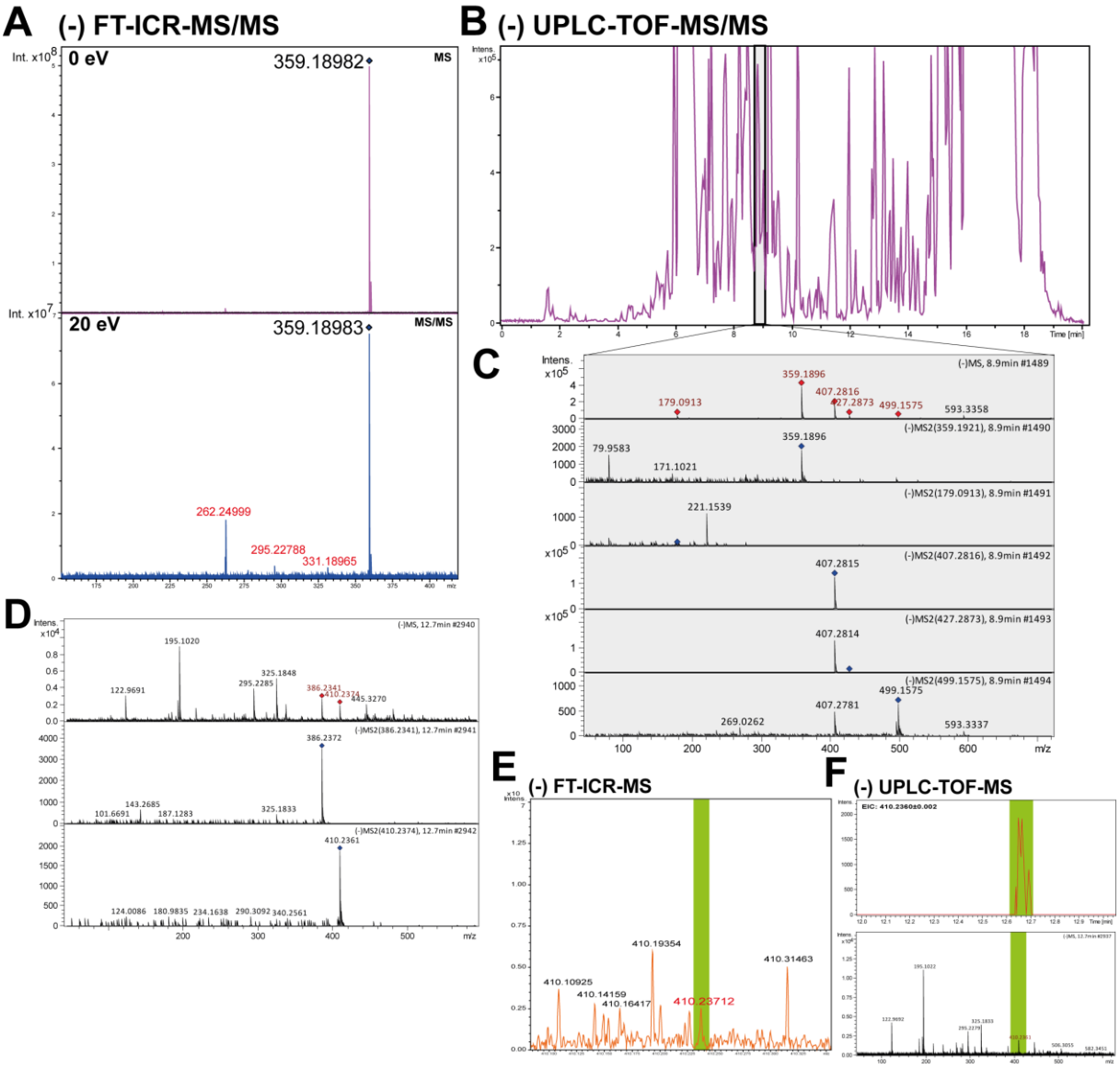

Figure 4-10 Procedure of identification experiments using MS/MS measurements using (-) FT-ICR-MS/MS and (-) UPLC-TOF-MS/MS; A: Mass spectrum from direct infusion in (-) FT-ICR-MS/MS, B and C: Automated MS/MS experiments by fragmentation of five highest MS peaks by using (-) UPLC-TOF-MS/MS, D: Precursor list based MS/MS experiments by fragmentation of selected MS peaks, E-F: An example of the mass signal 410.2371 in FT-ICR-MS or UPLC-TOF-MS experiments, FT-ICR-MS shows a plenty number of mass signals, which disturbed the fragmentation, in UPLC-TOF-MS a pre- performed separation allows to fragment the desired mass signal

Following parameters were applied: capillary voltage of 4000 V and end plate offset to -500 V, a dry gas flow rate of 8 L/min, the dry gas temperature to 200 °C and a nebulizer gas flow rate of 2.0 bar. The mass range was set from 50 to 1200 and the scan rate of 5 Hz with a rolling average of 2 by acquiring profile spectra in a switching mode between MS and

MS/MS mode. The isolation width window was set to 0.1 m/z. Afterwards the comparison of experimental MS/MS spectra was performed manually against the METLIN database within an error of 10 ppm (Smith, Maille et al. 2005).

4.5 Data processing for FT-ICR-MS analyses

Data processing of DI-FT-ICR-MS spectra is an important issue in order to derive meaningful data matrices for further data elaboration for multivariate statistical analyses and data interpretation. To present the procedure for data handling we took the (-) FT-ICR-MS analyses from the non-targeted metabolomics study of Chapter 3.In total, we had 53 spectra of methanolic extracts from cecal content of 53 individual mice. Every mass spectrum was processed first in Compass DataAnalysis 4.0© (Bruker Daltonik GmbH). The spectra were calibrated internally and then exported with a signal to noise ratio of four and a relative intensity ratio of 0.001 % (base peak). On average about 7982 mass signals were counted. The mass signal lists were aligned with the in-house software called Matrix Generator within an error of 1 ppm. The alignment resulted in a data matrix containing 37032 mass signals.

4.5.1 Raw data filtration

The data matrix containing 37032 mass signals was processed as follows. First, the abundance of each mass signal was counted, shown in Figure 4-11. For example 8906 mass signals were counted only once in n = 53 mass spectra. Roughly, we decided to exclude all mass signals that counted less than 10 times in n = 53 mass spectra (Figure 4-11, red color). The filtration resulted in x = 12200 mass signals with an abundance of n ≥10 (5%). For example, Hackstadt *et al*. proposed for the processing of multivariate data to exclude variables with abundances ≤50 % (Hackstadt and Hess 2009). This rough filtration would theoretically exclude all meaningful information about unique metabolites that represent specifically one subgroup, for example a subgroup with n = 10 mice.

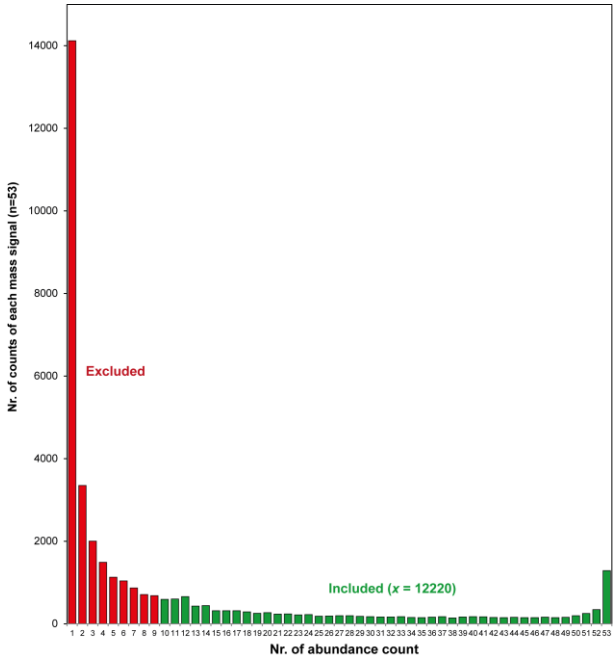

Figure 4-11 Raw data filtration, count of mass signals occurred in n=53 samples, red were excluded from further analysis, green one were included in further data processing

4.5.2 Mass defect filtration

This data matrix was further processed by evaluating the mass defect filter (MDF). The "mass defect" represents the difference between nominal mass (300.00000) and exact mass (e.g. 300.04889) (Hughey, Hendrickson et al. 2001). In the plot of Figure 4-12, the nominal mass (x-axis) is plotted against the mass defect (y-axis). The mass signals, highlighted in red, were excluded from further analyses. As an example, one of the mass signals that were excluded from further analyses was the experimental mass 296.61705 with high intensity values of $x10^9$, which is taurocholic acid sulfate bearing a double charged due carboxyl and sulfate group. The $[M-H]^-$ of taurocholic acid sulfate is also presented in the spectra with an experimental mass of 594.240876, which was included in further data evaluation. This filtration resulted in 11151 mass signals (green dots) that were chosen for further analyses.

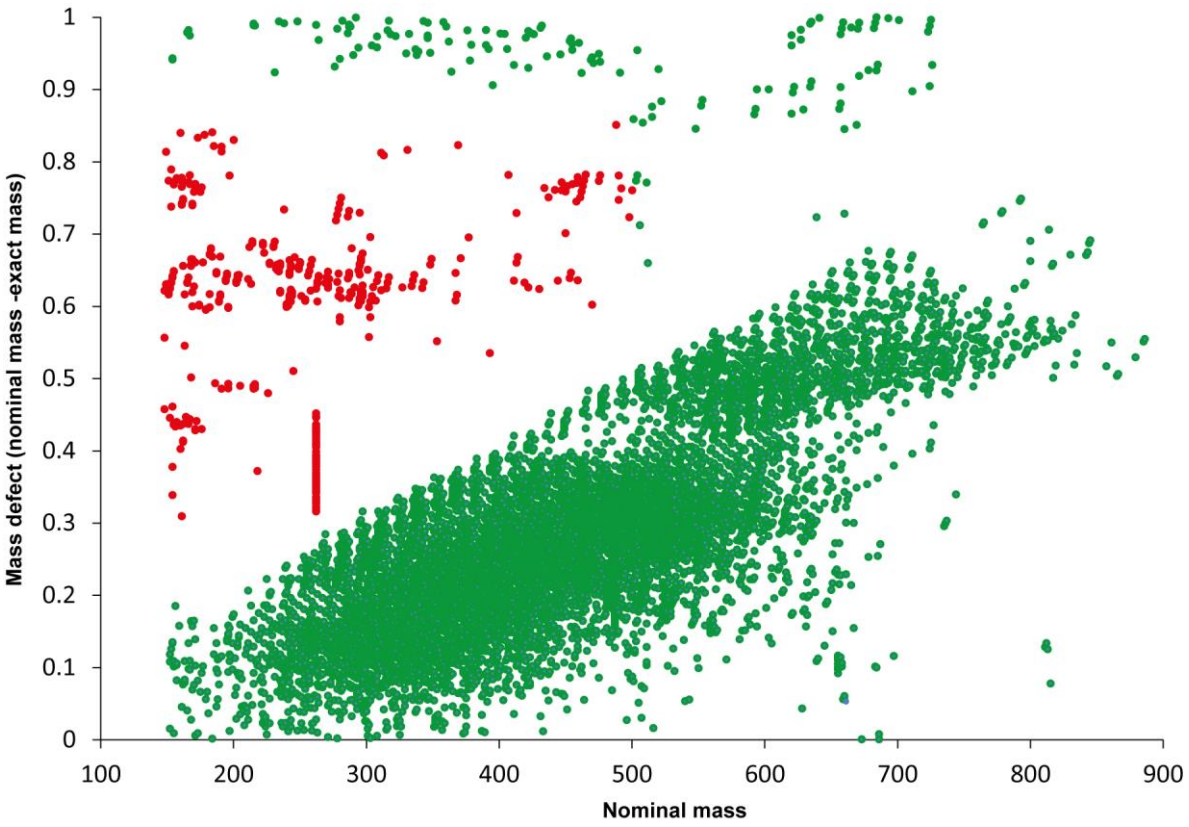

Figure 4-12 Mass defect plot

4.5.3 NetCalc – molecular formula calculation and deisotoping

For the last step, the in-house generated software NetCalc was used for molecular formula calculation, deisotoping and calculation of mass differences and subsequent network visualization in chapter 2.3.5 and 2.3.8 (Tziotis, Hertkorn et al. 2011). We included 22 mass differences containing the elemental composition of carbon, hydrogen, nitrogen, oxygen, sulfur and phosphor (CHNOSP), shown in Table 11. We decided to include common reaction and biotransformation steps such as hydrogenation, hydroxylation (Snyder and Hedli 1996), methylation, ß-oxidation (Harper, Garrity et al. 1986), introduction of water, carboxylation, sulfonation (Alnouti 2009), introduction of sulfur, conjugation with taurine (Swann, Want et al. 2011), hypotaurine, cysteine (Teichert, Sohr et al. 2005), homocysteine, glycine (Swann, Want et al. 2011), glucose (Sarda, Page et al. 2012), glucuronic acid (Sarda, Page et al. 2012), glucosamine, phosphate, the involvement of nitrogen (N) and the primary and secondary amidation (NH_2 and NH). Some of the mass differences were also adopted from Breitling *et al*. (Breitling, Ritchie et al. 2006).

Intentionally, we did not include mass differences between the mentioned elements and their stable isotopes (^{13}C, ^{15}N, ^{18}O and ^{34}S), to exclude all isotopic mass signals from further analysis. This is the mentioned deisotoping step in the filtration procedure. The calculation derived 3545 valid mass signals with their respective molecular formula. The calculation was performed with an error of 0.2 ppm.

Table 11 Mass difference list and their elemental composition applied for molecular formula calculation using NetCalc

Name	Mass difference exact mass (theoretical)	Elemental composition CHNOSP
+/- H_2	2.01565	H_2
+/- N	14.00307	N
+/- Methylation	14.01565	CH_2
+/- CH_3	15.02348	CH_3
+/- NH	15.01090	NH
+/- OH	15.99492	O
+/- NH_2	16.01872	NH_2
+/- H_2O	18.01057	H_2O
+/- ß-oxidation	28.03130	C_2H4
+/- Carboxylation	29.97418	CO_2
+/- Thiol	31.97207	S
+/- Glycine	57.02146	C_2H_3NO
+/- SO_2	63.96190	SO_2
+/- Sulfate	79.95682	SO_3
+/- Phosphate	79.96633	HPO_3
+/- Hypotaurine	91.00919	C_2H_5NOS
+/- Cysteine	103.00919	C_3H_5NOS
+/- Taurine	107.00410	$C_2H_5NO_2S$
+/- Homocysteine	117.02484	C_4H_7NOS
+/- Glucose	162.05283	$C_6H_{10}O5$
+/- Glucosamine	163.08446	$C_6H_{13}NO4$
+/- Glucuronic acid	176.03209	$C_6H_8O_6$

The combination of abundance filter and NetCalc calculation step should be enough to filter the MS data for valid mass signals with elemental composition of CHNOSP. The mass defect filter can be skipped in prospective data processing procedures. The data matrix was subsequently taken for mass signal annotation of putative metabolites. In chapter 2.3.8.2, we used mass difference analysis to reveal new metabolites of the AAM pathway, especially ß- and ω-oxidation, sulfate and taurine conjugated metabolites. This application was more specific in order to reveal new metabolites of a certain class or to describe unknown metabolites, which is explained in detail in chapter 4.5.4. A more global mass difference analysis is starting with all mass signals measured in an experiment. Here, we took the data matrix from the study of T2DM, including spectra from 4 different sample matrices and 2 different genotypes (cecum, middle, colon and feces samples from *wt* and *db/db* mice; n=74 spectra). The molecular formula calculation resulted here in 3360 mass signals, which then are taking part in the calculation of mass differences. Molecular formula calculation was performed with an error of 0.2 ppm. Overall, we could find 11986 mass differences, whereas the highest count of mass differences was found for the mass difference of hydrogenation, hydroxylation, methylation, ß-oxidation, and introduction of water or for carboxylation. The

distribution of the found mass differences is shown in Figure 4-13. Moreover, we concluded that 3 mass differences (+/-NH_2, CH_3 and N) were not essential for mass difference analysis due low count, shown in Figure 4-13 and could be excluded from further analysis.

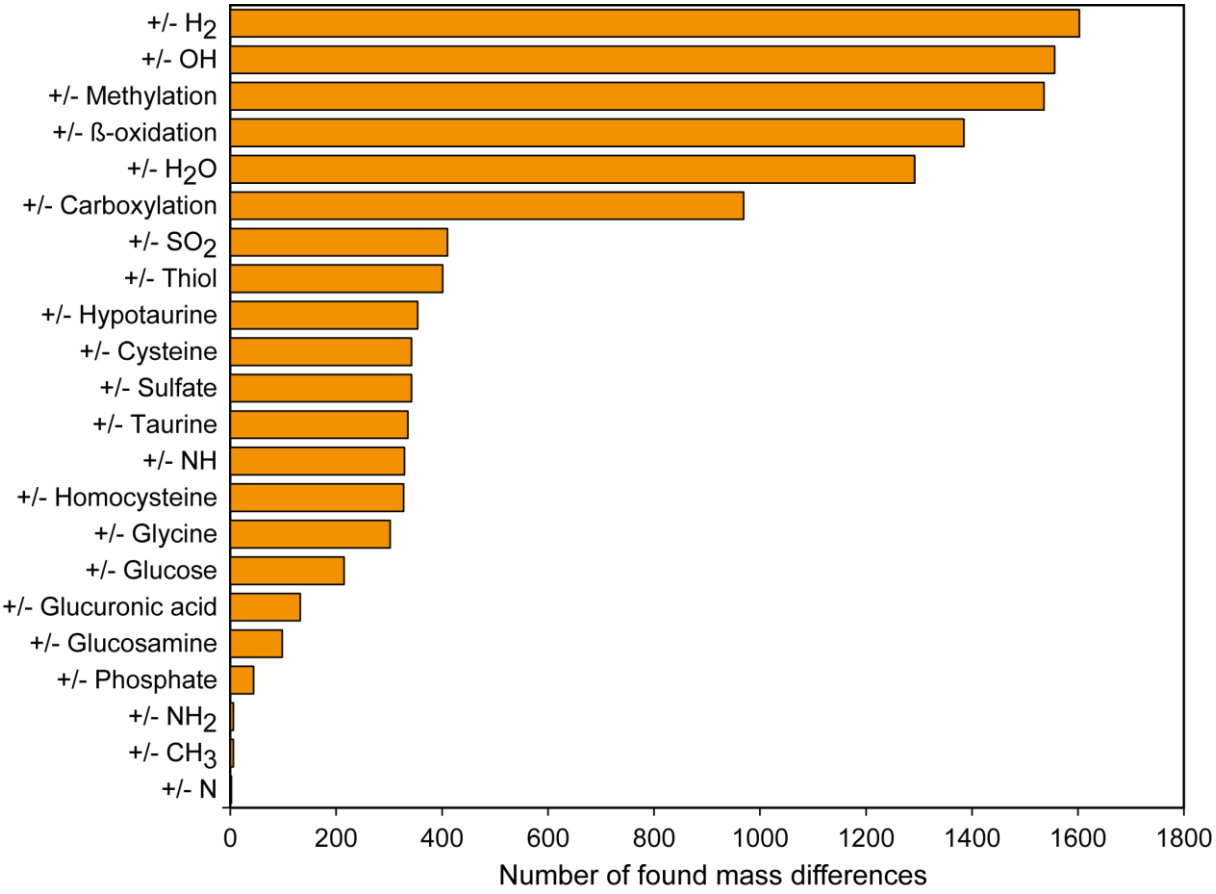

Figure 4-13 Count of found mass differences in the data matrices of T2DM study of chapter 2.

4.5.4 Data annotation

Following the data processing procedure, we achieved a data matrix of 3545 mass signals with their molecular formulas. This work could be accomplished by METLIN (Smith, Maille et al. 2005) or MassTRIX, which are web- based servers (Suhre and Schmitt-Kopplin 2008) and which are suitable for annotation of ESI-MS data. Both support the upload of MS data. While MassTRIX handles large amounts of mass signal data, the upload in METLIN is limited to a list of 500 mass signals in one analysis. Both offer the upload of experimental data by choosing a ionization mode with $[M-H]^-$ or $[M+H]^+$ plus a bunch of other adducts e.g. $[M+Na]^+$ or $[M+Cl]^-$. Additionally, the accuracy (error in ppm) can be defined and is dependent on the used MS instrument. For the FT-ICR-MS measurements, we were using an error of 1 ppm. MassTRIX performs the search against several metabolite databases including

the KEGG compound database (Kanehisa and Goto 2000), Human Metabolome Database (HMDB) (Wishart, Knox et al. 2009), the LIPID MAPS database (Sud, Fahy et al. 2007) and MetaCyc (Caspi, Altman et al. 2012). The annotation of KEGG compounds allows assigning the putative metabolites into metabolic pathways of KEGG by choosing a specific species for example *Mus musculus* (MMU). METLIN is also directly connected to the KEGG database. In terms of our dataset containing 3545 mass signals, we could annotate 1121 mass signals. From those 250 mass signals could be mapped onto KEGG metabolic pathways (Figure 4-14, A). About 2174 mass signals were not annotated and are so-called "Unknowns" which are now represented by their molecular elemental composition.

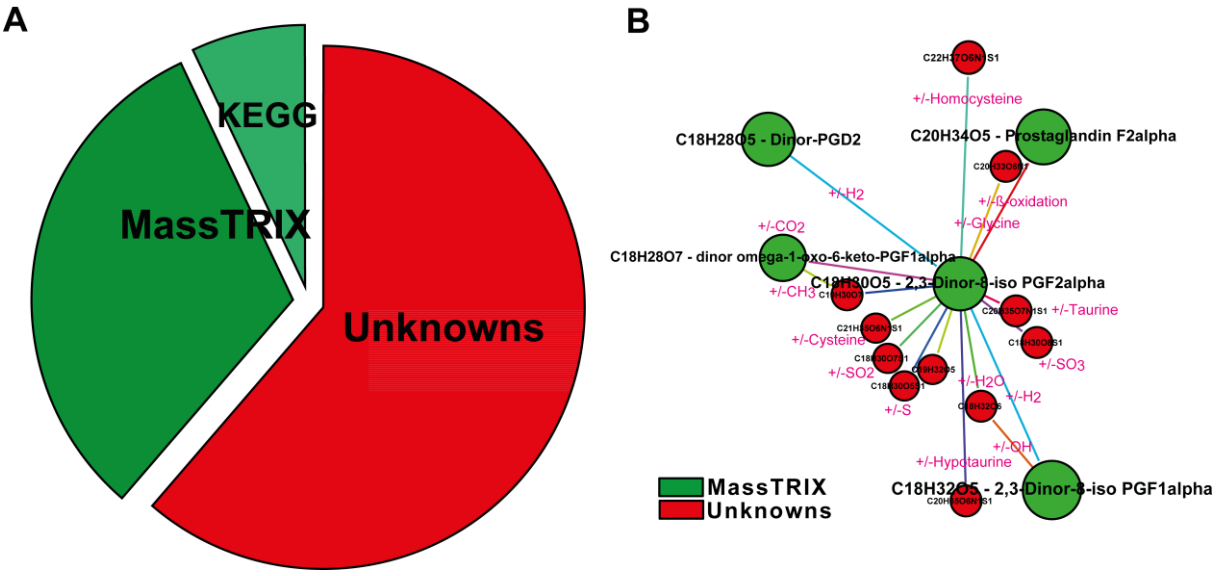

Figure 4-14 A: A pie diagram of all mass signals and their annotation through MassTRIX, the assignment of annotated metabolites into KEGG metabolic pathways and the remaining part consisting of Unknowns: In numbers we annotated 1121 mass signals, 250 were mapped into KEGG metabolic pathways and 2174 remained as not-annotated mass signals and are represented by their elemental composition, including CHNOSP as elements; B: Discovery of Unknowns by applying a mass difference analysis and subsequent network visualization of 2,3-Dinor-8-iso PGF2alpha

Based on molecular formula knowledge we were using two additional and comprehensive chemical databases, including ChemSpider (http://www.chemspider.com/) and Pubchem (http://pubchem.ncbi.nlm.nih.gov/) which allow searching by using molecular formulas. As an example for the annotation procedure, we selected the mass signal 514.284131 for $[M-H]^-$ with the calculated molecular formula of $C_{26}H_{45}O_7N_1S_1$ (already protonated species). First, we could annotate this mass signal into putative metabolites using MassTRIX and METLIN

which was successful and we annotated 11 putative metabolites in MassTRIX (isomeric substances), while in METLIN 6 putative metabolites were annotated (Table 12). Performing a molecular formula search using chemical databases like ChemSpider or PubChem resulted in 47 or 84 compounds, respectively. The search for molecular formulas and possible compounds in ChemSpider or PubChem is very time consuming, due to the lack of uploading of large datasets.

Table 12: Example for mass signal annotation using different databases with experimental mass signals or molecular formulas

Experimental mass [M-H]-	Neutral mass	Theoretical mass	Error in ppm	Molecular Formula	METLIN[a]	MassTRIX[a]	ChemSpider[b]	PubChem[b]
514.284131	515.291674	514.284397	-0.5172	$C_{26}H_{45}O_7N_1S_1$	6[x]	11[x]	47[x]	84[x]

a: annotation performed by using the experimental mass within an error of 1 ppm; b: molecular formula based search; x:nmber of isomeric compounds

The elucidation of unknowns can be derived by various ways. One approach was explained and applied in detail in chapter 2.3.5 by using the mass difference analyses and subsequent network visualization, to reveal new arachidonic acid co-metabolites. Therefore, we were using again Netcalc for finding possible mass differences between mass signals within an error of 0.2 ppm. For example, we elaborated the mass differences of one mass signal such as [M-H]-: 325.20204, which was annotated as 2,3-Dinor-8-iso PGF2alpha. We could find several possible mass differences such as the carboxylation to dinor omega-1-oxo-6-keto-PGF1alph. Found mass differences are for the metabolite 2,3-Dinor-8-iso PGF2alpha summarized in Table 13. This table is now the starting point to generate and visualize networks, shown in Figure 4-14, B. Then, it can be used in order to achieve an overview over possible connections to unknown metabolites, such as it is the case with the metabolite 2,3-Dinor-8-iso PGF2alpha, which showed 11 possible mass differences (pink labels) to Unknowns (red nodes), including taurine and sulfate conjugates which were not annotated before (Figure 4-14, B).

Table 13 Example of a mass difference table for generating networks of Figure 4-14 B

Experimental mass	Molecular Formula	Metabolite Name	Experimental mass	Molecular Formula	Metabolite Name	Name	Mass difference exact mass (theoretical)
323.18637	$C_{18}H_{28}O_5$	Dinor-PGD2	325.20204	$C_{18}H_{30}O_5$	2,3-Dinor-8-iso PGF2alpha	+/- H2	2.01565
325.20204	$C_{18}H_{30}O_5$	2,3-Dinor-8-iso PGF2alpha	355.17625	$C_{18}H_{28}O_7$	dinor omega-1-oxo-6-keto-PGF1alpha	+/- Carboxylation	29.97418
325.20204	$C_{18}H_{30}O_5$	2,3-Dinor-8-iso PGF2alpha	339.21769	$C_{19}H_{32}O_5$	Unknown	+/- Methylation	14.01565
325.20204	$C_{18}H_{30}O_5$	2,3-Dinor-8-iso PGF2alpha	343.21261	$C_{18}H_{32}O_6$	Unknown	+/- H_2O	18.010565
325.20204	$C_{18}H_{30}O_5$	2,3-Dinor-8-iso PGF2alpha	357.17412	$C_{18}H_{30}O_5S_1$	Unknown	+/- Thiol	31.97207
325.20204	$C_{18}H_{30}O_5$	2,3-Dinor-8-iso PGF2alpha	382.22347	$C_{20}H_{33}O_6N_1$	Unknown	+/- Glycine	57.021465
325.20204	$C_{18}H_{30}O_5$	2,3-Dinor-8-iso PGF2alpha	389.16392	$C_{18}H_{30}O_7S_1$	Unknown	+/- SO_2	63.961903
325.20204	$C_{18}H_{30}O_5$	2,3-Dinor-8-iso PGF2alpha	428.21127	$C_{21}H_{35}O_6N_1S_1$	Unknown	+/- Cysteine	103.00919
325.20204	$C_{18}H_{30}O_5$	2,3-Dinor-8-iso PGF2alpha	432.20617	$C_{20}H_{35}O_7N_1S_1$	Unknown	+/- Taurine	107.0041
325.20204	$C_{18}H_{30}O_5$	2,3-Dinor-8-iso PGF2alpha	442.22691	$C_{22}H_{37}O_6N_1S_1$	Unknown	+/- Homocysteine	117.02483
325.20204	$C_{18}H_{30}O_5$	2,3-Dinor-8-iso PGF2alpha	327.21769	$C_{18}H_{32}O_5$	2,3-Dinor-8-iso PGF1alpha	+/- H2	2.01565
325.20204	$C_{18}H_{30}O_5$	2,3-Dinor-8-iso PGF2alpha	353.23335	$C_{20}H_{34}O_5$	Prostaglandin F2alpha	+/- ß-oxidation	28.0313
325.20204	$C_{18}H_{30}O_5$	2,3-Dinor-8-iso PGF2alpha	416.21126	$C_{20}H_{35}O_6N_1S_1$	Unknown	+/- Hypotaurine	91.009186
325.20204	$C_{18}H_{30}O_5$	2,3-Dinor-8-iso PGF2alpha	405.15887	$C_{18}H_{30}O_8S_1$	Unknown	+/- Sulfate	79.95682
355.17625	$C_{18}H_{28}O_7$	dinor omega-1-oxo-6-keto-PGF1alpha	369.19187	$C_{19}H_{30}O_7$	Unknown	+/- Methylation	14.01565
327.21769	$C_{18}H_{32}O_5$	2,3-Dinor-8-iso PGF1alpha	343.21261	$C_{18}H_{32}O_6$	Unknown	+/- OH	15.994915

Another approach that was used to confirm metabolites but also identify new metabolites was the application of MS/MS experiments, described in chapter 4.4.2.

4.5.5 Data processing of (+/-) UPLC-TOF-MS: non-targeted metabolomics

The raw data were exported to .mzxml data format and processed with MZmine 2.0 (Pluskal, Castillo et al. 2010). The aligned data were then exported to .csv (comma separated) files and filtered in terms of abundance count of n≥10. The annotation was performed with MassTRIX with an absolute mass error of 0.005 Da and in METLIN within an error of 10 ppm.

Table 14 MZmine steps and their parameters for UPLC-TOF-MS data alignment

Steps	Parameters			
1. Mass detection	Mass detection		Noise level	
	Centroid		500 (+); 200 (-)	
2. Chromatogramm builder	Minimum span time		Minimum height	m/z tolerance
		0.1	500 (+); 200 (-)	10 ppm
3. Chromatogramm deconvolution	Minimum peak height		Peak duration [min]	Baseline level
(Baseline cutoff)	500 (+); 200 (-)		0.05-1.5	500 (+); 200 (-)
4. Alignment	m/z tolerance		RT tolerance [min]	
(Ransac)	10 ppm		0.5	
5: Export	Format		Integration	
	.csv		Peak area	

4.6 Multivariate statistical analyses

4.6.1 Unsupervised techniques: Principal component analysis

The evolving of metabolomics and the ongoing development of NMR, but also MS, increased the amount of the generated data. The containing multivariate data needs appropriate handling (here as example our data matrices contains n=53 observations and k=3545 variables, which represents the ***X*** matrix, Figure 4-15 A). In the field of metabolomics , two commonly used

methods for data handling emerged since the beginning of 1980s, in order to reduce the dimensionality and for recognizing patterns in multivariate data (van der Greef, Tas et al. 1983). These techniques are principal component analysis (PCA) and partial least squares regression (PLS). PCA belongs to the unsupervised and PLS to the supervised techniques in the multivariate data analyses. PCA is popular and widely used in the metabolomics research field, applying an - ISI Web of Science® – search with the keywords: metabolomics and PCA resulted in 411 articles (date: 21.08.2013). In PCA the data is reduced in several principal components (PCs), usually the first and second PC is showing and visualizing the majority of total variance existing in the data. In our example with n =53 observations and k=3545 variables the application of PCA resulted in the two-dimensional scores plot, representing the observations (Figure 4-15 B). In our example the first two PCs already describe 37.5 % of the total variance (Figure 4-15 B). In turn the variables are plotted in the so called loading plot, shown in Figure 4-15 C. Superimposing both plots allows to reveal which variables were responsible for the "pulling" or clustering of the observations (so called bi-plot). The application of PCA in the thesis served the aim to get a first overview over the behavior of the data, concerning the groups and their unsupervised clustering with no input of information of the group classification. In our example, we already observed a clustering of two main groups (Figure 4-15 B, 1 and 2), separated due to diets (HFD (1) and LFD (2)).

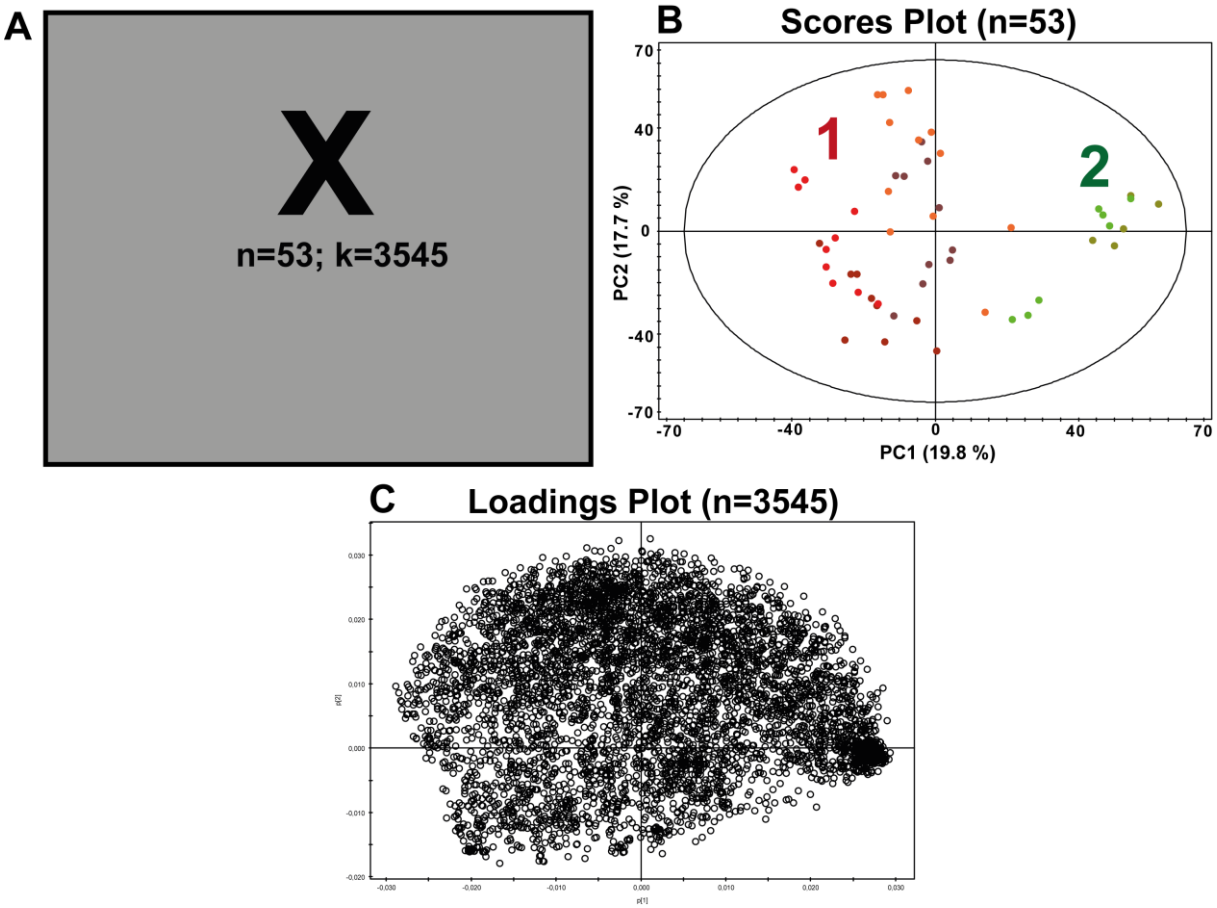

Figure 4-15 Principal component analysis scheme: A: *X* matrix, a data matrix containing multivariate data, which is reduced and projected into a two dimensional plot, shown in B, the so-called scores scatter plot which is summarized into two main principal components (PCs), displaying the largest variation; C: a loading plot visualizes the variables and their distribution along a two dimensional space, responsible for the projection of the scores in the score plot of B

4.6.2 Supervised techniques: PLS-DA and OPLS-DA

In order to classify the multivariate data here in the studies we were applying primarily the orthogonal partial least squares discriminant analysis (OPLS-DA). Now we want to present with our exemplary data the evolution from PCA to OPLS-DA and their impact on the data and group separation. Therefore, we were using a subset of the data consisting of two subgroups (C57J (orange dots) and C57N (brown dots) in the PCA scores plot of Figure 4-15 B). First, the application of PCA resulted in the scores plot shown in Figure 4-16 A. The separation of the two groups was whether neither clear nor good enough to discriminate the groups, thus the major variation comes from another unknown factor. For the classification we applied the partial least squares DA (PLS-DA), where we generated a dependent vector (Y) consisting of dummy variables, here zero and one for the two classes. The application of

PLS-DA to our dataset resulted in a good discrimination between the two groups, the scores plot shown in Figure 4-16 B with a $R^2Y(cum)$ value of 0.911 and $Q^2(cum)$ value of 0.68, which is satisfying due to the given criteria in the literature with suggested Q^2 value over 0.5 (Broadhurst and Kell 2006). Moreover, the difference between $R^2Y(cum)$ and $Q^2(cum)$ should not be too large. In addition, problems in terms of over fitting by using PLS-DA were discussed elsewhere (Westerhuis, Hoefsloot et al. 2008, Fonville, Richards et al. 2010). Additionally, a part from ***X*** matrix (red) which is not related to the ***Y*** vector disturbs, because it contributes to and influences the distribution or the separation of the scores, as shown in Figure 4-16 B. Thus, another approach was developed, called OPLS-DA. OPLS-DA was originally introduced by Trygg *et al.* (Trygg and Wold 2002), in order to "clean" the ***X*** matrix and remove all systemic variation (red part of the ***X*** matrices) that is orthogonal to ***Y*** vector and thus not correlated to the vector of ***Y***. Our data was also subjected to an extension of OPLS-DA called OPLS/O2PLS-DA, showing the scores plot in Figure 4-16 C. OPLS/O2PLS-DA is a development of OPLS-DA which takes into account the bi-direction between ***X*** matrix and ***Y*** vector, whereas PLS/OPLS-DA considered solely the direction from ***X*** to ***Y***. Moreover, the Q^2 was 0.61 and subsequent performed CV-ANOVA could show a valid model for this separation (p-value = 0.014). In all mentioned studies in chapter 2 and 3 we applied as first step a PCA to reduce and to get an overview of the data and then we classified the data by the usage of OPLS/O2PLS-DA. The cross-validation is always performed by CV-ANOVA.

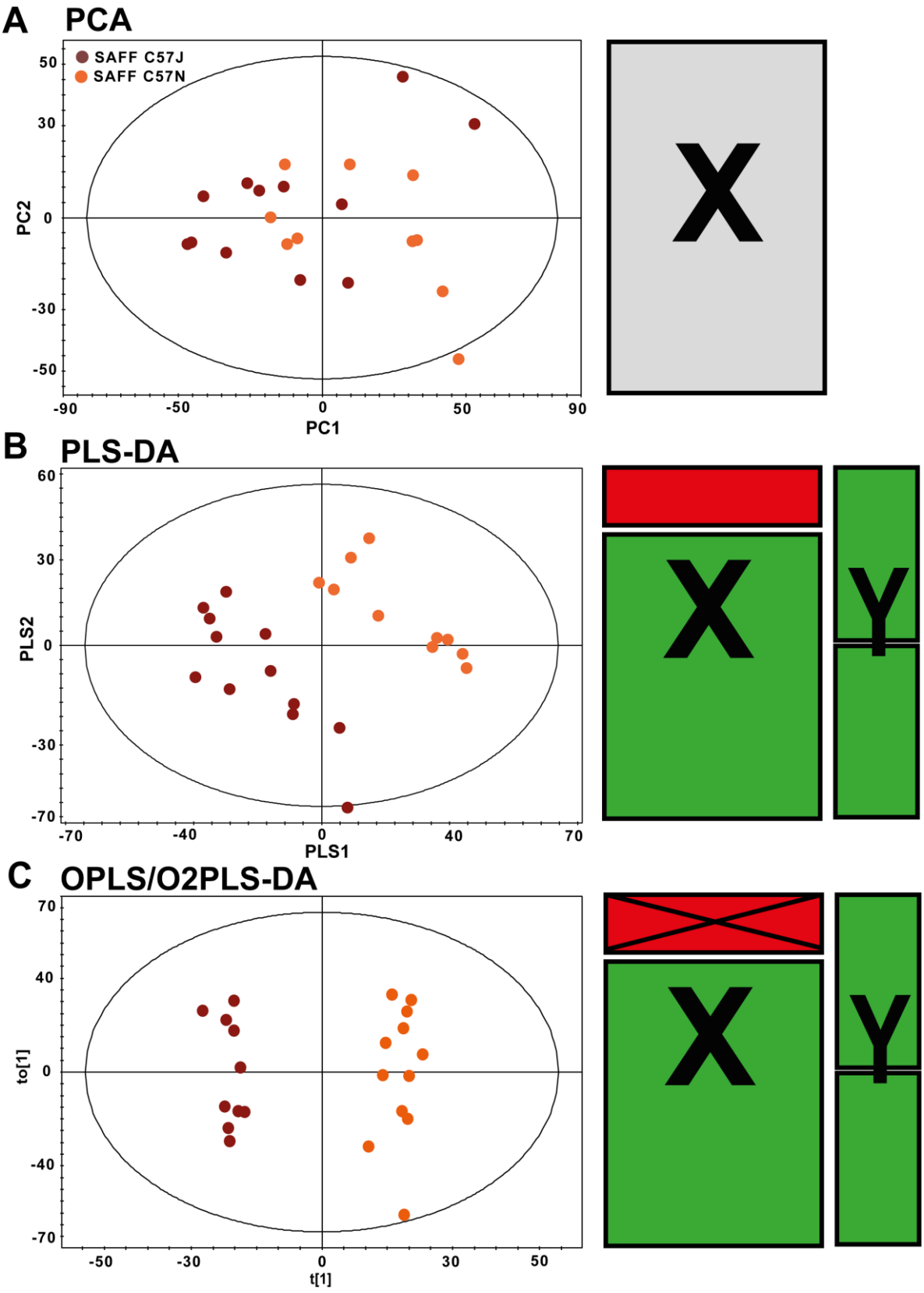

Figure 4-16 An example for the evolvement from unsupervised PCA to the supervised OPLS/O2PLS-DA analyses and the impact on the discrimination of the two groups (orange and brown)

4.6.3 Other data handling tools

Furthermore, handling and visualizing data, we used several software tools such as heatmaps which was performed by using Hierarchical Clustering Explorer 3.5 (Jinwook and Shneiderman 2002). Before visualization in heatmaps the data was normalized ($x-\bar{x}/\sigma$). Boxplots were plotted by using Rstudio (http://www.rstudio.org/). Other plots were generated by using Microsoft Office Excel 2007. MSA was performed using SIMCA-P 9.0 or 12.0 (Umetrics, Umea, Sweden). The data was always scaled to the unit variance before performing MSA. Univariate statistical analyses were performed by using MultiExperiment Viewer while applying a non-parametric univariate statistical Mann-Whitney test or ANOVA or Kruskal Wallis test (Saeed, Sharov et al. 2003).

Chapter V

5 Supplementary Information

5.1 Mouse Studies – experimental design

5.1.1 Type 2 Diabetes mouse model

Mice: Ten weeks old homozygous BKS.Cg-*dock7*^{m} *+/+ Lepr*^{db}*/J* (*db/db*) mice and their non-diabetic controls (*wt*) were used for the investigation of gastrointestinal meta- metabolome. Mice were housed in a specific pathogen-free (SPF) environment using single ventilated cages (SealsafePlus AERO IVC Greenline, Tecniplast GmbH, Hohenpeissenberg, Germany) with a 12/12 hour light-dark cycle at a constant temperature (22 ± 1°C) and controlled humidity. The maintenance of the mice was done in German Mouse Clinic. At an age of 3 weeks both *db/db* and *wt* mice were fed a high fat and high carb diet (S0372-E010, Ssniff, Germany). At the beginning of the drug challenge study, the mice were fasted for 4 hours. Afterwards body weight and tail blood glucose (Contour, Bayer Vital GmbH, Leverkusen, Germany) were measured. The db/db mice should fulfill two aspects having a body weight over 44 g and blood glucose levels over 19.43 mmol/L. All mice were single house during the study. *Db/db* mice or wt mice were treated daily orally with a 0.5% vehicle solution containing 95% hydroxyethylcellulose 250 g Pharm (Fagron GmbH & Co KG, Barsbüttel, Germany) and 5% solutol HS15 (BASF Chem-Trade GmbH, Ludwigshafen, Germany) and represented the control groups of diabetic and wt mice. The drug challenge was performed in db/db mice by using Metformin (MET) (Sigma Aldrich Chemie GmbH, Munich, Germany) and an SGLT-2 inhibitor AVE2268 (SGLT) (Sanofi-Aventis AG, Frankfurt, Germany). Metformin was dosed 300 mg/kg (mpk) body weight per day and AVE2268 30 mpk body weight per day. Drugs were weighed in (XA105 Dual Range, Mettler Toledo, Gießen, Germany) and dissolved in 0.5% vehicle solution containing 95% hydroxyethylcellulose 250G Pharm (HEC) (Fagron GmbH & Co KG, Barsbüttel, Germany) and 5% solutol HS15 (BASF ChemTrade GmbH, Ludwigshafen, Germany). Drug suspensions were applied by oral gavage to all mice. Vehicle solution was prepared by diluting 475 mg of hydroxyethylcellulose with 25 µl of preheated solutol into a 100 ml Ampuwa-water bottle

(Fresenius Medical Care, Bad Homburg, Germany). At 10 weeks of age, the mice were fasted for 4 hours, weighed and sacrificed with an overdose of isoflurane. Glucose was measured from tail blood. For CRP measurement, blood was taken from the *Vena cava* using Monovettes with cannulas (1.2 ml K3-EDTA S-Monovettes, Sarstedt AG, Nümbrecht, Germany) and centrifuged at 14 000 rpm for 2 minutes at 4°C (Fresco 21, Heraeus GmbH, Hanau, Germany). The upper plasma phase was transferred into fresh eppendorf tubes, snap frozen in liquid nitrogen and stored at -80°C. For metabolomics studies of gut luminal content, the complete gastrointestinal tract was removed with sterile instruments, flamed with ethanol. The gastrointestinal tract was divided into nine parts: stomach, duodenum, jejunum, ileum, cecum, the proximal, middle, distal and the rectal part of the colon. The luminal content of the cecum and the proximal, middle and the distal part of the colon of each group was collected in Eppendorf tubes and immediately snap-frozen, quenched in liquid nitrogen and preserved in -80°C prior to further experiments. Additionally, feces droppings were collected in the cages after scarification of the mice and stored at -80°C conditions.

After plasma samples were measured by means of BIOCRATES AbsoluteIDQ™ p180 kit for a targeted metabolomics approach, the supernatants were evaporated with an original volume of 10 µL of plasma. Evaporated plasma samples were kept under -80° C conditions. In order to perform a non-targeted metabolomics approach we reconstituted the evaporated samples in 0.1 % formic acid (500 µL). We performed a solid phase extraction by using C18 cartridges (Bond Elut™ Cartridge SPE, sorbent mass: 100 mg with 1 mL of volume; Varian, Inc., Walnut creek cA, USA). First, the cartridges were conditioned with 1 mL methanol and then with 1 mL of water. Then, the reconstituted plasma samples were loaded and wash step with 0.1 % formic acid (1 mL) was performed. The elution was performed with 1 mL of methanol. The samples were evaporated and reconstituted in 50 µL of pure methanol.

5.1.2 Diet induced obesity in C57J and C57N mice

Mice: C57BL/6NTac (C57N, Taconic Denmark) and C57BL/6J (C57J) were bred and housed under standard vivarium conditions (12:12 light dark cycle) in German Mouse Clinic. The diet study was started at an age of 14 weeks. Mice from every strain were switched to high fat diet (HFD, Ssniff, Germany) rich in safflower-oil (SAFF) or lard fat (LARD) or kept under low fat diet (LFD, Diet#1310, Altromin, Germany; 17.0KJ/g) for 3 weeks. Mice were bred, housed and handled according to the federal animal welfare guidelines. Mouse husbandry was conducted under a continuously controlled hygiene standard according to the Federation of

European Laboratory Animal Science Associations (FELASA). Body weight was measured before the beginning of high fat feeding and after 3 weeks.

At the terminal study-endpoint after a glucose tolerance test between 9-12 a.m. mice were killed with isoflurane. For gut metabolome, analysis the gastrointestinal tract was removed from each animal. The luminal content of the cecum of each mouse was collected and immediately snap-frozen in liquid nitrogen and preserved in -80°C prior to metabolomics experiments. All animals received humane care according to criteria outlined in the NAS "Guide for the Care and Use of Laboratory Animals". Animal experiments were approved by the Upper-Bavarian district government (Regierung von Oberbayern, Gz.55.2-1-54-2532-70-07, Gz. 55.2-1-54-2532-4-11).

5.2 MS/MS identification experiments

Confirmation of metabolites was performed using (-) TOF-MS/MS experiments as described in chapter 4.4.2. Experimental MS/MS spectra were compared manually with METLIN database (Smith, Maille et al. 2005).

5.2.1 (-) TOF-MS/MS spectra of metabolites of T2DM metabolomics study

5.2.1.1 Fatty acids

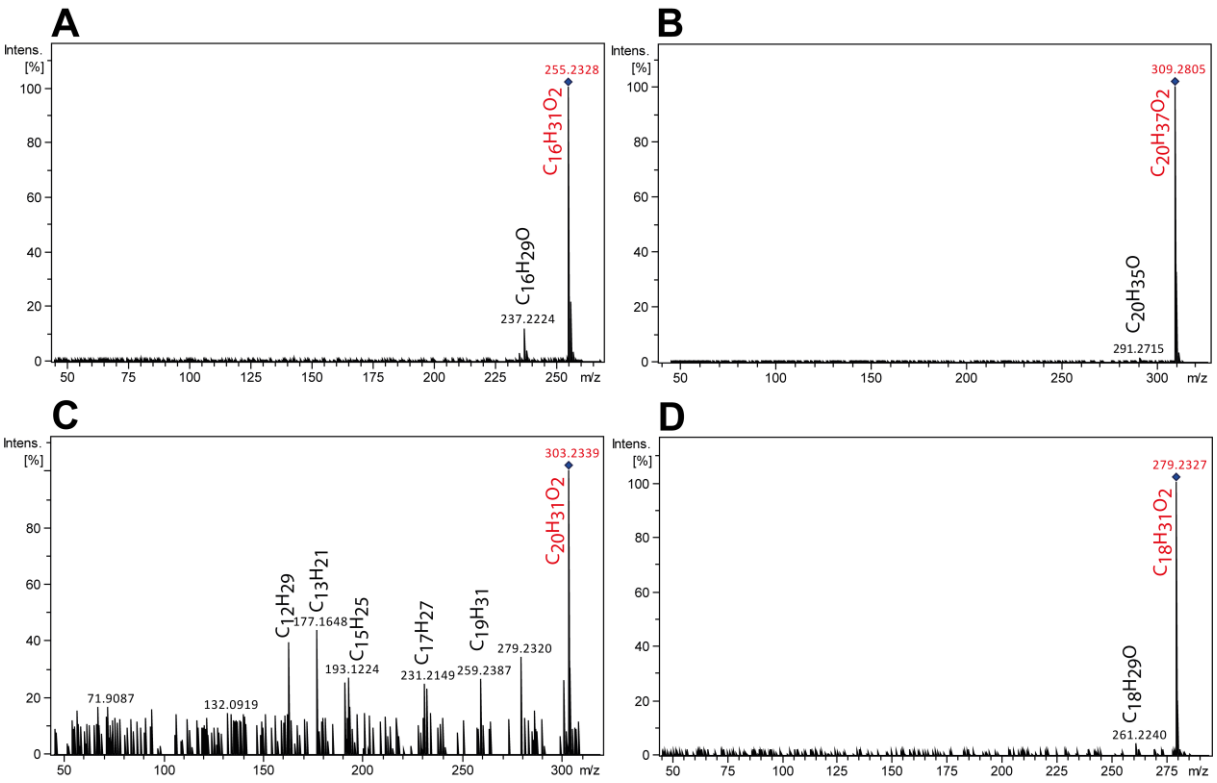

Figure 5-1 Experimental (-) TOF-MS/MS spectra: A: Palmitic acid C16:0; Icosenoic (C20:1) B: C: Arachidonic acid (20:4); D: Linoleic acid (C18:2)

5.2.1.2 Oxylipins

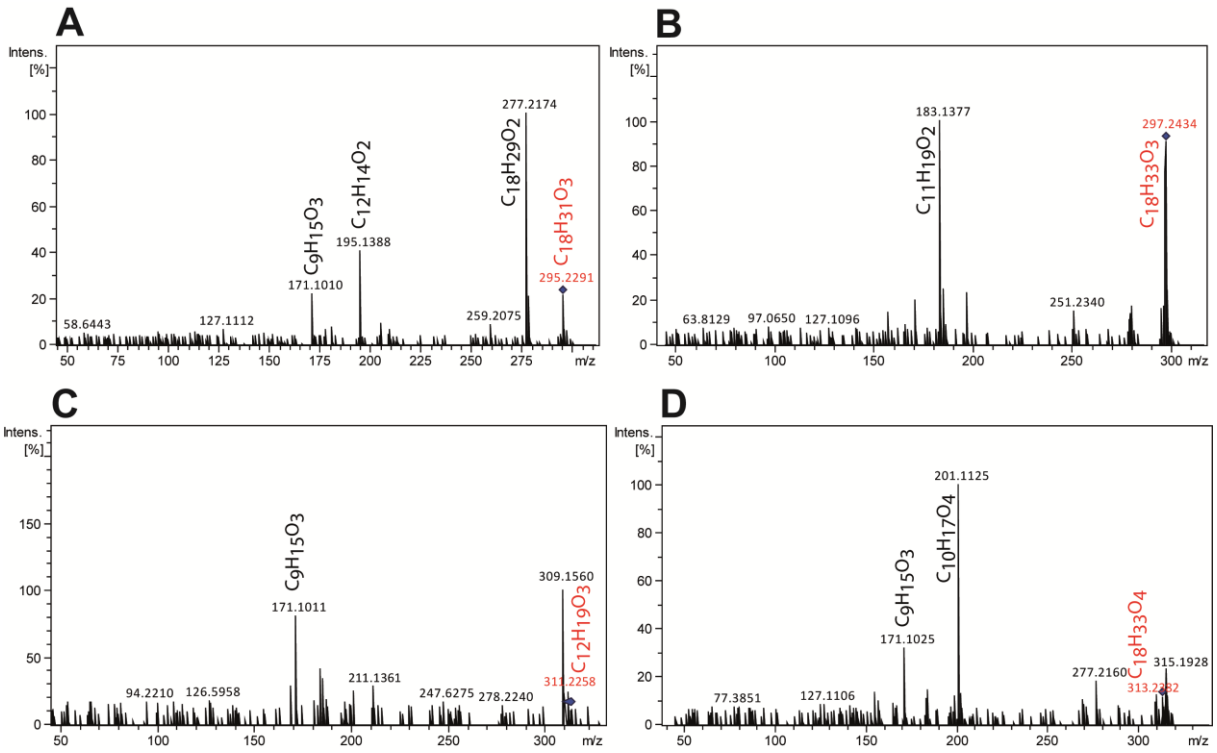

Figure 5-2 Experimental (-) TOF-MS/MS spectra: A: possible isomers of hydroxylinoleic acid (also known as HODE) with a possible hydroxyl position at C-13 or C-9, B: Hydroxyoleic acid; C: Hydroxyoxooleic acid: D: Dihydroxyoleic acid

5.2.1.3 N-acyltaurines

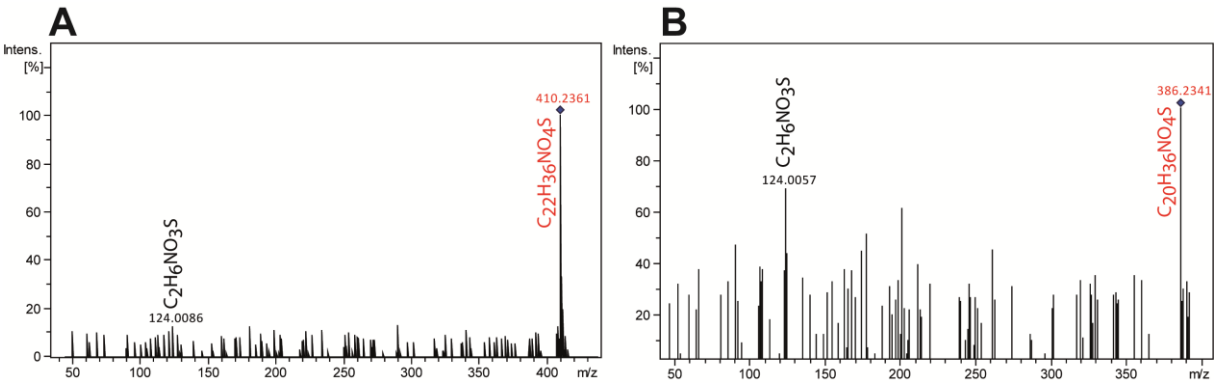

Figure 5-3 Experimental (-) TOF-MS/MS spectra: A: N-arachidonoyltaurine; B: N-linoleoyl taurine

5.2.1.4 Bile acids

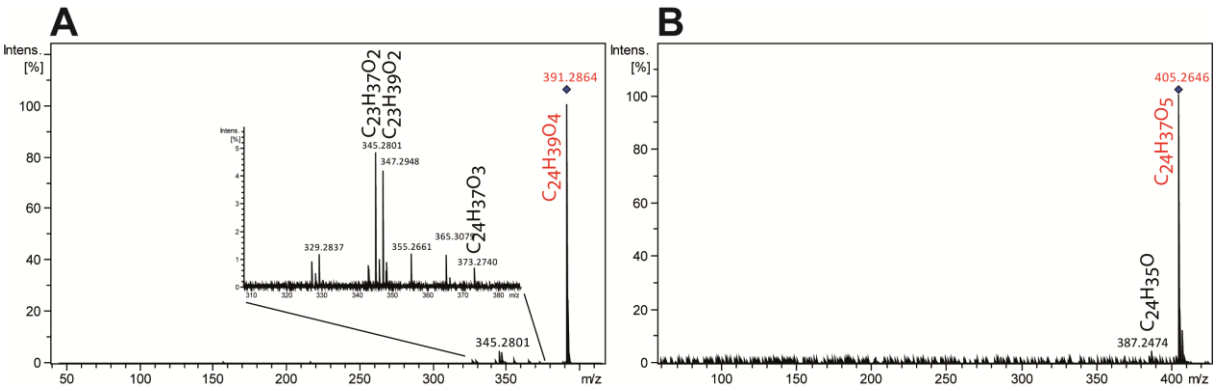

Figure 5-4 Experimental (-) TOF-MS/MS spectra: A: Deoxycholic acid; B: Ketodeoxycholic acid

5.2.1.5 Conjugates of bile acids and steroids

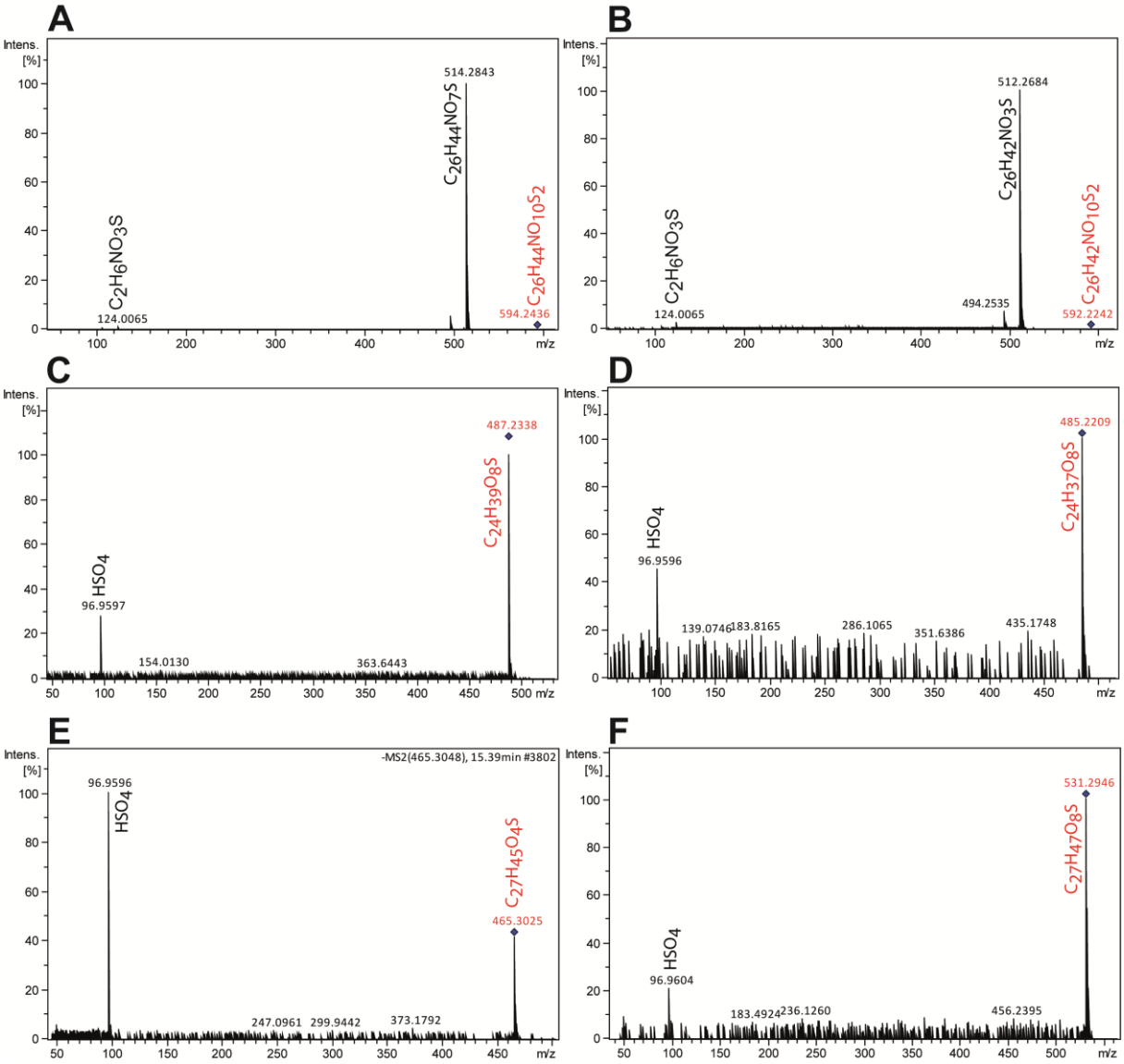

Figure 5-5 Experimental (-) TOF-MS/MS spectra: A: Taurocholic acid sulfate; B: Taurooxocholic acid sulfate; C: Sulfocholic acid; D: Oxocholic acid sulfate; E: Cholesterol sulfate; F: Cyprinolsulfate

5.2.1.6 Sulfated metabolites of AAM pathway

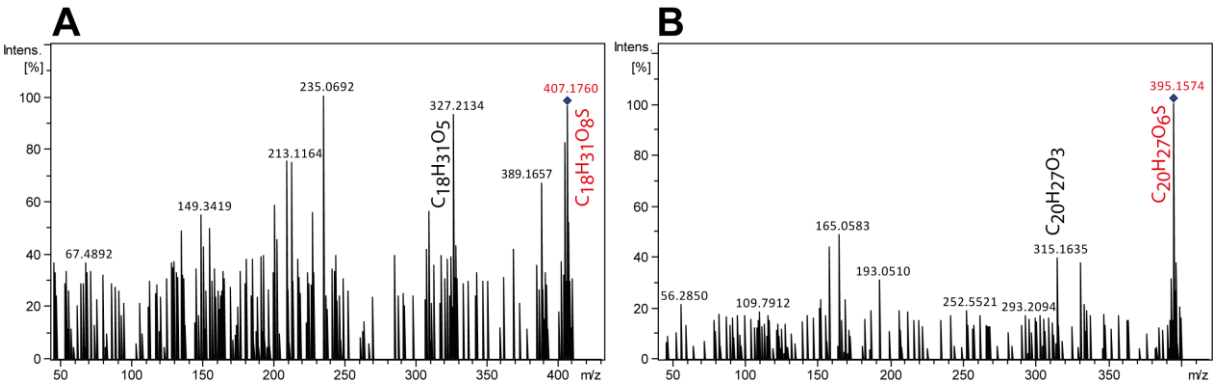

Figure 5-6 Experimental (-) TOF-MS/MS spectra: A: 2, 3-Dinor-8-iso prostaglandin F1alpha sulfate; B: 15-Deoxy-delta-12, 14-PGJ2 sulfate

5.2.1.7 Sulfate conjugated metabolites: Oxygenated fatty acids

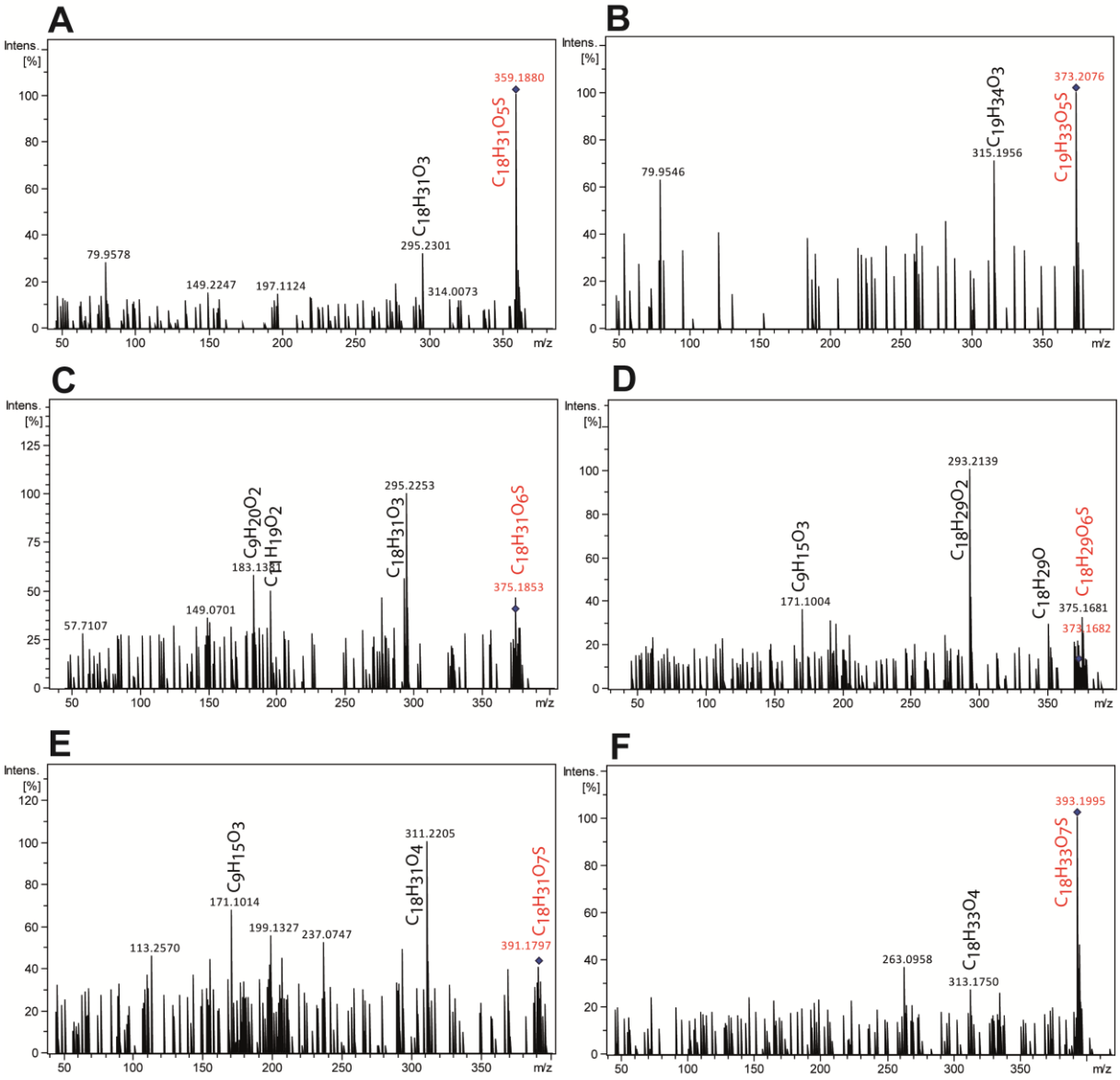

Figure 5-7 Experimental (-) TOF-MS/MS spectra: A: Sulfolinoleic acid; B: Nonadecadienoic acid sulfonate; C: Hydroxylinoleic acid sulfate; D: Hydroxylinolenic acid sulfate; D; Dihydroxylinoleic acid sulfate; E: Dihydroxyoleic acid sulfate

5.2.1.8 Taurine conjugated metabolites: oxygenated fatty acids

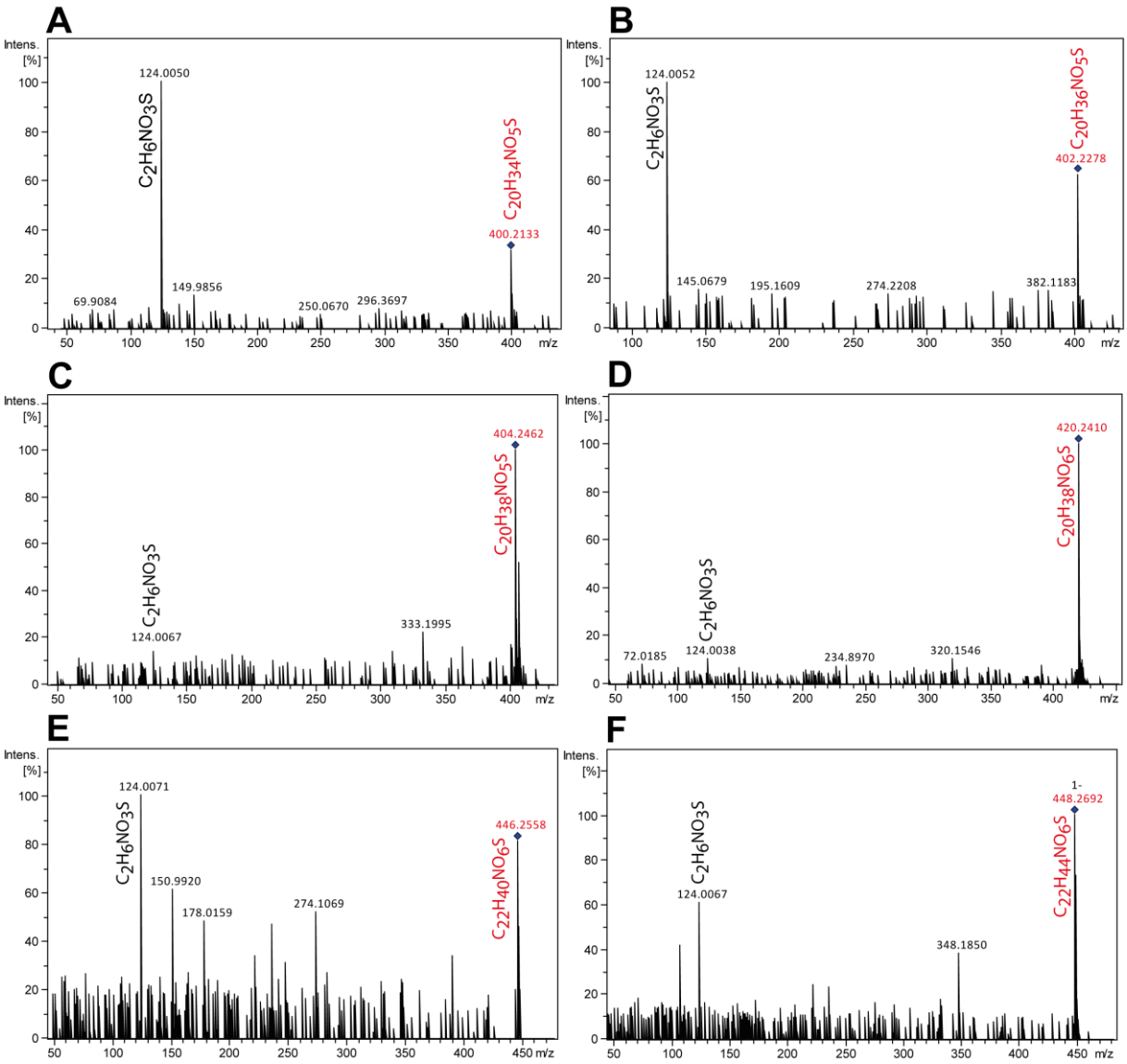

Figure 5-8 Experimental (-) TOF-MS/MS spectra: A: Hydroxylinolenic acid taurine B: Hydroxylinoleic acid taurine; C: Hydroxyoleic acid taurine; D: Dihydroxystearic acid taurine; E; Dihydroxyeicosadienic acid taurine; E: Dihydroxyeicosanoic acid taurine

5.2.1.9 Other N-acyl Fatty acids with amino acids

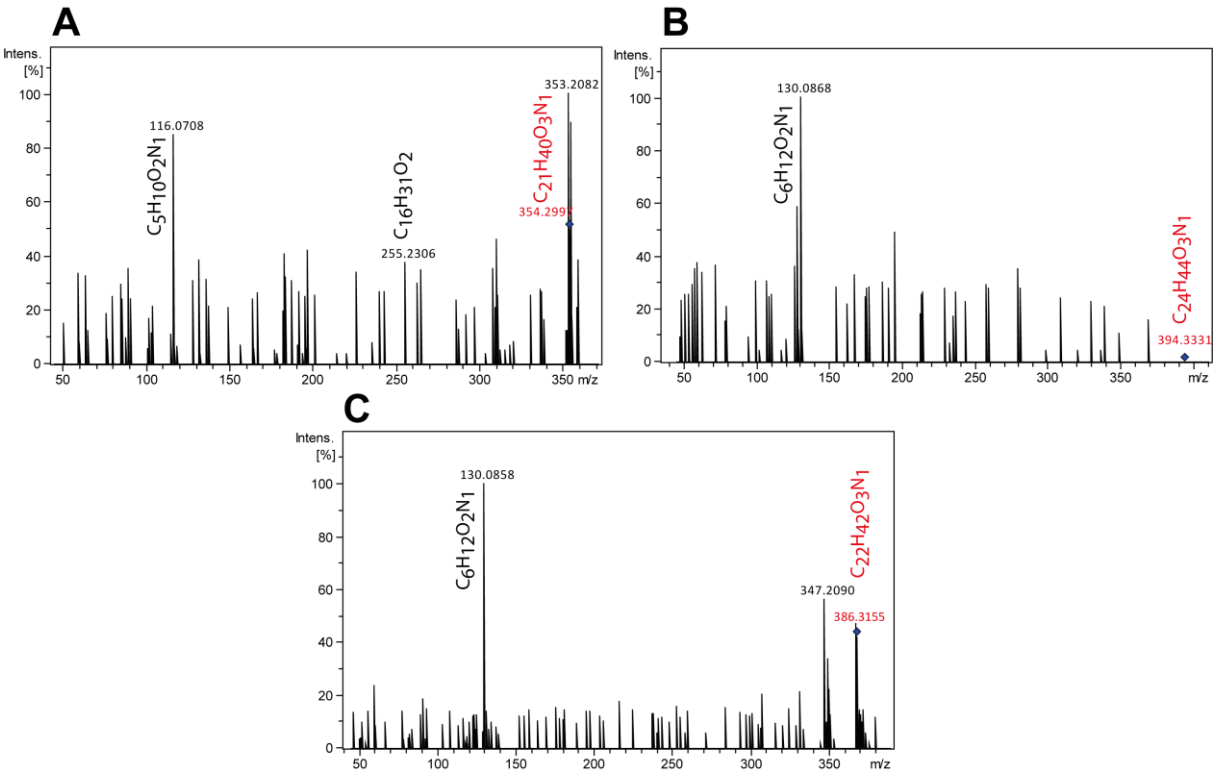

Figure 5-9 Experimental (-) TOF-MS/MS spectra: A: N-palmitoyl (iso)leucine B: N-oleoyl (iso)leucine C: N-palmitoyl (iso)leucine (compared with MS/MS spectra from Tan *et al.* (Tan, O'Dell et al. 2010)

5.2.2 (-) TOF-MS/MS spectra of metabolites of DIO metabolomics study

5.2.2.1 LTB4 sulfate

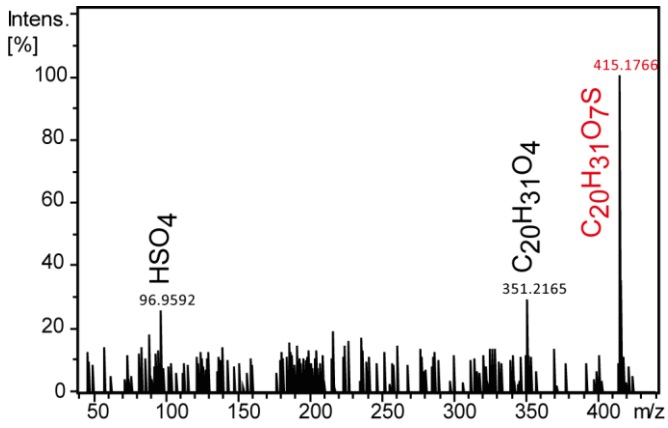

Figure 5-10 Experimental (-) TOF-MS/MS spectrum of LTB4

5.2.2.2 Unknown – $C_{15}H_{22}O_5$

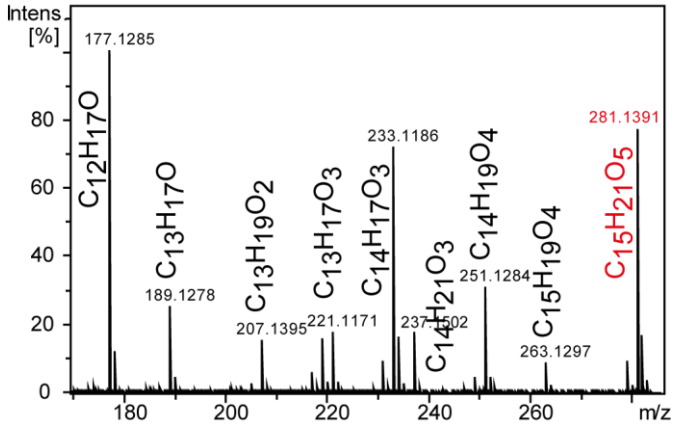

Figure 5-11 Experimental (-) TOF-MS/MS spectrum of an unknown metabolite with the molecular formula of $C_{15}H_{22}O_5$, the fragments are indicated by their molecular formula

5.2.2.3 C_{24} Bile acids

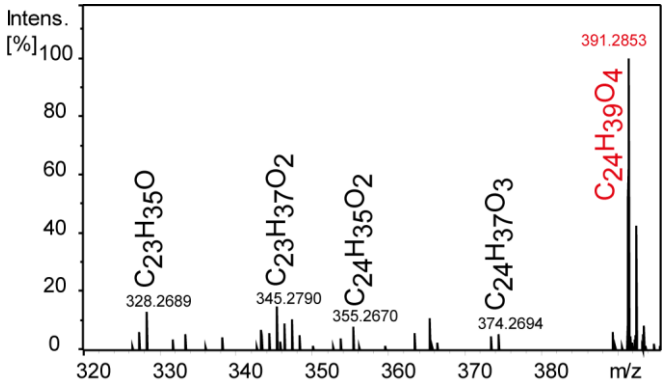

Figure 5-12 Experimental (-) TOF-MS/MS spectrum of deoxycholic acid (DCA)

5.2.2.4 C_{24} Taurine conjugated Bile acids

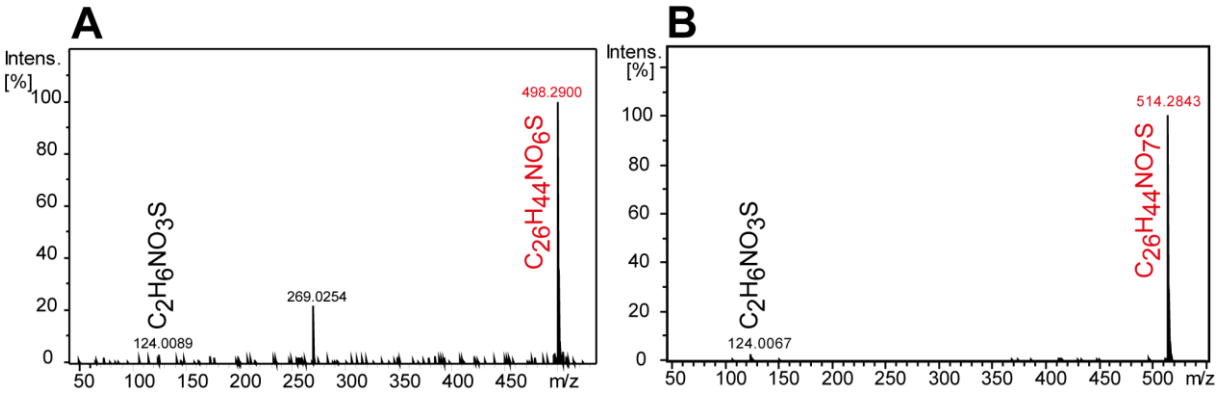

Figure 5-13 Experimental (-) TOF-MS/MS spectra: A: Taurodeoxycholic acid; B: Taurocholic acid

5.2.2.5 Taurine and Sulfates of C_{27} Bile acids

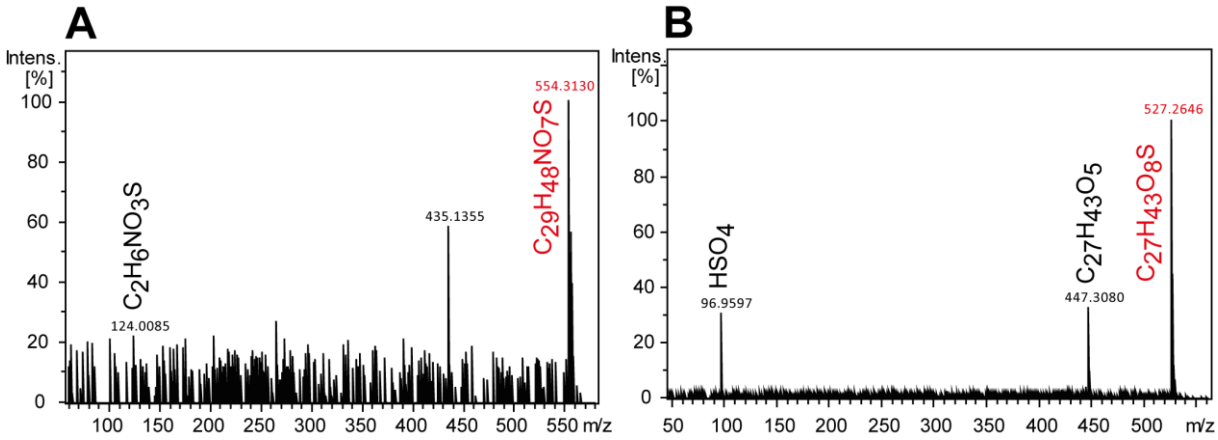

Figure 5-14 Experimental (-) TOF-MS/MS spectra: A: Taurodihydroxycholestenoic acid, B: Dihydroxyoxocholestanoic acid sulfate

5.2.2.6 Fatty acids

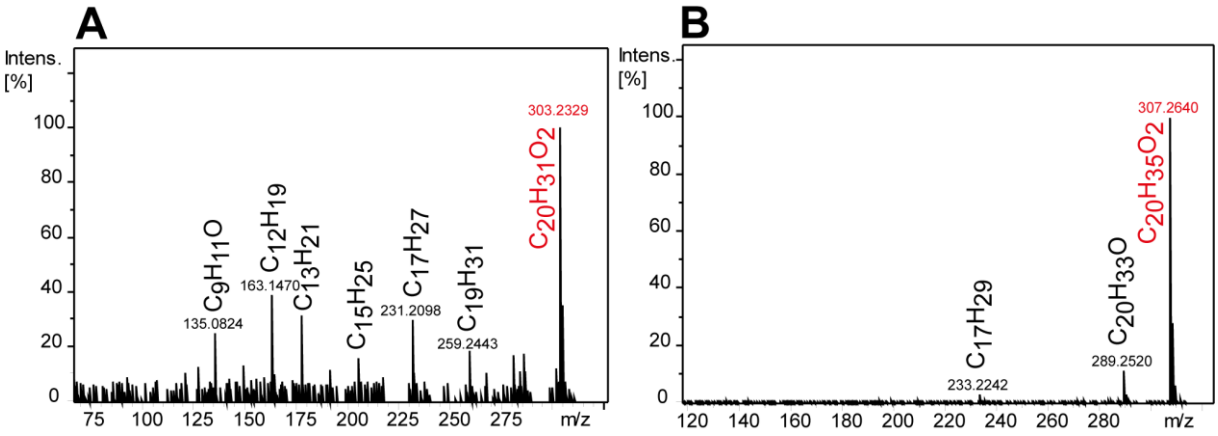

Figure 5-15 Experimental (-) TOF-MS/MS spectra: A: Arachidonic acid (C20:4); B: Eicosadienoic acid (C20:2)

5.2.2.7 Bacterial derived metabolites

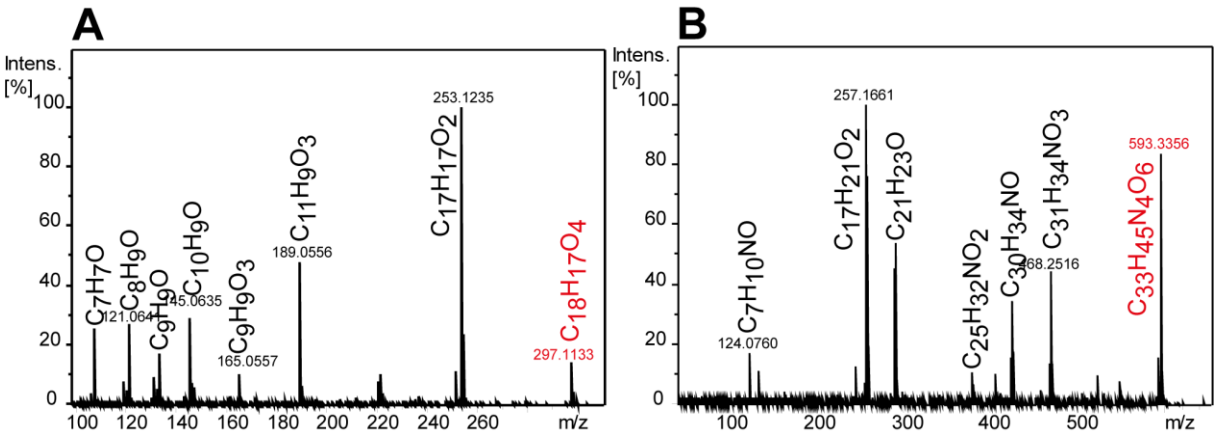

Figure 5-16 Experimental (-) TOF-MS/MS spectra: A: Enterolactone B: L-Urobilin

5.2.2.8 Novel metabolites – Diphloretoylputrescine

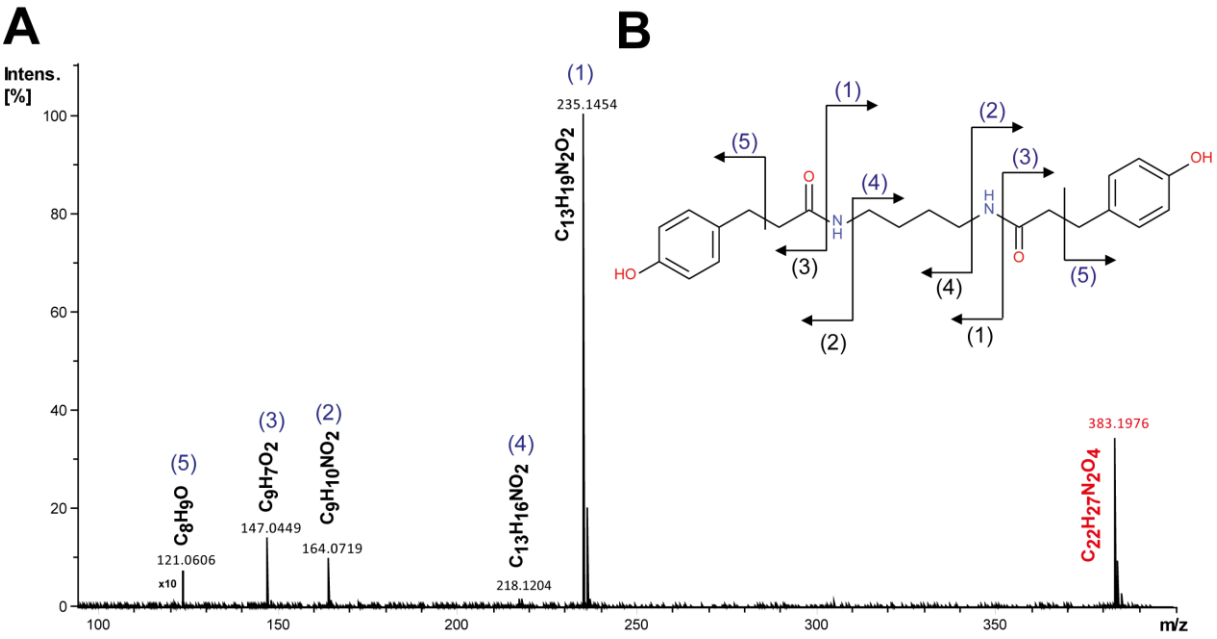

Figure 5-17 Experimental (-) TOF-MS/MS spectrum of diphloretoylputrescine in **A** and their most plausible structure in **B** due to no reference spectrum was given in METLIN database

5.2.2.9 Altered metabolites in C57J and C57N on LARD diet

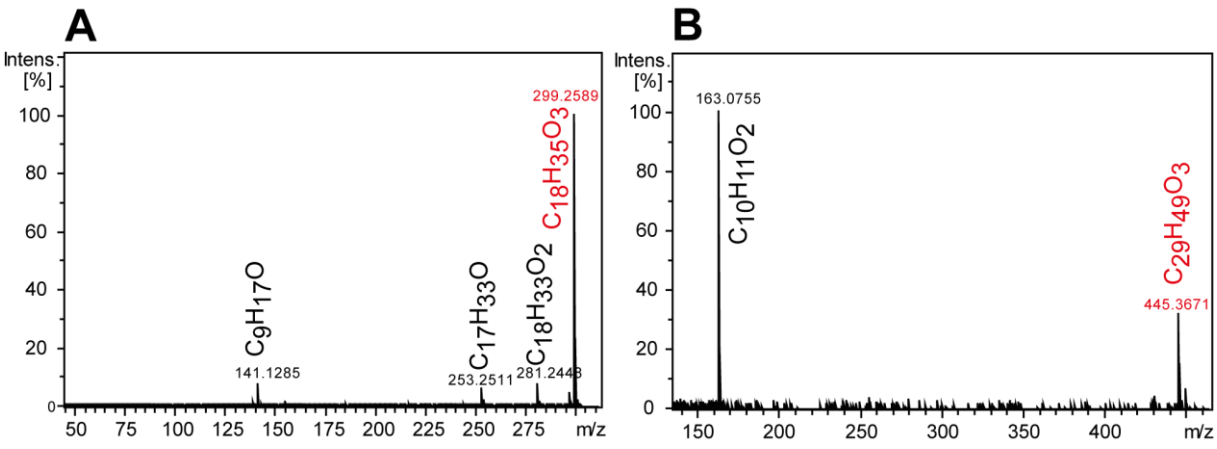

Figure 5-18 Experimental (-) TOF-MS/MS spectra: A: Hydroxystearic acid B: Hydroxyalphatocopherol

Chapter VI

6 Appendix

6.1 Tables of T2DM metabolomics study

6.1.1 Primary bile acid pathway and their metabolites

Table 15 Bile acids and cholesterol metabolites

Mass (avg.)	Compound Name	Monoisotopic mass	p-value (CECUM) db/db vs. wt	p-value (MIDDLE) db/db vs. wt	p-value (DISTAL) db/db vs. wt	p-value (FECES) db/db vs. wt	Molecular Formula
Bile acids							
391.285381	Deoxycholic acid	392.292644	n.s.	n.s.	n.s.	0.03376	$C_{24}H_{40}O_4$
407.280277	Cholic acid	408.287559	n.s.	0.00101	n.s.	0.00109	$C_{24}H_{40}O_5$
Cholesterol metabolites							
399.326853	Hydroxycholestenone	400.3341124	0.029084	n.s.	0.011440	0.00175	$C_{27}H_{44}O_2$
401.34253	Hydroxycholesterol	402.3497616	0.043003	0.00100	0.004136	0.00145	$C_{27}H_{46}O_2$
415.321805	Dihydroxycholestenone	416.3290274	0.046945	n.s.	0.001833	n.s.	$C_{27}H_{44}O_3$
417.337434	Dihydroxycholesterol	418.3446766	0.030510	0.00337	0.002050	0.00109	$C_{27}H_{46}O_3$
429.301041	Hydroxyoxocholestenoate	430.3082932	0.015169	n.s.	0.001461	n.s.	$C_{27}H_{42}O_4$
431.316709	Dihydroxycholestenoate	432.3239424	0.015169	n.s.	0.001031	n.s.	$C_{27}H_{44}O_4$
433.332348	Trihydroxycholestanal	434.3395916	0.030510	n.s.	0.000722	n.s.	$C_{27}H_{46}O_4$
435.348005	Tetrahydroxycholestane	436.3552408	0.030510	0.00038	0.004837	0.00550	$C_{27}H_{48}O_4$
449.327276	Trihydroxycholestanoate	450.3345066	0.046945	n.s.	0.001302	n.s.	$C_{27}H_{46}O_5$

6.1.2 Fecal meta-metabolome between *db/db* and *wt* mice

Table 16 Summary of all metabolites significantly differed between db/db and wt mice in feces

Mass (avg.)	Compound Name	Monoisotopic mass	MEAN wt	MEAN db/db	Log2 fold change db/db vs. wt	p-value	Molecular Formula
Fatty acids							
199.17036	Lauric acid	200.177620	1.99E+07	1.04E+07	-0.94	0.00427	$C_{12}H_{24}O_2$
227.201658	Myristic acid	228.208919	2.18E+08	5.38E+07	-2.02	0.00024	$C_{14}H_{28}O_2$
253.217297	Palmitoleic acid	254.224568	2.53E+08	1.18E+08	-1.10	0.00329	$C_{16}H_{30}O_2$
255.232921	Palmitic acid	256.240217	5.07E+10	1.00E+10	-2.34	0.00061	$C_{16}H_{32}O_2$
277.217277	Linolenic acid	278.224568	1.29E+09	8.42E+08	-0.62	0.02224	$C_{18}H_{30}O_2$
279.232917	Linoleic acid	280.240217	2.87E+10	1.96E+10	-0.55	0.02749	$C_{18}H_{32}O_2$
281.248583	Oleic acid	282.255866	3.79E+10	2.09E+10	-0.86	0.00705	$C_{18}H_{34}O_2$
283.264254	Stearic acid	284.271516	1.62E+10	6.27E+09	-1.37	0.00427	$C_{18}H_{36}O_2$
297.279872	Nonadecanoic acid	298.287165	1.09E+08	4.27E+07	-1.36	0.00192	$C_{19}H_{38}O_2$
301.217273	Icosapentanoic acid	302.224568	3.00E+08	5.60E+08	0.90	0.00705	$C_{20}H_{30}O_2$
309.27987	Icosenoic acid	310.287165	3.76E+09	5.31E+08	-2.82	0.00024	$C_{20}H_{38}O_2$
311.295565	Icosanoic acid	312.302814	2.01E+09	5.36E+08	-1.91	0.00024	$C_{20}H_{40}O_2$
327.232923	Docosahexaenoic acid	328.240217	2.31E+08	6.08E+08	1.39	0.00705	$C_{22}H_{32}O_2$
335.295565	Docosadienoic acid	336.302814	2.89E+07	1.78E+07	-0.70	0.02224	$C_{22}H_{40}O_2$
337.311213	Docosenoic acid	338.318463	6.29E+08	1.95E+08	-1.69	0.00061	$C_{22}H_{42}O_2$
339.326861	Docosanoic acid	340.334112	1.69E+09	7.71E+08	-1.13	0.00550	$C_{22}H_{44}O_2$
347.29553	Tricosatrienoic acid	348.302814	4.88E+05	2.34E+06	2.26	0.01186	$C_{23}H_{40}O_2$
365.342507	Nervonic acid	366.349762	1.72E+08	6.39E+07	-1.43	0.00705	$C_{24}H_{46}O_2$
367.358143	Tetracosanoic acid	368.365411	6.16E+08	3.98E+08	-0.63	0.02749	$C_{24}H_{48}O_2$
375.326825	Pentacosatrienoic acid	376.334112	3.23E+06	7.63E+06	1.24	0.00145	$C_{25}H_{44}O_2$
377.342485	Pentacosadienoic acid	378.349762	3.49E+06	7.24E+06	1.05	0.00252	$C_{25}H_{46}O_2$
389.342492	Hexacosatrienoic acid	390.349762	4.42E+06	6.93E+06	0.65	0.01789	$C_{26}H_{46}O_2$
405.373765	Heptacosadienoic acid	406.381060	1.45E+06	3.68E+06	1.34	0.00175	$C_{27}H_{50}O_2$
419.389443	Octacosadienoic acid	420.396709	3.13E+06	5.45E+06	0.80	0.01596	$C_{28}H_{52}O_2$
431.389481	Nonacosatrienoic acid	432.396709	3.07E+06	6.43E+06	1.06	0.00191	$C_{29}H_{52}O_2$
433.405114	Nonacosadienoic acid	434.412358	8.96E+05	3.59E+06	2.00	0.00663	$C_{29}H_{54}O_2$
471.420713	Dotriacontatetraenoic acid	472.428008	3.53E+05	4.36E+06	3.63	0.00200	$C_{32}H_{56}O_2$
527.483436	Hexatriacontatetraenoic acid	528.490604	4.35E+06	1.36E+07	1.65	0.00033	$C_{36}H_{64}O_2$
551.48342	Octatriacontahexaenoic acid	552.490604	8.86E+06	2.65E+07	1.58	0.00024	$C_{38}H_{64}O_2$
553.499134	Octatriacontapentaenoic acid	554.506254	4.90E+06	1.71E+07	1.80	0.00024	$C_{38}H_{66}O_2$
Oxylipins							
293.212199	Hydroxylinolenic acid	294.219483	2.34E+08	3.50E+08	0.58	0.00705	$C_{18}H_{30}O_3$
295.227856	Hydroxylinoleic acid	296.235132	9.27E+08	1.88E+09	1.02	0.00192	$C_{18}H_{32}O_3$
297.243522	Hydroxyoleic acid	298.250781	4.99E+08	8.45E+08	0.76	0.03376	$C_{18}H_{34}O_3$
309.207136	Dihydroxylinolenic acid	310.214398	1.11E+08	1.74E+08	0.66	0.00033	$C_{18}H_{30}O_4$
311.222786	Hydroxyoxooleic acid	312.230047	1.92E+08	4.00E+08	1.06	0.00024	$C_{18}H_{32}O_4$
313.238439	Dihydroxyoleic acid	314.245696	1.47E+08	3.00E+08	1.03	0.00109	$C_{18}H_{34}O_4$
315.254101	Dihydroxystearic acid	316.261346	9.30E+07	1.75E+08	0.91	0.00329	$C_{18}H_{36}O_4$
329.233318	Trihydroxyoleic acid	330.240611	1.35E+08	2.30E+08	0.77	0.00192	$C_{18}H_{34}O_5$
331.249002	Trihydroxystearic acid	332.256261	2.78E+07	8.15E+07	1.55	0.00427	$C_{18}H_{36}O_5$
345.228273	Dihydroxyoctadecanedioic acid	346.235526	7.82E+07	1.43E+08	0.88	0.00033	$C_{18}H_{34}O_6$
347.243918	Tetrahydroxyoctadecanoic acid	348.251176	1.32E+07	3.54E+07	1.43	0.00109	$C_{18}H_{36}O_6$

Fatty acids taurine							
354.174455	Hexadecatetraenoic acid taurine C16:4	355.181719	1.72E+07	4.56E+07	1.40	0.00033	$C_{18}H_{29}O_4N_1S_1$
356.190105	Hexadecatrienoic acid taurine C16:3	357.197369	1.38E+07	4.63E+07	1.74	0.00024	$C_{18}H_{31}O_4N_1S_1$
358.205771	Hexadecadienoic acid taurine C16:2	359.213018	6.80E+06	2.35E+07	1.79	0.00024	$C_{18}H_{33}O_4N_1S_1$
360.221408	Hexadecenoic acid taurine C16:1	361.228667	2.35E+06	5.00E+06	1.09	0.00081	$C_{18}H_{35}O_4N_1S_1$
362.237074	N-palmitoyl taurine C16:0	363.244316	1.51E+07	6.96E+06	-1.12	0.01784	$C_{18}H_{37}O_4N_1S_1$
380.189886	Octadecapentaenoic acid taurine C18:5	381.197369	7.42E+05	3.82E+06	2.36	0.00019	$C_{20}H_{31}O_4N_1S_1$
382.205662	Octadecatetraenoic acid taurine C18:4	383.213018	4.31E+06	1.07E+07	1.32	0.00033	$C_{20}H_{33}O_4N_1S_1$
384.221373	Octadecatrienoic acid taurine C18:3	385.228667	9.54E+06	2.19E+07	1.20	0.00061	$C_{20}H_{35}O_4N_1S_1$
386.237058	N-linoleoyl taurine C18:2	387.244316	5.15E+07	9.03E+07	0.81	0.01137	$C_{20}H_{37}O_4N_1S_1$
388.252679	N-oleoyl taurine C18:1	389.259965	3.14E+07	4.44E+07	0.50	0.04123	$C_{20}H_{39}O_4N_1S_1$
402.268341	Nonadecenoic acid taurine C19:1	403.275615	5.90E+05	6.28E+06	3.41	0.00016	$C_{21}H_{41}O_4N_1S_1$
408.221349	Icosapentaenoic acid taurine C20:5	409.228667	3.40E+06	7.74E+06	1.19	0.00252	$C_{22}H_{35}O_4N_1S_1$
474.362338	Lignoceric acid taurine C24:0	475.369510	1.06E+07	1.83E+07	0.79	0.02749	$C_{26}H_{53}O_4N_1S_1$
Bile acids							
355.264237	Cholandienoic acid	356.271516	2.87E+06	5.92E+06	1.05	0.01991	$C_{24}H_{36}O_2$
377.306117	Cholantriol	378.313378	1.91E+06	4.14E+06	1.11	0.00276	$C_{24}H_{42}O_3$
385.238413	Dioxocholenoic acid	386.245696	2.44E+07	4.60E+07	0.92	0.04123	$C_{24}H_{34}O_4$
391.285381	Deoxycholic acid	392.292644	1.05E+09	2.08E+09	0.99	0.03376	$C_{24}H_{40}O_4$
393.300976	Cholantetrol	394.308293	2.78E+06	7.56E+06	1.44	0.00248	$C_{24}H_{42}O_4$
399.217625	Trioxocholenoic acid	400.224962	5.91E+05	4.11E+06	2.80	0.00081	$C_{24}H_{32}O_5$
405.26465	Ketodeoxycholic acid	406.271910	8.14E+08	4.50E+08	-0.86	0.00427	$C_{24}H_{38}O_5$
407.280277	Cholic acid	408.287559	7.04E+09	3.52E+09	-1.00	0.00109	$C_{24}H_{40}O_5$
367.227582	Oxocholatrienoic acid	368.235132	5.58E+05	2.92E+06	2.39	0.00745	$C_{24}H_{32}O_3$
Bile acids sulfate							
485.221495	Oxocholic acid sulfate	486.228727	7.08E+07	1.44E+08	1.03	0.00705	$C_{24}H_{38}O_8S_1$
487.23714	Sulfocholic acid	488.244376	2.83E+08	9.81E+08	1.79	0.01789	$C_{24}H_{40}O_8S_1$
528.263745	Glycochenodeoxycholate sulfate	529.270924	7.93E+07	1.27E+08	0.68	0.00329	$C_{26}H_{43}O_8N_1S_1$
531.29978	Cyprinolsulfate	532.306973	1.41E+08	2.59E+08	0.88	0.01137	$C_{27}H_{48}O_8S_1$
544.2586	Glycocholate sulfate	545.265839	1.12E+07	2.52E+07	1.16	0.00024	$C_{26}H_{43}O_9N_1S_1$
592.22573	Taurooxocholic acid sulfate	593.232826	8.74E+06	2.16E+07	1.31	0.00145	$C_{26}H_{43}O_{10}N_1S_2$
594.241313	Taurocholic acid sulfate	595.248475	8.69E+07	2.81E+08	1.69	0.00082	$C_{26}H_{45}O_{10}N_1S_2$
363.217693	Urocortisone	364.224962	7.09E+07	2.29E+08	1.69	0.00024	$C_{21}H_{32}O_5$
365.233352	Urocortisol	366.240611	2.79E+08	1.05E+09	1.91	0.00082	$C_{21}H_{34}O_5$
367.158436	Dehydroepiandrosterone sulfate	368.165736	5.65E+06	1.13E+07	1.00	0.00082	$C_{19}H_{28}O_5S_1$
369.174088	Androsterone sulfate	370.181385	6.33E+06	1.15E+07	0.86	0.00252	$C_{19}H_{30}O_5S_1$
383.153383	Dihydroxyandrostenone sulfate	384.160651	9.02E+06	2.04E+07	1.17	0.00045	$C_{19}H_{28}O_6S_1$
441.158906	Cortisol sulfate	442.166130	6.07E+06	8.94E+06	0.56	0.00550	$C_{21}H_{30}O_8S_1$
465.304438	Cholesterol sulfate	466.311664	8.63E+08	1.71E+09	0.99	0.00550	$C_{27}H_{46}O_4S_1$
479.283785	Ketocholesterol sulfate	480.290929	2.41E+07	3.27E+07	0.44	0.02224	$C_{27}H_{44}O_5S_1$
481.299356	Hydroxycholesterol sulfate	482.306579	1.20E+08	1.88E+08	0.65	0.01431	$C_{27}H_{46}O_5S_1$
497.294258	Dihydroxycholesterol sulfate	498.301494	6.85E+07	1.48E+08	1.12	0.00192	$C_{27}H_{46}O_6S_1$
Arachidonic acid metabolites							
299.186352	Tetranor-PGF1alpha	300.193664	5.42E+07	6.78E+07	0.32	0.04123	$C_{16}H_{28}O_5$
303.23296	Arachidonic acid (ETE)	304.240217	1.54E+09	3.34E+09	1.12	0.00898	$C_{20}H_{32}O_2$
309.134358	16-COOH-dinor LTB4	310.141631	1.70E+07	2.23E+07	0.39	0.00705	$C_{16}H_{22}O_6$
315.181182	Hydroxy-tetranor-PGF1alpha	316.188579	2.10E+07	3.08E+07	0.55	0.00705	$C_{16}H_{28}O_6$
315.196583	15-Deoxy-delta-12,14-PGJ2	316.203834	2.66E+08	7.92E+08	1.57	0.00329	$C_{20}H_{28}O_3$
317.196916	Tetrahydroxyprostanoic acid	318.204228	1.81E+07	4.04E+07	1.16	0.00024	$C_{16}H_{30}O_6$
317.212206	OxoETE	318.219483	1.18E+08	2.95E+08	1.33	0.00329	$C_{20}H_{30}O_3$
319.227852	HydroxyETE	320.235132	4.39E+07	9.41E+07	1.10	0.00192	$C_{20}H_{32}O_3$
323.186366	Dinor-PGD2	324.193664	6.01E+07	9.33E+07	0.64	0.00109	$C_{18}H_{28}O_5$
325.20204	2,3-Dinor-8-iso PGF2alpha	326.209313	7.46E+07	1.16E+08	0.63	0.00061	$C_{18}H_{30}O_5$
327.217687	2,3-Dinor-8-iso PGF1alpha	328.224962	8.92E+07	1.68E+08	0.92	0.00024	$C_{18}H_{32}O_5$
333.207137	12-Keto-LTB4	334.214398	1.37E+08	2.78E+08	1.02	0.00192	$C_{20}H_{30}O_4$
335.222788	LTB4	336.230047	1.14E+08	2.46E+08	1.11	0.00705	$C_{20}H_{32}O_4$
337.238343	5,6-DHET	338.245696	3.15E+07	5.23E+07	0.73	0.01137	$C_{20}H_{34}O_4$
341.197026	2,3-Dinor-6-keto-prostaglandin F1alpha	342.204228	4.61E+07	8.63E+07	0.91	0.00033	$C_{18}H_{30}O_6$
351.217684	OH-LTB4	352.224962	6.92E+08	1.22E+09	0.82	0.00427	$C_{20}H_{32}O_5$
353.233346	Prostaglandin F2alpha	354.240611	9.54E+07	1.58E+08	0.72	0.00898	$C_{20}H_{34}O_5$
355.176252	dinor omega-1-oxo-6-keto-PGF1alpha	356.183494	1.56E+07	3.08E+07	0.98	0.00045	$C_{18}H_{28}O_7$
357.191887	dinor omega-1-hydroxy-6-keto-PGF1alpha	358.199143	2.24E+07	4.33E+07	0.95	0.00109	$C_{18}H_{30}O_7$
365.196962	COOH-LTB4	366.204228	3.65E+08	7.43E+08	1.03	0.00145	$C_{20}H_{30}O_6$
367.212633	6-Keto-PGE1	368.219877	3.55E+08	6.42E+08	0.86	0.00427	$C_{20}H_{32}O_6$
369.228266	6-Keto-PGF1alpha	370.235526	1.16E+08	1.99E+08	0.79	0.00192	$C_{20}H_{34}O_6$
371.171123	COOH-2,3-Dinor-6-keto-prostaglandin F1alpha	372.178409	5.27E+05	7.25E+06	3.78	0.00640	$C_{18}H_{28}O_8$
438.231906	LTE4	439.239231	2.66E+06	7.06E+06	1.41	0.00886	$C_{23}H_{37}O_5N_1S_1$
454.226858	OH-LTE4	455.234146	1.20E+07	2.56E+07	1.09	0.00145	$C_{23}H_{37}O_6N_1S_1$
AAM sulfates							
379.143216	Tetranor-PGF1alpha sulfate	380.150481	1.11E+06	4.83E+06	2.12	0.00029	$C_{16}H_{28}O_8S_1$
395.153386	15-Deoxy-delta-12,14-PGJ2 sulfate	396.160651	1.36E+07	3.74E+07	1.46	0.00024	$C_{20}H_{28}O_6S_1$
397.169059	OxoETE sulfate	398.176300	1.86E+07	6.09E+07	1.71	0.00024	$C_{20}H_{30}O_6S_1$
399.184703	HydroxyETE sulfate	400.191949	1.35E+07	3.49E+07	1.37	0.00024	$C_{20}H_{32}O_6S_1$
403.143229	Dinor-PGD2 sulfate	404.150481	5.20E+06	1.06E+07	1.03	0.00033	$C_{18}H_{28}O_8S_1$
405.158873	2,3-Dinor-8-iso PGF2alpha sulfate	406.166130	2.00E+07	5.24E+07	1.39	0.00024	$C_{18}H_{30}O_8S_1$
407.174515	2,3-Dinor-8-iso PGF1alpha sulfate	408.181779	8.14E+07	2.31E+08	1.51	0.00024	$C_{18}H_{32}O_8S_1$
413.163936	12-Keto-LTB4 sulfate	414.171215	2.85E+07	6.86E+07	1.27	0.00024	$C_{20}H_{30}O_7S_1$
415.179608	LTB4 sulfate	416.186864	3.09E+07	8.15E+07	1.40	0.00024	$C_{20}H_{32}O_7S_1$
421.153777	2,3-Dinor-6-keto-prostaglandin F1alpha sulfate	422.161045	7.73E+06	2.14E+07	1.47	0.00024	$C_{18}H_{30}O_9S_1$
431.174538	OH-LTB4 sulfate	432.181779	2.65E+07	8.53E+07	1.68	0.00024	$C_{20}H_{32}O_8S_1$
433.190235	Prostaglandin F2alpha sulfate	434.197428	1.36E+07	2.65E+07	0.97	0.00082	$C_{20}H_{34}O_8S_1$
437.148675	dinor omega-1-hydroxy-6-keto-PGF1alpha sulfate	438.155960	2.13E+06	6.54E+06	1.62	0.00023	$C_{18}H_{30}O_{10}S_1$
445.153793	COOH-LTB4 sulfate	446.161045	1.09E+07	2.91E+07	1.42	0.00024	$C_{20}H_{30}O_9S_1$
447.169453	6-Keto-PGE1 sulfate	448.176694	1.48E+07	4.21E+07	1.50	0.00024	$C_{20}H_{32}O_9S_1$
449.185157	6-Keto-PGF1alpha sulfate	450.192343	1.18E+07	2.80E+07	1.25	0.00024	$C_{20}H_{34}O_9S_1$
AAM taurines							
410.236997	N-arachidonoyl taurine	411.244316	9.65E+06	1.59E+07	0.72	0.03376	$C_{22}H_{37}O_4N_1S_1$
426.231955	HydroxyETE taurine	427.239231	9.35E+06	1.53E+07	0.71	0.01789	$C_{22}H_{37}O_5N_1S_1$
440.211265	12-Keto-LTB4 taurine	441.218497	2.23E+07	4.99E+07	1.16	0.00033	$C_{22}H_{35}O_6N_1S_1$
442.226906	Leukotriene B4 taurine	443.234146	4.54E+07	9.24E+07	1.03	0.00082	$C_{22}H_{37}O_6N_1S_1$
444.169713	18-COOH-dinor-LTB4 taurine	445.177029	1.13E+07	2.75E+07	1.29	0.00061	$C_{20}H_{31}O_8N_1S_1$
458.221817	OH-LTB4 taurine	459.229061	2.51E+07	4.79E+07	0.93	0.00427	$C_{22}H_{37}O_7N_1S_1$
460.237467	Prostaglandin F2alpha taurine	461.244710	4.40E+07	8.64E+07	0.97	0.00427	$C_{22}H_{39}O_7N_1S_1$
472.201017	COOH-LTB4 taurine	473.208327	1.51E+07	2.86E+07	0.92	0.02722	$C_{22}H_{35}O_8N_1S_1$
Oxylipins sulfates							
357.174122	Sulfolinonelic acid	358.181385	3.91E+07	1.65E+08	2.07	0.00033	$C_{18}H_{30}O_5S_1$
359.189773	Sulfolinoleic acid	360.197034	2.45E+09	8.89E+09	1.86	0.00024	$C_{18}H_{32}O_5S_1$
361.2054	(9Z)-Octadecenoic acid sulfate	362.212683	1.01E+07	3.05E+07	1.60	0.00024	$C_{18}H_{34}O_5S_1$
373.169038	Hydroxylinolenic acid sulfate	374.176300	3.56E+07	1.14E+08	1.68	0.00024	$C_{18}H_{30}O_6S_1$
373.20543	Nonadecadienoic acid sulfate	374.212683	3.20E+08	1.30E+09	2.02	0.01789	$C_{19}H_{34}O_5S_1$
375.184712	Hydroxylinoleic acid sulfate	376.191949	1.12E+08	2.76E+08	1.30	0.00145	$C_{18}H_{32}O_6S_1$

387.221075	Icosadienoic acid sulfate	388.228333	7.56E+06	1.32E+07	0.80	0.00427	$C_{20}H_{36}O_5S_1$
391.179603	Dihydroxylinoleic acid sulfate	392.186864	8.50E+07	2.41E+08	1.50	0.00024	$C_{18}H_{32}O_7S_1$
393.195257	Dihydroxyoleic acid sulfate	394.202513	7.98E+07	2.17E+08	1.44	0.00024	$C_{18}H_{34}O_7S_1$
Oxylipins taurines							
400.216337	Hydroxylinolenic acid taurine	401.223582	1.50E+08	8.12E+07	-0.88	0.02749	$C_{20}H_{35}O_5N_1S_1$
402.231992	Hydroxylinoleic acid taurine	403.239231	1.97E+08	1.11E+08	-0.82	0.02749	$C_{20}H_{37}O_5N_1S_1$
404.24763	Hydroxyoleic acid taurine	405.254880	2.19E+07	5.02E+07	1.20	0.00192	$C_{20}H_{39}O_5N_1S_1$
420.242555	Dihydroxystearic acid taurine	421.249795	2.04E+07	4.87E+07	1.26	0.00061	$C_{20}H_{39}O_6N_1S_1$
446.258188	Dihydroxyeicosadienic acid taurine	447.265445	1.63E+08	5.26E+08	1.69	0.00033	$C_{22}H_{41}O_6N_1S_1$
448.273855	Dihydroxyeicosanoic acid taurine	449.281094	7.72E+07	3.41E+08	2.14	0.00024	$C_{22}H_{43}O_6N_1S_1$

6.1.2.1 Fatty acids conjugated with taurine or other amino acids in four different gastrointestinal matrices between *db/db* and *wt* mice

Table 17 N-acyltaurines and other fatty acids with amino acids

Mass (avg.)	Compound Name	Monoisotopic mass	p-value (CECUM) db/db vs. wt	p-value (MIDDLE) db/db vs. wt	p-value (DISTAL) db/db vs. wt	p-value (FECES) db/db vs. wt	Molecular Formula
N-acyltaurines							
388.252679	N-oleoyl taurine C18:1	389.25998	n.s.	0.00769	0.01291	0.04123	$C_{20}H_{39}O_4N_1S_1$
410.236997	N-arachidonoyl taurine	411.24433	n.s.	0.03261	0.00655	0.03376	$C_{22}H_{37}O_4N_1S_1$
Other Fatty acids with amino acids							
354.301372	N-palmitoyl valine	355.308644	n.s.	n.s.	0.00020	0.01137	$C_{21}H_{41}O_3N_1$
368.317013	N-palmitoyl (iso)leucine	369.324294	n.s.	n.s.	0.00034	n.s.	$C_{22}H_{43}O_3N_1$
394.332688	N-oleoyl (iso)leucine	395.339944	n.s.	n.s.	0.00050	n.s.	$C_{24}H_{45}O_3N_1$

6.1.3 Plasma metabolome between *db/db* and *wt* mice

Table 18 Plasma metabolites differed significantly between db/db and wt mice

Mass (avg.)	Compound Name	Monoisotopic mass	MEAN wt	MEAN db/db	Log2 fold change db/db vs. wt	p-value	Molecular Formula
180.066558	L-Tyrosine	181.073834	1.78E+06	2.06E+05	8.64	0.01663	$C_9H_{11}NO_3$
203.082534	L-Tryptophan	204.08981	4.44E+06	1.89E+06	2.35	0.02050	$C_{11}H_{12}N_2O_2$
145.061808	L-Glutamine	146.069084	4.03E+06	2.73E+06	1.48	0.04095	$C_5H_{10}N_2O_3$
377.269628	2-Arachidonoylglycerol	378.276904	2.71E+06	6.92E+05	3.91	0.01376	$C_{23}H_{38}O_4$
328.045184	3',5'-Cyclic AMP	329.05246	6.61E+06	8.60E+06	0.77	0.01556	$C_{10}H_{12}N_5O_6P$
361.202114	Cortisol	362.20939	2.04E+07	4.75E+05	4.87	0.00007	$C_{21}H_{30}O_5$
435.348053	Tetrahydroxycholestane	436.355329	6.57E+06	2.62E+06	2.50	0.00147	$C_{27}H_{48}O_4$
514.284765	Taurocholate	515.292041	1.50E+08	2.81E+07	5.33	0.00029	$C_{26}H_{45}NO_7S$
251.078572	Deoxyinosine	252.085848	1.21E+07	6.43E+06	1.88	0.01556	$C_{10}H_{12}N_4O_4$
231.113862	Melatonin	232.121138	1.63E+08	8.70E+07	1.87	0.00115	$C_{13}H_{16}N_2O_2$
353.233413	Prostaglandin F2alpha	354.240689	3.36E+06	1.99E+06	1.69	0.03692	$C_{20}H_{34}O_5$
277.111481	Methylthioheptylmalic acid	278.118757	6.54E+06	2.63E+06	2.49	0.00088	$C_{12}H_{22}O_5S$
367.096954	Indolylmethyl-desulfoglucosinolate	368.10423	8.28E+06	4.45E+06	1.86	0.01911	$C_{16}H_{20}N_2O_6S$
207.07745	Formyl-5-hydroxykynurenamine	208.084726	6.26E+06	4.80E+06	1.30	0.03429	$C_{10}H_{12}N_2O_3$
217.098215	N-Acetylserotonin	218.105491	5.50E+07	3.12E+07	1.77	0.00407	$C_{12}H_{14}N_2O_2$
475.197557	2-Methoxyestrone 3-glucuronide	476.204833	4.96E+06	6.57E+05	7.54	0.01031	$C_{25}H_{32}O_9$
333.091319	Penicillin G	334.098595	7.99E+06	5.16E+06	1.55	0.00516	$C_{16}H_{18}N_2O_4S$
391.285568	Deoxycholic acid	392.292844	5.95E+06	3.16E+06	1.88	0.00319	$C_{24}H_{40}O_4$
369.228546	6-Keto-prostaglandin F1alpha	370.235822	2.99E+06	1.50E+06	1.99	0.03703	$C_{20}H_{34}O_6$
311.22278	Hydroxyoleic acid	312.230056	1.47E+07	1.03E+07	1.43	0.04937	$C_{18}H_{32}O_4$
305.248531	Eicosatrienoic acid C20:3	306.255807	2.14E+07	9.90E+06	2.16	0.01261	$C_{20}H_{34}O_2$
323.186444	Dinor-PGD2	324.193664	4.13E+06	1.74E+06	2.38	0.03057	$C_{18}H_{28}O_5$
356.190195	Hexadecatrienoic acid taurine C16:3	357.197369	2.18E+06	1.00E+06	2.18	0.01300	$C_{18}H_{31}O_4N_1S_1$
357.192006	dinor omega-1-hydroxy-6-keto-PGF1alpha	358.199143	6.22E+06	4.93E+06	1.26	0.00815	$C_{18}H_{30}O_7$
359.189711	Sulfolinoleic acid	360.197034	7.38E+07	4.71E+07	1.57	0.04937	$C_{18}H_{32}O_5S_1$
375.184689	Hydroxylinoleic acid sulfate	376.191949	1.97E+07	5.88E+06	3.35	0.00150	$C_{18}H_{32}O_6S_1$
388.252812	N-oleoyl taurine C18:1	389.259965	2.19E+06	4.87E+05	4.51	0.03292	$C_{20}H_{39}O_4N_1S_1$
465.304421	Cholesterol sulfate	466.311664	1.13E+09	5.52E+08	2.04	0.04125	$C_{27}H_{46}O_4S_1$

6.1.4 Fecal meta-metabolome analysis based on (-) UPLC-TOF-MS analysis

Table 19 Fecal metabolites differed significantly between db/db and wt mice of (-) UPLC-TOF-MS analysis

Mass (avg.)	Retention time in min.	Metabolite name	Monoisotopic mass	MEAN wt	MEAN db/db	p-value	Molecular Formula
243.04456	2.13	Kynuramine sulfate	244.051775	1.86E+03	2.06E+04	0.00327	$C_9H_{12}N_2O_4S$
365.19691	8.11	COOH-LTB4	366.204228	0.00E+00	6.87E+03	0.00466	$C_{20}H_{30}O_6$
351.21742	10.26	OH-LTB4	352.224962	2.93E+02	6.11E+03	0.00325	$C_{20}H_{32}O_5$
367.21192	10.80	6-Keto-PGE1	368.219877	0.00E+00	3.89E+03	0.00466	$C_{20}H_{32}O_6$
431.17442	10.82	OH-LTB4 sulfate	432.181779	0.00E+00	3.06E+03	0.02451	$C_{20}H_{32}O_8S_1$
413.16373	11.21	12-Keto-LTB4 sulfate	414.171215	0.00E+00	3.25E+03	0.01109	$C_{20}H_{30}O_7S_1$
415.17915	11.24	LTB4 sulfate	416.186864	0.00E+00	4.37E+03	0.00466	$C_{20}H_{32}O_7S_1$
407.17465	12.18	2,3-Dinor-8-iso PGF1alpha sulfate	408.181779	3.51E+02	6.99E+03	0.00325	$C_{18}H_{32}O_8S_1$
365.23318	12.26	Urocortisol	366.240611	4.48E+03	6.76E+04	0.00072	$C_{21}H_{34}O_5$
594.24069	12.44	Taurocholic acid sulfate	595.248475	6.91E+03	1.45E+03	0.01038	$C_{26}H_{45}O_{10}N_1S_2$
391.17894	12.44	Dihydroxylinoleic acid sulfate	392.186864	3.42E+03	1.50E+04	0.00922	$C_{18}H_{32}O_7S_1$
397.16894	12.58	OxoETE sulfate	398.176300	5.44E+02	1.14E+04	0.00029	$C_{20}H_{30}O_6S_1$
393.19433	12.61	Dihydroxyoleic acid sulfate	394.202513	2.80E+04	8.06E+04	0.00994	$C_{18}H_{34}O_7S_1$
363.21751	13.00	Urocortisone	364.224962	4.92E+02	1.61E+04	0.00096	$C_{21}H_{32}O_5$
375.18461	13.02	Hydroxylinoleic acid sulfate	376.191949	5.04E+03	1.75E+04	0.00873	$C_{18}H_{32}O_6S_1$
395.15345	13.21	15-Deoxy-delta-12,14-PGJ2 sulfate	396.160651	0.00E+00	6.52E+03	0.00466	$C_{20}H_{28}O_6S_1$
373.16908	13.40	Hydroxylinolenic acid sulfate	374.176300	0.00E+00	4.96E+03	0.01109	$C_{18}H_{30}O_6S_1$
440.21096	13.61	12-Keto-LTB4 taurine	441.218497	3.37E+02	9.09E+03	0.00325	$C_{22}H_{35}O_6N_1S_1$
434.22233	14.28	2,3-Dinor-8-iso PGF1alpha taurine	435.229061	9.04E+02	7.03E+03	0.00252	$C_{20}H_{37}O_7N_1S_1$
460.23768	14.45	Prostaglandin F2alpha taurine	461.244710	0.00E+00	2.69E+03	0.01109	$C_{22}H_{39}O_7N_1S_1$
405.26492	14.61	Ketodeoxycholic acid	406.271910	1.82E+04	5.16E+03	0.01194	$C_{24}H_{38}O_5$
333.20737	14.91	12-Keto-LTB4	334.214398	1.39E+03	3.65E+03	0.00538	$C_{20}H_{30}O_4$
335.22284	15.16	LTB4	336.230047	5.13E+02	3.33E+03	0.02818	$C_{20}H_{32}O_4$
402.23226	15.18	Hydroxylinoleic acid taurine	403.239231	3.79E+03	1.53E+04	0.00842	$C_{20}H_{37}O_5N_1S_1$
313.2387	15.19	Dihydroxyoleic acid	314.245696	0.00E+00	3.18E+03	0.00466	$C_{18}H_{34}O_4$
399.18614	15.27	HydroxyETE sulfate	400.191949	0.00E+00	2.02E+03	0.02451	$C_{20}H_{32}O_6S_1$
315.19695	15.33	15-Deoxy-delta-12,14-PGJ2	316.203834	0.00E+00	1.00E+04	0.01109	$C_{20}H_{28}O_3$
359.18939	15.37	Sulfolinoleic acid	360.197034	2.12E+06	7.76E+06	0.03297	$C_{18}H_{32}O_5S_1$
404.24777	15.82	Hydroxyoleic acid taurine	405.254880	1.48E+03	1.18E+04	0.00089	$C_{20}H_{39}O_5N_1S_1$
354.17467	16.01	Hexadecatetraenoic acid taurine C16:4	355.181719	3.19E+02	4.98E+03	0.00974	$C_{18}H_{29}O_4N_1S_1$
356.19052	16.02	Hexadecatrienoic acid taurine C16:3	357.197369	3.22E+02	1.12E+04	0.00440	$C_{18}H_{31}O_4N_1S_1$
373.20543	16.31	Nonadecadienoic acid sulfate	374.212683	7.17E+04	4.58E+05	0.03297	$C_{19}H_{34}O_5S_1$
315.25432	16.34	Dihydroxystearic acid	316.261346	6.03E+03	1.09E+04	0.02633	$C_{18}H_{36}O_4$
385.23872	16.86	Dioxocholenoic acid	386.245696	9.40E+02	4.70E+03	0.00794	$C_{24}H_{34}O_4$
319.22772	16.91	HydroxyETE	320.235132	7.39E+02	3.28E+03	0.03677	$C_{20}H_{32}O_3$
391.28525	16.97	Deoxycholic acid	392.292644	1.80E+05	3.61E+05	0.00997	$C_{24}H_{40}O_4$
446.25832	17.05	Dihydroxyeicosadienic acid taurine	447.265445	3.38E+04	1.36E+05	0.00073	$C_{22}H_{41}O_6N_1S_1$
297.24349	17.06	Hydroxyoleic acid	298.250781	4.94E+04	1.02E+05	0.00588	$C_{18}H_{34}O_3$
420.2428	17.15	Dihydroxystearic acid taurine	421.249795	0.00E+00	4.38E+03	0.00180	$C_{20}H_{39}O_6N_1S_1$
497.29433	17.43	Dihydroxycholesterol sulfate	498.301494	0.00E+00	2.06E+03	0.02451	$C_{27}H_{46}O_6S_1$
448.27412	17.55	Dihydroxyeicosanoic acid taurine	449.281094	1.09E+04	5.85E+04	0.00038	$C_{22}H_{43}O_6N_1S_1$
386.23689	17.57	N-linoleoyl taurine C18:2	387.244316	0.00E+00	9.56E+03	0.00466	$C_{20}H_{37}O_4N_1S_1$
301.21736	18.02	Icosapentanoic acid	302.224568	2.75E+03	9.27E+03	0.01194	$C_{20}H_{30}O_2$
327.23312	18.24	Docosahexaenoic acid	328.240217	7.42E+03	2.75E+04	0.00756	$C_{22}H_{32}O_2$
303.23295	18.29	Arachidonic acid (ETE)	304.240217	3.00E+04	7.05E+04	0.02633	$C_{20}H_{32}O_2$

6.1.5 Cecal and plasma meta-metabolome affected by COMBI treatment

Table 20 Cecal and plasma metabolites differed altered after COMBI treatment of db/db mice

Metabolites	p-value db/db vs. db/db COMBI
CECUM	
15-Deoxy-delta-12,14-PGJ2	0.015564411
OxoETE	0.023342201
Dihydroxyeicosadienic acid taurine	0.003185649
Dihydroxyeicosanoic acid taurine	0.000504076
Octatriacontahexaenoic acid	0.023342201
Tetrahydroxycholestane	0.023342201
N-linoleoyl taurine C18:2	0.001055822
Nonacosatrienoic acid	0.027184041
N-oleoyl taurine C18:1#LMFA08020081	0.038601913
Pentacosadienoic acid	0.015474393
Dihydroxystearic acid taurine	0.008913884
Pentacosatrienoic acid	0.020510329
Hexadecatetraenoic acid taurine C16:4	0.005175295
Hexadecadienoic acid taurine C16:2	0.021543097
LTE4	0.021101058
Nonadecenoic acid taurine C19:1	0.030570457
Hydroxyoxocholestenoate	0.010165202
Plasma	
L-Glutamine	0.005612996
Formyl-5-hydroxykynurenamine	0.049366195
Methylthioheptylmalic acid	0.028365506
dinor omega-1-hydroxy-6-keto-PGF1alpha	0.049366195

6.1.6 Topographical analysis of gastrointestinal luminal meta-metabolome in *wt* mice – correlation analysis

Table 21 Meta-metabolome distribution along the gastrointestinal luminal content of wt mice

Mass (avg.)	Compound Name	Monoisotopic mass	Pearson correlation R2	p-corr	Molecular Formula
Positive Correlation					
280.22837	Unknown	281.23547	0.68	5.8720E-06	$C_{17}H_{31}O_2N_1$
299.13222	Unknown	300.13952	0.67	1.2444E-05	$C_{15}H_{24}O_4S_1$
300.135595	Y	301.14263	0.67	1.1639E-05	$C_{16}H_{19}N_3O_3$
311.222786	Hydroxyoxooleic acid	312.23005	0.69	5.5581E-06	$C_{18}H_{32}O_4$
311.259131	Oxononadecanoic acid	312.26643	0.68	7.3460E-06	$C_{19}H_{36}O_3$
313.238439	Dihydroxyoleic acid	314.24570	0.73	7.6277E-07	$C_{18}H_{34}O_4$
315.254101	Dihydroxystearic acid	316.26135	0.68	6.2652E-06	$C_{18}H_{36}O_4$
354.301372	N-palmitoyl valine	355.30863	0.75	1.8465E-07	$C_{21}H_{41}O_3N_1$
359.181887	Unknown	360.18879	0.67	1.0444E-05	$C_{18}H_{33}O_3S_1P_1$
359.193705	Unknown	360.20087	0.68	7.6907E-06	$C_{15}H_{28}O_6N_4$
360.196956	Unknown	361.20417	0.67	1.1968E-05	$C_{24}H_{27}O_2N_1$
362.237074	N-palmitoyl taurine C16:0	363.24432	0.67	9.2066E-06	$C_{18}H_{37}O_4N_1S_1$
368.317013	N-palmitoyl (iso)leucine	369.32428	0.70	2.3043E-06	$C_{22}H_{43}O_3N_1$
384.221373	Octadecatrienoic acid taurine C18:3	385.22867	0.67	1.2575E-05	$C_{20}H_{35}O_4N_1S_1$
389.200244	Unknown	390.20760	0.67	1.2223E-05	$C_{19}H_{34}O_6S_1$
404.24763	Hydroxyoleic acid taurine	405.25488	0.67	1.0514E-05	$C_{20}H_{39}O_5N_1S_1$
405.195219	Unknown	406.20251	0.67	1.0215E-05	$C_{19}H_{34}O_7S_1$
410.236997	N-arachidonoyl taurine	411.24432	0.67	1.0754E-05	$C_{22}H_{37}O_4N_1S_1$
446.258188	Dihydroxyeicosadienic acid taurine	447.26544	0.68	8.2789E-06	$C_{22}H_{41}O_6N_1S_1$
458.258196	Unknown	459.26544	0.70	2.2976E-06	$C_{23}H_{41}O_6N_1S_1$
486.289508	Unknown	487.29674	0.67	8.7154E-06	$C_{25}H_{45}O_6N_1S_1$
504.299915	Unknown	505.30731	0.67	9.0684E-06	$C_{25}H_{47}O_7N_1S_1$
527.249867	Unknown	528.25705	0.67	1.0845E-05	$C_{26}H_{40}O_{11}$
541.462743	Y	542.46987	0.70	2.3403E-06	$C_{36}H_{62}O_3$
549.452625	Unknown	550.45970	0.67	9.4757E-06	$C_{34}H_{62}O_5$
Negative Correlation					
205.159793	Octylphenol	206.16706	-0.50	1.9859E-03	$C_{14}H_{22}O_1$
211.133959	Oxododecenoic acid	212.14124	-0.46	5.1608E-03	$C_{12}H_{20}O_3$
219.175432	Nonylphenol	220.18271	-0.55	5.7979E-04	$C_{15}H_{24}O_1$
221.049101	Methylthiopropylmalic acid	222.05619	-0.47	4.6128E-03	$C_8H_{14}O_5S$
225.113231	Tuberonic acid	226.12050	-0.46	5.1220E-03	$C_{12}H_{18}O_4$
229.144525	Dodecanedioic acid	230.15180	-0.45	6.4510E-03	$C_{12}H_{22}O_4$
233.15471	Y	234.16197	-0.51	1.8534E-03	$C_{15}H_{22}O_2$
235.133981	Heptyloxybenzoic acid	236.14124	-0.44	7.8455E-03	$C_{14}H_{20}O_3$
236.078433	Aminomethylsulfanyloctanoic acid	237.08572	-0.59	1.6730E-04	$C_9H_{19}O_2N_1S_2$
237.149628	Oxotetradecadienoic acid	238.15689	-0.43	1.0344E-02	$C_{14}H_{22}O_3$
239.165274	Oxotetradecenoic acid	240.17254	-0.49	2.8774E-03	$C_{14}H_{24}O_3$
249.185989	Hexadecatrienoic acid	250.19327	-0.41	1.3451E-02	$C_{16}H_{26}O_2$
252.073361	Unknown	253.08063	-0.53	1.0116E-03	$C_9H_{19}O_2N_1S_2$
261.222369	Dodecylphenol	262.22965	-0.68	7.2283E-06	$C_{18}H_{30}O_1$
265.180903	Hydroxyhexydecatrienoic acid	266.18818	-0.44	8.6148E-03	$C_{16}H_{26}O_3$
277.122765	Pantetheine	278.13002	-0.43	9.4352E-03	$C_{11}H_{22}O_4N_2S_1$
285.222392	Retinol	286.22965	-0.49	2.8741E-03	$C_{20}H_{30}O_1$
351.157761	Unknown	352.16508	-0.46	5.3042E-03	$C_{15}H_{29}O_5P_1$
353.173345	PA(12:0/0:0)	354.18073	-0.48	3.4397E-03	$C_{15}H_{31}O_7P_1$
373.199751	Unknown	374.20694	-0.47	4.0326E-03	$C_{15}H_{35}O_8P_1$
391.082295	Hydroxybenzylkaempferol	392.08960	-0.53	1.0501E-03	$C_{22}H_{16}O_7$
447.200157	Unknown	448.20734	-0.40	1.8275E-02	$C_{17}H_{37}O_{11}P_1$
450.177038	Unknown	451.18422	-0.49	2.5501E-03	$C_{22}H_{29}O_9N_1$
457.220782	Unknown	458.22807	-0.38	2.3932E-02	$C_{19}H_{39}O_{10}P_1$
473.218162	Y	474.22536	-0.55	5.6891E-04	$C_{26}H_{34}O_8$

Y= this mass signal was annotated but metabolite classification was not possible

6.2 Tables of DIO metabolomics study

6.2.1 Analysis of cecal metabolites of C57J and C57N

Table 22 Cecal meta-metabolome changes of C57J and C57N mice after SAFF, LARD and SD diet

Mass (avg.)	Compound Name	Monoisotopic mass	Mean (n=53)	p-value SAFF C57J vs. C57N	p-value LARD C57J vs. C57N	p-value SD C57J vs. C57N	Molecular Formula
377.233338	Y	378.2406114	3.76E+07	0.04095	0.01789	0.00737	$C_{22}H_{34}O_5$
395.243825	Y	396.2511756	3.46E+07	0.01222	0.04123	0.01853	$C_{22}H_{36}O_6$
415.179672	LTB4 sulfate	416.1868642	3.81E+07	0.02956	0.01431	0.04236	$C_{20}H_{32}O_7S_1$
419.243922	Unknown	420.2511756	5.78E+07	0.01012	0.04123	0.02835	$C_{24}H_{36}O_6$
265.253722	Y	266.2609514	3.51E+07	0.03486	0.02742	n.s.	$C_{18}H_{34}O_1$
267.269266	Y	268.2766006	6.10E+07	0.01222	0.03376	n.s.	$C_{18}H_{36}O_1$
281.158092	Unknown	282.1653416	2.90E+07	0.04095	0.00061	n.s.	$C_{16}H_{26}O_5S_1$
295.154935	Y	296.1623654	3.17E+07	0.01012	0.00024	n.s.	$C_{16}H_{24}O_5$
295.300709	Y	296.3078990	4.14E+07	0.01470	0.01137	n.s.	$C_{20}H_{40}O_1$
297.113129	Enterolactone	298.1205028	5.25E+08	0.03486	0.00550	n.s.	$C_{18}H_{18}O_4$
299.201693	Retinoic Acid	300.2089188	4.68E+07	0.00686	0.01137	n.s.	$C_{20}H_{28}O_2$
300.048895	N-Acetyl-D-glucosamine 6-phosphate	301.0562656	2.91E+07	0.02956	0.04087	n.s.	$C_8H_{16}NO_9P$
307.264205	Eicosadienoic acid (C20:2)	308.2715156	3.05E+09	0.01012	0.01137	n.s.	$C_{20}H_{36}O_2$
317.150749	Unknown	318.1579492	3.87E+07	0.03486	0.00427	n.s.	$C_{17}H_{22}O_4N_2$
333.279892	Docosatrienoic acid (C22:3)	334.2871648	2.53E+08	0.00194	0.01431	n.s.	$C_{22}H_{38}O_2$
341.106418	Unknown	342.1137032	7.05E+07	0.04095	0.00045	n.s.	$C_{16}H_{22}O_6S_1$
341.196952	2,3-dinor, 6-keto-PGF1alpha	342.2042280	3.50E+07	0.02956	0.00550	n.s.	$C_{18}H_{30}O_6$
357.101366	Unknown	358.1086182	4.21E+07	0.04791	0.00145	n.s.	$C_{16}H_{22}O_7S_1$
369.228286	6-Keto-prostaglandin F1alpha	370.2355264	6.62E+07	0.04095	0.01789	n.s.	$C_{20}H_{34}O_6$
379.21255	Unknown	380.2198772	3.78E+08	0.04791	0.04123	n.s.	$C_{21}H_{32}O_6$
383.091846	Unknown	384.0991170	3.22E+07	0.01222	0.02224	n.s.	$C_{16}H_{20}O_7N_2S_1$
383.197532	Diphloretoylputrescine	384.2048968	3.02E+07	0.00012	0.00007	n.s.	$C_{22}H_{28}N_2O_4$
383.265283	Unknown	384.2723040	4.20E+07	0.03486	0.03376	n.s.	$C_{18}H_{40}O_8$
411.238829	LysoPC(10:0)	412.2460906	3.50E+07	0.02497	0.01431	n.s.	$C_{22}H_{36}O_7$
426.195457	Unknown	427.2028478	3.54E+07	0.01222	0.01991	n.s.	$C_{21}H_{33}O_6N_1S_1$
427.32166	Y	428.3290274	2.96E+07	0.04791	0.00329	n.s.	$C_{28}H_{44}O_3$
431.352947	Y	432.3603258	7.65E+07	0.04791	0.03376	n.s.	$C_{28}H_{48}O_3$
445.190093	Y	446.1974284	3.20E+07	0.03486	0.00252	n.s.	$C_{21}H_{34}O_8S_1$
489.270523	Unknown	490.2777832	4.00E+07	0.03486	0.00420	n.s.	$C_{24}H_{42}O_{10}$
496.273817	Taurohydroxyoxocholanoic acid	497.2810938	8.02E+07	0.01470	0.00145	n.s.	$C_{26}H_{43}O_6N_1S_1$
498.289477	Taurodeoxycholic acid	499.2967430	3.57E+08	0.00562	0.03376	n.s.	$C_{26}H_{45}O_6N_1S_1$
509.3594	Unknown	510.3668680	3.92E+07	0.03486	0.00427	n.s.	$C_{28}H_{50}O_6N_2$
512.268599	Sulfolithocholylglycine	513.2760088	2.04E+08	0.00686	0.00192	n.s.	$C_{26}H_{43}O_7N_1S_1$
514.284132	Taurocholic acid	515.2916580	3.12E+09	0.00458	0.01789	n.s.	$C_{26}H_{45}O_7N_1S_1$
517.31693	Y	518.3243366	9.85E+07	0.02101	0.03376	n.s.	$C_{30}H_{46}O_7$
530.279358	Taurotetrahydroxycholanoic acid	531.2865730	3.50E+07	0.00632	0.00323	n.s.	$C_{26}H_{45}O_8N_1S_1$
536.266135	Unknown	537.2736398	4.46E+07	0.00686	0.01431	n.s.	$C_{21}H_{48}O_{10}N_1S_1P_1$
586.450686	Unknown	587.4583200	3.74E+07	0.02497	0.02749	n.s.	$C_{33}H_{65}O_5N_1S_1$
588.466295	Unknown	589.4739692	7.87E+08	0.00835	0.00329	n.s.	$C_{33}H_{67}O_5N_1S_1$
589.303054	D-Urobilinogen	590.3104192	6.02E+07	0.01467	0.01431	n.s.	$C_{33}H_{42}N_4O_6$
590.491772	Unknown	591.4991340	5.58E+07	0.01222	0.01789	n.s.	$C_{33}H_{70}O_5N_1P_1$
591.318793	I-Urobilinogen	592.3260684	3.59E+08	0.01222	0.00705	n.s.	$C_{33}H_{44}N_4O_6$
595.349929	L-Urobilinogen	596.3573668	6.13E+07	0.02101	0.00898	n.s.	$C_{33}H_{48}N_4O_6$
602.482356	Unknown	603.4896184	3.22E+08	0.01012	0.00109	n.s.	$C_{34}H_{69}O_5N_1S_1$
616.222806	Y	617.2304568	1.42E+08	0.01315	0.00082	n.s.	$C_{21}H_{48}O_{13}N_1S_2P_1$
616.461176	Unknown	617.4688842	2.09E+08	0.00458	0.00550	n.s.	$C_{34}H_{67}O_6N_1S_1$
616.497532	Unknown	617.5052676	4.69E+07	0.02497	0.00082	n.s.	$C_{35}H_{71}O_5N_1S_1$
630.476822	Unknown	631.4845334	7.08E+07	0.00242	0.00109	n.s.	$C_{35}H_{69}O_6N_1S_1$
632.197143	Unknown	633.2042434	4.06E+07	0.00494	0.00258	n.s.	$C_{24}H_{44}O_{12}N_1S_2P_1$
747.517607	Y	748.5254072	3.50E+07	0.04095	0.03376	n.s.	$C_{40}H_{77}O_{10}P$

Y= this mass signal was annotated but metabolite classification was not possible

6.2.2 Correlation analysis of body weight changes related to cecal meta-metabolome

Table 23 Pearson Correlation results of body weight changes with metabolome data

Mass (avg.)	Compound Name	Monoisotopic mass	Pearson R2	p-corr (n=53)	Molecular Formula
329.142735	Unknown	330.150087	0.75	5.92E-11	$C_{16}H_{26}O_5S_1$
602.482356	Unknown	603.489618	0.73	4.37188E-10	$C_{34}H_{69}O_5N_1S_1$
343.085698	Unknown	344.092969	0.73	5.65872E-10	$C_{15}H_{20}O_7S_1$
344.089025	Unknown	345.096081	0.72	8.52003E-10	$C_{16}H_{15}O_6N_3$
281.13936	Y	282.146716	0.72	1.41677E-09	$C_{15}H_{22}O_5$
417.141022	Unknown	418.148372	0.71	2.0341E-09	$C_{19}H_{30}O_6S_2$
327.127153	Y	328.134437	0.71	2.22861E-09	$C_{16}H_{24}O_5S_1$
339.090795	Unknown	340.098054	0.71	2.3975E-09	$C_{16}H_{20}O_6S_1$
321.127836	Unknown	322.135106	0.71	2.78726E-09	$C_{16}H_{22}O_3N_2S_1$
323.143564	Unknown	324.150755	0.71	2.99459E-09	$C_{16}H_{24}O_3N_2S_1$
351.094193	Unknown	352.101424	0.70	3.82773E-09	$C_{14}H_{24}O_6S_2$
317.124299	Unknown	318.131461	0.69	8.19183E-09	$C_{14}H_{22}O_8$
281.085348	Unknown	282.092575	0.69	8.34154E-09	$C_{14}H_{18}O_4S_1$
341.106418	Unknown	342.113703	0.69	8.47682E-09	$C_{16}H_{22}O_6S_1$
315.090757	Unknown	316.098054	0.69	8.66604E-09	$C_{14}H_{20}O_6S_1$
600.466695	Y	601.473969	0.69	8.78046E-09	$C_{34}H_{67}O_5N_1S_1$
295.100881	Unknown	296.108224	0.69	9.80734E-09	$C_{15}H_{20}O_4S_1$
342.109777	Unknown	343.116815	0.69	1.01012E-08	$C_{17}H_{17}O_5N_3$
357.101366	Unknown	358.108618	0.69	1.14264E-08	$C_{16}H_{22}O_7S_1$
285.116571	Unknown	286.123873	0.69	1.2762E-08	$C_{14}H_{22}O_4S_1$
391.212566	Y	392.219877	0.69	1.29505E-08	$C_{22}H_{32}O_6$
358.104714	Unknown	359.111730	0.68	1.72757E-08	$C_{17}H_{17}O_6N_3$
328.094125	Unknown	329.101166	0.68	1.79804E-08	$C_{16}H_{15}O_5N_3$
383.189695	Unknown	384.197034	0.67	2.64815E-08	$C_{20}H_{32}O_5S_1$
279.123875	Y	280.131067	0.67	2.70688E-08	$C_{15}H_{20}O_5$
343.122051	Unknown	344.129352	0.67	2.91404E-08	$C_{16}H_{24}O_6S_1$
359.116973	Unknown	360.124267	0.67	3.3171E-08	$C_{16}H_{24}O_7S_1$
283.100884	Unknown	284.108224	0.67	3.9353E-08	$C_{14}H_{20}O_4S_1$
199.097566	Y	200.104854	0.67	4.13684E-08	$C_{10}H_{16}O_4$
415.125465	Unknown	416.132723	0.67	4.74356E-08	$C_{19}H_{28}O_6S_2$
315.127029	Unknown	316.134437	0.66	4.88663E-08	$C_{15}H_{24}O_5S_1$
399.184673	Unknown	400.191949	0.66	5.28297E-08	$C_{20}H_{32}O_6S_1$
616.497532	Unknown	617.505268	0.66	5.43362E-08	$C_{35}H_{71}O_5N_1S_1$
331.085578	Unknown	332.092969	0.66	5.63186E-08	$C_{14}H_{20}O_7S_1$
295.154935	Y	296.162365	0.66	6.94802E-08	$C_{16}H_{24}O_5$
325.165794	Unknown	326.172930	0.66	7.38834E-08	$C_{17}H_{26}O_6$
225.113286	Y	226.120503	0.65	9.4271E-08	$C_{12}H_{18}O_4$
277.108224	Y	278.115418	0.65	1.15445E-07	$C_{15}H_{18}O_5$
603.48091	Unknown	604.488890	0.65	1.47086E-07	$C_{38}H_{68}O_3S_1$
385.168988	Unknown	386.176300	0.65	1.49163E-07	$C_{19}H_{30}O_6S_1$
327.093246	Unknown	328.100557	0.65	1.55782E-07	$C_{11}H_{20}O_{11}$
331.166394	Unknown	332.173598	0.64	1.94919E-07	$C_{18}H_{24}O_4N_2$
267.123862	Unknown	268.131067	0.64	2.07945E-07	$C_{14}H_{20}O_5$
317.150749	Unknown	318.157949	0.64	2.25218E-07	$C_{17}H_{22}O_4N_2$
323.295677	Y	324.302814	0.64	2.25939E-07	$C_{21}H_{40}O_2$
327.14479	Y	328.152195	0.64	2.40825E-07	$C_{16}H_{24}O_7$
393.104672	Unknown	394.111989	0.64	2.66539E-07	$C_{16}H_{26}O_7S_2$
223.097564	Y	224.104854	0.64	2.69005E-07	$C_{12}H_{16}O_4$
389.196979	Y	390.204228	0.64	2.76452E-07	$C_{22}H_{30}O_6$
311.186373	Unknown	312.193664	0.64	2.90278E-07	$C_{17}H_{28}O_5$

Y= this mass signal was annotated but metabolite classification was not possible

6.2.3 Cecal meta-metabolome changes between C57J and C57N mice on SAFF diet

Table 24 Metabolites classes affected after SAFF diet in C57J and C57N mice

Compound class	Mass (avg.)	Compound Name	Monoisotopic mass	MEAN SAFF C57J	MEAN SAFF C57N	log2 fold change C57J vs. C57N	p-value	Molecular Formula
C24 Bile acids								
	401.233323	Trixoxocholanoic acid	402.240611	1.65E+07	1.89E+07	-0.20	0.024968	$C_{24}H_{34}O_5$
	421.259526	Trihydroxyoxocholanoic acid	422.266825	2.18E+08	2.62E+08	-0.26	0.004578	$C_{24}H_{38}O_6$
	423.275108	Tetrahydroxycholanoic acid	424.282474	5.43E+08	7.15E+08	-0.40	0.017608	$C_{24}H_{40}O_6$
	375.29046	Lithocholic acid	376.297729	1.49E+09	9.91E+08	0.59	n.s.	$C_{24}H_{40}O_3$
	407.280086	Cholic acid	408.287559	8.58E+09	7.69E+09	0.16	n.s.	$C_{24}H_{40}O_5$
	355.264269	Cholandienoic acid	356.271516	1.14E+07	7.05E+06	0.70	0.029559	$C_{24}H_{36}O_2$
	371.259162	Oxocholenoic acid	372.266431	2.45E+07	1.56E+07	0.66	0.003005	$C_{24}H_{36}O_3$
	373.274756	Oxocholanoic acid	374.282080	9.79E+07	6.65E+07	0.56	n.s.	$C_{24}H_{38}O_3$
	391.285157	Deoxycholic acid	392.292644	1.57E+10	9.36E+09	0.75	0.024968	$C_{24}H_{40}O_4$
Fatty acids								
	435.25176	Lysophosphatidic Acid (18:1)	436.258977	9.42E+06	2.10E+07	-1.16	0.00453	$C_{21}H_{41}O_7P_1$
	269.24867	Margaric acid (C17:0)	270.255866	2.46E+08	2.84E+08	-0.21	0.02274	$C_{17}H_{34}O_2$
	333.279892	Docosatrienoic acid (C22:3)	334.287165	9.55E+07	3.03E+08	-1.66	0.00194	$C_{22}H_{38}O_2$
	335.295584	Docosadienoic acid (C22:2)	336.302814	7.78E+07	1.14E+08	-0.55	0.02101	$C_{22}H_{40}O_2$
	319.227887	Hydroxyarachidonic acid	320.235132	2.68E+07	1.42E+07	0.92	0.00835	$C_{20}H_{32}O_3$
	335.222773	LTB4	336.230047	4.92E+07	2.45E+07	1.01	0.00458	$C_{20}H_{32}O_4$
	299.201693	Retinoic Acid	300.208919	5.40E+07	2.74E+07	0.98	0.00686	$C_{20}H_{28}O_2$
	301.217307	Eicosapentaenoic acid (C20:5)	302.224568	5.46E+07	2.91E+07	0.91	0.01761	$C_{20}H_{30}O_2$
	327.233001	Docosahexanoic acid (C22:6)	328.240217	5.76E+08	1.59E+08	1.86	0.01222	$C_{22}H_{32}O_2$
	307.264205	Eicosadienoic acid (C20:2)	308.271516	2.01E+09	3.69E+09	-0.88	0.01012	$C_{20}H_{36}O_2$
	303.232832	Arachidonic Acid (C20:4)	304.240217	2.96E+09	9.30E+08	1.67	0.01761	$C_{20}H_{32}O_2$
Endocannabinoids								
	350.306468	Anandamide (20:2)	351.313713	2.94E+06	5.72E+06	-0.96	0.03922	$C_{22}H_{41}O_2N_1$
	352.322092	Anandamide (20:1)	353.329362	8.98E+06	1.42E+07	-0.66	0.01761	$C_{22}H_{43}O_2N_1$
	380.353453	Erucicoylethanolamine	381.360660	4.69E+05	1.79E+06	-1.93	0.02121	$C_{24}H_{47}O_2N_1$
	326.306606	Stearoylethanolamine	327.313713	1.24E+07	3.29E+07	-1.41	0.00686	$C_{20}H_{41}NO_2$
	324.290713	N-Oleoylethanolamine	325.298063	5.25E+06	1.31E+07	-1.32	0.02956	$C_{20}H_{39}O_2N_1$
Urobilinoids								
	593.334357	L-Urobilin	594.341718	5.20E+08	9.73E+08	-0.90	0.02497	$C_{33}H_{46}N_4O_6$
	587.287171	D-Urobilin	588.294770	2.69E+06	8.17E+06	-1.61	0.00698	$C_{33}H_{40}N_4O_6$
	595.349929	L-Urobilinogen	596.357367	5.05E+07	9.64E+07	-0.93	0.02101	$C_{33}H_{48}N_4O_6$
	591.318793	I-Urobilinogen	592.326068	2.12E+08	6.32E+08	-1.57	0.01222	$C_{33}H_{44}N_4O_6$
	589.303054	D-Urobilinogen	590.310419	2.04E+07	1.06E+08	-2.38	0.01467	$C_{33}H_{42}N_4O_6$
	583.255677	Bilirubin	584.263472	2.37E+07	2.92E+07	-0.30	n.s.	$C_{33}H_{36}N_4O_6$
Other conjugated C24 Bile acids								
	455.247299	Sulfolithocholic acid	456.254546	1.12E+07	3.14E+06	1.83	0.02649	$C_{24}H_{40}O_6S_1$
	471.24211	Sulfodeoxycholic acid	472.249461	2.61E+08	2.27E+08	0.20	n.s.	$C_{24}H_{40}O_7S_1$
	487.236698	Sulfocholic acid	488.244376	7.03E+09	4.75E+09	0.57	n.s.	$C_{24}H_{40}O_8S_1$
	512.268599	Sulfolithocholylglycine	513.276009	2.02E+08	1.08E+08	0.91	0.00686	$C_{26}H_{43}O_7N_1S_1$
	528.263526	Sulfodeoxycholylglycine	529.270924	3.70E+07	2.11E+07	0.81	0.02959	$C_{26}H_{43}O_8N_1S_1$
	544.258192	Sulfocholylglycine	545.265839	8.95E+06	1.40E+06	2.67	0.00093	$C_{26}H_{43}O_9N_1S_1$
	448.306922	Glycodeoxycholic Acid	449.314107	1.66E+06	1.00E+06	0.73	0.01869	$C_{26}H_{43}O_5N_1$
	464.301993	Glycocholic acid	465.309022	8.09E+06	2.12E+06	1.93	0.03425	$C_{26}H_{43}NO_6$

Table 25 C_{24} and C_{27} conjugated BAs affected in C57J and C57N mice after SAFF diet (taurine and sulfate)

Mass (avg.)	Compound Name	Monoisotopic mass	MEAN SAFF C57J	MEAN SAFF C57N	p-value	Molecular Formula
C_{24} Taurine conjugated Bile acids						
478.263234	Taurooxocholenoic acid	479.270530	5.51E+06	1.04E+06	0.00630	$C_{26}H_{41}O_5N_1S_1$
480.278841	Taurooxocholanoic acid	481.286179	7.49E+06	1.20E+06	0.02422	$C_{26}H_{43}O_5N_1S_1$
482.294473	Taurolithocholic acid	483.301828	1.20E+07	1.78E+06	0.01317	$C_{26}H_{45}O_5N_1S_1$
494.257970	Taurodioxocholanoic acid	495.265445	1.65E+07	4.78E+06	0.00458	$C_{26}H_{41}O_6N_1S_1$
496.273817	Taurohydroxyoxocholanoic acid	497.281094	1.27E+08	3.75E+07	0.01470	$C_{26}H_{43}O_6N_1S_1$
498.289477	Taurodeoxycholic acid	499.296743	5.34E+08	2.25E+08	0.00562	$C_{26}H_{45}O_6N_1S_1$
510.252936	Taurohydroxydioxocholanoic acid	511.260360	1.95E+07	7.31E+06	0.00123	$C_{26}H_{41}O_7N_1S_1$
514.284132	Taurocholic acid	515.291658	3.88E+09	1.10E+09	0.00458	$C_{26}H_{45}O_7N_1S_1$
530.279358	Taurotetrahydroxycholanoic acid	531.286573	5.93E+07	8.37E+06	0.00632	$C_{26}H_{45}O_8N_1S_1$
594.240876	Taurocholic acid 3-sulfate	595.248475	6.92E+07	2.92E+05	0.00671	$C_{26}H_{45}O_{10}N_1S_2$
C_{27} Taurine conjugated Bile acids						
520.309819	Taurodihydrocholestenoic acid	521.317477	2.09E+06	2.91E+05	0.02600	$C_{29}H_{47}O_5N_1S_1$
522.325673	Taurocholestenoic acid	523.333126	5.65E+06	1.16E+06	0.01058	$C_{29}H_{49}O_5N_1S_1$
536.304750	Taurodioxocholestanoic acid	537.312392	8.13E+06	7.68E+05	0.00397	$C_{29}H_{47}O_6N_1S_1$
538.320689	Taurodihydroxycholestenoic acid	539.328041	2.31E+07	3.57E+06	0.00457	$C_{29}H_{49}O_6N_1S_1$
540.336074	Taurodihydroxycholestanoic acid	541.343691	1.58E+07	3.69E+06	0.00457	$C_{29}H_{51}O_6N_1S_1$
552.299690	Taurodihydroxyoxocholestenoic acid	553.307307	1.02E+07	1.54E+06	0.00736	$C_{29}H_{47}O_7N_1S_1$
554.315510	Taurodihydroxycholestenoic acid	555.322956	4.06E+07	4.26E+06	0.00372	$C_{29}H_{49}O_7N_1S_1$
556.330806	Taurotrihydroxycholestanoic acid	557.338606	2.49E+07	3.79E+06	0.02253	$C_{29}H_{51}NO_7S$
570.310363	Taurotetrahydroxycholestenoic acid	571.317871	1.19E+07	1.43E+06	0.00774	$C_{29}H_{49}O_8N_1S_1$
572.326197	Taurotetrahydroxycholestanoic acid	573.333521	6.63E+06	1.33E+06	0.04102	$C_{29}H_{51}O_8N_1S_1$
Sulfates of C_{27} Bile acids						
511.273369	Dihydroxycholestenoic acid sulfate	512.280759	1.06E+08	7.57E+07	0.01761	$C_{27}H_{44}O_7S_1$
527.268213	Dihydroxyoxocholestanoic acid sulfate	528.275674	9.67E+08	6.10E+08	0.02956	$C_{27}H_{44}O_8S_1$

6.2.4 Cecal meta-metabolome analysis based on (-) UPLC-TOF-MS of C57J and C57N mice after SAFF diet

Table 26 Metabolites affected between C57J and C57N mice after SAFF diet derived from (-) UPLC-TOF MS analysis

Mass (avg.)	Retention time in min.	Compound Name	Monoisotopic mass	MEAN SAFF C57J	MEAN SAFF C57N	p-value	Molecular formula
301.14496	10.68	Enterodiol	302.151801	5.95E+03	1.18E+03	0.00060	$C_{18}H_{22}O_4$
383.19834	10.02	Diphloretoylputrescine	384.204897	8.14E+03	4.30E+02	0.00072	$C_{22}H_{28}N_2O_4$
365.23329	12.35	Urocortisol	366.240611	1.18E+04	5.41E+04	0.01758	$C_{21}H_{34}O_5$
333.28036	19.06	Docosatrienoic acid (C22:3)	334.287165	1.94E+03	7.82E+03	0.02951	$C_{22}H_{38}O_2$
538.31997	17.16	Taurodihydroxycholestenoic acid	539.328041	4.99E+03	1.43E+03	0.00556	$C_{29}H_{49}O_6N_1S_1$
299.20193	17.51	Retinoic Acid	300.208919	9.66E+03	3.25E+03	0.00242	$C_{20}H_{28}O_2$
297.11335	11.2	Enterolactone	298.120503	9.00E+04	3.12E+04	0.00458	$C_{18}H_{18}O_4$
591.31919	10.91	I-Urobilinogen	592.326068	9.76E+04	1.93E+05	0.02101	$C_{33}H_{44}N_4O_6$
589.30371	10.75	D-Urobilinogen	590.310419	1.72E+04	5.74E+04	0.01761	$C_{33}H_{42}N_4O_6$
512.26924	12.88	Sulfolithocholylglycine	513.276009	4.54E+04	1.36E+04	0.00562	$C_{26}H_{43}NO_7S$
464.30541	15	Glycocholic acid	465.309022	3.46E+03	7.31E+02	0.01647	$C_{26}H_{43}NO_6$
510.25527	12.58	Taurohydroxydioxocholanoic acid	511.260360	3.68E+03	6.29E+02	0.00339	$C_{26}H_{41}O_7N_1S_1$
530.28011	12.19	Taurotetrahydroxycholanoic acid	531.286573	3.36E+03	1.76E+02	0.00264	$C_{26}H_{45}O_8N_1S_1$
471.24316	16.26	Sulfodeoxycholic acid	472.246091	1.72E+05	1.50E+04	0.00686	$C_{27}H_{36}O_7$
514.28419	12.99	Taurocholic acid	515.291658	2.60E+06	3.71E+05	0.00155	$C_{26}H_{45}NO_7S$
496.27492	14.31	Taurohydroxyoxocholanoic acid	497.281094	1.33E+04	4.29E+03	0.00835	$C_{26}H_{43}O_6N_1S_1$
594.2426	14.15	Taurocholic acid sulfate	595.248475	3.05E+04	1.06E+03	0.01807	$C_{26}H_{45}NO_{10}S_2$

Table 27 Diet specific alterations between SAFF, LARD and SD fed C57J and C57N mice

Mass (avg.)	Compound Name	Monoisotopic mass	Mean (n=53)	ANOVA p-value	Molecular Formula
241.217339	Pentadecanoic acid	242.224568	4.76E+08	7.20640E-03	$C_{15}H_{30}O_2$
255.232971	Palmitic acid	256.2402172	4.11E+09	1.47061E-06	$C_{16}H_{32}O_2$
269.24867	Margaric acid (C17:0)	270.2558664	4.25E+08	2.98441E-06	$C_{17}H_{34}O_2$
281.13936	Unknown	282.1467162	5.73E+08	5.76977E-07	$C_{15}H_{22}O_5$
283.264138	Stearic acid	284.2715156	1.25E+10	3.77708E-09	$C_{18}H_{36}O_2$
297.113129	Enterolactone	298.1205028	5.25E+08	6.08204E-03	$C_{18}H_{18}O_4$
297.279888	Nonadecanoic acid	298.2871648	2.82E+08	1.25164E-03	$C_{19}H_{38}O_2$
309.279791	Icosenoic acid	310.2871648	2.69E+09	1.42644E-03	$C_{20}H_{38}O_2$
311.295613	Icosanoic acid	312.302814	1.24E+09	3.32692E-05	$C_{20}H_{40}O_2$
325.311213	Heneicosanoic acid	326.3184632	3.18E+08	1.59703E-04	$C_{21}H_{42}O_2$
329.248637	Docosapentaenoic acid	330.2558664	6.34E+08	4.84606E-04	$C_{22}H_{34}O_2$
336.327191	Docosenamide	337.3344468	5.62E+08	1.19747E-03	$C_{22}H_{43}O_1N_1$
337.311146	Docosenoic acid	338.3184632	1.33E+09	4.12928E-07	$C_{22}H_{42}O_2$
349.202011	TrihydroxyEPA	350.209313	5.40E+08	7.28204E-03	$C_{20}H_{30}O_5$
351.21769	OH-LTB4	352.2249622	3.84E+08	1.86971E-02	$C_{20}H_{32}O_5$
359.189777	Sulfolinoleic acid	360.1970342	2.42E+08	4.26401E-07	$C_{18}H_{32}O_5S_1$
365.196972	COOH-LTB4	366.204228	2.62E+08	7.31956E-03	$C_{20}H_{30}O_6$
365.233356	Urocortisol	366.2406114	3.96E+08	3.98576E-03	$C_{21}H_{34}O_5$
365.342439	Nervonic acid	366.3497616	4.34E+08	2.19582E-09	$C_{24}H_{46}O_2$
375.29046	Lithocholic acid	376.297729	8.30E+08	1.04025E-06	$C_{24}H_{40}O_3$
381.228178	Unknown	382.2355264	5.82E+08	8.62819E-03	$C_{21}H_{34}O_6$
381.337413	Hydroxytetracosenoic acid	382.3446766	5.06E+08	2.76702E-03	$C_{24}H_{46}O_3$
383.353082	Hydroxytetracosanoic acid	384.3603258	2.41E+08	1.32661E-02	$C_{24}H_{48}O_3$
389.269698	Ketodeoxycholic acid	390.2769948	1.28E+09	5.80113E-03	$C_{24}H_{38}O_4$
391.285157	Deoxycholic acid	392.292644	9.71E+09	9.20414E-04	$C_{24}H_{40}O_4$
421.259526	Trihydroxyoxocholanoic acid	422.2668248	2.39E+08	2.97215E-02	$C_{24}H_{38}O_6$
429.373694	Vitamin E	430.38106	7.57E+08	6.81139E-06	$C_{29}H_{50}O_2$
445.368713	Hydroxyl Vitamin E	446.375975	6.21E+08	2.68407E-08	$C_{29}H_{50}O_3$
455.316581	Unknown	456.3239424	5.17E+08	1.11022E-16	$C_{29}H_{44}O_4$
461.363466	Unknown	462.37089	3.96E+08	8.26725E-10	$C_{29}H_{50}O_4$
465.303966	Cholesterol sulfate	466.3116636	1.13E+10	2.15270E-07	$C_{27}H_{46}O_4S_1$
471.24211	Sulfodeoxycholic acid	472.249461	3.73E+08	3.40338E-04	$C_{24}H_{40}O_7S_1$
471.311515	Unknown	472.3188574	1.11E+09	1.55431E-15	$C_{29}H_{44}O_5$
479.319867	Unknown	480.3273128	3.29E+08	1.88592E-08	$C_{28}H_{48}O_4S_1$
485.221348	Oxocholic acid sulfate	486.2287268	2.48E+09	1.01074E-10	$C_{24}H_{38}O_8S_1$
485.290813	Unknown	486.2981232	2.29E+08	1.55431E-15	$C_{29}H_{42}O_6$
487.233767	Unknown	488.2410056	8.86E+08	1.08287E-09	$C_{27}H_{36}O_8$
487.236698	Sulfocholic acid	488.244376	1.28E+10	1.48034E-09	$C_{24}H_{40}O_8S_1$
493.335481	Unknown	494.342962	3.16E+08	2.55063E-05	$C_{29}H_{50}O_4S_1$
499.306195	Unknown	500.3137724	2.55E+08	<1.110223E-16	$C_{30}H_{44}O_6$
501.32199	Unknown	502.3294216	3.23E+08	1.11022E-15	$C_{30}H_{46}O_6$
527.268213	Dihydroxyoxocholestanoic acid sulfate	528.2756744	7.55E+08	2.56287E-08	$C_{27}H_{44}O_8S_1$
529.28378	Unknown	530.2913236	6.80E+08	1.46337E-06	$C_{27}H_{46}O_8S_1$
531.299656	Cyprinolsulfate	532.3069728	2.48E+08	5.26366E-07	$C_{27}H_{48}O_8S_1$
557.457339	Unknown	558.4647852	2.23E+08	1.94756E-03	$C_{36}H_{62}O_4$
574.4507	Unknown	575.45832	6.91E+08	4.06581E-05	$C_{32}H_{65}O_5N_1S_1$
589.450802	Unknown	590.4579856	3.51E+08	3.53817E-06	$C_{33}H_{66}O_6S_1$
591.318793	I-Urobilinogen	592.3260684	3.59E+08	6.54881E-03	$C_{33}H_{44}N_4O_6$
593.334357	L-Urobilin	594.3417176	5.81E+08	6.43153E-04	$C_{33}H_{46}N_4O_6$
602.482356	Unknown	603.4896184	3.22E+08	5.41655E-03	$C_{34}H_{69}O_5N_1S_1$

6.3 Parameters

6.3.1 FT-ICR-MS conditions

	(-) FT-ICR-MS	(+) FT-ICR-MS
Type 2 Diabetes study		
Flow rate µL/min	2	2
Mass range in Da	122.9-1000	147.4-2000
Time of flight in sec	0.5	0.5
Ion accumulation time in sec	0.3	0.1
Acquired scans	500	300
Capillary voltage in V	4000	3700
Drying gas flow rate in L/min	4	4
Drying gas temperature in °C	180	180
Nebulizer gas flow rate in bar	1	1
Spray shield in V	500	500
Time domain in megaword	2	2
Diet induced obesity in C57J and C57N mice		
Flow rate µL/min	2	2
Mass range in Da	147.4-1000	73.3-1000
Time of flight in µsec	0.5	0.5
Ion accumulation time in msec	0.5	0.5
Acquired scans	450	300
Capillary voltage in V	4000	4000
Drying gas flow rate in L/min	4	4
Drying gas temperature in °C	180	180
Nebulizer gas flow rate in bar	1	1
Spray shield in V	500	500
Time domain in megaword	2	2

6.3.2 (-) TOF-MS conditions

	(-) TOF-MS/MS
All experiments and studies	
Flow rate mL/min	0.2
Mass range in Da	50-1200
Spectrum rate in Hz	5
Capillary voltage in V	4000
Drying gas flow rate in L/min	8
Drying gas temperature in °C	200
Nebulizer gas flow rate in bar	2
Spray shield in V	500

6.3.3 Chemicals

Used chemicals	
Methanol	CHROMASOLV® LC-MS, Sigma-Aldrich, St.Louis, USA
Acetonitrile	CHROMASOLV® LC-MS, Sigma-Aldrich, St.Louis, USA
Water	CHROMASOLV® LC-MS, Sigma-Aldrich, ST.Louis, USA
Acetone	CHROMASOLV® LC-MS, Sigma-Aldrich, ST.Louis, USA
Formic acid	Formic acid 99% ULC/MS, Biosolve BV, Valkenswaard, Netherlands
Ammonium fluoride	≥98.0% purity, Sigma-Aldrich, St.Louis, USA
Ammonium acetate	Ammonium acetate ULC/MS, Biosolve BV, Valkenswaard, Netherlands
L-Arginine	>98% purity, Sigma-Aldrich, St.Louis, USA

Chapter VII

7 Literature

Abrahamsson, T. R., H. E. Jakobsson, A. F. Andersson, B. Bjorksten, L. Engstrand and M. C. Jenmalm (2012). "Low diversity of the gut microbiota in infants with atopic eczema." Journal of Allergy and Clinical Immunology **129**(2): 434-U244.

Al-Waiz, M., M. Mikov, S. C. Mitchell and R. L. Smith (1992). "The exogenous origin of trimethylamine in the mouse." Metabolism **41**(2): 135-136.

Alberti, K. G. M. M. and P. Z. Zimmet (1998). "Definition, diagnosis and classification of diabetes mellitus and its complications. Part 1: diagnosis and classification of diabetes mellitus. Provisional report of a WHO Consultation." Diabetic Medicine **15**(7): 539-553.

Alnouti, Y. (2009). "Bile Acid Sulfation: A Pathway of Bile Acid Elimination and Detoxification." Toxicological Sciences **108**(2): 225-246.

Altmaier, E., S. L. Ramsay, A. Graber, H.-W. Mewes, K. M. Weinberger and K. Suhre (2008). "Bioinformatics Analysis of Targeted Metabolomics—Uncovering Old and New Tales of Diabetic Mice under Medication." Endocrinology **149**(7): 3478-3489.

Antunes, L. C. M., J. Han, R. B. R. Ferreira, P. Lolić, C. H. Borchers and B. B. Finlay (2011). "Effect of antibiotic treatment on the intestinal metabolome." Antimicrobial agents and chemotherapy **55**: 1494-1503.

Arthur, J. C., E. Perez-Chanona, M. Mühlbauer, S. Tomkovich, J. M. Uronis, T.-J. Fan, B. J. Campbell, T. Abujamel, B. Dogan, A. B. Rogers, J. M. Rhodes, A. Stintzi, K. W. Simpson, J. J. Hansen, T. O. Keku, A. A. Fodor and C. Jobin (2012). "Intestinal Inflammation Targets Cancer-Inducing Activity of the Microbiota." Science **338**(6103): 120-123.

Arumugam, M., J. Raes, E. Pelletier, D. Le Paslier, T. Yamada, D. R. Mende, G. R. Fernandes, J. Tap, T. Bruls, J.-M. Batto, M. Bertalan, N. Borruel, F. Casellas, L. Fernandez, L. Gautier, T. Hansen, M. Hattori, T. Hayashi, M. Kleerebezem, K. Kurokawa, M. Leclerc, F. Levenez, C. Manichanh, H. B. Nielsen, T. Nielsen, N. Pons, J. Poulain, J. Qin, T. Sicheritz-Ponten, S. Tims, D. Torrents, E. Ugarte, E. G. Zoetendal, J. Wang, F. Guarner, O. Pedersen, W. M. de Vos, S. Brunak, J. Dore, J. Weissenbach, S. D. Ehrlich and P. Bork (2011). "Enterotypes of the human gut microbiome." Nature **473**(7346): 174-180.

Atherton, H. J., M. K. Gulston, N. J. Bailey, K. K. Cheng, W. Zhang, K. Clarke and J. L. Griffin (2009). "Metabolomics of the interaction between PPAR-alpha and age in the PPAR-alpha-null mouse." Molecular Systems Biology **5**.

Bäckhed, F., H. Ding, T. Wang, L. V. Hooper, G. Y. Koh, A. Nagy, C. F. Semenkovich and J. I. Gordon (2004). "The gut microbiota as an environmental factor that regulates fat storage." Proceedings of the National Academy of Sciences of the United States of America **101**: 15718-15723.

Bäckhed, F., J. K. Manchester, C. F. Semenkovich and J. I. Gordon (2007). "Mechanisms underlying the resistance to diet-induced obesity in germ-free mice." Proceedings of the National Academy of Sciences **104**(3): 979-984.

Bakke, J. E., J. A. Gustafsson and B. E. Gustafsson (1980). "Metabolism of propachlor by the germ-free rat." Science (Washington D C) **210**(4468): 433-435.

Bao, Y., T. Zhao, X. Wang, Y. Qiu, M. Su, W. Jia and W. Jia (2009). "Metabonomic Variations in the Drug-Treated Type 2 Diabetes Mellitus Patients and Healthy Volunteers." Journal of Proteome Research **8**(4): 1623-1630.

Bastian, M., S. Heymann and M. Jacomy (2009). Gephi: An Open Source Software for Exploring and Manipulating Networks.

Baumert, T., M. Huber, D. Mayer and D. Keppler (1989). "Ethanol-induced inhibition of leukotriene degradation by ω-oxidation." European Journal of Biochemistry **182**(2): 223-229.

Berer, K., M. Mues, M. Koutrolos, Z. A. Rasbi, M. Boziki, C. Johner, H. Wekerle and G. Krishnamoorthy (2011). "Commensal microbiota and myelin autoantigen cooperate to trigger autoimmune demyelination." Nature **479**(7374): 538-541.

Bergman, E. N. (1990). "Energy contributions of volatile fatty acids from the gastrointestinal tract in various species." Physiological Reviews **70**(2): 567-590.

Bertini, I., A. Calabrò, V. De Carli, C. Luchinat, S. Nepi, B. Porfirio, D. Renzi, E. Saccenti and L. Tenori (2008). "The Metabonomic Signature of Celiac Disease." Journal of Proteome Research **8**(1): 170-177.

Bertram, H. C., L. B. Larsen, X. P. Chen and P. B. Jeppesen (2012). "Impact of High-Fat and High-Carbohydrate Diets on Liver Metabolism Studied in a Rat Model with a Systems Biology Approach." Journal of Agricultural and Food Chemistry **60**(2): 676-684.

Bivona, B. J., S. Park and L. M. Harrison-Bernard (2011). "Glomerular filtration rate determinations in conscious type II diabetic mice." American Journal of Physiology - Renal Physiology **300**(3): F618-F625.

Booth, A. N., M. S. Masri, D. J. Robbins, O. H. Emerson, F. T. Jones and F. DeEds (1960). "Urinary Phenolic Acid Metabolites of Tyrosine." Journal of Biological Chemistry **235**(9): 2649-2652.

Bowey, E., H. Adlercreutz and I. Rowland (2003). "Metabolism of isoflavones and lignans by the gut microflora: a study in germ-free and human flora associated rats." Food and Chemical Toxicology **41**(5): 631-636.

Breitling, R., S. Ritchie, D. Goodenowe, M. L. Stewart and M. P. Barrett (2006). "Ab initio prediction of metabolic networks using Fourier transform mass spectrometry data." Metabolomics **2**(3): 155-164.

Breyer, M. D., E. Böttinger, F. C. Brosius, T. M. Coffman, R. C. Harris, C. W. Heilig, K. Sharma and f. t. AMDCC (2005). "Mouse Models of Diabetic Nephropathy." Journal of the American Society of Nephrology **16**(1): 27-45.

Broadhurst, D. and D. Kell (2006). "Statistical strategies for avoiding false discoveries in metabolomics and related experiments." Metabolomics **2**(4): 171-196.

Brown, S. C., G. Kruppa and J.-L. Dasseux (2005). "Metabolomics applications of FT-ICR mass spectrometry." Mass Spectrometry Reviews **24**(2): 223-231.

Brufau, G., F. Stellaard, K. Prado, V. W. Bloks, E. Jonkers, R. Boverhof, F. Kuipers and E. J. Murphy (2010). "Improved glycemic control with colesevelam treatment in patients with type 2 diabetes is not directly associated with changes in bile acid metabolism." Hepatology **52**(4): 1455-1464.

Calvani, R., A. Miccheli, G. Capuani, A. T. Miccheli, C. Puccetti, M. Delfini, A. Iaconelli, G. Nanni and G. Mingrone (2010). "Gut microbiome-derived metabolites characterize a peculiar obese urinary metabotype." International Journal of Obesity **34**(6): 1095-1098.

Capasso, R. and a. a. Izzo (2008). "Gastrointestinal regulation of food intake: general aspects and focus on anandamide and oleoylethanolamide." Journal of neuroendocrinology **20 Suppl 1**: 39-46.

Capasso, R., I. Matias, B. Lutz, F. Borrelli, F. Capasso, G. Marsicano, N. Mascolo, S. Petrosino, K. Monory, M. Valenti, V. Di Marzo and A. A. Izzo (2005). "Fatty Acid Amide Hydrolase Controls Mouse Intestinal Motility In Vivo." Gastroenterology **129**(3): 941-951.

Caspi, R., T. Altman, K. Dreher, C. A. Fulcher, P. Subhraveti, I. M. Keseler, A. Kothari, M. Krummenacker, M. Latendresse, L. A. Mueller, Q. Ong, S. Paley, A. Pujar, A. G. Shearer, M. Travers, D. Weerasinghe, P. Zhang and P. D. Karp (2012). "The MetaCyc database of metabolic pathways and enzymes and the BioCyc collection of pathway/genome databases." Nucleic Acids Research **40**(D1): D742-D753.

Castellarin, M., R. L. Warren, J. D. Freeman, L. Dreolini, M. Krzywinski, J. Strauss, R. Barnes, P. Watson, E. Allen-Vercoe, R. A. Moore and R. A. Holt (2012). "Fusobacterium nucleatum infection is prevalent in human colorectal carcinoma." Genome Research **22**(2): 299-306.

Chawla, a., J. J. Repa, R. M. Evans and D. J. Mangelsdorf (2001). "Nuclear receptors and lipid physiology: opening the X-files." Science (New York, N.Y.) **294**: 1866-1870.

Choi, S. W., S. K. Lee, E. O. Kim, J. H. Oh, K. S. Yoon, N. Parris, K. B. Hicks and R. A. Moreau (2007). "Antioxidant and Antimelanogenic Activities of Polyamine Conjugates from Corn Bran and Related Hydroxycinnamic Acids." Journal of Agricultural and Food Chemistry **55**(10): 3920-3925.

Christensen, K. L., M. S. Hedemann, H. Jorgensen, J. Stagsted and K. E. B. Knudsen (2012). "Liquid Chromatography-Mass Spectrometry Based Metabolomics Study of Cloned versus Normal Pigs Fed Either Restricted or Ad Libitum High-Energy Diets." Journal of Proteome Research **11**(7): 3573-3580.

Chuang, H.-L., Y.-T. Huang, C.-C. Chiu, C.-D. Liao, F.-L. Hsu, C.-C. Huang and C.-C. Hou (2012). "Metabolomics characterization of energy metabolism reveals glycogen accumulation in gut-microbiota-lacking mice." The Journal of Nutritional Biochemistry **23**(7): 752-758.

Claus, S. P., T. M. Tsang, Y. Wang, O. Cloarec, E. Skordi, F.-P. Martin, S. Rezzi, A. Ross, S. Kochhar, E. Holmes and J. K. Nicholson (2008). "Systemic multicompartmental effects of the gut microbiome on mouse metabolic phenotypes." Molecular systems biology **4**: 219.

Coleman, D. L., E. H. Leiter and N. Applezweig (1984). "Therapeutic Effects of Dehydroepiandrosterone Metabolites in Diabetes Mutant Mice (C57BL/KsJ-db/db)." Endocrinology **115**(1): 239-243.

Connor, S. C., M. K. Hansen, A. Corner, R. F. Smith and T. E. Ryan (2010). "Integration of metabolomics and transcriptomics data to aid biomarker discovery in type 2 diabetes." Molecular BioSystems **6**(5): 909-921.

Connor, S. C., W. Wu, B. C. Sweatman, J. Manini, J. N. Haselden, D. J. Crowther and C. J. Waterfield (2004). "Effects of feeding and body weight loss on the 1H-NMR-based urine metabolic profiles of male Wistar Han Rats: Implications for biomarker discovery." Biomarkers **9**(2): 156-179.

Cox, J., S. Williams, K. Grove, R. H. Lane and K. M. Aagaard-Tillery (2009). "A maternal high-fat diet is accompanied by alterations in the fetal primate metabolome." American Journal of Obstetrics and Gynecology **201**(3).

Curtius, H. C., M. Mettler and L. Ettlinger (1976). "Study of the intestinal tyrosine metabolism using stable isotopes and gas chromatography-mass spectrometry." Journal of Chromatography A **126**(0): 569-580.

Daniel, H., A. M. Gholami, D. Berry, C. Desmarchelier, H. Hahne, G. Loh, S. Mondot, P. Lepage, M. Rothballer, A. Walker, C. Bohm, M. Wenning, M. Wagner, M. Blaut, P. Schmitt-Kopplin, B. Kuster, D. Haller and T. Clavel (2013). "High-fat diet alters gut microbiota physiology in mice." ISME J.

Davies, P., P. J. Bailey, M. M. Goldenberg and A. W. Ford-Hutchinson (1984). "The role of arachidonic acid oxygenation products in pain and inflammation." Annu Rev Immunol **2**: 335-357.

Davis, V., D. Schiller, D. Eurich and M. Sawyer (2012). "Urinary metabolomic signature of esophageal cancer and Barrett's esophagus." World Journal of Surgical Oncology **10**(1): 271.

Deo, A. K. and S. M. Bandiera (2008). "Biotransformation of Lithocholic Acid by Rat Hepatic Microsomes : Metabolite Analysis by Liquid Chromatography / Mass Spectrometry." **36**: 442-451.

Devkota, S., Y. Wang, M. W. Musch, V. Leone, H. Fehlner-Peach, A. Nadimpalli, D. A. Antonopoulos, B. Jabri and E. B. Chang (2012). "Dietary-fat-induced taurocholic acid promotes pathobiont expansion and colitis in Il10-/- mice." Nature **advance online publication**.

Di Cagno, R., M. De Angelis, I. De Pasquale, M. Ndagijimana, P. Vernocchi, P. Ricciuti, F. Gagliardi, L. Laghi, C. Crecchio, M. Guerzoni, M. Gobbetti and R. Francavilla (2011). "Duodenal and faecal microbiota of celiac children: molecular, phenotype and metabolome characterization." BMC Microbiology **11**(1): 219.

Dinoto, A., A. Suksomcheep, S. Ishizuka, H. Kimura, S. Hanada, Y. Kamagata, K. Asano, F. Tomita and A. Yokota (2006). "Modulation of Rat Cecal Microbiota by Administration of Raffinose and Encapsulated Bifidobacterium breve." Applied and Environmental Microbiology **72**(1): 784-792.

Duboc, H., S. Rajca, D. Rainteau, D. Benarous, M.-A. Maubert, E. Quervain, G. Thomas, V. Barbu, L. Humbert, G. Despras, C. Bridonneau, F. Dumetz, J.-P. Grill, J. Masliah, L. Beaugerie, J. Cosnes, O. Chazouillères, R. Poupon, C. Wolf, J.-M. Mallet, P. Langella, G. Trugnan, H. Sokol and P. Seksik (2012). "Connecting dysbiosis, bile-acid dysmetabolism and gut inflammation in inflammatory bowel diseases." Gut.

Dumas, M.-E., R. H. Barton, A. Toye, O. Cloarec, C. Blancher, A. Rothwell, J. Fearnside, R. Tatoud, V. Blanc, J. C. Lindon, S. C. Mitchell, E. Holmes, M. I. McCarthy, J. Scott, D. Gauguier and J. K. Nicholson (2006). "Metabolic profiling reveals a contribution of gut microbiota to fatty liver phenotype in insulin-resistant mice." Proceedings of the National Academy of Sciences **103**(33): 12511-12516.

Duncan, S. H., G. E. Lobley, G. Holtrop, J. Ince, A. M. Johnstone, P. Louis and H. J. Flint (2008). "Human colonic microbiota associated with diet, obesity and weight loss." Int J Obes **32**(11): 1720-1724.

Dunn, W. (2013). "Diabetes - the Role of Metabolomics in the Discovery of New Mechanisms and Novel Biomarkers." Current Cardiovascular Risk Reports **7**(1): 25-32.

Eckel, R. H., S. M. Grundy and P. Z. Zimmet "The metabolic syndrome." The Lancet **365**(9468): 1415-1428.

El Aidy, S., C. a. Merrifield, M. Derrien, P. van Baarlen, G. Hooiveld, F. Levenez, J. Doré, J. Dekker, E. Holmes, S. P. Claus, D.-J. Reijngoud and M. Kleerebezem (2012). "The gut microbiota elicits a profound metabolic reorientation in the mouse jejunal mucosa during conventionalisation." Gut: 1-10.

Fahmy, K., C. H. Gray and D. C. Nicholson (1972). "Thin-layer chromatography Spectrophotometry Inocula of organisms The incubation of bile pigments with mixed faecal organisms." **264**: 85-97.

Fearnside, J. F., M.-E. Dumas, A. R. Rothwell, S. P. Wilder, O. Cloarec, A. Toye, C. Blancher, E. Holmes, R. Tatoud, R. H. Barton, J. Scott, J. K. Nicholson and D. Gauguier (2008). "Phylometabonomic Patterns of Adaptation to High Fat Diet Feeding in Inbred Mice." PLoS ONE **3**(2): e1668.

Federico, L., H. Ren, P. a. Mueller, T. Wu, S. Liu, J. Popovic, E. M. Blalock, M. Sunkara, H. Ovaa, H. M. Albers, G. B. Mills, A. J. Morris and S. S. Smyth (2012). "Autotaxin and its product lysophosphatidic acid suppress brown adipose differentiation and promote diet-induced obesity in mice." Molecular endocrinology (Baltimore, Md.) **26**: 786-797.

Fiedler, J., F. R. Simon, M. Iwahashi and R. C. Murphy (2001). "Effect of peroxisome proliferator-activated receptor alpha activation on leukotriene B4 metabolism in isolated rat hepatocytes." The Journal of pharmacology and experimental therapeutics **299**: 691-697.

Fiehn, O. (2002). Metabolomics - the link between genotypes and phenotypes.

Fiehn, O., W. T. Garvey, J. W. Newman, K. H. Lok, C. L. Hoppel and S. H. Adams (2010). "Plasma Metabolomic Profiles Reflective of Glucose Homeostasis in Non-Diabetic and Type 2 Diabetic Obese African-American Women." PLoS ONE **5**(12): e15234.

Fitzpatrick, F. A., R. R. Gorman, J. C. Mc Guire, R. C. Kelly, M. A. Wynalda and F. F. Sun (1977). "A radioimmunoassay for thromboxane B2." Analytical Biochemistry **82**(1): 1-7.

Fitzpatrick, F. A. and M. A. Wynalda (1981). "Albumin-lipid interactions: prostaglandin stability as a probe for characterizing binding sites on vertebrate albumins." Biochemistry **20**(21): 6129-6134.

Floegel, A., N. Stefan, Z. Yu, K. Mühlenbruch, D. Drogan, H.-G. Joost, A. Fritsche, H.-U. Häring, M. Hrabě de Angelis, A. Peters, M. Roden, C. Prehn, R. Wang-Sattler, T. Illig, M. B. Schulze, J. Adamski, H. Boeing and T. Pischon (2013). "Identification of Serum Metabolites Associated With Risk of Type 2 Diabetes Using a Targeted Metabolomic Approach." Diabetes **62**(2): 639-648.

Fonville, J. M., S. E. Richards, R. H. Barton, C. L. Boulange, T. M. D. Ebbels, J. K. Nicholson, E. Holmes and M.-E. Dumas (2010). "The evolution of partial least squares models and related chemometric approaches in metabonomics and metabolic phenotyping." Journal of Chemometrics **24**(11-12): 636-649.

Forcisi, S., F. Moritz, B. Kanawati, D. Tziotis, R. Lehmann and P. Schmitt-Kopplin "Liquid chromatography-mass spectrometry in metabolomics research: Mass analyzers in Ultra High Pressure Liquid Chromatography coupling." Journal of Chromatography A(0).

Friedrich, N. (2012). "Metabolomics in diabetes research." Journal of Endocrinology **215**(1): 29-42.

Fu, J., S. Gaetani, F. Oveisi, J. Lo Verme, A. Serrano, F. Rodríguez De Fonseca, A. Rosengarth, H. Luecke, B. Di Giacomo, G. Tarzia, D. Piomelli and F. Rodriguez de Fonseca (2003). "Oleylethanolamide regulates feeding and body weight through activation of the nuclear receptor PPAR-[alpha]." Nature **425**: 90-93.

Geurts, L., V. Lazarevic, M. Derrien, A. Everard, M. Van Roye, C. Knauf, P. Valet, M. Girard, G. G. Muccioli, P. Francois, W. M. de Vos, J. Schrenzel, N. M. Delzenne and P. D. Cani (2011). "Altered gut microbiota and endocannabinoid system tone in obese and diabetic leptin-resistant mice: impact on apelin regulation in adipose tissue." Frontiers in Microbiology **2**.

Gika, H. G., G. A. Theodoridis and I. D. Wilson (2008). "Hydrophilic interaction and reversed-phase ultra-performance liquid chromatography TOF-MS for metabonomic analysis of Zucker rat urine." Journal of Separation Science **31**(9): 1598-1608.

Gipson, G. T., K. S. Tatsuoka, R. J. Ball, B. A. Sokhansanj, M. K. Hansen, T. E. Ryan, M. P. Hodson, B. C. Sweatman and S. C. Connor (2008). "Multi-platform investigation of the metabolome in a leptin receptor defective murine model of type 2 diabetes." Molecular BioSystems **4**(10): 1015-1023.

Goodwin, B. L., C. R. J. Ruthven and M. Sandler (1994). "Gut flora and the origin of some urinary aromatic phenolic compounds." Biochemical Pharmacology **47**(12): 2294-2297.

Granger, J., R. Plumb, J. Castro-Perez and I. D. Wilson (2005). "Metabonomic studies comparing capillary and conventional HPLC-oa-TOF MS for the analysis of urine from Zucker obese rats." Chromatographia **61**(7-8): 375-380.

Grapov, D., S. H. Adams, T. L. Pedersen, W. T. Garvey and J. W. Newman (2012). "Type 2 Diabetes Associated Changes in the Plasma Non-Esterified Fatty Acids, Oxylipins and Endocannabinoids." PLoS ONE **7**(11): e48852.

Gross, J. H. (2011). Mass Spectrometry, Springer Berlin Heidelberg.

Gustafsson, B. E. and L. S. Lanke (1960). "Bilirubin and urobilins in germfree, ex-germfree and conventional rats." The Journal of Experimental Medicine **112**(6): 975-981.

Hackstadt, A. J. and A. M. Hess (2009). "Filtering for increased power for microarray data analysis." Bmc Bioinformatics **10**.

Hamberg, M., J. Svensson, T. Wakabayashi and B. Samuelsson (1974). "Isolation and Structure of Two Prostaglandin Endoperoxides That Cause Platelet Aggregation." Proceedings of the National Academy of Sciences **71**(2): 345-349.

Harper, T. W., M. J. Garrity and R. C. Murphy (1986). "Metabolism of leukotriene B4 in isolated rat hepatocytes. Identification of a novel 18-carboxy-19,20-dinor leukotriene B4 metabolite." Journal of Biological Chemistry **261**(12): 5414-5418.

Haslam, D. W. and W. P. T. James "Obesity." The Lancet **366**(9492): 1197-1209.

Hatley, M. E., S. Srinivasan, K. B. Reilly, D. T. Bolick and C. C. Hedrick (2003). "Increased Production of 12/15 Lipoxygenase Eicosanoids Accelerates Monocyte/Endothelial Interactions in Diabetic db/db Mice." Journal of Biological Chemistry **278**(28): 25369-25375.

Heeren, R. M. A., A. J. Kleinnijenhuis, L. A. McDonnell and T. H. Mize (2004). "A mini-review of mass spectrometry using high-performance FTICR-MS methods." Analytical and Bioanalytical Chemistry **378**(4): 1048-1058.

Henao-Mejia, J., E. Elinav, C. Jin, L. Hao, W. Z. Mehal, T. Strowig, C. A. Thaiss, A. L. Kau, S. C. Eisenbarth, M. J. Jurczak, J.-P. Camporez, G. I. Shulman, J. I. Gordon, H. M. Hoffman

and R. A. Flavell (2012). "Inflammasome-mediated dysbiosis regulates progression of NAFLD and obesity." Nature **482**(7384): 179-185.

Hildebrand, F., T. L. A. Nguyen, B. Brinkman, R. Yunta, B. Cauwe, P. Vandenabeele, A. Liston and J. Raes (2013). "Inflammation-associated enterotypes, host genotype, cage and inter-individual effects drive gut microbiota variation in common laboratory mice." Genome Biology **14**(1): R4.

Hildebrandt, M. A., C. Hoffmann, S. A. Sherrill-Mix, S. A. Keilbaugh, M. Hamady, Y. Y. Chen, R. Knight, R. S. Ahima, F. Bushman and G. D. Wu (2009). "High-Fat Diet Determines the Composition of the Murine Gut Microbiome Independently of Obesity." Gastroenterology **137**(5): 1716-1724.

Hirayama, A., K. Kami, M. Sugimoto, M. Sugawara, N. Toki, H. Onozuka, T. Kinoshita, N. Saito, A. Ochiai, M. Tomita, H. Esumi and T. Soga (2009). "Quantitative Metabolome Profiling of Colon and Stomach Cancer Microenvironment by Capillary Electrophoresis Time-of-Flight Mass Spectrometry." Cancer Research **69**(11): 4918-4925.

Holmes, E., J. V. Li, T. Athanasiou, H. Ashrafian and J. K. Nicholson (2011). "Understanding the role of gut microbiome–host metabolic signal disruption in health and disease." Trends in Microbiology **19**(7): 349-359.

Holmes, E., I. D. Wilson and J. K. Nicholson (2008). "Metabolic Phenotyping in Health and Disease." Cell **134**(5): 714-717.

Hooper, L. V. and J. I. Gordon (2001). "Commensal Host-Bacterial Relationships in the Gut." Science **292**(5519): 1115-1118.

Huang, Q., P. Yin, J. Wang, J. Chen, H. Kong, X. Lu and G. Xu (2011). "Method for liver tissue metabolic profiling study and its application in type 2 diabetic rats based on ultra performance liquid chromatography–mass spectrometry." Journal of Chromatography B **879**(13–14): 961-967.

Hughey, C. A., C. L. Hendrickson, R. P. Rodgers, A. G. Marshall and K. Qian (2001). "Kendrick Mass Defect Spectrum: A Compact Visual Analysis for Ultrahigh-Resolution Broadband Mass Spectra." Analytical Chemistry **73**(19): 4676-4681.

Ikeda, A., S. Nishiumi, M. Shinohara, T. Yoshie, N. Hatano, T. Okuno, T. Bamba, E. Fukusaki, T. Takenawa, T. Azuma and M. Yoshida (2012). "Serum metabolomics as a novel diagnostic approach for gastrointestinal cancer." Biomedical Chromatography **26**(5): 548-558.

Islam, K. B. M. S., S. Fukiya, M. Hagio, N. Fujii, S. Ishizuka, T. Ooka, Y. Ogura, T. Hayashi and A. Yokota (2011). "Bile Acid Is a Host Factor That Regulates the Composition of the Cecal Microbiota in Rats." Gastroenterology **141**(5): 1773-1781.

Jansson, J., B. Willing, M. Lucio, A. Fekete, J. Dicksved, J. Halfvarson, C. Tysk and P. Schmitt-Kopplin (2009). "Metabolomics Reveals Metabolic Biomarkers of Crohn's Disease." PLoS ONE **4**(7): e6386.

Jedlitschkys, G., A. Volkls, M. Muller, I. Leiers, J. Muller, W.-d. Lehmannz, H. D. Fahimi and D. Kepplers (1991). "Peroxisomal Degradation of Leukotrienes by & Oxidation from." **266**: 24763-24772.

Ji, B., B. Ernest, J. R. Gooding, S. Das, A. M. Saxton, J. Simon, J. Dupont, S. Metayer-Coustard, S. R. Campagna and B. H. Voy (2012). "Transcriptomic and metabolomic profiling of chicken adipose tissue in response to insulin neutralization and fasting." Bmc Genomics **13**.

Jiang, T., X. X. Wang, P. Scherzer, P. Wilson, J. Tallman, H. Takahashi, J. Li, M. Iwahashi, E. Sutherland, L. Arend and M. Levi (2007). "Farnesoid X Receptor Modulates Renal Lipid Metabolism, Fibrosis, and Diabetic Nephropathy." Diabetes **56**(10): 2485-2493.

Jinwook, S. and B. Shneiderman (2002). "Interactively exploring hierarchical clustering results [gene identification]." Computer **35**(7): 80-86.

Johnson, Andrew M. F. and Jerrold M. Olefsky (2013). "The Origins and Drivers of Insulin Resistance." Cell **152**(4): 673-684.

Jones, R. D., J. J. Repa, D. W. Russell, J. M. Dietschy and S. D. Turley (2012). "Delineation of biochemical, molecular, and physiological changes accompanying bile acid pool size restoration in Cyp7a1−/− mice fed low levels of cholic acid." American Journal of Physiology - Gastrointestinal and Liver Physiology **303**(2): G263-G274.

Jubiz, W., O. Rådmark, C. Malmsten, G. Hansson, J. A. Lindgren, J. Palmblad, A. M. Udén and B. Samuelsson (1982). "A novel leukotriene produced by stimulation of leukocytes with formylmethionylleucylphenylalanine." Journal of Biological Chemistry **257**(11): 6106-6110.

Kahn, B. B. and J. S. Flier (2000). "Obesity and insulin resistance." The Journal of Clinical Investigation **106**(4): 473-481.

Kahn, S. E., R. L. Hull and K. M. Utzschneider (2006). "Mechanisms linking obesity to insulin resistance and type 2 diabetes." Nature **444**(7121): 840-846.

Kalhan, S. C., L. Guo, J. Edmison, S. Dasarathy, A. J. McCullough, R. W. Hanson and M. Milburn (2011). "Plasma metabolomic profile in nonalcoholic fatty liver disease." Metabolism **60**(3): 404-413.

Kanehisa, M. and S. Goto (2000). "KEGG: kyoto encyclopedia of genes and genomes." Nucleic acids research **28**: 27-30.

Kau, A. L., P. P. Ahern, N. W. Griffin, A. L. Goodman and J. I. Gordon (2011). "Human nutrition, the gut microbiome and the immune system." Nature **474**(7351): 327-336.

Kim, E. O., K. J. Min, T. K. Kwon, B. H. Um, R. A. Moreau and S. W. Choi (2012). "Anti-inflammatory activity of hydroxycinnamic acid derivatives isolated from corn bran in lipopolysaccharide-stimulated Raw 264.7 macrophages." Food and Chemical Toxicology **50**(5): 1309-1316.

Kim, H.-J., J. H. Kim, S. Noh, H. J. Hur, M. J. Sung, J.-T. Hwang, J. H. Park, H. J. Yang, M.-S. Kim, D. Y. Kwon and S. H. Yoon (2010). "Metabolomic Analysis of Livers and Serum from High-Fat Diet Induced Obese Mice." Journal of Proteome Research **10**(2): 722-731.

Kim, I. Y., J. Jung, M. Jang, Y. G. Ahn, J. H. Shin, J. W. Choi, M. R. Sohn, S. M. Shin, D. G. Kang, H. S. Lee, Y. S. Bae, D. H. Ryu, J. K. Seong and G. S. Hwang (2010). "H-1 NMR-based metabolomic study on resistance to diet-induced obesity in AHNAK knock-out mice." Biochemical and Biophysical Research Communications **403**(3-4): 428-434.

Kim, K.-B., J.-Y. Yang, S. J. Kwack, H. S. Kim, D. H. Ryu, Y.-J. Kim, J. Y. Bae, D. S. Lim, S. M. Choi, M. J. Kwon, D. Y. Bang, S. K. Lim, Y. W. Kim, G.-S. Hwang and B.-M. Lee (2012). "Potential metabolomic biomarkers for evaluation of adriamycin efficacy using a urinary 1H-NMR spectroscopy." Journal of Applied Toxicology: n/a-n/a.

Kim, S.-H., S.-O. Yang, H.-S. Kim, Y. Kim, T. Park and H.-K. Choi (2009). "1H-nuclear magnetic resonance spectroscopy-based metabolic assessment in a rat model of obesity induced by a high-fat diet." Analytical and Bioanalytical Chemistry **395**(4): 1117-1124.

Kindahl, H., L.-E. Edqvist, E. Granström and A. Bane (1976). "The release of prostaglandin F2α as reflected by 15-keto-13,14-dihydroprostaglandin F2α in the peripheral circulation during normal luteolysis in heifers." Prostaglandins **11**(5): 871-878.

Klaassen, C. D. and J. W. Boles (1997). "Sulfation and sulfotransferases 5: the importance of 3'-phosphoadenosine 5'-phosphosulfate (PAPS) in the regulation of sulfation." The FASEB Journal **11**(6): 404-418.

Koren, O., A. Spor, J. Felin, F. Fåk, J. Stombaugh, V. Tremaroli, C. J. Behre, R. Knight, B. Fagerberg, R. E. Ley and F. Bäckhed (2011). "Human oral, gut, and plaque microbiota in patients with atherosclerosis." Proceedings of the National Academy of Sciences **108**(Supplement 1): 4592-4598.

Krey, G., O. Braissant, F. L'Horset, E. Kalkhoven, M. Perroud, M. G. Parker and W. Wahli (1997). "Fatty acids, eicosanoids, and hypolipidemic agents identified as ligands of peroxisome proliferator-activated receptors by coactivator-dependent receptor ligand assay." Molecular endocrinology (Baltimore, Md.) **11**: 779-791.

Krych, L., C. H. F. Hansen, A. K. Hansen, F. W. J. van den Berg and D. S. Nielsen (2013). "Quantitatively Different, yet Qualitatively Alike: A Meta-Analysis of the Mouse Core Gut Microbiome with a View towards the Human Gut Microbiome." PLoS ONE **8**(5): e62578.

Larsen, N., F. K. Vogensen, F. W. J. van den Berg, D. S. Nielsen, A. S. Andreasen, B. K. Pedersen, W. A. Al-Soud, S. J. Sørensen, L. H. Hansen and M. Jakobsen (2010). "Gut Microbiota in Human Adults with Type 2 Diabetes Differs from Non-Diabetic Adults." PLoS ONE **5**(2): e9085.

Lawson, A. M., M. J. Madigan, D. Shortland and P. T. Clayton (1986). "Rapid diagnosis of Zellweger syndrome and infantile Refsum's disease by fast atom bombardment—mass spectrometry of urine bile salts." Clinica Chimica Acta **161**(2): 221-231.

Lee, S. H., J. H. An, H.-M. Park and B. H. Jung (2012). "Investigation of endogenous metabolic changes in the urine of pseudo germ-free rats using a metabolomic approach." Journal of Chromatography B **887–888**(0): 8-18.

Lefebvre, P., B. Cariou, F. Lien, F. Kuipers and B. Staels (2009). "Role of Bile Acids and Bile Acid Receptors in Metabolic Regulation." Physiological Reviews **89**(1): 147-191.

Leiter, E. H., H. D. Chapman and C. N. Falany (1991). "Synergism of Obesity Genes With Hepatic Steroid Sulfotransferases to Mediate Diabetes in Mice." Diabetes **40**(10): 1360-1363.

Ley, R. E., F. Bäckhed, P. Turnbaugh, C. a. Lozupone, R. D. Knight and J. I. Gordon (2005). "Obesity alters gut microbial ecology." Proceedings of the National Academy of Sciences of the United States of America **102**: 11070-11075.

Li, J. V., H. Ashrafian, M. Bueter, J. Kinross, C. Sands, C. W. le Roux, S. R. Bloom, A. Darzi, T. Athanasiou, J. R. Marchesi, J. K. Nicholson and E. Holmes (2011). "Metabolic surgery profoundly influences gut microbial–host metabolic cross-talk." Gut **60**(9): 1214-1223.

Li, L. O., Y.-F. Hu, L. Wang, M. Mitchell, A. Berger and R. A. Coleman (2010). "Early Hepatic Insulin Resistance in Mice: A Metabolomics Analysis." Molecular Endocrinology **24**(3): 657-666.

Li, M. J., X. F. Wang, J. Y. Aa, W. S. Qin, W. B. Zha, Y. C. Ge, L. S. Liu, T. Zheng, B. Cao, J. Shi, C. Y. Zhao, X. W. Wang, X. Y. Yu, G. J. Wang and Z. H. Liu (2013). "GC/TOFMS analysis of metabolites in serum and urine reveals metabolic perturbation of TCA cycle in

db/db mice involved in diabetic nephropathy." American Journal of Physiology-Renal Physiology **304**(11): F1317-F1324.

Li, T., J. M. Francl, S. Boehme, A. Ochoa, Y. Zhang, C. D. Klaassen, S. K. Erickson and J. Y. L. Chiang (2012). "Glucose and insulin induction of bile acid synthesis: mechanisms and implication in diabetes and obesity." The Journal of biological chemistry **287**: 1861-1873.

Li, T., E. Owsley, M. Matozel, P. Hsu, C. M. Novak and J. Y. L. Chiang (2010). "Transgenic expression of cholesterol 7alpha-hydroxylase in the liver prevents high-fat diet-induced obesity and insulin resistance in mice." Hepatology (Baltimore, Md.) **52**: 678-690.

Li, T., E. Owsley, M. Matozel, P. Hsu, C. M. Novak and J. Y. L. Chiang (2010). "Transgenic expression of cholesterol 7α-hydroxylase in the liver prevents high-fat diet–induced obesity and insulin resistance in mice." Hepatology **52**(2): 678-690.

Li, X., Z. Xu, X. Lu, X. Yang, P. Yin, H. Kong, Y. Yu and G. Xu (2009). "Comprehensive two-dimensional gas chromatography/time-of-flight mass spectrometry for metabonomics: Biomarker discovery for diabetes mellitus." Analytica Chimica Acta **633**(2): 257-262.

Libert, R., D. Hermans, J. P. Draye, F. Van Hoof, E. Sokal and E. de Hoffmann (1991). "Bile acids and conjugates identified in metabolic disorders by fast atom bombardment and tandem mass spectrometry." Clinical Chemistry **37**(12): 2102-2110.

Lieberman, L. S. (2003). "DIETARY, EVOLUTIONARY, AND MODERNIZING INFLUENCES ON THE PREVALENCE OF TYPE 2 DIABETES." Annual Review of Nutrition **23**(1): 345-377.

Lin, H.-M., N. A. Helsby, D. D. Rowan and L. R. Ferguson (2011). "Using metabolomic analysis to understand inflammatory bowel diseases." Inflammatory Bowel Diseases **17**(4): 1021-1029.

Lin, S., Z. Yang, H. Liu, L. Tang and Z. Cai (2011). "Beyond glucose: metabolic shifts in responses to the effects of the oral glucose tolerance test and the high-fructose diet in rats." Molecular BioSystems **7**(5): 1537-1548.

Lindeque, J. Z., J. Hidalgo, R. Louw and F. H. van der Westhuizen (2013). "Systemic and organ specific metabolic variation in metallothionein knockout mice challenged with swimming exercise." Metabolomics **9**(2): 418-432.

Lu, J., G. Xie, W. Jia and W. Jia (2013). "Metabolomics in human type 2 diabetes research." Frontiers of Medicine **7**(1): 4-13.

Lucio, M., A. Fekete, C. Weigert, B. Wägele, X. Zhao, J. Chen, A. Fritsche, H.-U. Häring, E. D. Schleicher, G. Xu, P. Schmitt-Kopplin and R. Lehmann (2010). "Insulin Sensitivity Is Reflected by Characteristic Metabolic Fingerprints - A Fourier Transform Mass Spectrometric Non-Targeted Metabolomics Approach." PLoS ONE **5**(10): e13317.

Lupp, C., M. L. Robertson, M. E. Wickham, I. Sekirov, O. L. Champion, E. C. Gaynor and B. B. Finlay (2007). "Host-Mediated Inflammation Disrupts the Intestinal Microbiota and Promotes the Overgrowth of Enterobacteriaceae." Cell host & microbe **2**(2): 119-129.

Ma, B., Q. Zhang, G. J. Wang, J. Y. A, D. Wu, Y. Liu, B. Cao, L. S. Liu, Y. Y. Hu, Y. L. Wang and Y. Y. Zheng (2011). "GC-TOF/MS-based metabolomic profiling of estrogen deficiency-induced obesity in ovariectomized rats." Acta Pharmacologica Sinica **32**(2): 270-278.

MacMillan, D. and R. Murphycor (1995). "Analysis of lipid hydroperoxides and long-chain conjugated keto acids by negative ion electrospray mass spectrometry." Journal of The American Society for Mass Spectrometry **6**(12): 1190-1201.

Major, H. J., R. Williams, A. J. Wilson and I. D. Wilson (2006). "A metabonomic analysis of plasma from Zucker rat strains using gas chromatography/mass spectrometry and pattern recognition." Rapid Communications in Mass Spectrometry **20**(22): 3295-3302.

Makino, I., K. Shinozaki, S. Nakagawa and K. Mashimo (1974). "Measurement of sulfated and nonsulfated bile acids in human serum and urine." Journal of Lipid Research **15**(2): 132-138.

Manichanh, C., L. Rigottier-Gois, E. Bonnaud, K. Gloux, E. Pelletier, L. Frangeul, R. Nalin, C. Jarrin, P. Chardon, P. Marteau, J. Roca and J. Dore (2006). "Reduced diversity of faecal microbiota in Crohn's disease revealed by a metagenomic approach." Gut **55**(2): 205-211.

Marchesi, J. R., E. Holmes, F. Khan, S. Kochhar, P. Scanlan, F. Shanahan, I. D. Wilson and Y. Wang (2007). "Rapid and Noninvasive Metabonomic Characterization of Inflammatory Bowel Disease." Journal of Proteome Research **6**(2): 546-551.

Marcobal, A., P. C. Kashyap, T. A. Nelson, P. A. Aronov, M. S. Donia, A. Spormann, M. A. Fischbach and J. L. Sonnenburg (2013). "A metabolomic view of how the human gut microbiota impacts the host metabolome using humanized and gnotobiotic mice." ISME J.

Mariat, D., O. Firmesse, F. Levenez, V. Guimaraes, H. Sokol, J. Dore, G. Corthier and J.-P. Furet (2009). "The Firmicutes/Bacteroidetes ratio of the human microbiota changes with age." BMC Microbiology **9**(1): 123.

Marshall, A. G. (2000). "Milestones in fourier transform ion cyclotron resonance mass spectrometry technique development." International Journal of Mass Spectrometry **200**(1–3): 331-356.

Marshall, A. G. and P. B. Grosshans (1991). "Fourier transform ion cyclotron resonance mass spectrometry: the teenage years." Analytical Chemistry **63**(4): 215A-229A.

Marshall, A. G., C. L. Hendrickson and G. S. Jackson (1998). "Fourier transform ion cyclotron resonance mass spectrometry: A primer." Mass Spectrometry Reviews **17**(1): 1-35.

Martin, F.-P. J., M.-E. Dumas, Y. Wang, C. Legido-Quigley, I. K. S. Yap, H. Tang, S. Zirah, G. M. Murphy, O. Cloarec, J. C. Lindon, N. Sprenger, L. B. Fay, S. Kochhar, P. van Bladeren, E. Holmes and J. K. Nicholson (2007). "A top-down systems biology view of microbiome-mammalian metabolic interactions in a mouse model." Molecular systems biology **3**: 112.

Martin, F.-P. J., S. Rezzi, I. Montoliu, D. Philippe, L. Tornier, A. Messlik, G. Hölzlwimmer, P. Baur, L. Quintanilla-Fend, G. Loh, M. Blaut, S. Blum, S. Kochhar and D. Haller (2009). "Metabolic Assessment of Gradual Development of Moderate Experimental Colitis in IL-10 Deficient Mice." Journal of Proteome Research **8**(5): 2376-2387.

Martin, F.-P. J., Y. Wang, N. Sprenger, E. Holmes, J. C. Lindon, S. Kochhar and J. K. Nicholson (2007). "Effects of Probiotic Lactobacillus Paracasei Treatment on the Host Gut Tissue Metabolic Profiles Probed via Magic-Angle-Spinning NMR Spectroscopy." Journal of Proteome Research **6**(4): 1471-1481.

Martin, F.-P. J., Y. Wang, I. K. S. Yap, N. Sprenger, J. C. Lindon, S. Rezzi, S. Kochhar, E. Holmes and J. K. Nicholson (2009). "Topographical Variation in Murine Intestinal Metabolic

Profiles in Relation to Microbiome Speciation and Functional Ecological Activity." Journal of Proteome Research **8**(7): 3464-3474.

Martin, F. P. J., Y. Wang, I. K. S. Yap, N. Sprenger, J. C. Lindon, S. Rezzi, S. Kochhar, E. Holmes and J. K. Nicholson (2009). "Topographical Variation in Murine Intestinal Metabolic Profiles in Relation to Microbiome Speciation and Functional Ecological Activity." Journal of Proteome Research **8**(7): 3464-3474.

Matsumoto, K., E. Kurosawa, H. Terui, T. Hosoya, K. Tashima, T. Murayama, J. V. Priestley and S. Horie (2009). "Localization of TRPV1 and contractile effect of capsaicin in mouse large intestine: high abundance and sensitivity in rectum and distal colon." American Journal of Physiology - Gastrointestinal and Liver Physiology **297**(2): G348-G360.

Matsumoto, M., R. Kibe, T. Ooga, Y. Aiba, S. Kurihara, E. Sawaki, Y. Koga and Y. Benno (2012). "Impact of Intestinal Microbiota on Intestinal Luminal Metabolome." Sci. Rep. **2**.

Medini, D., C. Donati, H. Tettelin, V. Masignani and R. Rappuoli (2005). "The microbial pan-genome." Current Opinion in Genetics & Development **15**(6): 589-594.

Meinl, W., S. Sczesny, R. Brigelius-flohe, M. Blaut and H. Glatt (2009). "Impact of Gut Microbiota on Intestinal and Hepatic Levels of Phase 2 Xenobiotic-Metabolizing Enzymes in the Rat." **37**: 1179-1186.

Mekada, K., K. Abe, A. Murakami, S. Nakamura, H. Nakata, K. Moriwaki, Y. Obata and A. Yoshiki (2009). "Genetic Differences among C57BL/6 Substrains." Experimental Animals **58**(2): 141-149.

Messana, I., F. Forni, F. Ferrari, C. Rossi, B. Giardina and C. Zuppi (1998). "Proton nuclear magnetic resonance spectral profiles of urine in type II diabetic patients." Clinical Chemistry **44**(7): 1529-1534.

Mihalik, S. J., B. H. Goodpaster, D. E. Kelley, D. H. Chace, J. Vockley, F. G. S. Toledo and J. P. DeLany (2010). "Increased Levels of Plasma Acylcarnitines in Obesity and Type 2 Diabetes and Identification of a Marker of Glucolipotoxicity." Obesity **18**(9): 1695-1700.

Mihalik, S. J., S. F. Michaliszyn, J. de las Heras, F. Bacha, S. Lee, D. H. Chace, V. R. DeJesus, J. Vockley and S. A. Arslanian (2012). "Metabolomic Profiling of Fatty Acid and Amino Acid Metabolism in Youth With Obesity and Type 2 Diabetes: Evidence for enhanced mitochondrial oxidation." Diabetes Care **35**(3): 605-611.

Moreau, R., A. Nuñez and V. Singh (2001). "Diferuloylputrescine and p-coumaroyl-feruloylputrescine, abundant polyamine conjugates in lipid extracts of maize kernels." Lipids **36**(8): 839-844.

Muccioli, G. G., D. Naslain, F. Bäckhed, C. S. Reigstad, D. M. Lambert, N. M. Delzenne, P. D. Cani and F. Backhed (2010). "The endocannabinoid system links gut microbiota to adipogenesis." Molecular systems biology **6**: 392.

Murdoch, T. B., H. Fu, S. MacFarlane, B. C. Sydora, R. N. Fedorak and C. M. Slupsky (2008). "Urinary Metabolic Profiles of Inflammatory Bowel Disease in Interleukin-10 Gene-Deficient Mice." Analytical Chemistry **80**(14): 5524-5531.

Mutch, D. M., M. Grigorov, A. Berger, L. B. Fay, M. A. Roberts, S. M. Watkins, G. Williamson and J. B. German (2005). "An integrative metabolism approach identifies stearoyl-CoA desaturase as a target for an arachidonate-enriched diet." Faseb Journal **19**(1): 599-+.

Naccache, P. H., T. F. P. Molski, P. Borgeat and R. I. Sha'afi (1984). "Association of leukotriene B4 with the cytoskeleton of rabbit neutrophils, effect of chemotactic factor and phorbol esters." Biochemical and Biophysical Research Communications **124**(3): 963-969.

Narushima, S., K. Itoha, Y. Miyamoto, S.-H. Park, K. Nagata, K. Kuruma and K. Uchida (2006). "Deoxycholic acid formation in gnotobiotic mice associated with human intestinal bacteria." Lipids **41**: 835-843.

Nicholls, A. W., R. J. Mortishire-Smith and J. K. Nicholson (2003). "NMR Spectroscopic-Based Metabonomic Studies of Urinary Metabolite Variation in Acclimatizing Germ-Free Rats." Chemical Research in Toxicology **16**(11): 1395-1404.

Nicholson, A., P. C. Reifsnyder, R. D. Malcolm, C. A. Lucas, G. R. MacGregor, W. Zhang and E. H. Leiter (2010). "Diet-induced Obesity in Two C57BL/6 Substrains With Intact or Mutant Nicotinamide Nucleotide Transhydrogenase (Nnt) Gene." Obesity **18**(10): 1902-1905.

Nicholson, J., E. Holmes and I. Wilson (2005). "Gut microorganisms, mammalian metabolism and personalized health care." Nat Rev Microbiol **3**: 431 - 438.

Nicholson, J. K., E. Holmes, J. Kinross, R. Burcelin, G. Gibson, W. Jia and S. Pettersson (2012). "Host-Gut Microbiota Metabolic Interactions." Science **336**(6086): 1262-1267.

Nicholson, J. K., J. C. Lindon and E. Holmes (1999). "'Metabonomics': understanding the metabolic responses of living systems to pathophysiological stimuli via multivariate statistical analysis of biological NMR spectroscopic data." Xenobiotica **29**(11): 1181-1189.

Nicholson, J. K. and I. D. Wilson (2003). "Understanding 'Global' Systems Biology: Metabonomics and the Continuum of Metabolism." Nat Rev Drug Discov **2**(8): 668-676.

Nobusue, H., D. Kondo, M. Yamamoto and K. Kano (2010). "Effects of lysophosphatidic acid on the in vitro proliferation and differentiation of a novel porcine preadipocyte cell line." Comparative biochemistry and physiology. Part B, Biochemistry & molecular biology **157**: 401-407.

Oberbach, A., M. Bluher, H. Wirth, H. Till, P. Kovacs, Y. Kullnick, N. Schlichting, J. M. Tomm, U. Rolle-Kampczyk, J. Murugaiyan, H. Binder, A. Dietrich and M. von Bergen (2011). "Combined Proteomic and Metabolomic Profiling of Serum Reveals Association of the Complement System with Obesity and Identifies Novel Markers of Body Fat Mass Changes." Journal of Proteome Research **10**(10): 4769-4788.

Ohta, T., N. Masutomi, N. Tsutsui, T. Sakairi, M. Mitchell, M. V. Milburn, J. A. Ryals, K. D. Beebe and L. Guo (2009). "Untargeted Metabolomic Profiling as an Evaluative Tool of Fenofibrate-Induced Toxicology in Fischer 344 Male Rats." Toxicologic Pathology **37**(4): 521-535.

Olgun, A. (2009). "Converting NADH to NAD+ by nicotinamide nucleotide transhydrogenase as a novel strategy against mitochondrial pathologies during aging." Biogerontology **10**(4): 531-534.

Oliver, S. G., M. K. Winson, D. B. Kell and F. Baganz (1998). "Systematic functional analysis of the yeast genome." Trends in Biotechnology **16**(9): 373-378.

Oresic, M., T. Seppanen-Laakso, L. Yetukuri, F. Backhed and V. Hanninen (2009). "Gut microbiota affects lens and retinal lipid composition." Experimental Eye Research **89**(5): 604-607.

Oscar Hammerstein II, R. R. (1945). You'll Never Walk Alone, Carousel Broadway Musical.

Pace-Asciak, C. R., M. C. Carrara and Z. Domazet (1977). "Identification of the major urinary metabolites of 6-ketoprostaglandin F1α (6K-PGF1α) in the rat." Biochemical and Biophysical Research Communications **78**(1): 115-121.

Pan, X.-d., F.-q. Chen, T.-x. Wu, H.-g. Tang and Z.-y. Zhao (2009). "Prebiotic oligosaccharides change the concentrations of short-chain fatty acids and the microbial population of mouse bowel." Journal of Zhejiang University SCIENCE B **10**(4): 258-263.

Patterson, A. D., J. A. Bonzo, F. Li, K. W. Krausz, G. S. Eichler, S. Aslam, X. Tigno, J. N. Weinstein, B. C. Hansen, J. R. Idle and F. J. Gonzalez (2011). "Metabolomics Reveals Attenuation of the SLC6A20 Kidney Transporter in Nonhuman Primate and Mouse Models of Type 2 Diabetes Mellitus." Journal of Biological Chemistry **286**(22): 19511-19522.

Pérez-Cobas, A. E., M. J. Gosalbes, A. Friedrichs, H. Knecht, A. Artacho, K. Eismann, W. Otto, D. Rojo, R. Bargiela, M. von Bergen, S. C. Neulinger, C. Däumer, F.-A. Heinsen, A. Latorre, C. Barbas, J. Seifert, V. M. dos Santos, S. J. Ott, M. Ferrer and A. Moya (2012). "Gut microbiota disturbance during antibiotic therapy: a multi-omic approach." Gut.

Peter, A. T., W. T. K. Bosu and C. W. Luker (1987). "Plasma endotoxin and concentrations of stable metabolites of prostacyclin, thromboxane A2, and prostaglandin E2 in postpartum dairy cows." Prostaglandins **34**(1): 15-24.

Pifer, D. D., L. M. Cagen and C. M. Chesney (1981). "Stability of prostaglandin I2 in human blood." Prostaglandins **21**(2): 165-175.

Plumb, R. S., K. A. Johnson, P. Rainville, J. P. Shockcor, R. Williams, J. H. Granger and I. D. Wilson (2006). "The detection of phenotypic differences in the metabolic plasma profile of three strains of Zucker rats at 20 weeks of age using ultra-performance liquid chromatography/orthogonal acceleration time-of-flight mass spectrometry." Rapid Communications in Mass Spectrometry **20**(19): 2800-2806.

Pluskal, T., S. Castillo, A. Villar-Briones and M. Oresic (2010). "MZmine 2: Modular framework for processing, visualizing, and analyzing mass spectrometry-based molecular profile data." Bmc Bioinformatics **11**.

Ponnusamy, K., J. N. Choi, J. Kim, S.-Y. Lee and C. H. Lee (2011). "Microbial community and metabolomic comparison of irritable bowel syndrome faeces." Journal of Medical Microbiology **60**(6): 817-827.

Popkin, B. M., S. Kim, E. R. Rusev, S. Du and C. Zizza (2006). "Measuring the full economic costs of diet, physical activity and obesity-related chronic diseases." Obesity Reviews **7**(3): 271-293.

Qin, J., R. Li, J. Raes, M. Arumugam, K. S. Burgdorf, C. Manichanh, T. Nielsen, N. Pons, F. Levenez, T. Yamada, D. R. Mende, J. Li, J. Xu, S. Li, D. Li, J. Cao, B. Wang, H. Liang, H. Zheng, Y. Xie, J. Tap, P. Lepage, M. Bertalan, J.-M. Batto, T. Hansen, D. Le Paslier, A. Linneberg, H. B. Nielsen, E. Pelletier, P. Renault, T. Sicheritz-Ponten, K. Turner, H. Zhu, C. Yu, S. Li, M. Jian, Y. Zhou, Y. Li, X. Zhang, S. Li, N. Qin, H. Yang, J. Wang, S. Brunak, J. Dore, F. Guarner, K. Kristiansen, O. Pedersen, J. Parkhill, J. Weissenbach, P. Bork, S. D. Ehrlich and J. Wang (2010). "A human gut microbial gene catalogue established by metagenomic sequencing." Nature **464**(7285): 59-65.

Qiu, Y., G. Cai, M. Su, T. Chen, Y. Liu, Y. Xu, Y. Ni, A. Zhao, S. Cai, L. X. Xu and W. Jia (2010). "Urinary Metabonomic Study on Colorectal Cancer." Journal of Proteome Research **9**(3): 1627-1634.

Rajilić–Stojanović, M., E. Biagi, H. G. H. J. Heilig, K. Kajander, R. A. Kekkonen, S. Tims and W. M. de Vos (2011). "Global and Deep Molecular Analysis of Microbiota Signatures in Fecal Samples From Patients With Irritable Bowel Syndrome." Gastroenterology **141**(5): 1792-1801.

Raman, M., I. Ahmed, P. M. Gillevet, C. S. Probert, N. M. Ratcliffe, S. Smith, R. Greenwood, M. Sikaroodi, V. Lam, P. Crotty, J. Bailey, R. P. Myers and K. P. Rioux (2013). "Fecal Microbiome and Volatile Organic Compound Metabolome in Obese Humans With Nonalcoholic Fatty Liver Disease." Clinical Gastroenterology and Hepatology **11**(7): 868-+.

Reilly, S.-J., E. M. O'Shea, U. Andersson, J. O'Byrne, S. E. H. Alexson and M. C. Hunt (2007). "A peroxisomal acyltransferase in mouse identifies a novel pathway for taurine conjugation of fatty acids." The FASEB Journal **21**(1): 99-107.

Ricciotti, E. and G. A. FitzGerald (2011). "Prostaglandins and Inflammation." Arteriosclerosis, Thrombosis, and Vascular Biology **31**(5): 986-1000.

Ridlon, J. M., D.-J. Kang and P. B. Hylemon (2006). "Bile salt biotransformations by human intestinal bacteria." Journal of Lipid Research **47**(2): 241-259.

Robertson, D. G., P. B. Watkins and M. D. Reily (2011). "Metabolomics in Toxicology: Preclinical and Clinical Applications." Toxicological Sciences **120**(suppl 1): S146-S170.

Rodriguez, L., L. D. Roberts, J. LaRosa, N. Heinz, R. Gerszten, S. Nurko and A. M. Goldstein (2013). "Relationship between postprandial metabolomics and colon motility in children with constipation." Neurogastroenterology & Motility **25**(5): 420-e299.

Rosenkranz, B., C. Fischer, I. Reimann, K. E. Weimer, G. Beck and J. C. Frölich (1980). "Identification of the major metabolite of prostacyclin and 6-ketoprostaglandin F1α in man." Biochimica et Biophysica Acta (BBA) - Lipids and Lipid Metabolism **619**(2): 207-213.

Saadat, N., H. B. Iglay Reger, M. G. Myers, P. Bodary and S. V. Gupta (2012). "Differences in metabolomic profiles of male db/db and s/s, leptin receptor mutant mice." Physiological Genomics **44**(6): 374-381.

Saeed, A. I., V. Sharov, J. White, J. Li, W. Liang, N. Bhagabati, J. Braisted, M. Klapa, T. Currier, M. Thiagarajan, A. Sturn, M. Snuffin, A. Rezantsev, D. Popov, A. Ryltsov, E. Kostukovich, I. Borisovsky, Z. Liu, A. Vinsavich, V. Trush and J. Quackenbush (2003). "TM4: A free, open-source system for microarray data management and analysis." Biotechniques **34**(2): 374-+.

Saghatelian, A., M. K. McKinney, M. Bandell, A. Patapoutian and B. F. Cravatt (2006). "A FAAH-Regulated Class of N-Acyl Taurines That Activates TRP Ion Channels†." Biochemistry **45**(30): 9007-9015.

Saghatelian, A., S. A. Trauger, E. J. Want, E. G. Hawkins, G. Siuzdak and B. F. Cravatt (2004). "Assignment of Endogenous Substrates to Enzymes by Global Metabolite Profiling†." Biochemistry **43**(45): 14332-14339.

Salek, R. M., M. L. Maguire, E. Bentley, D. V. Rubtsov, T. Hough, M. Cheeseman, D. Nunez, B. C. Sweatman, J. N. Haselden, R. D. Cox, S. C. Connor and J. L. Griffin (2007). "A metabolomic comparison of urinary changes in type 2 diabetes in mouse, rat, and human." Physiological Genomics **29**(2): 99-108.

Samad, F., K. D. Hester, G. Yang, Y. A. Hannun and J. Bielawski (2006). "Altered Adipose and Plasma Sphingolipid Metabolism in Obesity: A Potential Mechanism for Cardiovascular and Metabolic Risk." Diabetes **55**(9): 2579-2587.

Samuel, B. S. and J. I. Gordon (2006). "A humanized gnotobiotic mouse model of host–archaeal–bacterial mutualism." Proceedings of the National Academy of Sciences **103**(26): 10011-10016.

Sarda, S., C. Page, K. Pickup, T. Schulz-Utermoehl and I. Wilson (2012). "Diclofenac metabolism in the mouse: Novel in vivo metabolites identified by high performance liquid chromatography coupled to linear ion trap mass spectrometry." Xenobiotica **42**(2): 179-194.

Scanlan, P. D., F. Shanahan, Y. Clune, J. K. Collins, G. C. O'Sullivan, M. O'Riordan, E. Holmes, Y. Wang and J. R. Marchesi (2008). "Culture-independent analysis of the gut microbiota in colorectal cancer and polyposis." Environmental Microbiology **10**(3): 789-798.

Schmitt-Kopplin, P., Z. Gabelica, R. D. Gougeon, A. Fekete, B. Kanawati, M. Harir, I. Gebefuegi, G. Eckel and N. Hertkorn (2010). "High molecular diversity of extraterrestrial organic matter in Murchison meteorite revealed 40 years after its fall." Proceedings of the National Academy of Sciences of the United States of America **107**(7): 2763-2768.

Schmitt-Kopplin, P., A. Gelencsér, E. Dabek-Zlotorzynska, G. Kiss, N. Hertkorn, M. Harir, Y. Hong and I. Gebefügi (2010). "Analysis of the Unresolved Organic Fraction in Atmospheric Aerosols with Ultrahigh-Resolution Mass Spectrometry and Nuclear Magnetic Resonance Spectroscopy: Organosulfates As Photochemical Smog Constituents†." Analytical Chemistry **82**(19): 8017-8026.

Sekirov, I., S. L. Russell, L. C. M. Antunes and B. B. Finlay (2010). "Gut Microbiota in Health and Disease." Physiological Reviews **90**(3): 859-904.

Seo, K. I., M. S. Choi, U. J. Jung, H. J. Kim, J. Yeo, S. M. Jeon and M. K. Lee (2008). "Effect of curcumin supplementation on blood glucose, plasma insulin, and glucose homeostasis related enzyme activities in diabetic db/db mice." Molecular Nutrition & Food Research **52**(9): 995-1004.

Serkova, N. J., M. Jackman, J. L. Brown, T. Liu, R. Hirose, J. P. Roberts, J. J. Maher and C. U. Niemann (2006). "Metabolic profiling of livers and blood from obese Zucker rats." Journal of hepatology **44**(5): 956-962.

Sharma, K., P. McCue and S. R. Dunn (2003). "Diabetic kidney disease in the db/dbmouse." American Journal of Physiology - Renal Physiology **284**(6): F1138-F1144.

Shearer, J., G. Duggan, A. Weljie, D. S. Hittel, D. H. Wasserman and H. J. Vogel (2008). "Metabolomic profiling of dietary-induced insulin resistance in the high fat–fed C57BL/6J mouse." Diabetes, Obesity and Metabolism **10**(10): 950-958.

Shi, X., B. Wahlang, X. L. Wei, X. M. Yin, K. C. Falkner, R. A. Prough, S. H. Kim, E. G. Mueller, C. J. McClain, M. Cave and X. Zhang (2012). "Metabolomic Analysis of the Effects of Polychlorinated Biphenyls in Nonalcoholic Fatty Liver Disease." Journal of Proteome Research **11**(7): 3805-3815.

Shirley, M. A. and R. C. Murphy (1990). "Metabolism of leukotriene B4 in isolated rat hepatocytes. Involvement of 2,4-dienoyl-coenzyme A reductase in leukotriene B4 metabolism." Journal of Biological Chemistry **265**(27): 16288-16295.

Shirley, M. A. and R. C. Murphy (1990). "Metabolism of leukotriene B4 in isolated rat hepatocytes. Involvement of 2,4-dienoyl-coenzyme A reductase in leukotriene B4 metabolism." Journal of Biological Chemistry **265**(27): 16288-16295.

Smith, C. A., G. O. Maille, E. J. Want, C. Qin, S. A. Trauger, T. R. Brandon, D. E. Custodio, R. Abagyan and G. Siuzdak (2005). "METLIN: A Metabolite Mass Spectral Database." Therapeutic Drug Monitoring **27**(6): 747-751.

Snyder, R. and C. C. Hedli (1996). "An overview of benzene metabolism." Environmental Health Perspectives **104**: 1165-1171.

Sommer, F. and F. Backhed (2013). "The gut microbiota - masters of host development and physiology." Nature Reviews Microbiology **11**(4): 227-238.

Sonestedt, E., S. Borgquist, U. Ericson, B. Gullberg, H. Olsson, H. Adlercreutz, G. Landberg and E. Wirfält (2008). "Enterolactone is differently associated with estrogen receptor beta-negative and -positive breast cancer in a Swedish nested case-control study." Cancer epidemiology, biomarkers & prevention : a publication of the American Association for Cancer Research, cosponsored by the American Society of Preventive Oncology **17**: 3241-3251.

Song, X. F., J. S. Wang, P. R. Wang, N. Tian, M. H. Yang and L. Y. Kong (2013). "H-1 NMR-based metabolomics approach to evaluate the effect of Xue-Fu-Zhu-Yu decoction on hyperlipidemia rats induced by high-fat diet." Journal of Pharmaceutical and Biomedical Analysis **78-79**: 202-210.

Spagou, K., G. Theodoridis, I. Wilson, N. Raikos, P. Greaves, R. Edwards, B. Nolan and M. I. Klapa (2011). "A GC-MS metabolic profiling study of plasma samples from mice on low- and high-fat diets." Journal of Chromatography B-Analytical Technologies in the Biomedical and Life Sciences **879**(17-18): 1467-1475.

Stobbe, M. D., S. M. Houten, A. H. C. van Kampen, R. J. A. Wanders and P. D. Moerland (2012). "Improving the description of metabolic networks: the TCA cycle as example." The FASEB Journal **26**(9): 3625-3636.

Sud, M., E. Fahy, D. Cotter, A. Brown, E. A. Dennis, C. K. Glass, A. H. Merrill, R. C. Murphy, C. R. H. Raetz, D. W. Russell and S. Subramaniam (2007). "LMSD: LIPID MAPS structure database." Nucleic Acids Research **35**(suppl 1): D527-D532.

Suhre, K., C. Meisinger, A. Döring, E. Altmaier, P. Belcredi, C. Gieger, D. Chang, M. V. Milburn, W. E. Gall, K. M. Weinberger, H.-W. Mewes, M. Hrabé de Angelis, H. E. Wichmann, F. Kronenberg, J. Adamski and T. Illig (2010). "Metabolic Footprint of Diabetes: A Multiplatform Metabolomics Study in an Epidemiological Setting." PLoS ONE **5**(11): e13953.

Suhre, K. and P. Schmitt-Kopplin (2008). "MassTRIX: mass translator into pathways." Nucleic acids research **36**: W481-484.

Sun, F. F. and B. M. Taylor (1978). "Metabolism of prostacyclin in rat." Biochemistry **17**(19): 4096-4101.

Sun, J. C., L. K. Schnackenberg, S. Khare, X. Yang, J. Greenhaw, W. Salminen, D. L. Mendrick and R. D. Beger (2013). "Evaluating effects of penicillin treatment on the metabolome of rats." Journal of Chromatography B-Analytical Technologies in the Biomedical and Life Sciences **932**: 134-143.

Swann, J. R., E. J. Want, F. M. Geier, K. Spagou, I. D. Wilson, J. E. Sidaway, J. K. Nicholson and E. Holmes (2011). "Systemic gut microbial modulation of bile acid metabolism in host tissue compartments." Proceedings of the National Academy of Sciences of the United States of America **108**: 4523-4530.

Szymanska, E., J. Bouwman, K. Strassburg, J. Vervoort, A. J. Kangas, P. Soininen, M. Ala-Korpela, J. Westerhuis, J. P. M. van Duynhoven, D. J. Mela, I. A. Macdonald, R. J. Vreeken, A. K. Smilde and D. M. Jacobs (2012). "Gender-Dependent Associations of Metabolite

Profiles and Body Fat Distribution in a Healthy Population with Central Obesity: Towards Metabolomics Diagnostics." Omics-a Journal of Integrative Biology **16**(12): 652-667.

Tan, B., D. K. O'Dell, Y. W. Yu, M. F. Monn, H. V. Hughes, S. Burstein and J. M. Walker (2010). "Identification of endogenous acyl amino acids based on a targeted lipidomics approach." Journal of Lipid Research **51**(1): 112-119.

Teichert, J., R. Sohr, F. Baumann, L. Hennig, K. Merkle, K. Caca and R. Preiss (2005). "Synthesis and characterization of some new phase II metabolites of the alkylator bendamustine and their identification in human bile, urine, and plasma from patients with cholangiocarcinoma." Drug Metabolism and Disposition **33**(7): 984-992.

Tian, Y., L. Zhang, Y. Wang and H. Tang (2011). "Age-Related Topographical Metabolic Signatures for the Rat Gastrointestinal Contents." Journal of Proteome Research **11**(2): 1397-1411.

Tiribelli, C. and J. D. Ostrow (2005). "Intestinal flora and bilirubin." Journal of hepatology **42**: 170-172.

Tominaga, S., K. Nishi, S. Nishimoto, K. Akiyama, S. Yamauchi and T. Sugahara (2012). "(-)-Secoisolariciresinol attenuates high-fat diet-induced obesity in C57BL/6 mice." Food & function **3**: 76-82.

Toye, A. A., J. D. Lippiat, P. Proks, K. Shimomura, L. Bentley, A. Hugill, V. Mijat, M. Goldsworthy, L. Moir, A. Haynes, J. Quarterman, H. C. Freeman, F. M. Ashcroft and R. D. Cox (2005). "A genetic and physiological study of impaired glucose homeostasis control in C57BL/6J mice." Diabetologia **48**(4): 675-686.

Trygg, J. and S. Wold (2002). "Orthogonal projections to latent structures (O-PLS)." Journal of Chemometrics **16**(3): 119-128.

Tsutsui, H., T. Maeda, J. Z. Min, S. Inagaki, T. Higashi, Y. Kagawa and T. Toyo'oka (2011). "Biomarker discovery in biological specimens (plasma, hair, liver and kidney) of diabetic mice based upon metabolite profiling using ultra-performance liquid chromatography with electrospray ionization time-of-flight mass spectrometry." Clinica Chimica Acta **412**(11-12): 861-872.

Turman, M. V., P. J. Kingsley, C. A. Rouzer, B. F. Cravatt and L. J. Marnett (2008). "Oxidative Metabolism of a Fatty Acid Amide Hydrolase-Regulated Lipid, Arachidonoyltaurine†." Biochemistry **47**(12): 3917-3925.

Turnbaugh, P. J. and J. I. Gordon (2008). "An Invitation to the Marriage of Metagenomics and Metabolomics." Cell **134**(5): 708-713.

Turnbaugh, P. J., R. E. Ley, M. A. Mahowald, V. Magrini, E. R. Mardis and J. I. Gordon (2006). "An obesity-associated gut microbiome with increased capacity for energy harvest." Nature **444**: 1027-1131.

Tziotis, D., N. Hertkorn and P. Schmitt-Kopplin (2011). "Kendrick-analogous network visualisation of ion cyclotron resonance Fourier transform mass spectra: improved options for the assignment of elemental compositions and the classification of organic molecular complexity." European Journal of Mass Spectrometry **17**(4): 415-421.

Ubeda, C., L. Lipuma, A. Gobourne, A. Viale, I. Leiner, M. Equinda, R. Khanin and E. G. Pamer (2012). "Familial transmission rather than defective innate immunity shapes the distinct intestinal microbiota of TLR-deficient mice." The Journal of Experimental Medicine **209**(8): 1445-1456.

Ugarte, M., M. Brown, K. Hollywood, G. Cooper, P. Bishop and W. Dunn (2012). "Metabolomic analysis of rat serum in streptozotocin-induced diabetes and after treatment with oral triethylenetetramine (TETA)." Genome Medicine **4**(4): 35.

Um, S. Y., J. H. Park, M. W. Chung, K.-B. Kim, S. H. Kim, K. H. Choi and H. J. Lee (2012). "Nuclear magnetic resonance-based metabolomics for prediction of gastric damage induced by indomethacin in rats." Analytica Chimica Acta **722**(0): 87-94.

van der Greef, J., A. C. Tas, J. Bouwman, M. C. Ten Noever de Brauw and W. H. P. Schreurs (1983). "Evaluation of field-desorption and fast atom-bombardment mass spectrometric profiles by pattern recognition techniques." Analytica Chimica Acta **150**(0): 45-52.

Van Doorn, M., J. Vogels, A. Tas, E. J. Van Hoogdalem, J. Burggraaf, A. Cohen and J. Van Der Greef (2007). "Evaluation of metabolite profiles as biomarkers for the pharmacological effects of thiazolidinediones in Type 2 diabetes mellitus patients and healthy volunteers." British Journal of Clinical Pharmacology **63**(5): 562-574.

Van Eldere, J., J. Robben, G. De Pauw, R. Merckx and H. Eyssen (1988). "Isolation and identification of intestinal steroid-desulfating bacteria from rats and humans." Applied and environmental microbiology **54**: 2112-2117.

Vaziri, N. D., J. Wong, M. Pahl, Y. M. Piceno, J. Yuan, T. Z. DeSantis, Z. Ni, T.-H. Nguyen and G. L. Andersen (2013). "Chronic kidney disease alters intestinal microbial flora." Kidney Int **83**(2): 308-315.

Velagapudi, V. R., R. Hezaveh, C. S. Reigstad, P. Gopalacharyulu, L. Yetukuri, S. Islam, J. Felin, R. Perkins, J. Boren, M. Oresic and F. Backhed (2010). "The gut microbiota modulates host energy and lipid metabolism in mice." Journal of Lipid Research **51**(5): 1101-1112.

Vítek, L., J. Zelenka, M. Zadinová and J. Malina (2005). "The impact of intestinal microflora on serum bilirubin levels." Journal of hepatology **42**: 238-243.

Waldram, A., E. Holmes, Y. Wang, M. Rantalainen, I. D. Wilson, K. M. Tuohy, A. L. McCartney, G. R. Gibson and J. K. Nicholson (2009). "Top-Down Systems Biology Modeling of Host Metabotype−Microbiome Associations in Obese Rodents." Journal of Proteome Research **8**(5): 2361-2375.

Waluk, D. P., K. Vielfort, S. Derakhshan, H. Aro and M. C. Hunt (2013). "N-Acyl taurines trigger insulin secretion by increasing calcium flux in pancreatic β-cells." Biochemical and Biophysical Research Communications **430**(1): 54-59.

Wang-Sattler, R., Z. H. Yu, C. Herder, A. C. Messias, A. Floegel, Y. He, K. Heim, M. Campillos, C. Holzapfel, B. Thorand, H. Grallert, T. Xu, E. Bader, C. Huth, K. Mittelstrass, A. Doring, C. Meisinger, C. Gieger, C. Prehn, W. Roemisch-Margl, M. Carstensen, L. Xie, H. Yamanaka-Okumura, G. H. Xing, U. Ceglarek, J. Thiery, G. Giani, H. Lickert, X. Lin, Y. X. Li, H. Boeing, H. G. Joost, M. H. de Angelis, W. Rathmann, K. Suhre, H. Prokisch, A. Peters, T. Meitinger, M. Roden, H. E. Wichmann, T. Pischon, J. Adamski and T. Illig (2012). "Novel biomarkers for pre-diabetes identified by metabolomics." Molecular Systems Biology **8**.

Wang, T. J., M. G. Larson, R. S. Vasan, S. Cheng, E. P. Rhee, E. McCabe, G. D. Lewis, C. S. Fox, P. F. Jacques, C. Fernandez, C. J. O'Donnell, S. A. Carr, V. K. Mootha, J. C. Florez, A. Souza, O. Melander, C. B. Clish and R. E. Gerszten (2011). "Metabolite profiles and the risk of developing diabetes." Nat Med **17**(4): 448-453.

Wang, Y., E. Holmes, E. M. Comelli, G. Fotopoulos, G. Dorta, H. Tang, M. J. Rantalainen, J. C. Lindon, I. E. Corthésy-Theulaz, L. B. Fay, S. Kochhar and J. K. Nicholson (2007). "Topographical Variation in Metabolic Signatures of Human Gastrointestinal Biopsies

Revealed by High-Resolution Magic-Angle Spinning 1H NMR Spectroscopy." Journal of Proteome Research **6**(10): 3944-3951.

Wang, Y., E. Holmes, J. K. Nicholson, O. Cloarec, J. Chollet, M. Tanner, B. H. Singer and J. Utzinger (2004). "Metabonomic investigations in mice infected with Schistosoma mansoni: An approach for biomarker identification." Proceedings of the National Academy of Sciences of the United States of America **101**(34): 12676-12681.

Wang, Y., H. Tang, E. Holmes, J. C. Lindon, M. E. Turini, N. Sprenger, G. Bergonzelli, L. B. Fay, S. Kochhar and J. K. Nicholson (2005). "Biochemical Characterization of Rat Intestine Development Using High-Resolution Magic-Angle-Spinning 1H NMR Spectroscopy and Multivariate Data Analysis." Journal of Proteome Research **4**(4): 1324-1329.

Wang, Z., E. Klipfell, B. J. Bennett, R. Koeth, B. S. Levison, B. DuGar, A. E. Feldstein, E. B. Britt, X. Fu, Y.-M. Chung, Y. Wu, P. Schauer, J. D. Smith, H. Allayee, W. H. W. Tang, J. A. DiDonato, A. J. Lusis and S. L. Hazen (2011). "Gut flora metabolism of phosphatidylcholine promotes cardiovascular disease." Nature **472**(7341): 57-63.

Watanabe, M. and J. Ayugase (2010). "Effects of Buckwheat Sprouts on Plasma and Hepatic Parameters in Type 2 Diabetic db/db Mice." Journal of Food Science **75**(9): H294-H299.

Watanabe, M., Y. Horai, S. M. Houten, K. Morimoto, T. Sugizaki, E. Arita, C. Mataki, H. Sato, Y. Tanigawara, K. Schoonjans, H. Itoh and J. Auwerx (2011). "Lowering bile acid pool size with a synthetic farnesoid X receptor (FXR) agonist induces obesity and diabetes through reduced energy expenditure." The Journal of biological chemistry **286**: 26913-26920.

Watanabe, M., S. M. Houten, C. Mataki, M. A. Christoffolete, B. W. Kim, H. Sato, N. Messaddeq, J. W. Harney, O. Ezaki, T. Kodama, K. Schoonjans, A. C. Bianco and J. Auwerx (2006). "Bile acids induce energy expenditure by promoting intracellular thyroid hormone activation." Nature **439**(7075): 484-489.

Watanabe, M., S. M. Houten, C. Mataki, M. a. Christoffolete, B. W. Kim, H. Sato, N. Messaddeq, J. W. Harney, O. Ezaki, T. Kodama, K. Schoonjans, A. C. Bianco and J. Auwerx (2006). "Bile acids induce energy expenditure by promoting intracellular thyroid hormone activation." Nature **439**: 484-489.

Welters, C. F. M., C. H. C. Dejong, N. E. P. Deutz and E. Heineman (1999). "Effects of Parenteral Arginine Supplementation on the Intestinal Adaptive Response after Massive Small Bowel Resection in the Rat." Journal of Surgical Research **85**(2): 259-266.

Welthagen, W., R. Shellie, J. Spranger, M. Ristow, R. Zimmermann and O. Fiehn (2005). "Comprehensive two-dimensional gas chromatography–time-of-flight mass spectrometry (GC × GC-TOF) for high resolution metabolomics: biomarker discovery on spleen tissue extracts of obese NZO compared to lean C57BL/6 mice." Metabolomics **1**(1): 65-73.

Westerhuis, J., H. J. Hoefsloot, S. Smit, D. Vis, A. Smilde, E. J. Velzen, J. M. Duijnhoven and F. Dorsten (2008). "Assessment of PLSDA cross validation." Metabolomics **4**(1): 81-89.

WHO (2010). "International Classification of Diseases ICD-10." World Health Organization.

Wiklund, S., E. Johansson, L. Sjostrom, E. J. Mellerowicz, U. Edlund, J. P. Shockcor, J. Gottfries, T. Moritz and J. Trygg (2007). "Visualization of GC/TOF-MS-Based Metabolomics Data for Identification of Biochemically Interesting Compounds Using OPLS Class Models." Analytical Chemistry **80**(1): 115-122.

Wikoff, W. R., A. T. Anfora, J. Liu, P. G. Schultz, S. A. Lesley, E. C. Peters and G. Siuzdak (2009). "Metabolomics analysis reveals large effects of gut microflora on mammalian blood metabolites." Proceedings of the National Academy of Sciences **106**(10): 3698-3703.

Williams, H. R. T., I. J. Cox, D. G. Walker, B. V. North, V. M. Patel, S. E. Marshall, D. P. Jewell, S. Ghosh, H. J. W. Thomas, J. P. Teare, S. Jakobovits, S. Zeki, K. I. Welsh, S. D. Taylor-Robinson and T. R. Orchard (2009). "Characterization of Inflammatory Bowel Disease With Urinary Metabolic Profiling." Am J Gastroenterol **104**(6): 1435-1444.

Williams, R. E., H. W. Eyton-Jones, M. J. Farnworth, R. Gallagher and W. M. Provan (2002). "Effect of intestinal microflora on the urinary metabolic profile of rats: A 1H-nuclear magnetic resonance spectroscopy study." Xenobiotica **32**(9): 783-794.

Williams, R. E., E. M. Lenz, J. A. Evans, I. D. Wilson, J. H. Granger, R. S. Plumb and C. L. Stumpf (2005). "A combined 1H NMR and HPLC–MS-based metabonomic study of urine from obese (fa/fa) Zucker and normal Wistar-derived rats." Journal of Pharmaceutical and Biomedical Analysis **38**(3): 465-471.

Willing, B. P., J. Dicksved, J. Halfvarson, A. F. Andersson, M. Lucio, Z. Zheng, G. Järnerot, C. Tysk, J. K. Jansson and L. Engstrand (2010). "A Pyrosequencing Study in Twins Shows That Gastrointestinal Microbial Profiles Vary With Inflammatory Bowel Disease Phenotypes." Gastroenterology **139**(6): 1844-1854.e1841.

Wimmer, R., S. Hohenester, T. Pusl, G. U. Denk, C. Rust and U. Beuers (2008). "Tauroursodeoxycholic acid exerts anticholestatic effects by a cooperative cPKC alpha-/PKA-dependent mechanism in rat liver." Gut **57**: 1448-1454.

Wishart, D. S., C. Knox, A. C. Guo, R. Eisner, N. Young, B. Gautam, D. D. Hau, N. Psychogios, E. Dong, S. Bouatra, R. Mandal, I. Sinelnikov, J. Xia, L. Jia, J. A. Cruz, E. Lim, C. A. Sobsey, S. Shrivastava, P. Huang, P. Liu, L. Fang, J. Peng, R. Fradette, D. Cheng, D. Tzur, M. Clements, A. Lewis, A. De Souza, A. Zuniga, M. Dawe, Y. Xiong, D. Clive, R. Greiner, A. Nazyrova, R. Shaykhutdinov, L. Li, H. J. Vogel and I. Forsythe (2009). "HMDB: a knowledgebase for the human metabolome." Nucleic Acids Research **37**(suppl 1): D603-D610.

Wong, N., A. R. Blair, G. Morahan and S. Andrikopoulos (2010). "The Deletion Variant of Nicotinamide Nucleotide Transhydrogenase (Nnt) Does Not Affect Insulin Secretion or Glucose Tolerance." Endocrinology **151**(1): 96-102.

Wostmann, B. S. (1981). "The Germfree Animal in Nutritional Studies." Annual Review of Nutrition **1**(1): 257-279.

Woting, A., T. Clavel, G. Loh and M. Blaut (2010). "Bacterial transformation of dietary lignans in gnotobiotic rats." FEMS microbiology ecology **72**: 507-514.

Wu, H., R. Xue, C. Lu, C. Deng, T. Liu, H. Zeng, Q. Wang and X. Shen (2009). "Metabolomic study for diagnostic model of oesophageal cancer using gas chromatography/mass spectrometry." Journal of Chromatography B **877**(27): 3111-3117.

Würtz, P., V.-P. Mäkinen, P. Soininen, A. J. Kangas, T. Tukiainen, J. Kettunen, M. J. Savolainen, T. Tammelin, J. S. Viikari, T. Rönnemaa, M. Kähönen, T. Lehtimäki, S. Ripatti, O. T. Raitakari, M.-R. Järvelin and M. Ala-Korpela (2012). "Metabolic Signatures of Insulin Resistance in 7,098 Young Adults." Diabetes **61**(6): 1372-1380.

Xie, G. X., M. M. Su, P. Li, X. Gu, C. Yan, Y. P. Qiu, H. K. Li and W. Jia (2007). "Analysis of urinary metabolites for metabolomic study by pressurized CEC." Electrophoresis **28**(23): 4459-4468.

Xu, J., J. Zhang, S. Cai, J. Dong, J. Yang and Z. Chen (2009). "Metabonomics studies of intact hepatic and renal cortical tissues from diabetic db/db mice using high-resolution magic-

angle spinning 1H NMR spectroscopy." Analytical and Bioanalytical Chemistry **393**(6-7): 1657-1668.

Yanes, O., R. Tautenhahn, G. J. Patti and G. Siuzdak (2011). "Expanding Coverage of the Metabolome for Global Metabolite Profiling." Analytical Chemistry **83**(6): 2152-2161.

Yetukuri, L., M. Katajamaa, G. Medina-Gomez, T. Seppanen-Laakso, A. Vidal-Puig and M. Oresic (2007). "Bioinformatics strategies for lipidomics analysis: characterization of obesity related hepatic steatosis." Bmc Systems Biology **1**.

Yetukuri, L., M. Katajamaa, G. Medina-Gomez, T. Seppänen-Laakso, A. Vidal-Puig and M. Oresic (2007). "Bioinformatics strategies for lipidomics analysis: characterization of obesity related hepatic steatosis." BMC systems biology **1**: 12.

Young, N. L., D. J. McNamara, C. D. Saudek, J. Krasovsky, D. R. Lopez and G. Levy (1983). "Hyperphagia alters cholesterol dynamics in diabetic rats." Diabetes **32**(9): 811-819.

Zhang, X., Y. Wang, F. Hao, X. Zhou, X. Han, H. Tang and L. Ji (2009). "Human Serum Metabonomic Analysis Reveals Progression Axes for Glucose Intolerance and Insulin Resistance Statuses." Journal of Proteome Research **8**(11): 5188-5195.

Zhang, X., L. Xu, J. Shen, B. Cao, T. Cheng, T. Zhao, X. Liu and H. Zhang (2013). "Metabolic signatures of esophageal cancer: NMR-based metabolomics and UHPLC-based focused metabolomics of blood serum." Biochimica et Biophysica Acta (BBA) - Molecular Basis of Disease **1832**(8): 1207-1216.

Zhao, L.-C., X.-D. Zhang, S.-X. Liao, H.-C. Gao, H.-Y. Wang and D.-H. Lin (2010). "A Metabonomic Comparison of Urinary Changes in Zucker and GK Rats." Journal of Biomedicine and Biotechnology **2010**.

Zhao, X., J. Fritsche, J. Wang, J. Chen, K. Rittig, P. Schmitt-Kopplin, A. Fritsche, H.-U. Häring, E. Schleicher, G. Xu and R. Lehmann (2010). "Metabonomic fingerprints of fasting plasma and spot urine reveal human pre-diabetic metabolic traits." Metabolomics **6**(3): 362-374.

Zhao, X., A. Peter, J. Fritsche, M. Elcnerova, A. Fritsche, H.-U. Häring, E. D. Schleicher, G. Xu and R. Lehmann (2009). "Changes of the plasma metabolome during an oral glucose tolerance test: is there more than glucose to look at?" American Journal of Physiology - Endocrinology And Metabolism **296**(2): E384-E393.

Zhao, Y., J. Wu, J. V. Li, N.-Y. Zhou, H. Tang and Y. Wang (2013). "Gut Microbiota Composition Modifies Fecal Metabolic Profiles in Mice." Journal of Proteome Research **12**(6): 2987-2999.

Zoppi, G. (1997). "Probiotics and prebiotics in the treatment of infections due to vancomycin-dependent Enterococcus faecalis and of imbalance of the intestinal ecosystem (dysbiosis)." Acta Pædiatrica **86**(10): 1148-1150.

Scientific communications

Posters and Oral presentations

2011:

Non-targeted metabolomics to study the metabolic impact of gut microbiome, International Scientific Conference on Probiotics and Prebiotics, IPC 2011, June 14-16, Kosice, Slovakia. (Poster)

2012:

Discovery of metabolic patterns of gut microbiome in C57BL/6J and C57BL/6N mice using high resolution mass spectrometry, Metabomeeting, September 24-27, Manchester, UK. (Oral presentation)

Gut microbial ecology: DZD meeting, (Oral presentation)

2013:

In depth characterization of gut microbial sulfometabolome in a mouse model of Crohn`s disease (oral presentation) at Schwerpunktsprogramm "INTESTINAL MICROBIOTA at the edge between immune homeostasis and inflammation" (SPP 1656), (Oral presentation)

Discovery of gut microbial metabolome in type 2 Diabetes (Oral presentation): Seeon Conference "Microbiota, Probiota and Host", (Oral presentation)

Publications

Kunert, C.; Walker, A.; Hofmann, T. (2011) J. Agric. Food Chem., 59, 8366-8374. Taste Modulating N-(1-Methyl-4-oxoimidazolidin-2-ylidene) α-Amino Acids Formed from Creatinine and Reducing Carbohydrates.

Wörmann, K., A. Walker, F. Moritz, S. Forcisi, D. Tziotis, M. Lucio, S. S. Heinzmann, J. Adamski, R. Lehmann, H.-U. Häring and P. Schmitt-Kopplin (2012). "Revolution in der Diabetesdiagnostik dank -omics - Biomarker mittels Metabolomics." Diabetes aktuell 10(03): 129-133.

Daniel, H., A. M. Gholami, D. Berry, C. Desmarchelier, H. Hahne, G. Loh, S. Mondot, P. Lepage, M. Rothballer, A. Walker, C. Bohm, M. Wenning, M. Wagner, M. Blaut, P. Schmitt-Kopplin, B. Kuster, D. Haller and T. Clavel (2013). "High-fat diet alters gut microbiota physiology in mice." ISME J: Multidisciplinary Journal of Microbial Ecology

2014:

Walker, A., B. Pfitzner, S. Neschen, M. Kahle, M. Harir, M. Lucio, F. Moritz, D. Tziotis, M. Witting, M. Rothballer, M. Engel, M. Schmid, D. Endesfelder, M. Klingenspor, T. Rattei, W. z. Castell, M. H. de Angelis, A. Hartmann and P. Schmitt-Kopplin (2014). "Distinct signatures of host-microbial meta-metabolome and gut microbiome in two C57BL/6 strains under high-fat diet." ISME J: Multidisciplinary Journal of Microbial Ecology

Walker, A., M. Lucio, B. Pfitzner, M. F. Scheerer, S. Neschen, M. H. de Angelis, A. Hartmann and P. Schmitt-Kopplin (2014). "Importance of Sulfur-Containing Metabolites in Discriminating Fecal Extracts between Normal and Type-2 Diabetic Mice." Journal of proteome research 13(10): 4220-4231.

Fernsebner, K., J. Zorn, B. Kanawati, A. Walker and B. Michalke (2014). "Manganese leads to an increase in markers of oxidative stress as well as to a shift in the ratio of Fe(II)/(III) in rat brain tissue." Metallomics 6(4): 921-931.